Geotechnical Design of Tailings Dams - A Stochastic Analysis Approach

By

Tarek Hamade

Department of Mining and Materials Engineering
McGill University, Montreal

March 2013

A thesis submitted to McGill University in partial fulfillment of the requirements of the degree of Doctorate of Philosophy

ABSTRACT

Mine tailings dams are geotechnical structures that are designed to provide adequate and safe storage of tailings materials both during and after the end of mine life. The design of tailings dams is currently based on limit equilibrium methods (LEM) which are used to calculate slope stability safety factors under various operational loads. The minimum safety factor obtained from these analyses is retained to be the design safety factor. LEM's however suffer from a number of shortcomings most notably the lack of information on dam deformation and the interaction between effective stress and pore pressure. For this, advanced numerical modeling techniques accounting for the hydro-mechanical coupling occurring in the dam structure have been developed. These models provide much greater insight into the geotechnical behavior of the tailings dam. However, both LEM and numerical modeling approaches are deterministic in nature; thus, they do not take into consideration the inherent uncertainty of the construction material properties – a fact that is well known to the geotechnical engineer, yet, needs to be addressed.

In this thesis, stochastic analysis approaches such as the Monte Carlo (MC) method are adopted to investigate the effect of the inherent uncertainty in material properties on the design factor of safety. Both LEM and coupled hydro-mechanical numerical models are first developed and the results for deterministic models are compiled. These are then compared with the result obtained from stochastic analyses.

A case study of a new water retention tailings dam project design with well documented geotechnical data is adopted throughout the thesis study. First the LEM analysis was pursued followed by a sensitivity analysis to determine the most influential parameters on the design safety factor.

Next, a fully coupled hydro-mechanical model was developed with FLAC2D in which the construction sequence was simulated in seven stages. The factor of safety (FOS) was calculated at the end of every stage using the Strength

Reduction Technique (SRT). Following that, the Point Estimate Method (PEM) was then used to obtain the probability of unsatisfactory performance by considering the dam's core angle of friction, cohesion and permeability as stochastic variables. The coefficient of variation for the material properties was varied and its consequence on the probability was recorded. Next, the MC method was adopted to calculate the tailings dam's probability of unsatisfactory performance as well as its reliability. The effect of changing the probability density function (PDF) of the stochastic input parameter on the output reliability was further analyzed. Furthermore, the effect of randomness at the local level was studied using the Random Monte-Carlo (RMC) method and compared to the output of the MC method.

Finally, the effect of the coefficient of correlation between the dam's core angle of friction and its cohesion on the impoundment's reliability was analyzed. This was followed by an advanced stochastic analysis using the MC method that included a third stochastic variable, the dam's core permeability. The incorporation of both mechanical and hydraulic parameters as stochastic variables lowered the impoundment's reliability; thus, highlighting the power and novelty in the hydro-mechanical stochastic analysis hybrid approach. The results of all analyses are presented in the thesis along with the findings in the conclusion.

RÉSUMÉ

Les digues des résidus miniers sont des ouvrages géotechniques conçus pour offrir un stockage adéquat et sécuritaire des résidus et ce pendant et après la fin de la vie de la mine. La conception des digues à résidus est actuellement basée sur les méthodes d'équilibre limite (LEM) qui sont utilisés pour calculer les facteurs de sécurité de la stabilité des pentes sous diverses charges opérationnelles. Le facteur de sécurité minimal obtenu à partir de ces analyses est considéré comme facteur de sécurité de conception. Ils sont présentement utilisés dans la conception géotechnique. Cependant, LEM a des lacunes notamment le manque d'information sur la déformation d'une digue et de l'interaction entre les contraintes effectives et la pression interstitielle. Ainsi, les techniques de modélisation numérique avancées qui considèrent le couplage hydro-mécanique survenant dans la structure de la digue ont été développées. Ces modèles procurent un aperçu plus précis du comportement géotechnique de la digue à résidus. Cependant, les deux approches LEM et modélisation numérique sont déterministe. Par conséquent, ces approches ne tiennent pas compte de l'incertitude inhérente aux propriétés des matériaux de construction et ceci est un fait bien connu par l'ingénieur géotechnicien et pourtant ceci doit être abordé.

Dans cette thèse, les approches d'analyse stochastiques tels que le Monte Carlo (MC) sont adoptées pour étudier l'effet de l'incertitude inhérente aux propriétés du matériau sur le coefficient de sécurité. Les deux LEM et les modèles numériques hydro- mécaniques couplés sont d'abord développés et après les résultats des modèles déterministes sont compilés. Ces derniers sont ensuite comparés aux résultats obtenus à partir des analyses stochastiques.

Une étude de cas d'une nouvelle conception d'une digue à rétention d'eau à résidus avec des données géotechniques bien documentées est adoptée dans cette étude. Tout d'abord, l'analyse LEM a été poursuivi et suivi par une analyse de sensibilité pour déterminer les paramètres les plus influents sur le facteur de sécurité de la conception.

Ensuite, un model couplé d'hydro-mécanique a été développé avec FLAC2D dans lequel la séquence de construction a été simulée en sept étapes. Le

coefficient de sécurité (FOS) a été calculé à la fin de chaque étape en utilisant la technique de réduction de la résistance (SRT). Par la suite, la méthode d'estimation ponctuelle (PEM) a été utilisée pour obtenir la probabilité d'un rendement insatisfaisant en tenant compte de l'angle de base de la digue, de la friction, de la cohésion et de la perméabilité comme variables stochastiques.

Le coefficient de variation des propriétés du matériau a été varié et ses conséquences sur la probabilité ont été enregistrées. Ensuite, la méthode de MC a été adoptée pour calculer la probabilité de rendement insatisfaisant de la digue à résidus ainsi que sa fiabilité. Par ailleurs, l'effet de la modification de la fonction de densité de probabilité (PDF) du paramètre d'entrée stochastique sur la fiabilité de sortie a encore été analysé. En outre, l'effet du hasard au niveau local a été étudiée en utilisant le hasard Monte-Carlo (RMC) et la méthode par rapport à la sortie de la méthode de MC. Enfin, l'effet du coefficient de corrélation entre l'angle de friction du noyau et la cohésion sur la fiabilité de la digue a été analysé. Ceci a été suivi d'une analyse stochastique avancé à l'aide de la méthode MC qui comprenait une troisième variable stochastique qui est la perméabilité du noyau. L'incorporation de paramètres à la fois mécaniques et hydrauliques en tant que variables stochastiques ont réduit la fiabilité de la digue, ainsi, mettant en évidence l'impact de l'analyse stochastique hydro-mécanique avec l'approche hybride. Les résultats de toutes les analyses sont présentés dans la thèse suivante ainsi que les découvertes dans la conclusion.

DEDICATION

This work is dedicated to my parents: Nadim and Ahlam,

with all the warmth of a thankful son;

and my siblings: Firas, Bachar and Diala,

with all the joy of a lucky brother

ACKNOWLEDGEMENTS

There is a long list of people that have shaped my years at McGill and have made my journey an enjoyable one.

Foremost, I would like to thank Professor Hani Mitri. Hani was not just my supervisor; he was my coach, mentor, and motivator to say the least. Hani, your guidance over the past years has shaped my career, and has provided me the confidence I needed to venture into unchartered waters and prove myself time after time. I shall always cherish the valuable advice you have given me and I know that I will be knocking on your door in the future for further coaching. The research guidance and dedication that you have provided me with have been priceless, and the financial assistance much appreciated. To many more things, I am also very thankful.

I would like to also thank Dr. Bassam Saad for his technical input and valuable advice in this research. Bassam, you greatly assisted in this research; the ideas and challenges that you brought to the table made this a better piece of work.

Moreover, I would like to thank Sandra Pouliot and Pascal Lavoie at Agnico-Eagle Mines Ltd. for embracing and providing the necessary financial support to complete this research. Our meetings and lunches together shall always be remembered.

My colleagues at the Mine Design Lab (each and every one of you) have been very supportive during this journey, but I especially would like to thank my long time officemates Dr. Shahé Shnorhokian and Hind Zniber for all the good laughs we had in Room 102. They are already missed.

I had a big circle of friends and loved ones, and including them all would make the pages run on and on. Nevertheless, I would like to thank my long time childhood friend and roommate from our days at Cornell, Dr. Imad Agha, for always being there for me during both the ups and downs. I also want to thank one

of my best friends, Razan Francis, for always hearing me out and laughing away the problems that I shared with her. I also want to salute my long time friend, Dr. Mona Hammami, for being a great supporter and a source of encouragement during this roller coaster journey. In addition, I would like to thank Nour El Houda El Mostaqim for her unwavering encouragement, and supporting me in keeping the course to overcome the numerous obstacles while working on this thesis.

I also want to thank the folks at Thomson House for their encouragement and support during my tenure as an Elections Commissioner for the Post Graduate Students' Society (PGSS) at McGill.

Last but not least, the biggest thank you goes to my family for showering me with their love and care and cheering me on every step of the way. Mom and Dad: you are my number 1. Firas, Bachar and Diala: I love you guys!

TABLE OFCONTENTS

LIST OF TABLES

LIST OF FIGURES

LIST OF APPENDICES

LIST OF ABBREVIATIONS AND SYMBOLS

LEM: Limit Equilibrium Method

FEM: Finite Element Models

FDM: Finite Difference models

PEM: Point Estimate Method

MC: Monte Carlo

MCS: Monte Carlo Simulation

RMC: Random Monte Carlo

RMCS: Random Monte Carlo Simulation

WRD: Water Retention Dam

ESA: Effective Stress Analysis

TSA: Total Stress Analysis

USA: Undrained Strength Analysis

VRT: Variance Reduction Techniques

RFEM: Random Finite Element Method

FORM: First Order Reliability Method

FOSM: First Order Second Moment

AFOSM: Advanced First-Order Second Moment

PDF: Probability Density Function

PMF: Probability Mass Function

CDF: Cumulative Distribution Function

FOS or F: Factor of Safety

M-P: Morgenstern-Price Method

CDA: Canadian Dam Association

n_g: Seismic Coefficient

ϕ: Friction Angle

c: Cohesion

C_c: Compression Index

C_v: Coefficient of Consolidation

σij: Cauchy stress

ρ: Mass Density or Correlation Coefficient

k^e_{ij}: effective permeability

k_{ij}: permeability

g: gravity

S: degree of saturation

p_w: pore water pressure

ρ_w: density of water

α: Biot's effective stress parameter

ε_{ii}: volumetric strain

ϕ^{DP}: Drucker Prager Friction Angle

c^{DP}: Drucker Prager Cohesion

COV: Coefficient of Variation

X_i: Variable

Z: Performance Function

p_f: Probability of Failure

R: Resistance

S: Load

μ: Mean

σ: Standard Deviation

Φ: Cumulative Distribution Function

β: Safety Index

λ_x and ζ_x: Two parameters of the lognormal distribution

$Cov(X_i, X_j)$: Covariance of X_i and X_j

β_{HL}: Hasofer-Lind Reliability Index

x'*: design point or the most probable point of failure

υ_x: Skewness

W: total weight of the slice of width *b* and height *h*

P: total normal force on the base of the slice over a length *l*

S_m: shear force mobilized on the base of the slice

R: radius or the moment arm associated with the mobilized shear force S_m

f: perpendicular offset of the normal force from the center of rotation

x: horizontal distance from the slice to the center of rotation

α: angle between the tangent to the center of the base of each slice and the horizontal

E: horizontal interslice forces

L: subscript designating left side

R: subscript designating right side

X: vertical interslice forces

k: seismic coefficient to account for a dynamic horizontal force

e: vertical distance from the centroid of each slice to the center of rotation

L: line load (force per unit width)

ω: angle of the line load from the horizontal

d: perpendicular distance from the line load to the center of rotation

A: resultant water forces

a: perpendicular distance from the resultant water force to the center of rotation

X: vertical interslice forces in the LEM

E: horizontal interslice forces in the LEM

q_i: pecific discharge vector

k_{ij}: mobility coefficient

$\hat{k}(s)$: relative permeability (which is a function of the saturation s)

P: fluid pressure

ρ_w :mass density of the fluid

g_i , i = 1,2 are the two components of the gravity vector

ζ: variation of fluid content (variation of fluid volume per unit volume of porous material)

q_v: volumetric fluid source intensity

M : Biot modulus

α: Biot coefficient

ε: volumetric strain

K: drained bulk modulus of the porous medium

K_w: fluid bulk modulus

$\dot{\epsilon_{kk}}$: is the volumetric strain increment

Q: flow rate

M: “stiffness” matrix

k: isotropic mobility coefficient

V: total volume associated with the node

P: pore pressure

$\Delta Vmech$: equivalent nodal volume increase arising from mechanical deformations of the grid

K: mechanical bulk modulus of a zone

t_c^m: characteristic time

K_u: undrained bulk modulus

G: shear modulus

ρ: mass density

L_c : characteristic length

c: diffusivity

k: mobility coefficient

S: storativity

CHAPTER : 1 **INTRODUCTION**

1.1 GENERAL

The disposal and management of mine waste, mainly tailings, is an ever evolving field (Vick 1990). An increase in the social awareness regarding the risks and liabilities associated with the permanent existence of tailings impoundment facilities coupled with the intense regulatory attention and public scrutiny have delineated a conceptual framework within which all stakeholders have to work collectively to ensure the safety of these impoundments, from cradle to grave.

Historically, mining operations started small and mainly in remote areas away from inhabited communities and the naked eye; and tailings were mainly disposed off in nearby streams before progressing to the empirical design of impoundments by operators using trial and error (Vick 1983). Over the past few decades, the principles of geotechnical engineering have been applied to tailings impoundments, starting with the design practices for water retention dams. However, now, the management, planning and design of tailings impoundment facilities is of a multidisciplinary nature requiring an integrated approach, and as such, necessitating the development of novel analysis techniques that shall address the hidden uncertainties governing the system's dynamics.

1.2 TAILINGS IMPOUNDMENT FACILITIES

Wherever one finds a milling operation, one will find a tailings impoundment facility to handle the tailings. However, every impoundment facility is unique in its nature and content, and as such the geotechnical and environmental regimes governing the impoundment's behavior vary from site to site. Moreover, ensuring the proper operations of these impoundments remains a challenge as the factors contributing to their stability change over their lifetime. A

breach in the embankment of a tailings impoundment will typically unleash a tidal wave of slimes and sediments that could be heavily contaminated with toxic compounds. Moreover, the fact that these tailings impoundments are built over time while enduring changing operational conditions adds to their complexity. All dams built are designed based on common current practices that simplify the design process by neglecting uncertainties in the model built and compromising on various critical and realistic features of the impoundment. This remains one of the many causes why the current numerical models have failed to predict failure, as all dams built are designed as "safe". As a result, there is an ominous need for further understanding these systems to better design and operate them and mitigate against their failure.

1.3 PROBLEM DEFINITION

All mining sites running milling operations aspire for the safe performance of their tailings impoundment facilities throughout their life cycle. Unfortunately some fail, and are failing at an increasing rate. The following set of figures/schematics presented below and published by the International Commission of Large Dams, (ICOLD 2001), support this observation. It was not until recently that the ICOLD along with the United States Commission of Large Dams (USCOLD) and the United Nations Environment Programme (UNEP) took over the task of recording the failures of tailings impoundment facilities as a result of the catastrophic environmental and socio-economic consequences associated with their breach. And given that at the present, impoundments remain operational for extended periods, guidelines have to be worked in place for their construction, maintenance and operation, as is the case for water retention dams (WRDs).

Figure 1-1illustrates the number of failures of tailings dams as a function of the cause of failure. From the figure, it can be seen that "slope stability" dominates the chart as the primary cause of the incident followed by overtopping, earthquake, seepage and foundation. Moreover, the number of failures for tailings

dams is comparable to that of water retaining dams, with relative consequences of failure (ICOLD 2001).

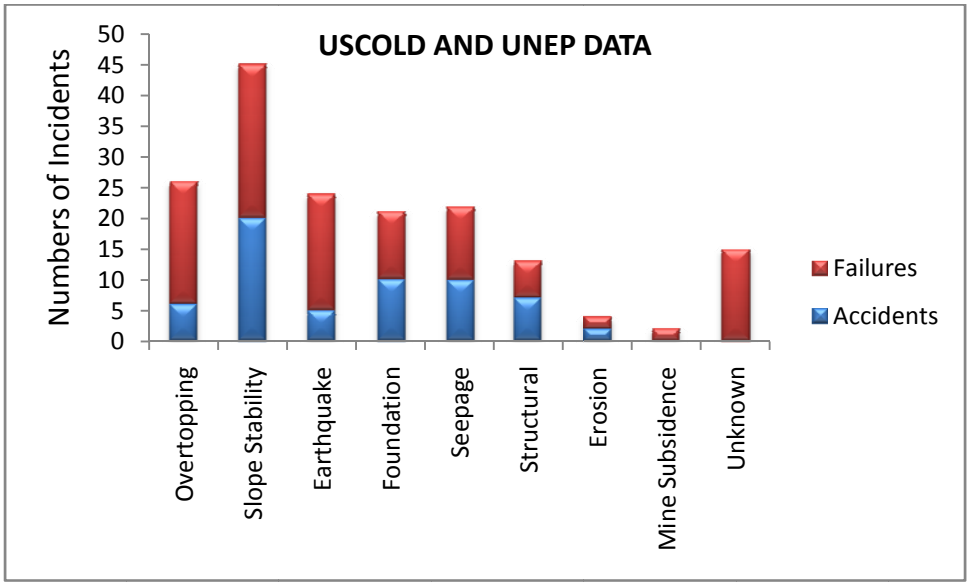

Figure 1-1: Tailings dam incident cause comparison with incident type for active dams (After ICOLD 2001).

Further statistics presented by the USCOLD and UNEP have shown that the majority of the tailings dams that have failed belong to the upstream construction technique as well as the water retaining type and which, according to Engels (Engels 2005), form at least 60% of the world's tailings impoundment facilities. This finding is illustrated in Figure 1-2 and Figure 1-3.

Thus, there is a clear need for further research on tailings dams' stability not only to better understand the causes of past failures, but also to provide tools capable of operating such facilities reliably and safely.

The latest edition of the "Guide to the Management of Tailings Facilities" published in 2011 by the Mining Association of Canada (MAC) is a sixty eight page descriptive report that is far from being technical and provides simple guidelines on managing tailings (MAC 2011). At the present, the Canadian Dam Association (CDA) is working on formally rolling out technical guidelines for the design and operations of tailings impoundments.

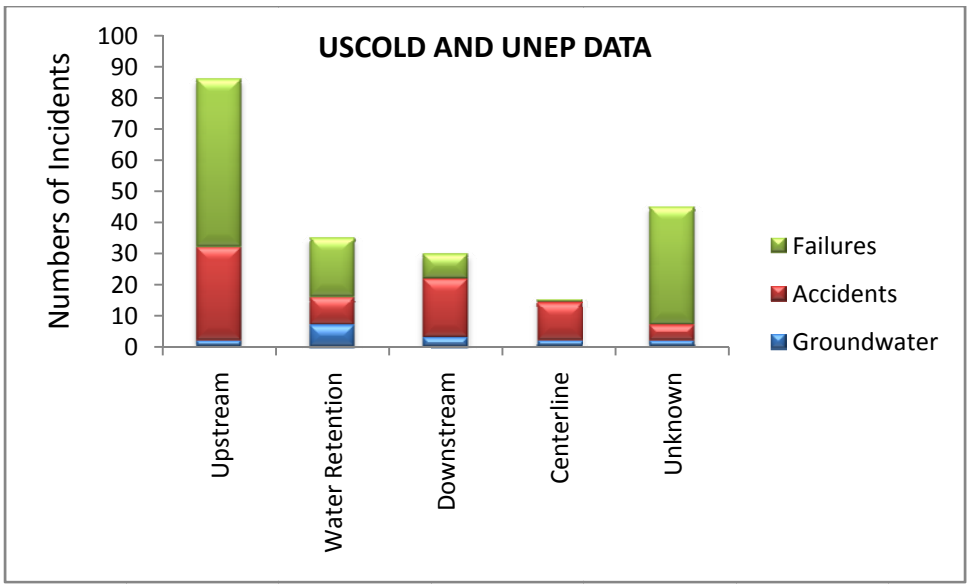

Figure 1-2: Tailings dam type comparison (After ICOLD 2001).

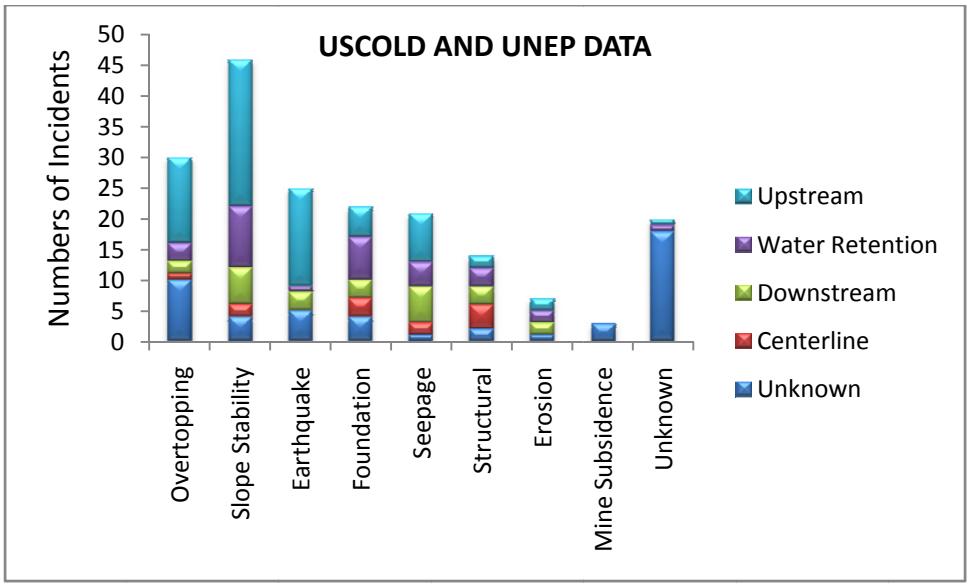

Figure 1-3: Tailings dam incident cause comparison with dam type (After ICOLD 2001).

Thus, there is the need for continuous research in this area to provide the community of tailings impoundment designers with the necessary tools and understanding of the mechanics governing the "well-being" of tailings impoundment facilities until the end of construction phase as well as post construction and closure.

1.4 SCOPE AND OBJECTIVES

Different classical geotechnical slope stability analyses such as the limit equilibrium method (LEM) have been applied for calculating a factor of safety for the design of tailings impoundments. Also, many stability analyses included the use of finite element models (FEMs) and finite difference models (FDM). Furthermore, several researchers have worked on defining the material properties of different zones within the impoundment to help tune up their models. The latest developments in this area was by developing a finite element model capable of performing a hydromechanical transient coupled analysis for upstream tailings disposal facilities (Saad and Mitri 2010). They reported a number of findings, including: "Unlike LEM, all the impoundments analyzed showed that the maximum plastic shear strain zones do not appear along surfaces of well defined shapes, but rather they spread over a volume of irregular shape. Such findings confirm the shortcomings in the use of LEM for the prediction of potential failure surface in upstream tailings disposal facilities."

However, both the current simple and advanced numerical models fail to incorporate uncertainty in the analysis. Consequently, they fall short of delivering a probability of failure for such impoundments that can then be used in further quantitative risk analysis models.

As a result, there is a looming need for developing adequate models that can address the inherent uncertainty of soil properties. Such models must be able to identify the critical parameters and their respective degrees of uncertainty influencing the stability of the tailings impoundment throughout its life cycle, i.e. till the end of construction and closure.

The research carried out in this dissertation presents a new framework for the stability analysis of tailings dams, whereby existing probabilistic methods are applied to a fully coupled hydromechanical model, with the final outcome being a distribution for the factor of safety that will define the probability of unsatisfactory performance of the impoundment. A case study of a newly

constructed water retention tailings dam of a gold mine is adopted in this thesis to demonstrate the analysis approaches developed.

Thus the research objectives are:

1. Further defining failure, the probability of failure and the probability of unsatisfactory performance.

2. Further defining reliability methods.

3. Identifying the model input parameters and their statistical distributions.

4. Filtering the model input parameters for the purpose of identifying which input parameter will be defined statistically depending on their degree of influence in the model.

5. Develop the hybrid approach which combines a deterministic model with a reliability model

6. Comparing the output of both deterministic and probabilistic models, as the latter complements the former.

1.5 THESIS OUTLINE

Aside from this chapter that provides a general background overview through a series of snap shots of today's tailings impoundments, the thesis includes the following chapters:

Chapter 2 provides a broad literature review on tailings impoundments, highlighting the tailings' different engineering properties, construction methods and practices and emerging approaches for tailings management.

Chapter 3 presents a detailed literature review on the current stability analyses applied to tailings dams. This includes an overview of the classical

stability analysis approaches, a comparison between the deterministic and probabilistic approaches and their applications in geotechnical engineering.

Chapter 4 presents the case study and the performed limit equilibrium analysis. This was followed by a sensitivity analysis and a section summarizing the limitation of the Limit Equilibrium Methods.

Chapter 5 presents the hydro-mechanical coupled analysis applied to the case study. It starts with an overview of the fluid-mechanical interaction, followed by the numerical model setup and output.

Chapter 6 presents the application of the different stochastic analysis to the case study. This included: the Point Estimate Method (PEM), the Monte Carlo (MC) method and the Random Mont Carlo (RMC) method.

Chapter 7 presents the reliability analysis pursued using the hybrid stochastic hydro-mechanical coupled analysis. First, the performance criteria was outlined; then stochastic variables were varied and the discussion of results was presented.

Chapter 8 presents the research summary, conclusions and recommendations for further research.

CHAPTER : 2 TAILINGS IMPOUNDMENTS OVERVIEW

2.1 MINERAL PROCESSING

Tailings result from mineral processing, which includes crushing, grinding, concentration, dewatering, and finally tailings slurry disposal as illustrated in Figure 2-1. Rock fragments are reduced from mine-run size to accepted feed to grinding via crushing which generally consists of a two stage system, primary and secondary crushing. The latter reduces the fragments to about 20 mesh size. Using rod mills and ball mills, the grinding phase reduces the crushed rock to adequate feed size to the concentration phase. Depending on the type of mineral to be extracted, leaching and/or heating will be deployed. The dewatering phase is crucial in reducing the water content of the mill output to that of tailings-water slurry, which is disposed off in the impoundment.

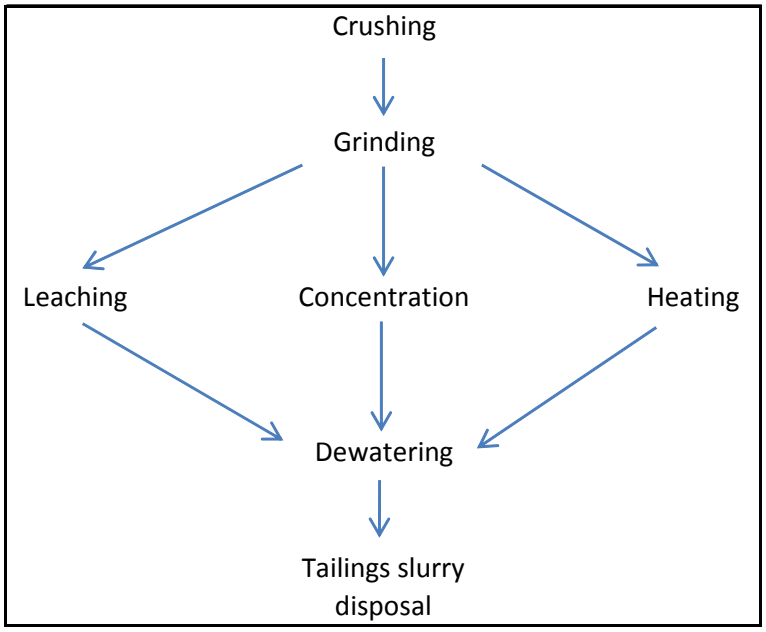

Figure 2-1: Procedures in tailings production (After Vick 1983.)

2.2 TAILINGS HANDLING AND MILL WATER RETURN

Pulp density is the most common measure of slurry density, defined as the weight of solids per unit weight of slurry, typically in the range of 30 – 50% depending on the type of thickener, thus making them abrasive and of high viscosity. The coarseness and size distribution of the tailings, pulp density of the slurry, and other factors all dictate the tailings velocity in the pipeline, which commonly ranges between 1.5 and 3m/sec.

As illustrated in Figure 2-2, beach deposition can take place either via spigotting or single-point discharge. Typically, coarse particles settle close to the point of discharge and finer and colloidal particles settle farther away in the standing water forming the decant pond. However, this remains a function of the tailings properties. Tailings that are not clayey in nature will tend to have a higher homogeneity relative to other tailings materials rich in clay size particles, thus leading to a lower concentration of suspended solids.

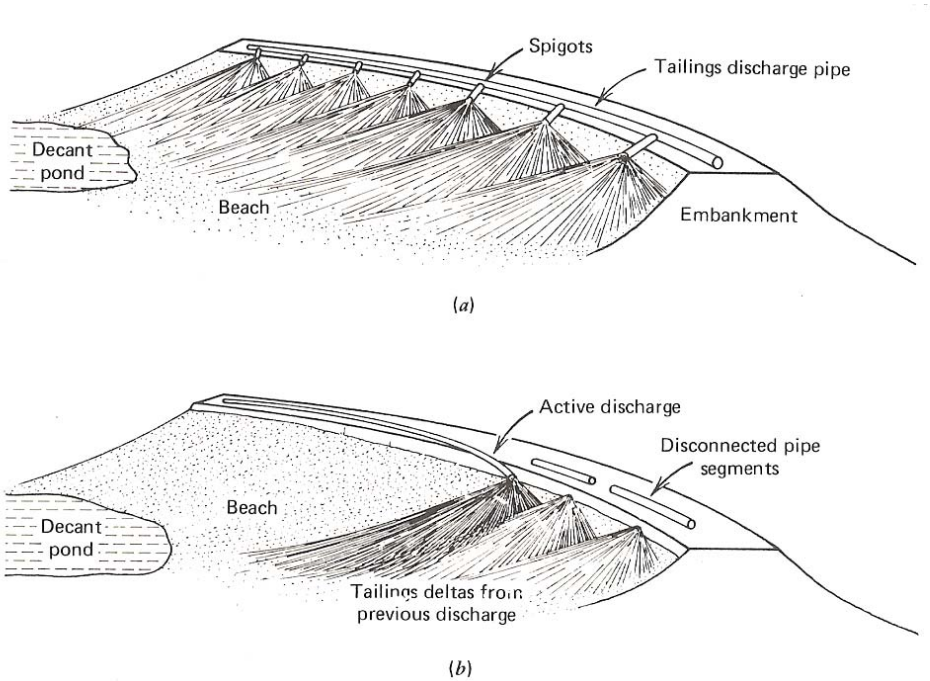

Figure 2-2: Peripheral discharge methods. (a) Spigotting. (b) Single-point discharge (after Vick 1983)

Furthermore, in mines where water is of limited availability, efforts are made to decant the pond and reuse the water back in the mill. Moreover, strict environmental regulations such as those imposed locally and in other developed nations require mines to re-circulate approximately 90% of the water consumed in the milling operations. Such regulations ensure minimal environmental impact on the surrounding habitats and ensure that the goals outlined by the Mining Association of Canada (MAC's) "Towards Sustainable Mining" guidelines will be achieved.

Figure 2-3 is a schematic illustrating the difference between spigotting and cycloning on the crest of the dyke. In the spigotting process, the tailings line is directed towards the pond and the dyke is raised by scooping sandy tailings from the beach. Moreover, it is worth noting that the separation line forming both the sand and slime zones in Figure 2-3a is merely conceptual and far from realistic. The reason simply being that operational procedures for spigotting dictate filling up the impoundment and that is seldom uniform, and the fact that spigotting is more of an "open tap" discharge approach where the slurry is released freely.

On the other hand, the cyclone includes two outlets, the overflow and the underflow which allow for the separation of the coarse and finer material in the tailings. This separation of the sands and slimes in the tailings provides a permeability difference between the adjacent zones of about two orders of magnitude which in turn leads to a major reduction in the phreatic surface. Moreover, as further illustrated in Figure 2-3b, cycloning takes place on the crest of the dyke where sand is being deposited and the slimes are discharged farther out onto the beach, forming the two zones. Depending on the ratio of sand recovery versus the fine contents, a second stage of cycloning might be necessary. It is important to note, though, that if the water level rises sufficiently to infringe on the sand zone, then higher seepage outflows could be observed at the toe of the embankment, resulting in stability issues because of the zone’s higher permeability.

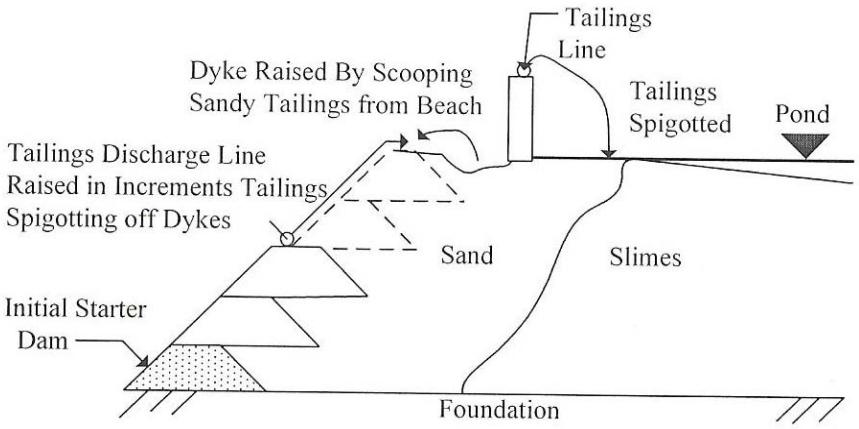

(a)

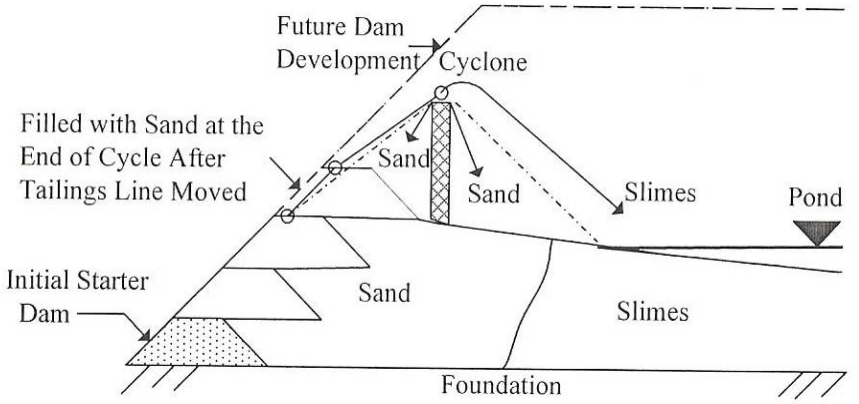

(b)

Figure 2-3: Upstream tailings dam construction using (a) spigotting (b) cycloning

2.3 TYPES OF TAILINGS

The kind of ore being milled as well as the particular processing operation defines the nature of tailings. The following Figures (Figure 2-4, Figure 2-5, and Figure 2-6) illustrate the particle size distribution of tailings samples from coal, tar sands, and gold-silver ore milling operations, respectively. A common theme in the three figures below presents itself: that the grain size distribution is unique for a specific tailings impoundments site (Vick 1983). This is justified by the variety observed in the tailings grain size distribution for processing the same type of ore mineral at different mine sites. As an example, the tailings characteristics generated from a milling operation processing gold by gravity separation will be

completely different than another milling operation processing gold using chemical means, such as introducing cyanide, which gold has a great affinity to. Moreover, it's important to note the location where the sample was obtained to define the grain size distribution; i.e. if the tailings are characterized with high clay content then collecting a sample far out in the impoundment will generate a different distribution than one collected close to the discharge point.

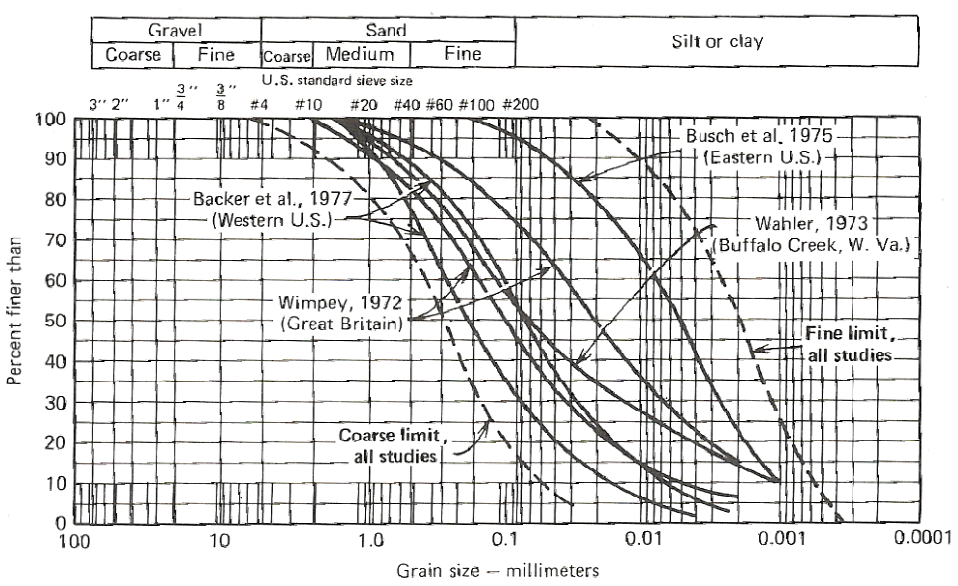

Figure 2-4: Average gradations of fine coal refuse (After Vick 1983)

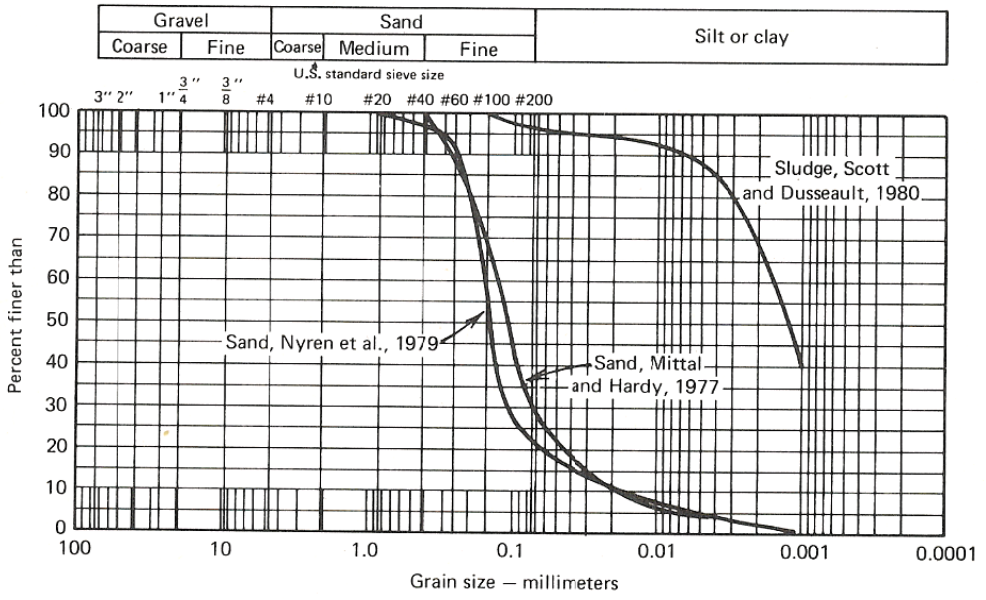

Figure 2-5: Gradations of tar sands tailings (After Vick 1983)

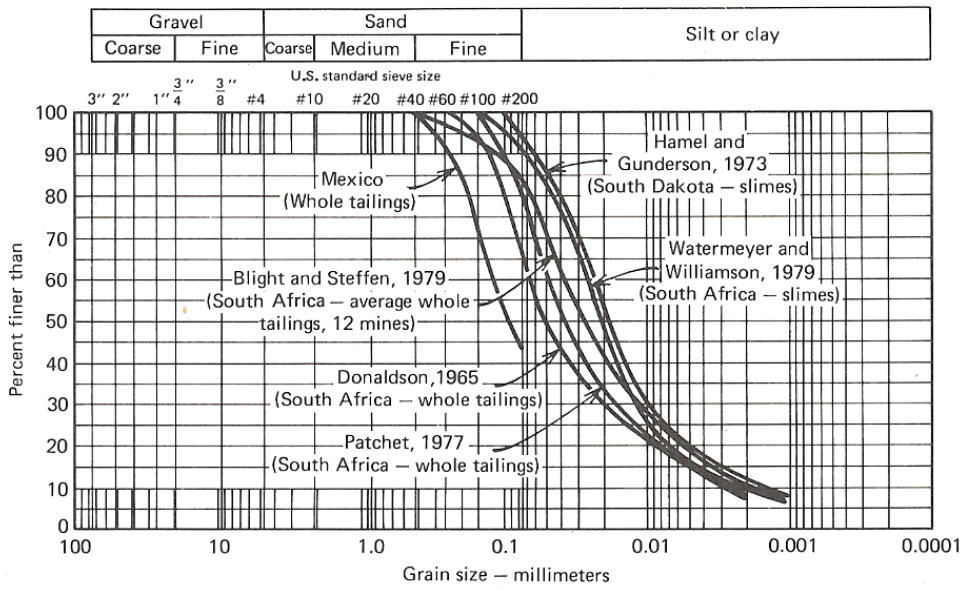

Figure 2-6: Gradations of gold-silver tailings (After Vick 1983)

2.4 ENGINEERING PROPERTIES OF TAILINGS

2.4.1. PERMEABILITY

It is quite difficult to generalize and define a permeability parameter for the whole tailings impoundment, given that it can vary more than five orders of magnitude within the same impoundment. It can take values ranging from 10^{-2} cm/sec for clean, coarse sand tailings to 10^{-7}cm/sec for well-consolidated slimes (Vick 1983). Moreover, given the layered nature of the tailings, the effects of anisotropy are highly visible in both the horizontal and vertical directions. For beach sand deposits, the literature suggests that the ratio of horizontal to vertical permeability, k_h/k_v, is in the range of 2 to 10 (Vick 1983). However, the ratio of k_h/k_v can assume values up to 100 or more for tailings deposits where discharge procedures are not well controlled, resulting in extensive sand-slime interlaying.

Given the nature of tailings discharge, i.e. spigotting or cycloning, coarser material is expected to land close to the point of discharge and finer material is expected to settle in the decant pond furthest away. This generates different

permeability zones that vary as a function of distance from the point of discharge. Kealy and Busch (Kealy and Busch 1971) suggest in Figure 2-7 a way of illustrating this variability by dividing the impoundment into three distinct zones: a zone of high permeability sands near the point of discharge, a zone of intermediate permeability, and a low permeability slimes zone. However, this remains a conceptual model that one has to further scrutinize to justify its applicability to a specific tailings impoundment study.

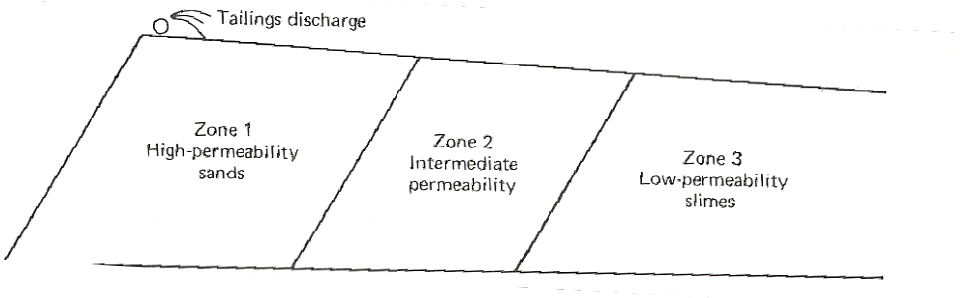

Figure 2-7: Conceptual model of permeability variation within a tailings deposit. (After Kealy and Busch, 1971)

2.4.2. COMPRESSIBILITY

Both tailings sands and slimes are more compressible than most natural soils because of their loose depositional state, high angularity, and grading characteristics (Vick 1983). The one-dimensional compression test used to evaluate compressibility of clays in conventional soil mechanics is used to determine the compressibility. The compression index, C_c, for sands is typically in the range of 0.05 and 0.10, and for slimes in the range of 0.20 to 0.30 (Vick 1983). Moreover, the density that the materials assume upon deposition for both the sands and the slimes dictates the compression level, i.e. the stiffer the initial state, the lower the compression under loading.

2.4.3. CONSOLIDATION

The primary and secondary phases define the time rate of consolidation for materials conforming to the Terzaghi theory (Lambe and Whitman 1969). As is commonly known, the rate of pore pressure dissipation under constant load is governed by the primary consolidation. For beach sand deposits, the coefficient of consolidation, c_v, ranges between 0.5 to 100 cm^2/sec thus making the primary consolidation for sand tailings occur so rapidly. As for the slimes, the c_v is reported to be in the range of 0.0001 and 0.01 cm^2/sec (Vick 1983). Moreover, the change in permeability and the rate of change in strain as a function of stress dictate the change in c_v with the void ratio.

The secondary compression of tailings, which involves particle rearrangement after the complete dissipation of pore pressure and any creep effects, is deemed to be small and relatively insignificant from a practical standpoint compared to primary consolidation (Vick 1983).

2.4.4. DRAINED SHEAR STRENGTH

The high degree of particle angularity associated with tailings gives it a higher effective friction angle, φ, than similar natural soils, typically 3 to 5° more (Vick 1983). Moreover, tailings are usually cohesion-less materials. Thus, the consolidated drained (CD) or consolidated undrained (CU) triaxial tests are suitable for measuring the tailings φ. Typical values for φ fall between 28° and 40° (Vick 1983).

2.4.5. UNDRAINED SHEAR STRENGTH

The tailings's capacity to withstand quick pore pressure build up generated by rapidly applied shear stresses is best defined by measuring its undrained shear strength, which is commonly determined by the CU triaxial tests on undisturbed and normally consolidated samples.

2.5 CONSTRUCTION METHODS

Different methods exist for constructing tailings dams: the upstream construction, the downstream construction and the centerline construction. All three of them differ from the classical water retention dams (WRDs), and share the following fundamental dam engineering principles for a tailings dam design: first, locating the dam to minimize the catchment area; second, maintaining a wide beach to control internal seepage from the free water pond; third, enhancing internal drainage by constructing pervious initial starter dykes; and fourth, exploiting pervious foundation conditions (Bjelkevik 2005). The area between the crest of the dam and the free water pond is named the beach, and it consists mainly of the coarser particles of the tailings that settle during deposition. The starter dyke is the initial dam constructed in the staged construction life cycle of the tailings impoundment from which subsequent raises of the dam are constructed (Vick 1990). Figure 2-8 illustrates the three different construction techniques.

A fundamental difference between the construction of tailings dams and WRDs is that the latter are built to their full design capacity prior to the dam's operation, whereas tailings dams are built in stages during the operation of the tailings impoundment until the end of the mine's life cycle. Moreover, one of the most crucial advantages of the staged construction is that it allows the cost of the construction to spread over the operating life of the impoundment. Furthermore, spreading the construction activities over multiple stages allows for design corrections to take place depending on the newly existing as-built conditions.

In the downstream construction technique, the staged construction progresses outward by placing embankment fill on the downstream slope of the previous raise, as illustrated in Figure 2-8a. In the centerline method, the embankment fill is placed sequentially onto the beach and onto the downstream slope of the previous raise (Figure 2-8b). Lastly, in the upstream construction method, after the construction of the starter dyke and the tailings deposition, the

beach then becomes the foundation for a second perimeter dyke, as shown in Figure 2-8c.

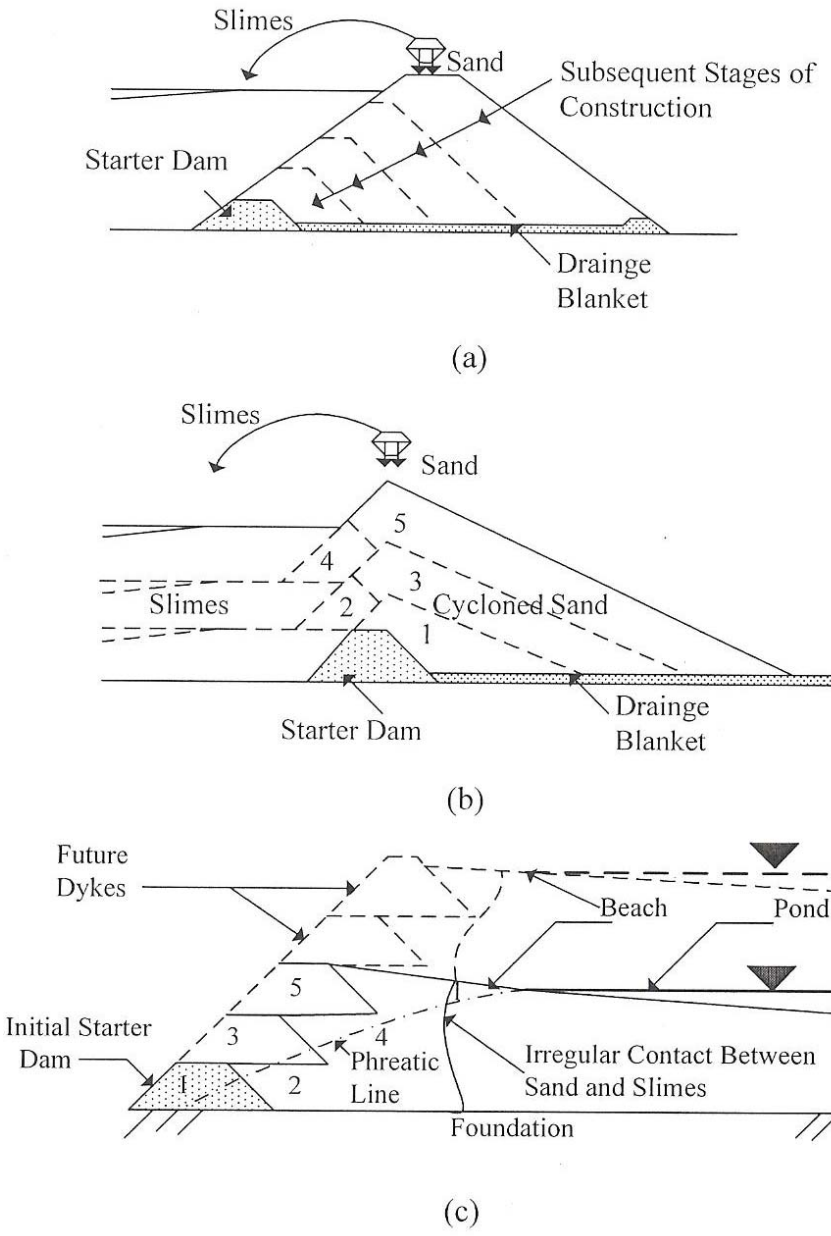

Figure 2-8: Scheme of tailings dam constructed with (a) Downstream Method (b) Centerline Method (c) Upstream Method.

The upstream staged construction technique is illustrated in Figure 2-9, and will be described in greater detail as follows. As shown in Figure 2-9a, a starter dyke is constructed typically from borrow material as no tailings are

produced yet from the milling operation. Then the spigots are placed on the perimeter of the crest where the tailings are discharged leading to the buildup of both the beach and slime zones. Prior to the impoundment reaching its initial capacity, the second dyke is constructed on the settled and consolidated tailings. This process is repeated until the design height is reached, which typically reflects the end of the operation of the mine. This sequential staged construction is illustrated in Figure 2-9a-d.

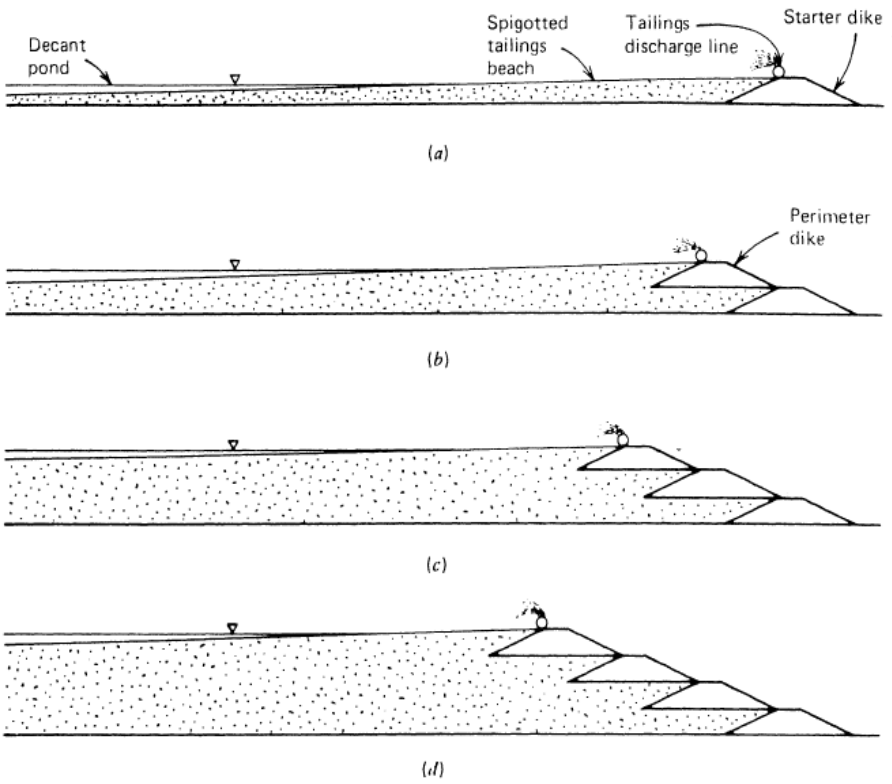

Figure 2-9: Sequential raising using the upstream construction technique (After Vick 1983).

Many advantages make the upstream construction technique the most preferable among the three techniques. First, it is considered the lowest cost option. Second, the material constituting the staged dykes could be made from the compacted cycloned tailings. Third, requiring a long beach allows for a low hydraulic gradient. Fourth, design adjustments to the downstream face of the dam during the upstream staged construction are feasible.

On the other hand it does suffer from some disadvantages, namely: controlling the hydraulic gradient, minimal water storage capacity, high susceptibility to seismic liquefaction, sensitivity to the rate of raise, and dust control in high winds.

The dam stability is highly influenced by the location of the hydraulic gradient, which is basically influenced by three parameters: first, the hydraulic conductivity of the foundation material as well as the dykes relative to the tailings in the impoundment. Second, the lateral hydraulic conductivity variations within the tailings, as well as the degree of grain size segregation. Third, the location of the decant pond's water surface relative to the crest.

The hydraulic gradient can be controlled by including design measures such as underdrains and extensive use of cyclones. The underdrains play a vital role in increasing the hydraulic gradient in the foundation, thus decreasing the chances of having an exit gradient at the downstream face of the tailings dam. Moreover, cyclones separate the incoming mill pulp into the coarse fraction and the slime. The coarse fraction will be used as building materials for the staged construction of the dykes. It is important to note that given the flat surface of the beach, a minute increase in the elevation of the decant pond will result in a large horizontal movement of the pond water towards the crest. Thus, if a high fluctuation in the water surface elevation of the decant pond is anticipated, then the designer must opt away from the upstream construction technique, as they are not suitable for storing large volumes of water where the water level may change a lot.

A rapid rate of raise will not provide the discharged slimes the necessary time to consolidate and dissipate the excess pore water pressure build-up. Thus, increased pore water pressures within the tailings will lower the effective stresses and lead to reduced shear strength, which in turn increases the impoundment's susceptibility to liquefaction.

Figure 2-10 illustrates the fundamental design difference that differentiates WRDs from the three construction techniques presented above. First, WRDs include an impervious core which is designed to retain the water. Second, a filter zone is used to capture all fine particles escaping the core. Third, a drainage layer is used to protect the downstream face of the WRD from erosion. It is worth noting that WRDs typically cost more than upstream construction dams due to the different material components making up the dam, most of which not found on site. However, in situations where WRDs have to be built and impervious materials for the core are not available on site, then thick geomembrane liners can be introduced and placed on the dam's face retaining the water as per the design guidelines for construction. Typically, the geomembranes will be sandwiched between protective layers of filter sands.

Furthermore, due to the stricter environmental regulations necessitating the recycling of the majority of the water in the tailings impoundments while also retaining the water run-off from the spring freshet and allowing for a capacity to absorb a 1:100 years flood and a 1:100 years snow storm, it has become quite common to find a hybrid model including WRDs and upstream dykes. As such, the WRD is built to its maximum full height and used to retain tailings and the water runoff from the spring freshet. Once the impoundment reaches its full capacity while respecting the free board restrictions, it is raised by constructing a smaller dyke on the beach, and so on.

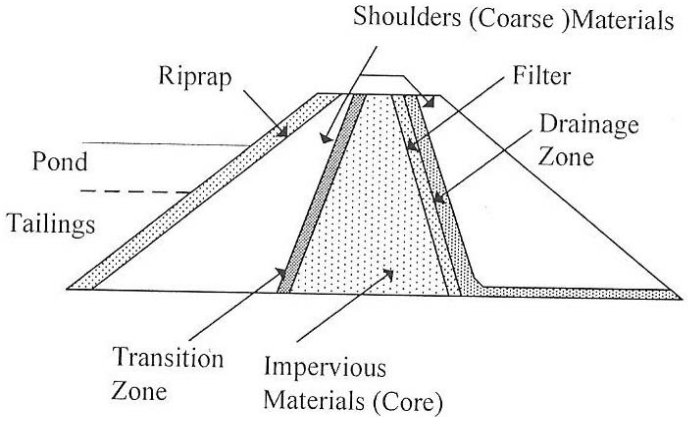

Figure 2-10: Typical section of a zoned water-retention dam used for tailings storage.

2.6 IMPOUNDMENT LAYOUTS

Different layouts currently exist in the industry, including: ring dykes, cross-valley impoundments, side-hill impoundments, and valley-bottom impoundments. Picking the impoundment layout depends heavily on the geographical and topographical location of the mine. The ring dike is among the most popular and is illustrated in the schematic of Figure 2-11. It is applicable mostly to flat terrains where natural topographic depressions are not available.

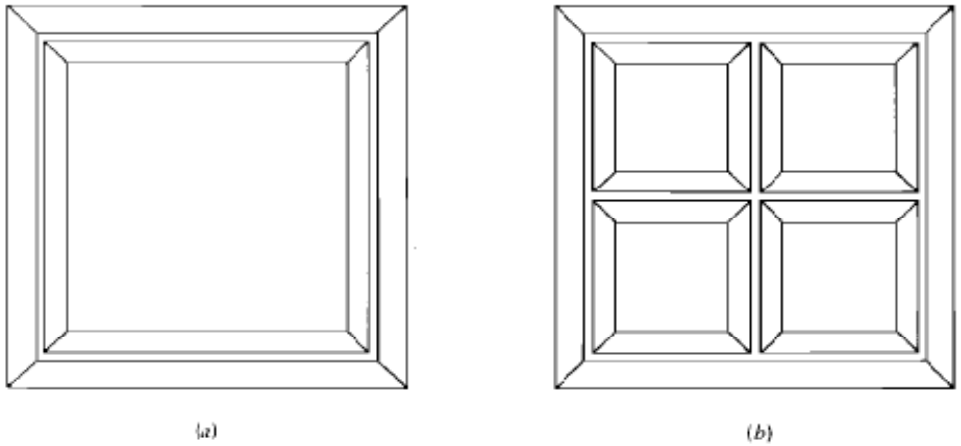

Figure 2-11: Ring dyke configuration. (a) Single impoundment. (b) Segmented impoundment (After Vick 1983).

2.7 IMPROVED CONSTRUCTION PRACTICES

Most failures of constructed tailings dams are due to one or a combination of the following reasons: steep slopes, poor phreatic surface control, earthquakes, high raising rates leading to high saturation levels, poor construction techniques that include poor material properties forming the dykes, static liquefaction and failure of the drainage system. To mitigate against the above failures, the following improvements have been presented: finger or blanket drains are being installed to lower the phreatic level, the beaches made from the cyclone sands are compacted, and building flatter slopes set at least at 3 horizontal to 1 vertical. Figure 2-12 illustrates the use of finger drains and Figure 2-13 presents the use of liners (Davies, Lighthall et al. 2002).

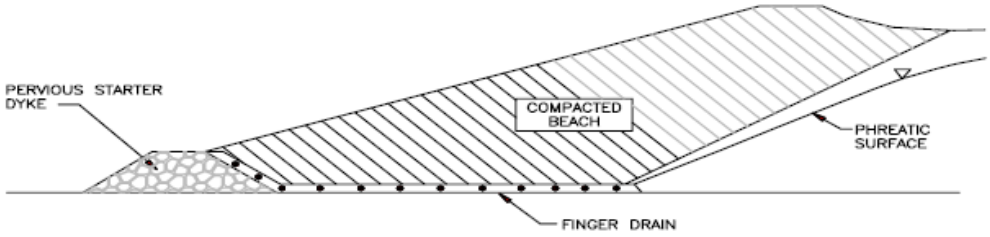

Figure 2-12: Typical section of improved upstream tailings dam design (Davies, Lighthall et al. 2002).

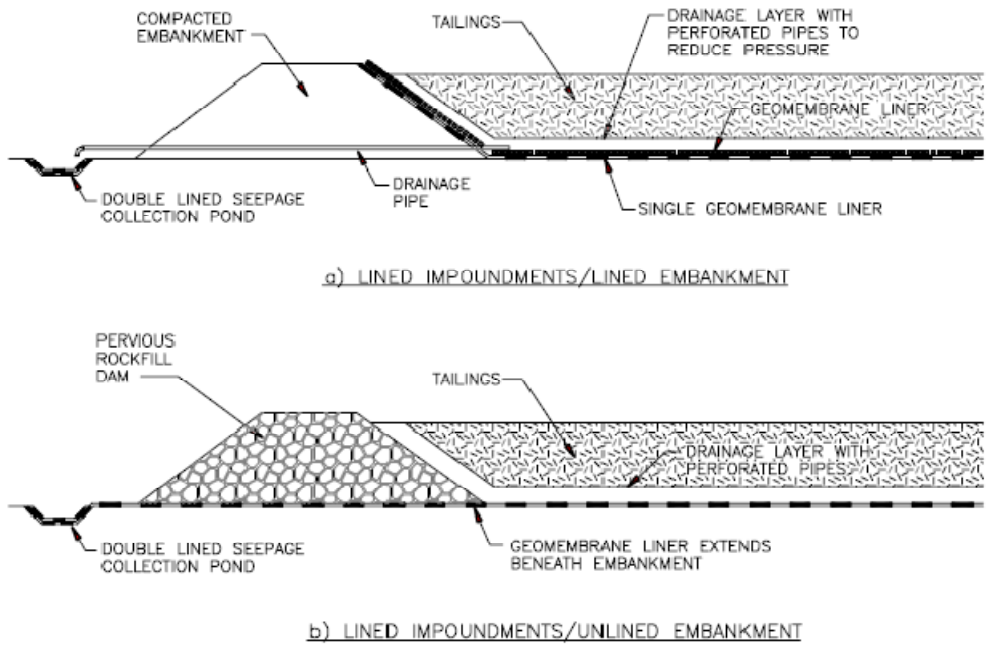

Figure 2-13: Conceptual sections of lined impoundments with underdrains (Davies, Lighthall et al. 2002).

2.8 EMERGING APPROACHES FOR TAILINGS MANAGEMENT

In recent years, a few emerging approaches have been studied with the effort to reduce the water consumption and maximize water reuse. As such, three forms of densified tailings exist: thickened tailings (solids content between 50% and 70%, mixture behaves like a viscous fluid rather than a suspended particle slurry), paste tailings (solids content between 70% and 85%), and filtered tailings

(solids content between 80% and 90%). Figure 2-14, Figure 2-15 and Figure 2-16 provide illustrations of these applications.

Figure 2-14: Slurry of tailings discharged in a tailings impoundment (Bussiere 2007).

Figure 2-15: Views showing transport placement of paste backfills (left) and hydraulic slurry (right), (Archibald)

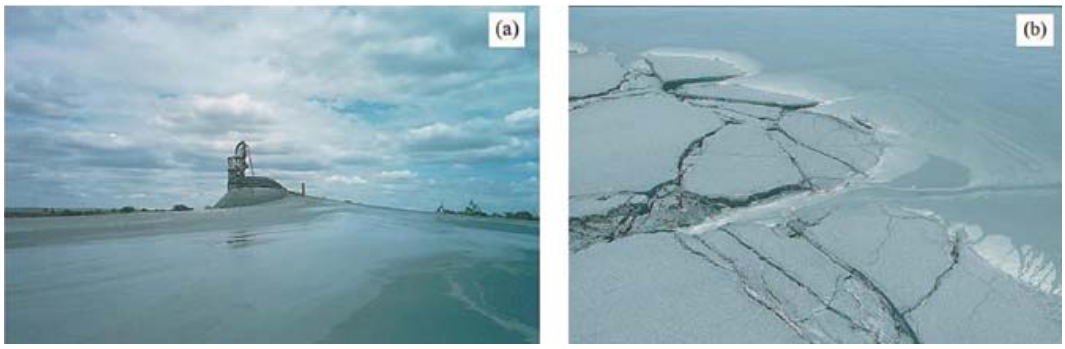

Figure 2-16: Paste tailings: (a) end-pipe discharge from one of the towers, (b) new layer of paste flowing over a desiccated sheet of paste (Bussiere 2007).

CHAPTER : 3 STABILITY ANALYSIS OF TAILINGS DAMS

3.1 CLASSICAL STABILITY ANALYSIS APPROACHES

Three categories define the stability analyses currently performed in the industry: steady state, seismic, and transient analysis.

3.1.1. STEADY STATE

A steady state analysis is usually performed on a system that is expected to perform in a constant manner under a prescribed set of loading and boundary conditions independent of time. In the steady state case, first a seepage analysis is performed to define the seepage and erosion potential, the discharge rate and to locate the phreatic surface. This is followed by developing a slope stability analysis to determine the factor of safety against slope sliding with the consideration of the effect of the predicted phreatic surface. These techniques are commonly referred to fall under the Limit Equilibrium Method (LEM) analysis. Typical slope stability analysis conducted using the LEM adopts the slices approach. The slices methodology allows the designer to account for the non-homogenous soil properties in each slice as well as the pore water pressure and vary the normal stress along the potential failure surface.

Furthermore, the steady state stability analysis is outlined in the following two analyses:

First, the effective stress analysis (ESA), which assumes a fully drained condition or a full dissipation of the pore pressure as a result of the operating loading and boundary conditions and hence the shear-induced pore pressure and the build-up generated from consolidation, is not taken into account in such an analysis. The factor of safety in this case is calculated using the effective shear

strength parameters obtained from the consolidated drained shear testing in the LEM stability computations.

Second, the Total Stress Analysis (TSA) assumes undrained conditions whereby no consolidation of the soil takes place under the applied stresses, and no pore pressure dissipation occurs. Their assumptions are due to the abrupt application of the load; e.g. rapid raising of embankment due to high tailings production rates. As a result, the undrained shear strength of the soil obtained from the undrained unconsolidated test will be used in calculating the factor of safety.

3.1.2. SEISMIC ANALYSIS

A seismic study is usually conducted in sites located in seismically active regions, where the system response is considered a function of time due to earthquake effect. Three simplified analytical approaches are considered for conducting seismic slope stability analysis.

First, the pseudo static approach assumes that a constant horizontal force equal to n_gW acts on the sliding mass that has a weight W. The parameter n_g ranges in value between 0.1 (severe) and 0.5 (catastrophic) (Seed 1979).

Second, Newmark's sliding block analogy (Newmark 1965) is considered. In this analysis, a friction block resting on an inclined plane subjected to the same accelerations as the modeled slope is considered to mimic a slope subjected to earthquake-induced acceleration. The block will displace when in each instance the sum of the static and dynamic forces exceed the shear resistance of the sliding interface. Thus, summing up the displacement resulting from each instance at which the shear resistance is exceeded during the associated ground shaking will result in calculating the total induced displacement.

Third, statistically, where the hazard is assessed through the correlations of past landslides with several influential factors. An estimated probability of failure will then be developed from the statistic analysis.

3.1.3. TRANSIENT ANALYSIS

As the name suggests the system performance changes slowly with time under transient phenomena. When investigating the stability of a tailings impoundment where the response of the system being raised is a function of time, a transient analysis should be undertaken.

The undrained strength analysis (USA) is used in this case. This analysis considers the undrained strength gain produced by the combination of the partial drainage and applied loading. Given that the time influence is reflected on the stability of the impoundment during its staged construction, it is done in combination with a consolidation analysis. For this reason the USA is considered a transient analysis in contrast with the TSA and ESA. Moreover, the dissipation of the shear-induced pore pressure is excluded in the USA as in the case of the TSA. As a result, the USA aims at predicting the available shear strength on the most realistic potential failure surface.

3.2 FAILURE MODES

Impoundments failure can be categorized under three headers: piping, which is caused predominantly by internal erosion in the embankment, localized failure that could stem from the presence of a shear band, and diffusive failure set off by liquefaction. However, it is important to differentiate between local and global failure, as it is not necessary for a local failure to lead to a whole system failure, since the soil may adjust itself kinematically by redistributing the stress states within it and further using the available strength (Saad 2008).

Furthermore, rigorous limits on the collapse conditions of a system consisting of a perfectly plastic material obeying normality (associated flow rule) can be provided by the following two bound theorems. The lower-bound theorem which states: "Collapse will not occur if any state of stress can be found that satisfies the equations of equilibrium and the traction boundary conditions and is everywhere below yield" (Davis and Selvadurai 2002); and the upper-bound theorem, which states: "Collapse must occur if, for any compatible plastic deformation, the rate of working of the external forces on the body equals or exceeds the rate of internal energy dissipation" (Davis and Selvadurai 2002). Thus, the lower-bound theorem refers to local equilibrium, whereas the upper-bound theorem refers to deformation that satisfies all displacement boundary conditions.

As such, the failure modes mentioned above can serve as an umbrella encompassing the different failure mechanisms: foundation settlement or shearing and slope instability or sliding. The factors responsible for such failure mechanisms are many, but the following shall highlight those deemed the most relevant: static liquefaction induced by excessive pore pressure build-up during the filling up of the tailings impoundment; a rapid rise in the impoundment's phreatic surface caused by flash floods; localized shearing and/or settlement of the foundation attributed to excessive loading.

In this thesis, the focus is on the overall stability of the tailings dam. Limit equilibrium is adapted in the first place to shed light on the dam's factor of safety. However, there are multiple limitations associated with the limit equilibrium method (LEM) as will be highlighted in Chapter 4. A more rigorous approach involving the hydro-mechanical coupling will be adopted in this thesis enabling the user to capture the global stability of the tailings dam.

3.3 THE NON-LINEAR TRANSIENT COUPLED ANALYSIS APPROACH USING NUMERICAL METHODS

Predicting the stress regime and its evolution in the tailings dams during their staged construction can be limited using one of the above LEMs (ESA, TSA, USA). However, the full interaction between the pore pressure evolution and the on-going deformation induced by the construction process could be accounted for with greater accuracy if a coupled deformation-based analysis is made, particularly with the use of appropriate mechanical constitutive laws.

Biot (Biot 1941) analyzed the three dimensional consolidation in porous media. This entailed understanding the coupled relationship between the deformation of the soil skeleton causing the flow and the imposed flow causing soil skeleton deformation. His derivations were based for fully saturated linear isotropic media with incompressible fluid phase governed by Darcy's flow (Biot 1941). Lately, Zienkiewicz et al. (Zienkiewicz, Chan et al. 1999) developed the coupled finite element formulations for Biot's theory.

This section of the chapter focuses on the work undertaken by Saad and Mitri (Saad and Mitri 2010; Saad and Mitri 2011) in developing a numerical modelling technique based on the deformation-pore pressure fully coupled response (Biot 1941), that can more rationally predict the pore pressure regime and thus more accurately evaluate the stability of tailings disposal facilities during their staged construction.

The response of the upstream tailings dam, when analyzed by the coupled finite element analysis, was evaluated by measuring: 1- pore pressure, 2- horizontal displacement, 3- maximum plastic shear strain, and 4- vertical settlement of the ground surface. And the evaluation of these results is assessed at the end of each construction stage.

Figure 3-1: below illustrates the components of the model built. The finite element software ABAQUS was used for this purpose (HKS 2004).

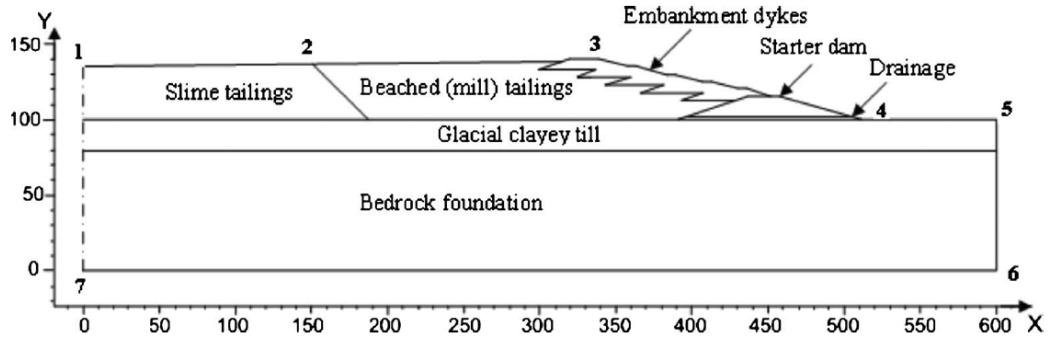

Figure 3-1:Section showing the modeled zones for the numerical simulations, dimensions are in meters (Saad and Mitri 2011).

The main features of the upstream tailings dam accounted for in their research are the following (Saad and Mitri 2010; Saad and Mitri 2011).

First, partially saturated flow under the transient state two dimensional consolidation response of the dam components under both the partially and fully saturated cases while considering:

(a) The large deformation-nature of the tailings and

(b) The fully coupled response between the fluid and the solid phases which can be expressed for a partially saturated soil mixture subjected to a static load by:

$$\sigma_{ij,\,j} + \rho\, B_i = 0 \qquad (3\text{-}1)$$

$$(k^e_{ij}\,(-\,p_{w},\,j + S\,\rho_w\,B_j)),\,i + \alpha\,\dot{\varepsilon}_{ii} + \dot{p}_w / Q = 0 \qquad (3\text{-}2)$$

Where σ_{ij} is Cauchy stress, ρ is the mass density of the soil mixture, B_i is the body force, k^e_{ij} is the effective permeability: $k^e_{ij} = k_{ij} / (\rho_w\, g)$, k_{ij} (length/time) is the permeability and g is the magnitude of the gravity acceleration, S is the degree of saturation, p_w is the pore water pressure, ρ_w is the mass density of the water in the mixture, α is Biot's effective stress parameter, ε_{ii} is the volumetric strain, Q for incompressible water and soil

skeleton is given by Q = (1/n) ($\partial p_w/\partial S$), and n is the medium porosity. The dot overlying ε_{ii} and p_w in equation (3-2) above means derivative with respect to time whereas the subscripts *i* and *j* are notations used to represent the tensors in an indicial form.

Second, the elastoplastic strain hardening/softening mechanical behavior of the soil and tailings components of the upstream tailings dam by utilizing the appropriate constitutive laws, namely:

(a) The Drucker-Prager model: this model can simulate non associative response exhibited by frictional materials of the starter dam and the compacted sandy materials of the embankment dykes zone; refer to Figure 3-2.

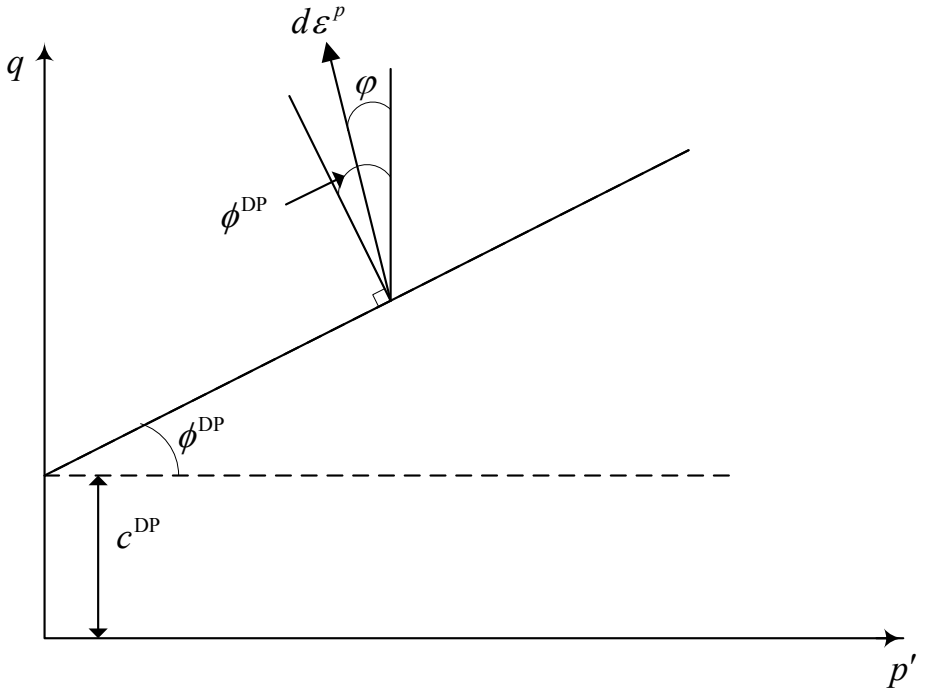

Figure 3-2: Drucker-Prager yield-failure surface is a straight line in (*p'*,*q*) plane and a circle in the II plane.

(b) Drucker-Prager Cap model: (HKS 2004) which can reflect the elastoplastic hardening/softening behavior exhibited by the frictional noncohesive materials that exist in the beach and maybe in slime zone. As

illustrated in Figure 3-3, a cap yield surface is added to the underlying Drucker-Prager failure surface (HKS 2004) to (1) bound the yield surface in the hydrostatic compression and hence provide a plastic hardening mechanism to simulate the plastic consolidation, and (2) help control the volume dilation when the material yields in shear by providing softening as a function of inelastic volume increase created when the material yields on the Drucker-Prager shear failure surface; refer to Figure 3-3.

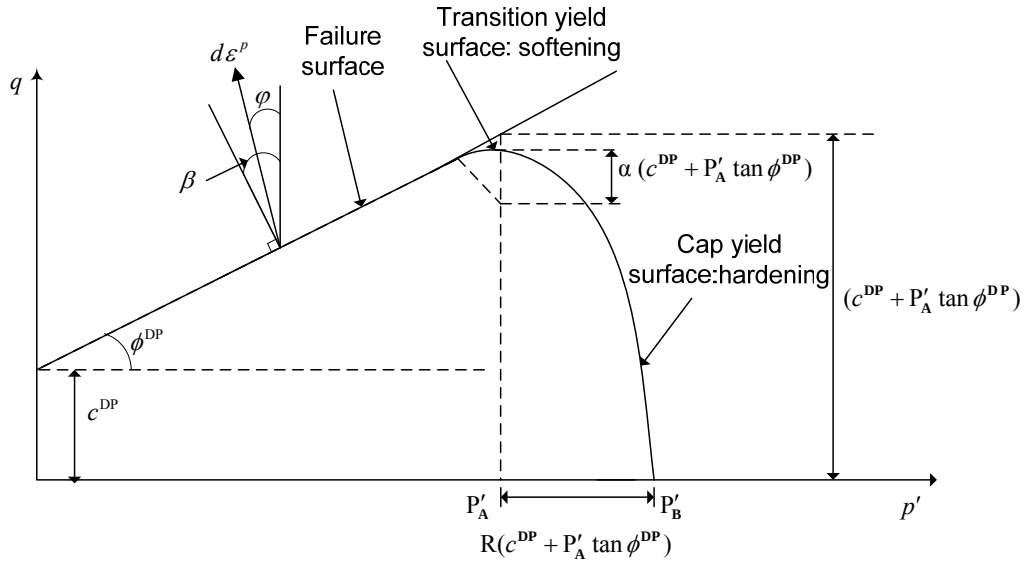

Figure 3-3: Yield and failure surfaces of the DPCM (HKS 2004)

(c) Modified Cam Clay: This model is based on the critical state theory and is used to model the response of the cohesive zones existing in the upstream tailings dam. These zones may include the tailings materials existing in the slime zone, if they possess a plasticity index (PI) > 15; refer to Figure 3-4.

In conclusion, the use of the different constitutive models should be addressed on a case by case basis depending on the nature of the numerical model being built and its sought output. In this thesis, the classical Mohr-Coulomb is adopted given that the case study concerned a water retention tailings dam; and its performance was dictated by the dam's core mechanical properties.

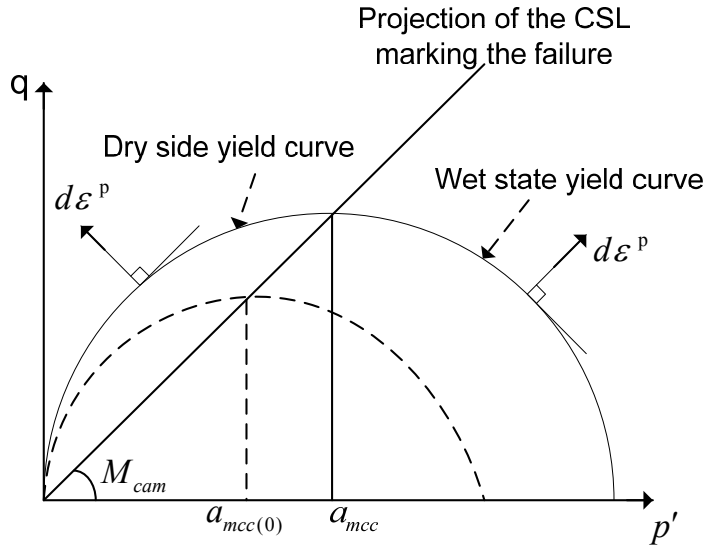

Figure 3-4: Yield and failure surfaces of the Modified Cam Clay Model

3.4 DETERMINISTIC VERSUS PROBABILISTIC APPROACHES

Engineers have always utilized deterministic approaches for their design analyses. This approach, which leads to calculating the factor of safety, does not deal with the uncertainties in the input soil parameters, as it uses one set of values for the input parameters to generate a single result for the factor of safety. Moreover, the advantage of easily interpreting the results in terms of safety factor terms has made the deterministic approach both popular and effective in many respects. However, in recent years, geotechnical engineers have recognized the need to deal with the inherent uncertainty in soil properties and its variation both spatially and temporally (e.g. due to erosion with time). In recent years, both developers and regulators have been pushing for the need of risk assessment. Bowles et al. (Bowles, Anderson et al. 1996) highlight the application of risk assessment in dam engineering, as the factor of safety, in and by itself, is no longer a sufficient measure of risk. Whitman (Whitman 2000) and Duncan (Duncan 2000) argue that it is difficult to evaluate how much safer a structure becomes as the factor of safety increases. Theoretically, a structure with a factor of safety greater than 1.0 is deemed stable, but in practice the design factor of

safety is typically taken significantly greater than unity, due to uncertainties related to material variability, measurement and model transformation uncertainty (Phoon and Kulhawy 1999). As such, mathematical frameworks that take into account the uncertainties in design parameters are developed using the probabilistic approach. Such an approach establishes a direct linkage between uncertainty in the design parameters and the probability of failure or reliability (Babu, Srivastava et al. 2007).

Babu et al. (Babu, Srivastava et al. 2007) add that most of the present literature indicates that the material parameters follow normal or lognormal distributions for input random variables (USACE 1997).

In the Thirty-Ninth Terzaghi Lecture presented at the 2003 ASCE Civil Engineering Conference and Exposition, Nashville, Tenn., John T. Christian presented the topic: "Geotechnical Engineering Reliability: How Well Do We Know What We Are Doing?". This lecture was later published in the Journal of Geotechnical and Geoenvironmental Engineering in 2004. In the abstract he notes that (*verbatim*) "Uncertainty and risk are central features of geotechnical and geological engineering. Engineers can deal with uncertainty by ignoring it, by being conservative, by using the observational method, or by quantifying it."

Christian (Christian 2004) continues by defining the current geotechnical applications of probabilistic methods and summarizes them under the following categories: 1. Design, Construction, and Operation of Offshore Platforms for Petroleum Industry, 2. Studies of Safety of Dams, Dikes, and Embankments, 3. Probabilistic Seismic Hazard Analysis, 4. Mining, 5. Nuclear Waste Repositories, and 6. Limit State Design or Load and Resistance Factor Design. It is worth noting that the section on mining included this paragraph, solely (*verbatim*): "Designs of open pit mine slopes and underground excavations have always involved tradeoffs between costs on the one hand and reliability on the other. Hoek (Hoek 1998) provides a brief exposition of reliability methods suitable for underground openings. Riela et al. (Riela, Urzua et al. 1999) and Calderon et al.

(Calderon, Catalan et al. 2003) describe the application of reliability methods for studying the stability of open pit mines."

Thus, there is a need to move beyond the different deterministic approaches discussed earlier and research the use of various probabilistic approaches in analyzing the geotechnical performance of tailings dams. The main objective of the probability approach is to determine the probability of failure or the probability of exceedance of a certain threshold. These probabilities will later be plugged into various quantitative risk assessment tools capable of generating risk matrices that will define the tailings impoundment risk level at a certain point in time.

Risk is defined as the product of probability of occurrence and consequence of an event. Typically, the probability is that of failure and the consequence is the cost of failure; refer to Figure 3-5. Prior to defining the probability of failure, one ought to define failure. Clearly, this is a subjective argument, as the probability of failure is not necessarily defined by a catastrophic failure, and as such, a system will encounter degrees of failure. For example, significant horizontal movement of the tailings dam components are often anticipated due to staged construction and seepage flow. Excessive horizontal movements, however, could lead to instability due to localized shear failure in the beach and dyke zones. Thus, it is possible to define failure by a threshold or a limit for the maximum horizontal deformation occurring in the tailings dam, beyond which the geotechnical performance of the dam is considered unsatisfactory, even though such threshold does not constitute dam failure. Moreover, a factor of safety less than one implies failure; so, calculating the probability of occurrence of a factor of safety less than one is another way of measuring the impoundment performance. Thus, in this research, the notion of defining failure by "unsatisfactory performance" will be adopted. The Corps of Engineers uses the term "*probability of unsatisfactory performance*" in recognition of the distinction between catastrophic failure and less significant performance problems (USACE 1998).

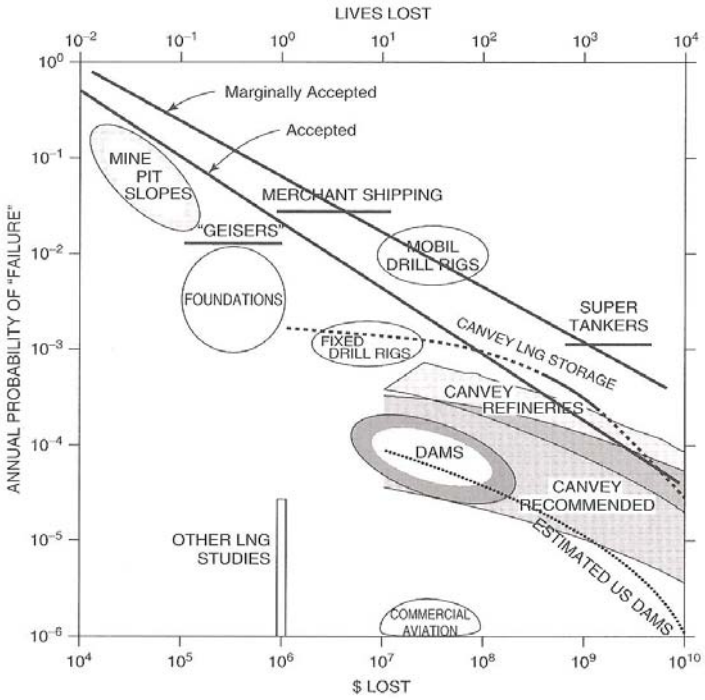

Figure 3-5: Average annual risks posed by a variety of traditional civil facilities and other large structures or projects (Baecher and Christian 2003)

3.5 UNCERTAINTY WITHIN THE SOIL STRUCTURE

Although a soil column within a single borehole consisting of multiple strata can be designated its respective soil classification, every soil sample from every borehole remains distinct in nature, resulting in the conclusion that almost all natural soils are highly variable in their properties and rarely homogenous. Elkateb et al. (Elkateb, Chalatumyk et al. 2003) define soil heterogeneity into two main categories: the first is lithological heterogeneity, described as the layering of different materials within the soil body and the second is the inherent spatial soil variability depicted in the changing soil properties from one point to another in space due to different deposition conditions and different loading histories.

In the past, designers relied on increasing the safety factors within a system as a means of combating the intrinsic uncertainty associated with the ground heterogeneity. Up to 70 % of the different geotechnical application cases considered by Morgenstern (Morgenstern 2000) resulted in poor to bad

predictions when relying solely on engineering judgment. Thus, incorporating ground heterogeneity in a rather quantitative scheme amenable to engineering design is a current need and necessity. The introduction of reliability-based design methods that combined limit equilibrium analysis with Monte Carlo simulation techniques were among the early attempts to rationally deal with the variability of soil properties in geotechnical engineering. Moreover, other effective ways to incorporate soil variability into a numerical analysis framework included implementing the stochastic finite element method.

At present, statistical design schemes using either of the above approaches or by implementing the outcome of MonteCarlo simulations into deterministic numerical analysis schemes have been recently adopted in order to incorporate correlation between soil properties.

Most geotechnical analyses are deterministic since a single average value is assumed for each parameter, as representative of the material properties in the system. Using the factor of safety and implementing local experience and engineering judgment have been deployed to address the uncertainties in these properties and their variation from one point to another in space. As a result, the selection of these design parameters contains a certain degree of uncertainty and consequently a degree of unavoidable risk.

Phoon and Kulhawy (Phoon and Kulhawy 1999) attributed those uncertainties to the following factors (*verbatim)*:

"(1) Soil inherent spatial variability due to variation in deposition conditions and stress history from one point to another in space

(2) Measurement errors due to insufficient control of testing procedure and equipment

(3) Deterministic trends in soil properties, such as the increase in soil strength with depth due to the increase in confining pressure

(4) The collection of field data over long time periods."

Christian et al. (Christian, Ladd et al. 1994) depicted the uncertainty in material properties as stemming out from two sources: data scatter, arising from the inherent spatial variability in the properties and random testing errors in their measurement; and systematic error in the estimate of the properties, which consists of systematic statistical errors due to sampling process and bias in the measurement process itself. The uncertainty in the soil properties is illustrated in Figure 3-6 below.

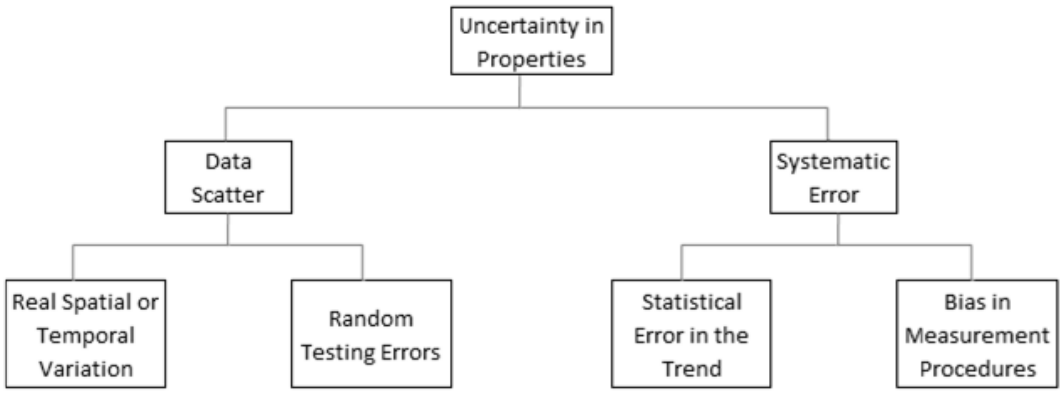

Figure 3-6: Conceptual separation of uncertainties in properties for geotechnical applications (after Christian et al. 1994).

Elements of soil spatial variability have to be identified to proceed with a stochastic analysis to assess the effect of the type of variability (Elkateb, Chalatumyk et al. 2003). Mainly, the statistical characteristics such as mean, coefficient of variation (COV), and probability distribution of the soil data, the spatial correlation structure that describes the variation of soil properties from one point to another in space and the limit of spatial continuity, beyond which no or small correlation between soil data exists.

Accounting for the variability in soil properties can be done by employing stochastic analysis techniques along with developing algorithms to estimate the soil design parameters on a probabilistic basis, thus enabling us to quantify the associated risk. These stochastic techniques have been applied to multiple geotechnical problems including: liquefaction assessment, slope stability analysis, seepage through an earth fill dam, and foundation settlement. Elkateb et al. (2003)

identified three different stochastic techniques in the literature, and they are (*verbatim*): *"first, application of reliability principles to limit equilibrium analyses, second, stochastic finite element analysis, and third, application of stochastic input soil parameters into deterministic numerical analysis (Elkateb, Chalatumyk et al. 2003)*".

3.6 PROBABILISTIC METHODS IN GEOTECHNICAL ENGINEERING

Many methods that address the application of reliability methods in geotechnical engineering have progressed over the years. The most common include: (i) the First Order Reliability Method (FORM), (ii) Point-Estimate Methods, and (iii) Monte Carlo Simulation. The following sections will provide a brief overview of these methods along with their present applications in geotechnical engineering.

3.6.1. FIRST ORDER RELIABILITY METHOD (FORM)

Baecher and Christian (2003) note that the first step in evaluating the reliability or probability of failure of a structure is to decide on specific performance criteria and the relevant input parameters, called the basic variables X_i, and the functional relationships among them corresponding to each performance criterion. Mathematically, this relationship or performance function can be described as (Haldar and Mahadevan 2000)

$$Z = g(X1, X2, \ldots, Xn) \qquad (3\text{-}3)$$

The failure surface or the limit state of interest can then be defined as $Z = 0$. This is the boundary between the safe and unsafe regions in the design parameter space, and it also represents a state beyond which a structure can no longer fulfill the function for which it was designed for. Figure 3-7 illustrates the representation of the limit state equation for a two parameter input problem, where X_1 and X_2 are the two basic random variables. Moreover, it illustrates the important role the limit state equation plays in the development of reliability

analysis methods. From Eq. (3-3) one observes that the failure occurs when Z < 0; and therefore the probability of failure is given by the integral (Haldar and Mahadevan 2000)

$$p_f = \int \ldots \int_{g()<0} f_X\left(x_1, x_2, \ldots, x_n\right) dx_1 dx_2 \ldots dx_n \qquad \textbf{(3-4)}$$

In which $f_X(x_1, x_2, \ldots, x_n)$ is the joint probability density function for the basic random variables X_1, X_2, …, X_n and the integration is performed over the failure region, i.e. g(…)<0. But, if the random variables are statistically independent, then the joint probability density function may be replaced by the product of the individual probability density functions in the integral.

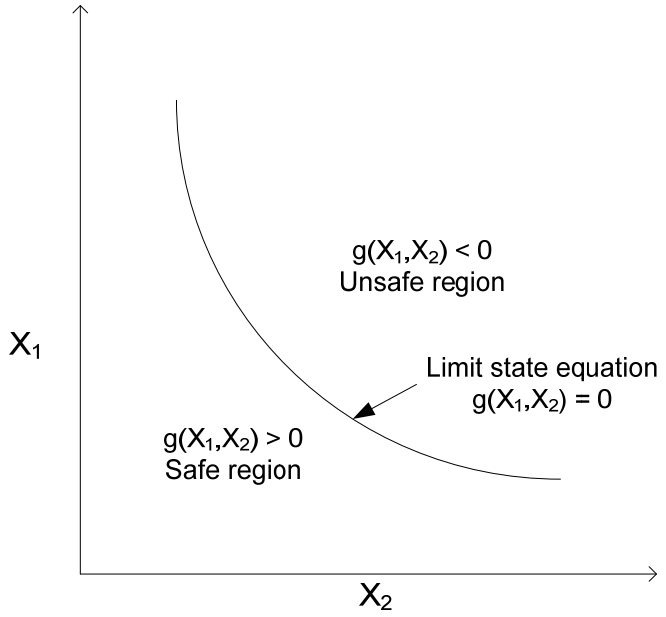

Figure 3-7 : Limit State Concept (After (Haldar and Mahadevan 2000))

The computation of p_f by Eq. (3-4) is called the full distributional approach and can be considered to be the fundamental equation of reliability analysis. However, the joint probability density function of random variables is practically impossible to obtain, and even if it was easy to attain, evaluating the multiple integral is extremely difficult (Haldar and Mahadevan 2000). Thus, one has to use analytical approximations of this integral that are simpler to compute. One such

method is the FORM. But, its application is limited to evaluating Eq. (3-4) when the limit state function is a linear function of uncorrelated normal variables or when the nonlinear limit state function is represented by a first-order (linear) approximation with equivalent normal variables. The FORM can be represented by two methods. These are the First-Order Second-Moment (FOSM) and the Advanced First-Order Second-Moment (AFOSM). In FOSM methods, the information on the distribution of random variables is ignored; however, in AFOSM methods, the distributional information is appropriately used.

3.6.1.1 First Order Second Moment (FOSM) method

The FOSM is based on a first-order Taylor series approximation of the performance function linearized at the mean values of the random variables using second-moment statistics (means and covariances) of the random variables. The original formulation was first presented by Cornell (1969) and incorporated two variables. In current applications, they commonly are the resistance (R) and the load (S) and are used to define the margin of safety

$$Z = R - S \tag{3-5}$$

Typically, the R and S are both assumed to be statistically independent normally distributed random variables, i.e. N (μ_R, σ_R) and N (μ_S, σ_S); and consequently Z can be inferred to be a random normal variable as well with $N(\mu_R - \mu_S, \sqrt{\sigma_R^2 + \sigma_S^2})$. As such, the event of failure is defined as R<S or Z<0 with the probability of failure as

$$p_f = P(Z < 0) \tag{3-6}$$

or

$$p_f = \Phi\left[\frac{0 - (\mu_R - \mu_S)}{\sqrt{\sigma_R^2 + \sigma_S^2}}\right] \tag{3-7}$$

or

$$p_f = 1 - \Phi\left[\frac{\mu_R - \mu_S}{\sqrt{\sigma_R^2 + \sigma_S^2}}\right] \tag{3-8}$$

Where Φ is the cumulative distribution function (CDF) of the standard normal variate. Eq. (3-8) can then be rewritten as

$$\mu_R \geq \mu_S + \Phi^{-1}\left(1 - p_f\right)\sqrt{\sigma_R^2 + \sigma_S^2} \tag{3-9}$$

And if one considers $\beta = \Phi^{-1}(1 - p_f)$ then Eq. 3-9 can be rewritten as

$$\mu_R = \mu_S + \beta\sqrt{\sigma_R^2 + \sigma_S^2} \tag{3-10}$$

And consequently

$$\beta = \Phi^{-1}\left(1 - p_f\right) = \frac{\mu_R - \mu_S}{\sqrt{\sigma_R^2 + \sigma_S^2}} = \frac{\mu_Z}{\sigma_Z} \tag{3-11}$$

Therefore, the probability of failure in terms of the safety index (β) can be obtained by rewriting Eq. (3-8)

$$p_f = \Phi(-\beta) = 1 - \Phi\left(\beta\right) \tag{3-12}$$

However, geotechnical engineers are more accustomed to working with the factor of safety F, defined as

$$F = R / S \tag{3-13}$$

The calculations of the reliability index are more difficult when expressed in terms of their factor of safety because F is the ratio of two uncertain quantities while Z is their difference. In this situation, the variables R and S are assumed to be statistically independent lognormal random variables, i.e. $LN(\lambda_R, \zeta_R)$ **and** $LN(\lambda_S, \zeta_S)$. This restricts the variables to having positive values which is a favorable, but not binding, representation of many engineering parameters that physically cannot take a negative value. Hence, the logarithm of

their ratio becomes the difference between their logarithms. As such the performance function can be transformed to

$$\ln F = Z = \ln R - \ln S \tag{3-14}$$

Furthermore, the failure event can be defined at F<1.0 or Z<0.0. Since R and S are lognormal then *ln R* and *ln S* are normal, and consequently $Z \sim N(\lambda_R - \lambda_S, \sqrt{\zeta_R^2 + \zeta_S^2})$ with the probability of failure defined as

$$p_f = 1 - \Phi\left[\frac{\lambda_R - \lambda_S}{\sqrt{\zeta_R^2 + \zeta_S^2}}\right] \tag{3-15}$$

The formulations presented above may be generalized for many random variables, denoted by a vector X. The Taylor series expansion of the performance function, Eq. 3-3, about the mean value gives

$$Z = g(\mu_X) + \sum_{i=1}^{n} \frac{\partial g}{\partial X_i}\left(X_i - \mu_{X_i}\right) + \frac{1}{2}\sum_{i=1}^{n}\sum_{j=1}^{n} \frac{\partial^2 g}{\partial X_i \partial X_j}\left(X_i - \mu_{X_i}\right)\left(X_j - \mu_{X_j}\right) + \ldots \tag{3-16}$$

Where the derivatives are evaluated at the mean values of the random variables (X_1, X_2, …, X_n), and μ_{Xi} is the mean value of X_i. Truncating the series at the linear terms allows us to obtain the first order approximate mean and variance of Z as

$$\mu_Z \approx g\left(\mu_{X_1}, \mu_{X_2}, \ldots, \mu_{X_n}\right) \tag{3-17}$$

And

$$\sigma_Z^2 \approx \sum_{i=1}^{n}\sum_{j=1}^{n} \frac{\partial g}{\partial X_i}\frac{\partial g}{\partial X_j} Cov\left(X_i, X_j\right) \tag{3-18}$$

Where $Cov(X_i, X_j)$ is the covariance of X_i and X_j.

If the variables are uncorrelated, then the variance is simply

$$\sigma_Z^2 \approx \sum_{i=1}^{n}\left(\frac{\partial g}{\partial X_i}\right)^2 Var\left(X_i\right) \tag{3-19}$$

As such, the safety or reliability index can be calculated by taking the ratio of the mean and standard deviation of Z, where the performance function is linearized at the mean values of the random variables, reflecting the concept behind the FOSM method. However, in most cases it is not likely that all the variables are statistically independent normals or lognormals, nor is it likely that the performance function is a simple additive or multiplicative function of these variables. Consequently, the safety index cannot be directly related to the probability of failure; nevertheless, it does provide a rough idea of the level of reliability in the design. Moreover, as was mentioned earlier the FOSM method does not use the distribution information about the variables when it is available. The performance function g( ) is linearized at the mean values of the X_i variables; as such, errors will arise by neglecting higher order terms when g( ) is nonlinear. The AFOSM solves some of the FOSM's shortcomings as elaborated below.

3.6.1.2 Advanced First Order Second Moment (AFOSM):

Hasofer and Lind (1974) addressed the concerns with the FOSM method mentioned above by proposing a different definition of the reliability index that is based on a geometric interpretation. The Hasofer-Lind (H-L) method, which is applicable for normal random variables, starts first by reducing the variables as

$$X_i' = \frac{X_i - \mu X_i}{\sigma X_i} \; for\left(i = 1,2,...,n\right) \tag{3-20}$$

Where X_i' is a random variable with zero mean and unit standard deviation. Eq. (3-20) is used to transform the original limit state g(X) = 0 to the reduced limit state, g(X') = 0. As illustrated in Figure 3-8 the safety index β_{HL} in the transformed or reduced coordinate system is defined as the minimum distance from the origin of the axes in the reduced coordinate system to the design point or checking point on the limit state surface (failure surface) and can be expressed as

$$\beta_{HL} = \sqrt{\left(x'^{*}\right)^{T}\left(x'^{*}\right)} \tag{3-21}$$

Where x' is the vector of the x_i's in the original coordinate system and x'* is the vector in the reduced coordinate system (Haldar and Mahadevan 2000). The superscript T indicates the transpose of a matrix or vector.

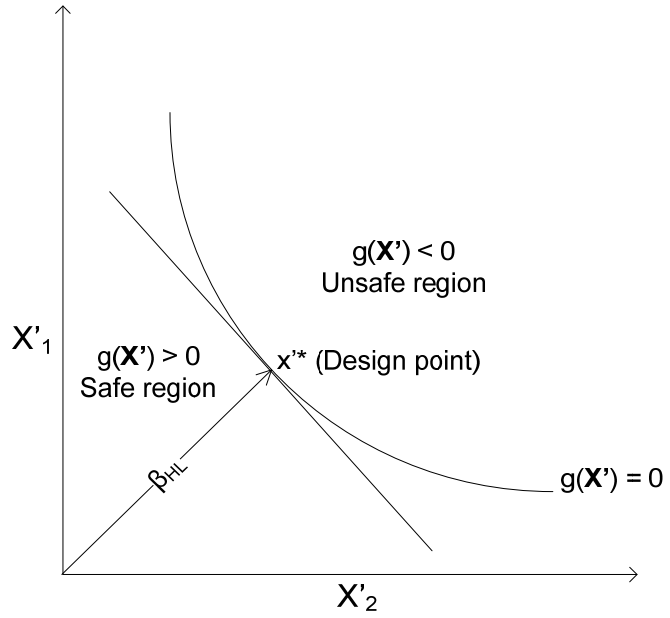

Figure 3-8: Hasofer-Lind Reliability Index: Nonlinear Performance Function (After (Haldar and Mahadevan 2000)

For the linear limit state equation in two variables

$$Z = R - S \tag{3-22}$$

and

$$R' = \frac{R - \mu_R}{\sigma_R} \tag{3-23}$$

and

$$S' = \frac{S - \mu_S}{\sigma_S} \tag{3-24}$$

And finally

$$\beta_{HL} = \frac{\mu_R - \mu_S}{\sqrt{\sigma_R^2 + \sigma_S^2}} \tag{3-25}$$

It is the same as the reliability index defined by FOSM where both R and S are normal variables, but obtained differently based on geometry, and as such $p_f = \Phi(-\beta_{HL})$.

From Figure 3-8, it is also evident that if the failure line or the limit state line is closer to the origin in the reduced coordinate system, then the failure region is larger and smaller if it is farther away. The same conclusion applies to the design point x'*. Therefore the point of minimum distance from the origin to the limit surface, x'*, represents the worst combination of the stochastic variables and thus named the design point or the most probable point of failure.

As such, for nonlinear limit states, the computation of the minimum distance becomes an optimization problem

Minimize

$$D = \sqrt{(x')^T (x')} \tag{3-26}$$

Subject to the constraint

$$g(x) = g(x') = 0 \tag{3-27}$$

Using the method of Lagrange multipliers, the minimum distance is calculated to be (Haldar and Mahadevan 2000)

$$\beta_{HL} = -\frac{\sum_{i=1}^{n} x_i'^{*} \left(\frac{\partial g}{\partial X_i'} \right)^{*}}{\sqrt{\sum_{i=1}^{n} \left(\frac{\partial g}{\partial X_i'} \right)^{2*}}} \tag{3-28}$$

Where $\left(\frac{\partial g}{\partial X_i'}\right)^*$ is the ith partial derivative evaluated at the design point with coordinates $\left(x_1'^*, x_2'^*, ..., x_n'^*\right)$. And the design point in the reduced coordinates is

$$x_i'^* = -\alpha_i \beta_{HL} \left(i = 1,2,...,n\right) \tag{3-29}$$

Where

$$\alpha_i = -\frac{\left(\frac{\partial g}{\partial X_i'}\right)^*}{\sqrt{\sum_{i=1}^{n}\left(\frac{\partial g}{\partial X_i'}\right)^{2*}}} \tag{3-30}$$

Are the direction cosines along the coordinate axes X_i'. The design point in the space of the original coordinates is then calculated to be

$$x_i^* = \mu X_i - \alpha_i \sigma_{X_i} \beta_{HL} \tag{3-31}$$

The analysis outlined above assumes the random variables to be uncorrelated. Several modifications to the FORM are available in the literature to include correlated random variables.

In terms of geotechnical applications, the FORM methods have been used to study the effects of spatial variability of soil properties on slope stability (Cho 2007); as well as conducting two and three-dimensional reliability analysis of earth slopes (Auvinet and González 2000) among other applications presented by (Christian, Ladd et al. 1994); (Fenton and Griffiths 2005); (Babu, Srivastava et al. 2006); (El-Ramly, Morgenstern et al. 2002); (Duncan 2000); (Hsu, Lin et al. 2007).

3.6.2. POINT ESTIMATE METHOD (PEM):

Rosenblueth (1975) published a method for numerically approximating the moments of functions of random variables. The method provides approximations for the low-order moments for the dependent variable Y starting from the low-order moments of the independent variable X. For the function Y=g(x), the random variable X could represent soil properties, geometric parameters and loading parameters and Y could be a factor of safety, settlement or flow, among other outputs.

Rosenblueth presented three cases from his 1975 paper (Rosenblueth 1975), namely (Baecher and Christian 2003) *verbatim*: *"(1) when Y is a function of one variable X, whose mean, variance and skewness are known; (2) when Y is a function of one variable X whose distribution is symmetrical and approximately Gaussian; and (3) when Y is a function of n variables X_1, X_2,..., X_n, whose distributions are symmetric and which may be correlated*". In most cases the calculations are made at two points, and Rosenblueth uses the following notation:

$$E\left[Y^m\right] \approx P_+ y_+^m + P_- y_-^m \tag{3-32}$$

Where:

Y is a deterministic function of X, Y = g(X),

$E[Y^m]$ is the expected value of Y raised to the power m,

y+ is the value of Y evaluated at a point x+, which is greater than the mean, μ_x,

y- is the value of Y evaluated at a point x-, which is less than μ_x, and

P+, P- are weights;

and the problem then reduces to finding the appropriate values of x+, x-, P+, and P-.

3.6.2.1 The First Case:

Rosenblueth gives four conditions that must be satisfied for the low-order moments of X to be modeled accurately:

$P_+ + P_- = 1$ (3-33)

$P_+x_+ + P_-x_- = \mu_x$ (3-34)

$$P_+\left(x_+ - \mu_x\right)^2 + P_-\left(x_- - \mu_x\right)^2 = \sigma_x^2 \quad (3\text{-}35)$$

$$P_+\left(x_+ - \mu_x\right)^3 + P_-\left(x_- - \mu_x\right)^3 = \upsilon_x\sigma_x^3 \quad (3\text{-}36)$$

where σ_x is the standard deviation of X and υ_x is the skewness $\left(\upsilon_x = \mu_X^3/\sigma_X^3\right)$

Rosenblueth (1981) (Rosenblueth 1981) presented a solution to the above set of equations.

$$x_+ = \mu_x + \left[\frac{\upsilon_x}{2} + \sqrt{1+\left(\frac{\upsilon_x}{2}\right)^2}\right]\sigma_x \quad (3\text{-}37)$$

$$x_- = \mu_x + \left[\frac{\upsilon_x}{2} - \sqrt{1+\left(\frac{\upsilon_x}{2}\right)^2}\right]\sigma_x \quad (3\text{-}38)$$

$$P_+ = \frac{1}{2}\left[1 - \frac{\upsilon_x}{2}\frac{1}{\sqrt{1+\left(\upsilon_x/2\right)^2}}\right] \quad (3\text{-}39)$$

$$P_- = 1 - P_+ \quad (3\text{-}40)$$

The above set of equations are further simplified when the skewness is zero or negligible. The distribution of X is then symmetric and

$$P_+ = P_- = \frac{1}{2}; \quad x_+ = \mu_x + \sigma_x; \quad x_- = \mu_x - \sigma_x \quad (3\text{-}41)$$

3.6.2.2 The Second Case:

Rosenblueth proposed that x can be estimated at more than two points if X is symmetric and approximately Gaussian. A one example would be a three point estimate using a central point ($x=\mu_x$) and two points x_+ and x_- symmetrically distributed about the mean. As such, we get

$$2P_+ + P = 1 \tag{3-42}$$

$$2P_+ (x_+ - \mu_x)^2 = \sigma_x^2 \tag{3-43}$$

$$2P_+ (x_+ - \mu_x)^4 = 3\sigma_x^4 \tag{3-44}$$

The solution to the above set of equations is

$$P = \frac{2}{3}, P_+ = P_- = \frac{1}{6} \tag{3-45}$$

$$x_\pm = \mu_x \pm \sqrt{3\sigma_x} \tag{3-46}$$

and consequently

$$E[Y^m] \approx P_-(y_-)^m + P(y_\mu)^m + P_+(y_+)^m \tag{3-47}$$

where y_μ is the value of Y evaluated at $x = \mu_x$.

3.6.2.3 The Third Case:

It is considered to be the most popular application of the Rosenblueth method where Y is a function of n variables whose skewness is zero but which may be correlated. The procedure chooses 2^n points selected so that the value of each variable is one standard deviation above or below its mean (Baecher and Christian 2003). Thus if there exists two variables X_1 and X_2, then the four points will be $(\mu_{X_1} + \sigma_{X_1}, \mu_{X_2} + \sigma_{X_2}), (\mu_{X_1} + \sigma_{X_1}, \mu_{X_2} - \sigma_{X_2}), (\mu_{X_1} - \sigma_{X_1}, \mu_{X_2} + \sigma_{X_2})$ and $(\mu_{X_1} - \sigma_{X_1}, \mu_{X_2} - \sigma_{X_2})$. In the event that the variables are not correlated then the function Y is evaluated at each of the four points, and the weight for each point is

0.25. If they are correlated with a correlation coefficient ρ then the weights will change as illustrated in Figure 3-9 (Christian and Baecher 1999).

When Y is a function of three variables, X_1, X_2, and X_3, then there are eight points in total, which are located at each combination one standard deviation above or below the mean of all the variables. As such, Rosenblueth defined a convention for the weight's nomenclature where the first sign refers to X_1 and the second to X_2 and so on and so forth; also if the point is at $\mu_{x_i} + \sigma_{x_i}$, then the sign is positive, otherwise it's negative; and finally ρ_{12} represents the correlation coefficient between X_1 and X_2 and so on.

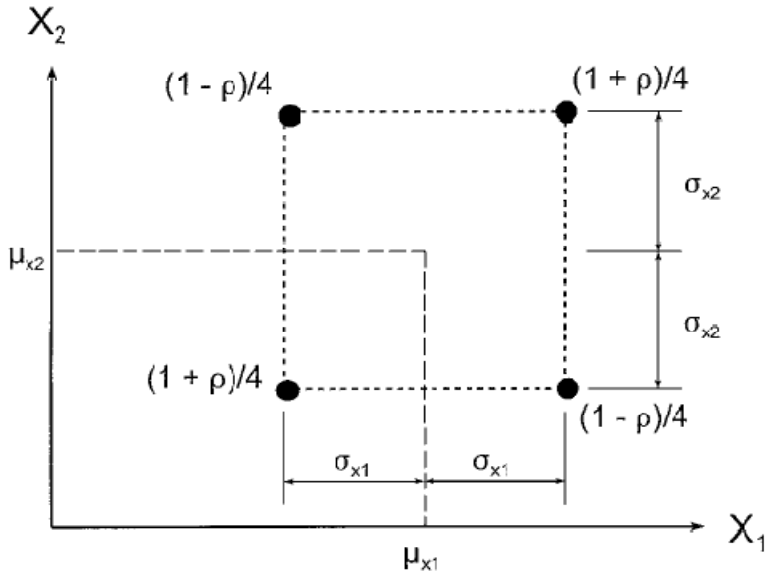

Figure 3-9: Rosenblueth's points and weights for two variables, correlated or uncorrelated (After (Christian and Baecher 1999)).

The convention is presented in Figure 3-10 and represented in the following set of equations

$$P_{+++} = P_{---} = \frac{1}{8}\left(1 + \rho_{12} + \rho_{23} + \rho_{31}\right) \tag{3-48}$$

$$P_{++-} = P_{--+} = \frac{1}{8}\left(1 + \rho_{12} - \rho_{23} - \rho_{31}\right) \tag{3-49}$$

$$P_{+-+} = P_{-+-} = \frac{1}{8}\left(1 - \rho_{12} - \rho_{23} + \rho_{31}\right) \tag{3-50}$$

$$P_{+--} = P_{-++} = \frac{1}{8}\left(1 - \rho_{12} + \rho_{23} - \rho_{31}\right) \tag{3-51}$$

In conclusion, for n variables, then 2^n points are chosen to include all possible combinations with each variable one standard deviation above or below the mean (Baecher and Christian 2003); and the generalization equation for the weights results in

$$P_{(S1S2...Sn)} = \frac{1}{2^n}\left[1 + \sum_{i=1}^{n-1}\sum_{j=i=1}^{n}\left(s_i\right)\left(s_j\right)\rho_{ij}\right] \tag{3-52}$$

and

$$E\left[Y^m\right] \approx \sum P_i\left(y_i\right)^m \tag{3-53}$$

where s_i is +1 when the value of the i^{th} variable is one standard deviation above the mean and -1 when the value is one standard deviation below the mean.

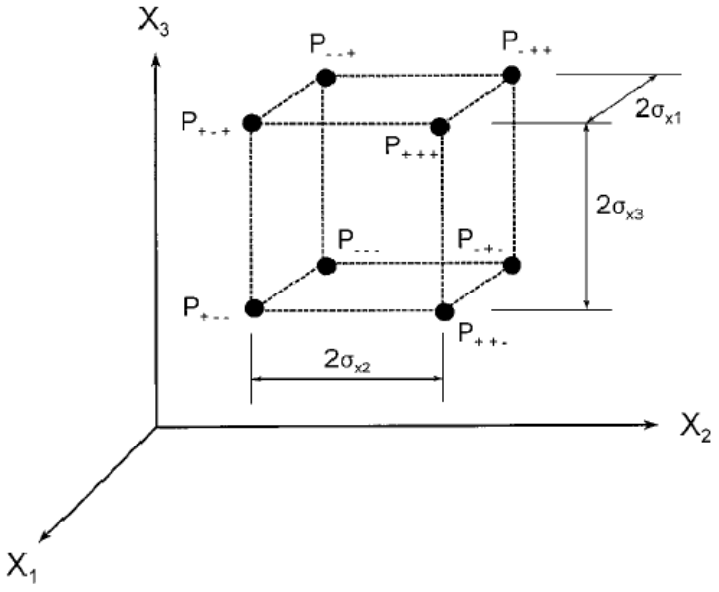

Figure 3-10: Rosenblueth's points and weights for three variables, correlated or uncorrelated (After (Christian and Baecher 1999))

The PEM remains an appealing choice given that it is less computationally expensive than other probabilistic methods. One application is illustrated in Hammah et al. (2009), where the PEM was used to perform a probabilistic slope analysis study using the finite element method by including two random variables, the cohesion and friction angles (Hammah, Yacoub et al. 2009).

3.6.3. MONTE CARLO SIMULATION (MCS):

The name "Monte Carlo" has no significance, except that it was used first by von Neumann during World War II as a code word for nuclear weapons work at the Los Alamos National Laboratory in New Mexico; but most it is associated with a place where gamblers take risk (Haldar and Mahadevan 2000) *verbatim*. Haldar and Mahadevan (2000) have illustrated the six essential elements forming the Monte Carlo simulation technique as follows (*verbatim*): *"(1) defining the problem in terms of all random variables, (2) quantifying the probabilistic characteristics of all the random variables in terms if their PDFs or PMFs and the corresponding parameters, (3) generating the values of these random variables, (4) evaluating the problem deterministically for each set of realizations of all the random variables, that is, numerical experimentation, (5) extracting probabilistic information from N such realizations and (6) determining the accuracy and efficiency of the simulation. Note that the Monte Carlo simulation technique can be used for both correlated and uncorrelated random variables"*.

As mentioned above, a random number generator will be used to generate N random numbers for each of the random variables in the problem, thus creating N realizations and N output points that can be used to calculate the sample statistics, the histogram, the frequency diagram, the Probability Density Function (PDF) and the corresponding Cumulative Density Function (CDF), and ultimately the probability of failure considering various performance criteria.

The accuracy of the MC simulation technique increases with the increase in the number of simulations N. However this can be computationally expensive,

and as such the analyst's task is to increase the efficiency of the simulation by expediting the execution and minimizing the computer storage requirements (Haldar and Mahadevan 2000). For this purpose, several Variance Reduction Techniques (VRTs) were developed that can increase efficiency by reducing the variance or the error of the estimated output variable without disturbing the expected or mean value and without increasing the sample size (Haldar and Mahadevan 2000). The VRTs are commonly grouped according to their purpose, mainly: sampling methods, correlation methods, and special methods. The commonly used sampling methods are the importance sampling, stratified sampling, adaptive sampling, and conditional expectation (Haldar and Mahadevan 2000). The most frequently used correlation-based VRT is the antithetic variates, which can be further combined with the conditional expectation as one of the special methods.

Efficient modern computers have made the Monte Carlo method both computationally plausible and affordable, especially after the improvements recently introduced to the method using VRT(Fishman 1995), as previously discussed. However, this remains to be a subjective statement as the complexity of the problem being solved will dictate how computationally exhaustive the process may be.

Furthermore, a spin-off on the use of MCS for geotechnical applications has been the development of the Random Monte-Carlo Simulation (RMCS). The fundamental difference between RMCS and MCS is that the former deals with spatial uncertainty at the local level, whereas the latter addresses uncertainty at the global level. Griffiths and Fenton (Griffiths and Fenton 2004) applied the Random Finite Element Method (RFEM), which includes spatially random soil profiles, on slope stability analysis problems. Furthermore, Griffiths and Fenton took their newly developed RFEM tool and applied it to different geotechnical applications including: settlements of shallow foundations, bearing capacity of shallow foundations, seepage and retaining walls (Griffiths and Fenton 1998; Griffiths, Fenton et al. 2002; Griffiths, Fenton et al. 2002; Griffiths and Fenton 2004;

Griffiths, Fenton et al. 2006; Griffiths and Fenton 2007). However, the RFEM's theoretical complexity makes the method unappealing for industrial practitioners. Moreover, the RFEM was first developed to incorporate a single soil layer. Currently, researchers are working on extending the tool to incorporate additional soil layers.

CHAPTER : 4 CASE STUDY AND LIMIT EQUILIBRIUM ANALYSIS

4.1 OVERVIEW

For the purpose of this research thesis a case study of a new tailings impoundment project is adopted. The name, location and design for construction plans of the site will be omitted from this thesis for reasons of confidentiality agreement.

The impoundment is an extension of an existing facility and is designed for a production rate of 7000 tons/day, which translate to over 2 million metric tonnes of annual tailings management. The service life of the extension impoundment is ten years or more.

In addition to the expansion in the mining operations, water management has been an issue for the owners. Effluents not meeting the physical and chemical environmental requirements, as prescribed by Direcive 019 in Quebec's provincial code, cannot be discharged to the environment. And complying to the toxicity limits has proven to be difficult given that the technology for large scale treatments of target chemicals was still under development. As such, the owners chose to retain the effluent while maintaining the production levels until the toxicity issue was resolved. A biological treatment plant was installed and improved over the years. Figure 4-1 illustrates the location of the extension project with reference to the existing impoundment.

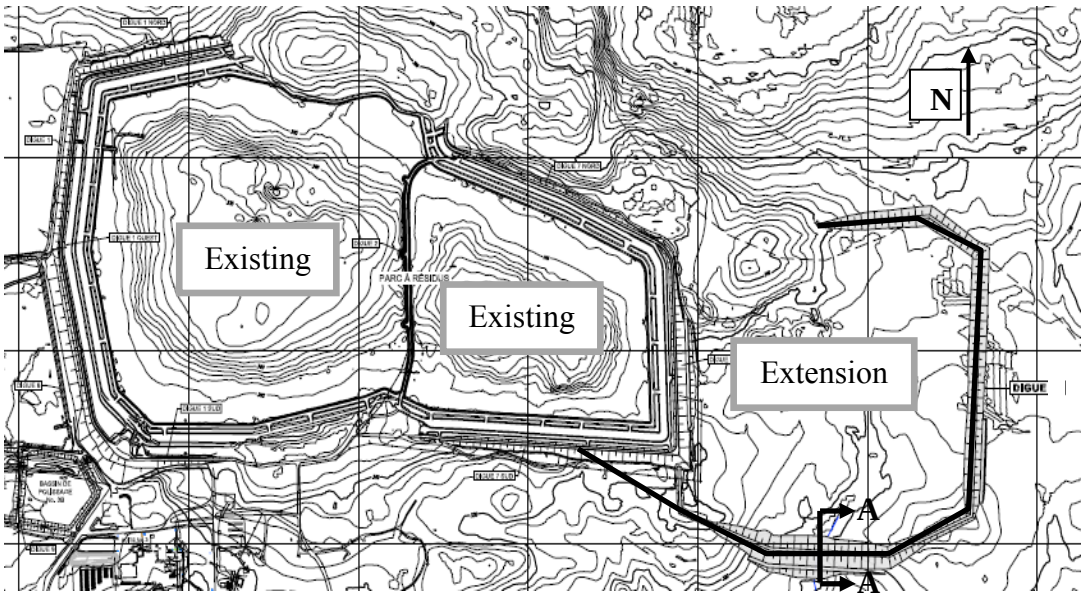

Figure 4-1: Tailings impoundment expansion site layout. Cross-section A-A refers to area of study.

4.2 DAM DESIGN

Given the fact that the new tailings expansion site will have the dual functionality of retaining both tailings and large water volumes with elevated toxicity, it was designed to be a water retention tailings dam with an impermeable core. The dam is widest and highest and hence most vulnerable to instability at the cross-section A-A highlighted in Figure 4-1, and as a result, this section will be the main focus of the study in this thesis. The ground surface elevation in this section is at 316m above mean sea level. The crest of the dam is designed to be at 332m. Once the tailings impoundment fills up to an elevation of 330m (respecting a 2 m free board), an upstream dyke will be built to increase the capacity of the impoundments and tailings will continue to be discharged behind the new dyke up to an elevation of 332m.

The dam crest is designed to be 8m wide and the dam's core at section A-A is designed to be keyed into the bedrock. The slopes both upstream and downstream of the dam will be 2.5H:1V. The downstream side of the dam

includes a toe to increase stability. The details of cross-section A-A will be presented in subsequent sections.

The tailings grain size distribution for the mine's tailings impoundment is presented in Figure 4-2.

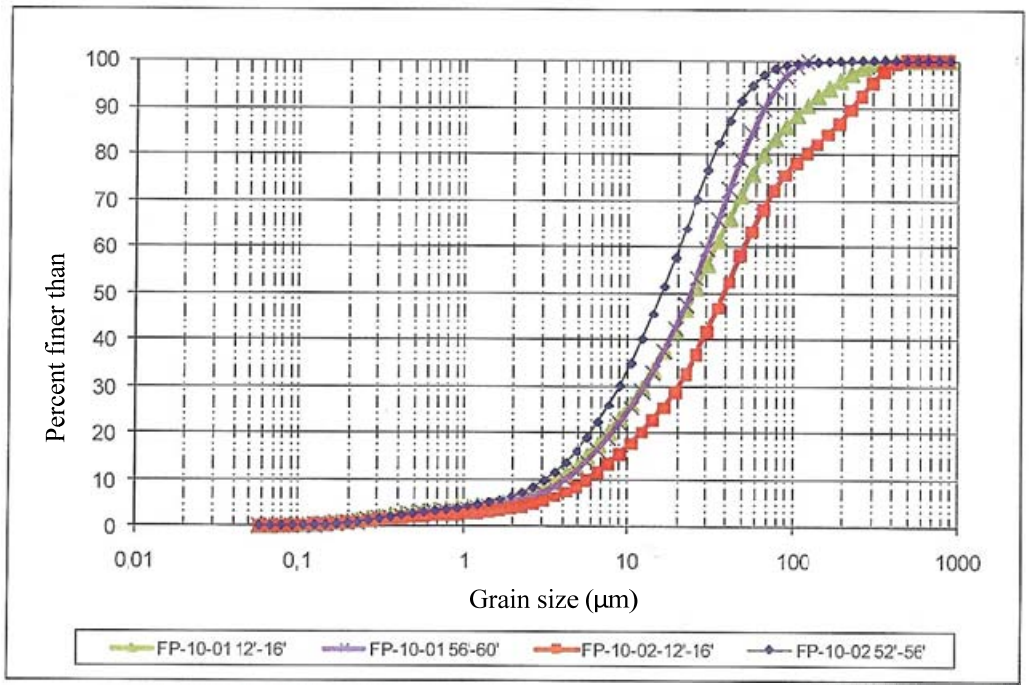

Figure 4-2: Cumulative grain size distribution from four samples

The geotechnical properties of the foundation and dam component materials provided by the owner are listed in Table 4-1.

Table 4-1: Tailings impoundment material properties

Material	Properties				
	γ (kN/m^3)	c (kPa)	Ø (°)	k (m/s)	n
Core	21.5	12	28	1E-07	0.25
Borrow	18.5	0	35	1E-3	0.3
Tailings	16	0	28	1E-6	0.4
Silty Clay	16.5	50	0	1E-7	0.2
Bedrock	27	6000	42	1E-8	0.1

γ=unit weight; c=cohesion; Φ=angle of friction; k=permeability; n=porosity

4.3 LIMIT EQUILIBRIUM METHOD (LEM) APPROACH

In this section, the classical geotechnical approach of using the LEM was used to analyze the stability of the tailings impoundment. First, a brief overview of the LEM is presented, followed by the application of the case study to calculate the Factor of Safety (FOS).

4.3.1. BRIEF OVERVIEW

A brief overview on the LEM is presented in this section, with emphasis on the Morgenstern-Price method. For more information, the reader is referred to the work of Morgenstern and Price (1967), and Fredlund and Krahn (1977) (Morgenst.Nr and Price 1967; Fredlund and Krahn 1977).

Figure 4-3 presents the different forces and variable associated with each slice to define and solve a slope stability problem. The definitions for the variables in Figure 4-3 are presented in Table 4-2.

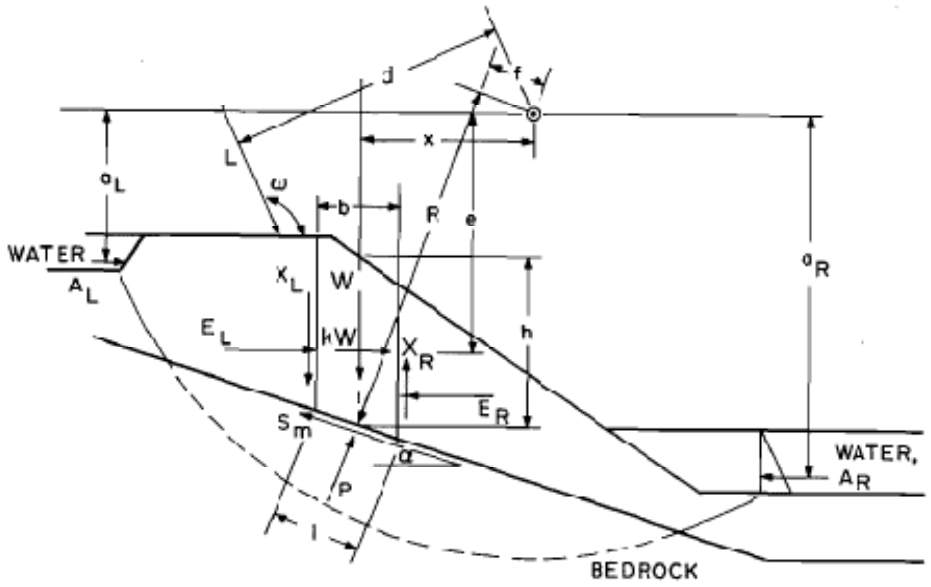

Figure 4-3: Forces acting for the method of slices applied to a composite sliding surface (from (Fredlund and Krahn 1977) p. 430).

Table 4-2: variables associated with each slice in Figure 4-3 (*verbatim from (Fredlund and Krahn 1977), p.2)*

W =	total weight of the slice of width b and height h
P =	total normal force on the base of the slice over a length l
S_m =	shear force mobilized on the base of the slice. It is a percentage of the shear strength as defined by the Mohr-Coulomb equation. That is, $S_m = l\{c' + [P/l - u]\tan +\phi')/F$ where c' = effective cohesion parameter, ϕ'= effective angle of internal friction, F = factor of safety, and u = porewater pressure
R =	radius or the moment arm associated with the mobilized shear force S_m
f =	perpendicular offset of the normal force from the center of rotation
x =	horizontal distance from the slice to the center of rotation
α =	angle between the tangent to the center of the base of each slice and the horizontal
E =	horizontal interslice forces
L =	subscript designating left side
R =	subscript designating right side
X =	vertical interslice forces
k =	seismic coefficient to account for a dynamic horizontal force
e =	vertical distance from the centroid of each slice to the center of rotation
L =	line load (force per unit width)
ω =	angle of the line load from the horizontal
d =	perpendicular distance from the line load to the center of rotation
A =	resultant water forces
a =	perpendicular distance from the resultant water force to the center of rotation

The fundamental difference between Morgentern-Price methods and other LEMs such as the Ordianry, Simplified Bishop, Spencer's, and Janbu's, is that Morgenstern-Price methods assume that the shear and normal forces are related via an arbitrary mathematical function (Fredlund and Krahn 1977):

$$\lambda f(x) = X/E \qquad (4\text{-}1)$$

Where X are the vertical interslice forces, E are the horizontal interslice forces, $f(x)$ is a known function that varies with respect to x, i.e. the location at each slice boundary, and λ is another unknown commonly referred to as the scaling factor to be solved for while solving for the factor of safety.

Figure 4-4 illustrates the different forms which the function f(x) can take and Figure 4-5 presents an example where the half sine function and λ are used to designate the direction of the interslice forces.

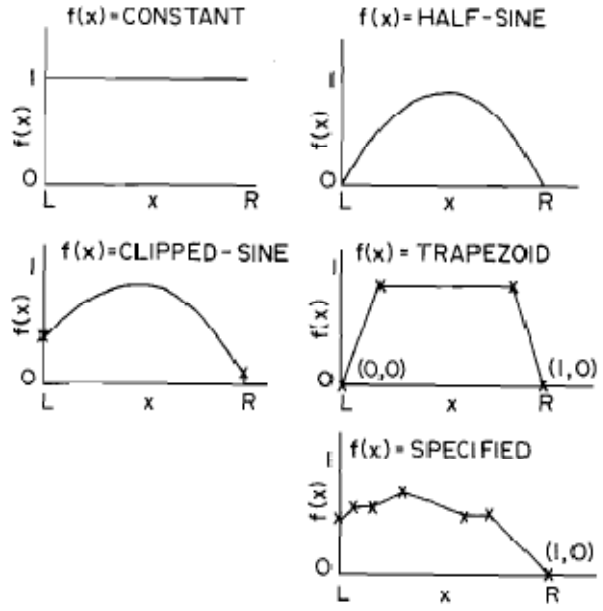

Figure 4-4: Functional variation of the direction of the side force with respect to the x direction (from (Fredlund and Krahn 1977), p. 434).

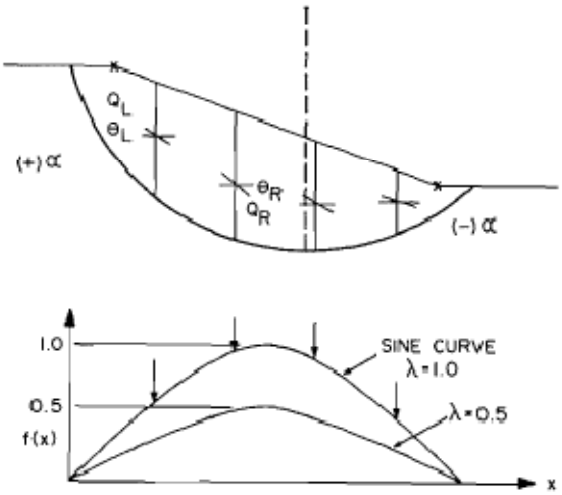

Figure 4-5: Side force designation for the Morgenstern-price method(from (Fredlund and Krahn 1977), p. 434).

As such, once the unknowns (F, λ, N, E, and the location of the interslice forces) are calculated using the equilibrium equations, the vertical component of the interslice forces is calculated from equation 4-1 (Duncan and Wright 2005).

If *f(x)* in Figure 4-4 is constant, then the Morgenstern-Price method reduces to the Spencer's method, where two factors of safety are solved for: one based on the summation of moments about a common point and another based on the summation of forces in a direction parallel to the interslice forces (Fredlund and Krahn 1977).

The set of equations are the following (Fredlund and Krahn 1977):

$$\sum M_o = 0 \tag{4-2}$$

$$P = W\cos\alpha - kW\sin\alpha \tag{4-3}$$

$$\sum W_x - \sum S_m R - \sum Pf + \sum kWe \pm Aa + Ld = 0 \tag{4-4}$$

$$FOS = \frac{\sum \{c'lR + (P - ul)R\tan\phi'\}}{\sum Wx - \sum Pf + \sum kWe \pm Aa + Ld} \tag{4-5}$$

$$\sum F_H = 0 \tag{4-6}$$

$$\sum (E_L - E_R) + \sum P\sin\alpha - \sum S_m\cos\alpha + \sum kW \pm A - L\cos\omega = 0 \tag{4-7}$$

$$FOS = \frac{\sum \{c'l\cos\alpha + (P - ul)\tan\phi'\cos\alpha\}}{\sum P\sin\alpha + \sum kW \pm A - L\cos\omega} \tag{4-8}$$

Numerous commercial software were developed based on the LEM and have been packaged for commercial use in the industry. In the subsequent sections the LEM analysis is conducted by GEO-SLOPE software: SLOPE/W, and Rocscience software: Slide.

4.3.2. LEM SLOPE STABILITY ANALYSIS USING SLOPE/W

Cross-section A-A outlined in Figure 4-1 is presented in Figure 4-6 with the respective regions defining the model. Furthermore, as was mentioned earlier, once the tailings impoundment fills up to Elevation 330m, the impoundment's capacity is increased by building an upstream dyke on the tailings and continuing discharge behind it up to Elevation 332m. Thus, the water elevation is considered to be at El. 332m behind the dyke and at El. 316m or ground surface elevation on the right side of the model after the dam's toe.

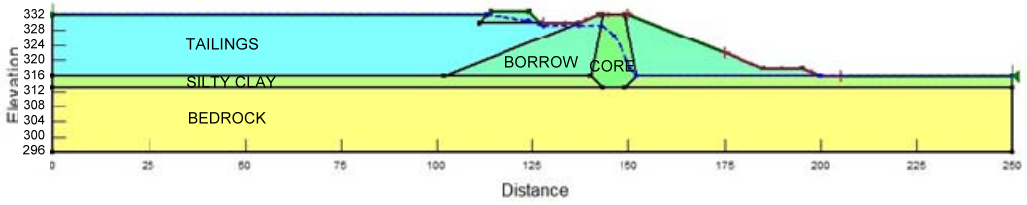

Figure 4-6: Tailings impoundment cross-section illustrating the different zones. The dashed line in the core corresponds to the phreatic surface. (Dimensions in meters)

After defining the geometry, material properties, the piezometric line in the model and the Mohr-Coulomb constitutive model, the factor of safety (FOS) was calculated using the Morgenstern-Price (MP) LEM method of slices, and the result was FOS=1.285, as presented in Figure 4-7.

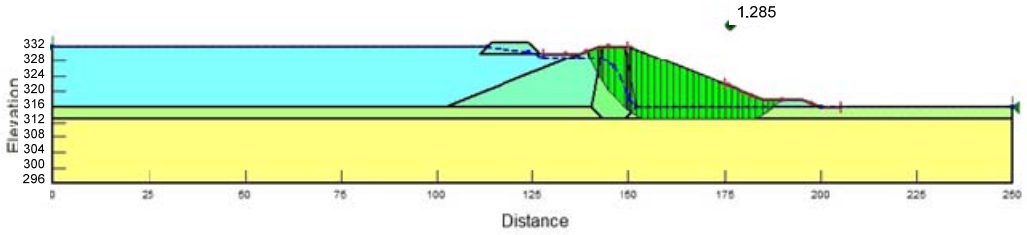

Figure 4-7: Slip surface corresponding to the minimum calculated FOS using the M-P LEM.

SLOPE/W, like many other LEM commercial software, calculates the FOS corresponding to a predefine slip surface. In the past, the slip surfaces were defined based on the historic Grid and Radius method. One of its disadvantages is

that it is difficult to visualize the extent and/or range of trial slip surfaces (GEO-SLOPE and SLOPE/W 2010). However, recent advancements in SLOPE/W allow the user to specify the entry and exit locations for the slip surfaces, thus enabling more flexibility in identifying further slip surfaces by connecting a point along the entry area with a point along the exit area, and then the process continues until the lowest FOS is found. This approach was used in the current analysis. Moreover, it is very important for the user to not just observe the slip surface corresponding to the minimum FOS out of the hundreds or thousands of calculated FOSs, but also verify the slip surfaces corresponding to the five or ten lowest ranked FOSs. The output for the next four lowest is presented in the figures below.

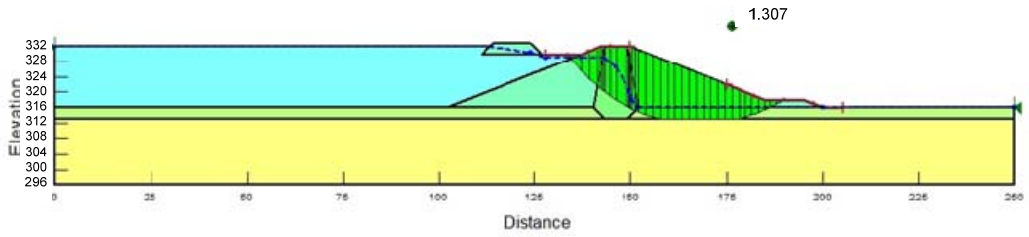

Figure 4-8: Slip surface corresponding to second lowest FOS; FOS=1.307

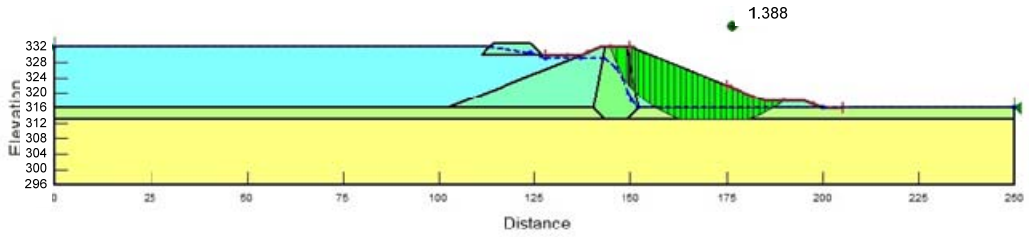

Figure 4-9: Slip surface corresponding to third lowest FOS; FOS=1.388

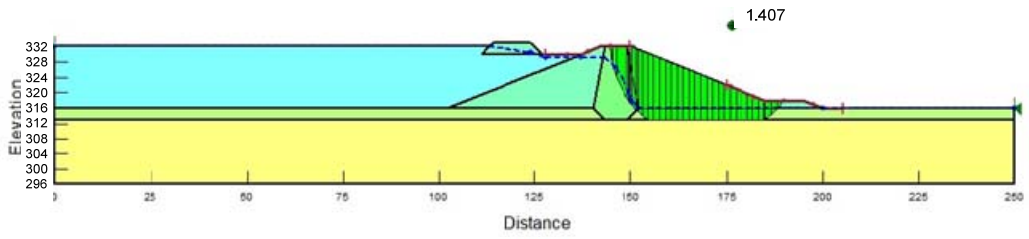

Figure 4-10: Slip surface corresponding to fourth lowest FOS; FOS=1.407

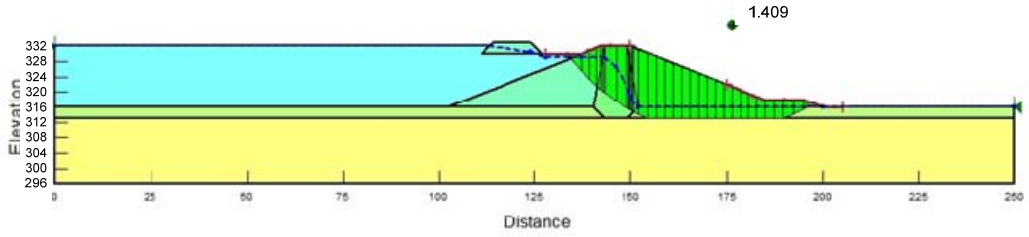

Figure 4-11: Slip surface corresponding to fifth lowest FOS; FOS=1.409

Thus, one can observe that by just presenting the five lowest values for the FOS, the results varied between 1.285 and 1.409, close to a 10% difference. This shows how sensitive the LEM is to the position of the predefined slip surface. Moreover, this exercise will allow the engineer to verify if the failure surfaces are passing through the same zones, which is the case in this scenario. The five slip surfaces are summarized in Figure 4-12.

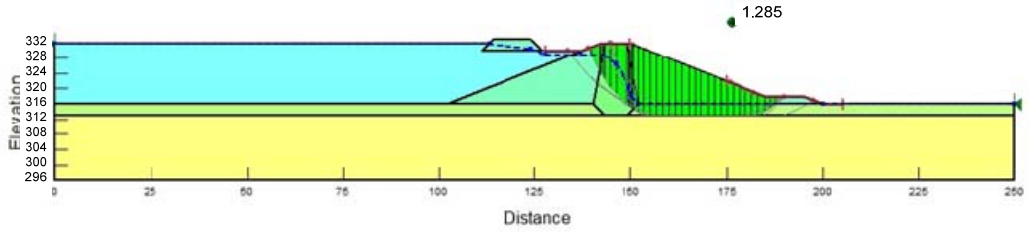

Figure 4-12: Illustration delineating the location of the five lowest FOSs with the lowest highlighted.

4.3.3. LEM SLOPE STABILITY ANALYSIS USING "SLIDE" SOFTWARE

The same geometry and material properties for cross-section A-A were modelled in Slide. The first step in this analysis involves performing a steady state seepage analysis using the Finite Element Analysis option in Slide. Then the generated phreatic surface is plugged in the slope stability component to calculate the FOS using the LEMs while incorporating the Mohr-Coulomb constitutive

model for all materials. Again, in this analysis, the Morgentern-Price option was chosen to calculte the FOS output (RocScience and Slide 2011).

Figure 4-13 illustrates the output for the steady state seepage analysis, where the contour lines correspond to the pressure head, along with the global minimum FOS calculated using the Morgenstern-Price (M-P) method to be 1.394. Simialr to the previous section boundary conditions, the tailings discharged behind the dyke are fully staurated, as such the water elevation is set to El. 332m and on the downstream end, the water elevation is assumed to be at the ground surface elkevation of El. 316m. As expected, given the low permeability of the core relative to the borrow material, the phreatic surface drops in the core and exits along the interface of the foundation with the borrow material.

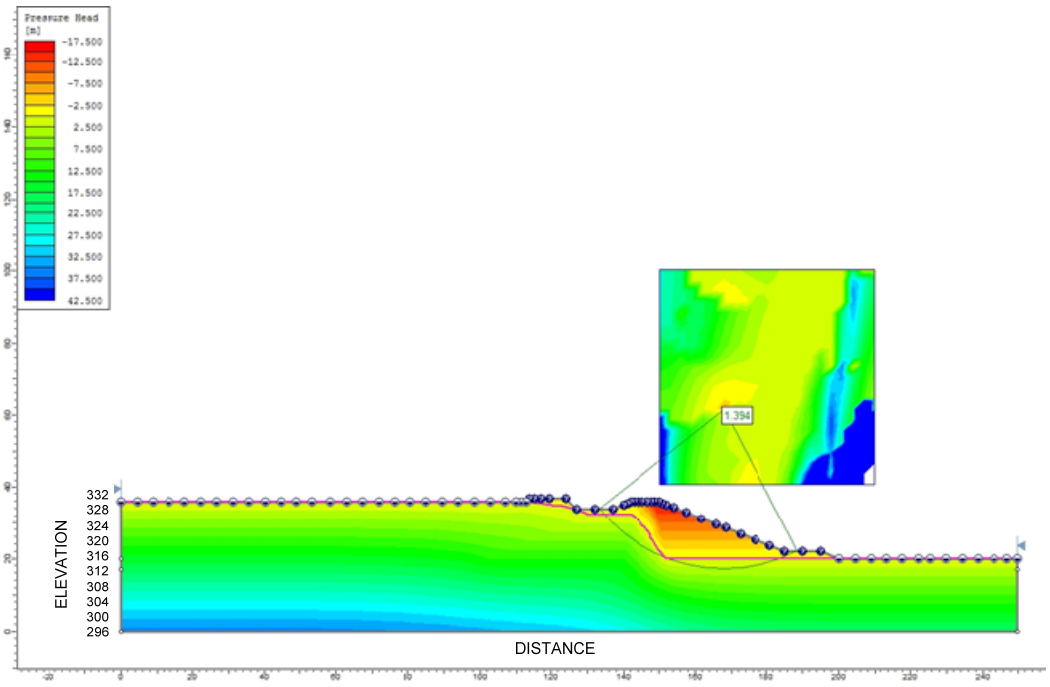

Figure 4-13: Phreatic surface output for steady state seepage analysis along with the calculated FOS using the M-P LEM (Dimensions in meters); FOS=1.394

Figure 4-14 illustrates the slices used in the calculations for the factor of safety of 1.394. Similar to the methodology adopted in the previous section, the output the for the next four lowest FOS calculations will be presented therafter

followed by a figure showing the failure surfaces corresponding to the five lowest FOSs.

As presented in Figure 4-15, the second lowest FOS corresponds to a value of 1.510; which reflects an 8.3% increase between the global minimum and the second lowest calculated. As such, the results for the five lowest FOSs range between 1.394 and 1.598 which reflects a 14.6% difference. Once again, this illustration shows how sensitive the LEM is to the position of the failure surface in calculating the FOS. This is further highlighted by the fact that the failure surfaces corresponding to the global minimum calculated by both SLOPE/W (FOS=1.285) and Slide (FOS=1.394) are very close to each other yet the results recorded from Slide are 8.5% higher.

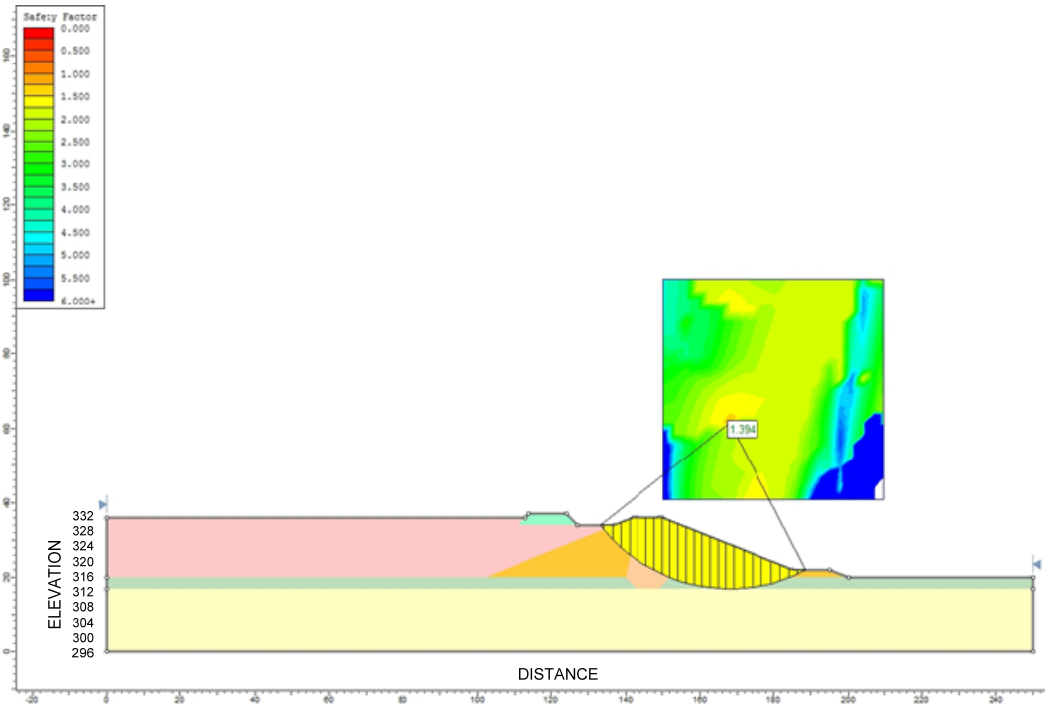

Figure 4-14: FOS calculation using the M-P method showing the slices; FOS=1.394

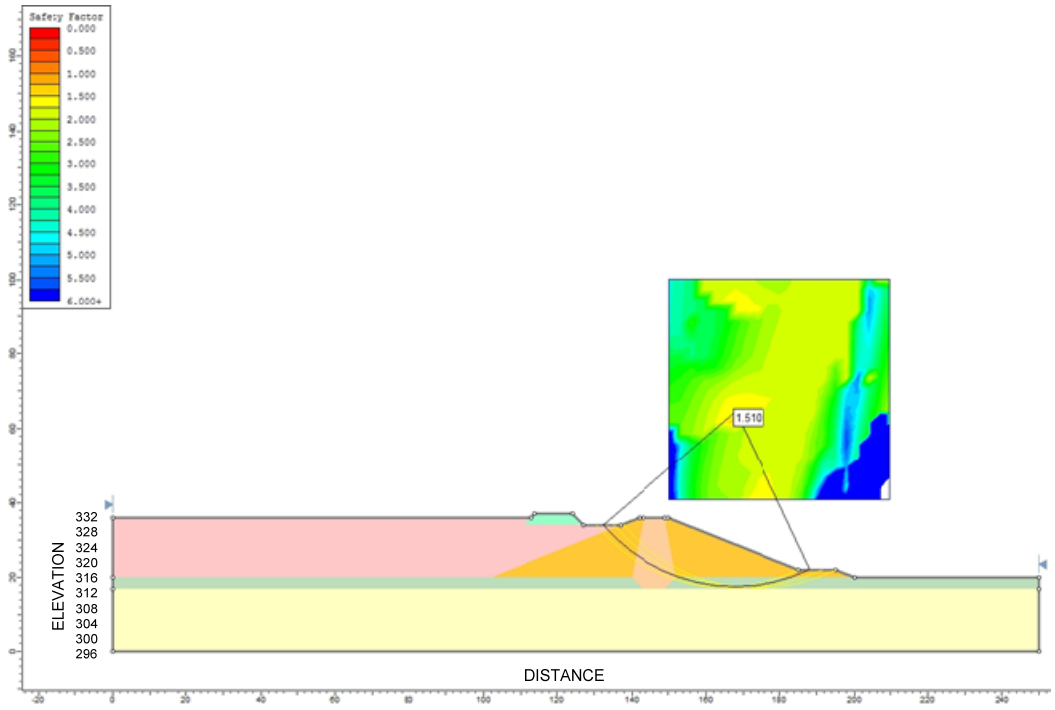

Figure 4-15: Slip surface corresponding to second lowest FOS; FOS=1.510

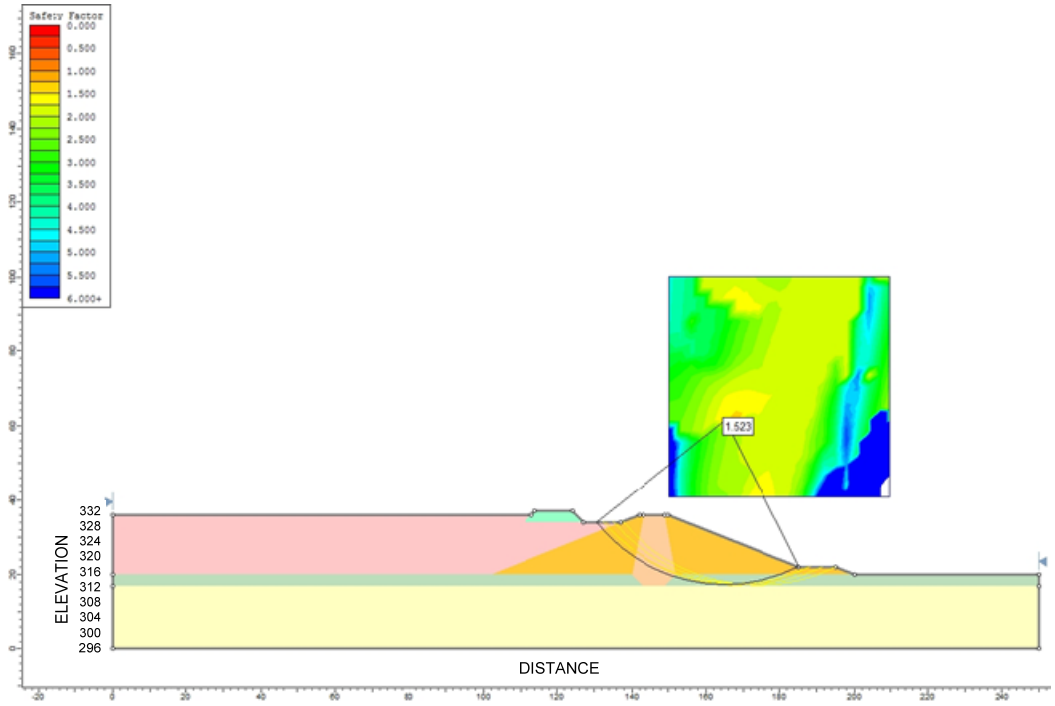

Figure 4-16: Slip surface corresponding to third lowest FOS; FOS=1.523

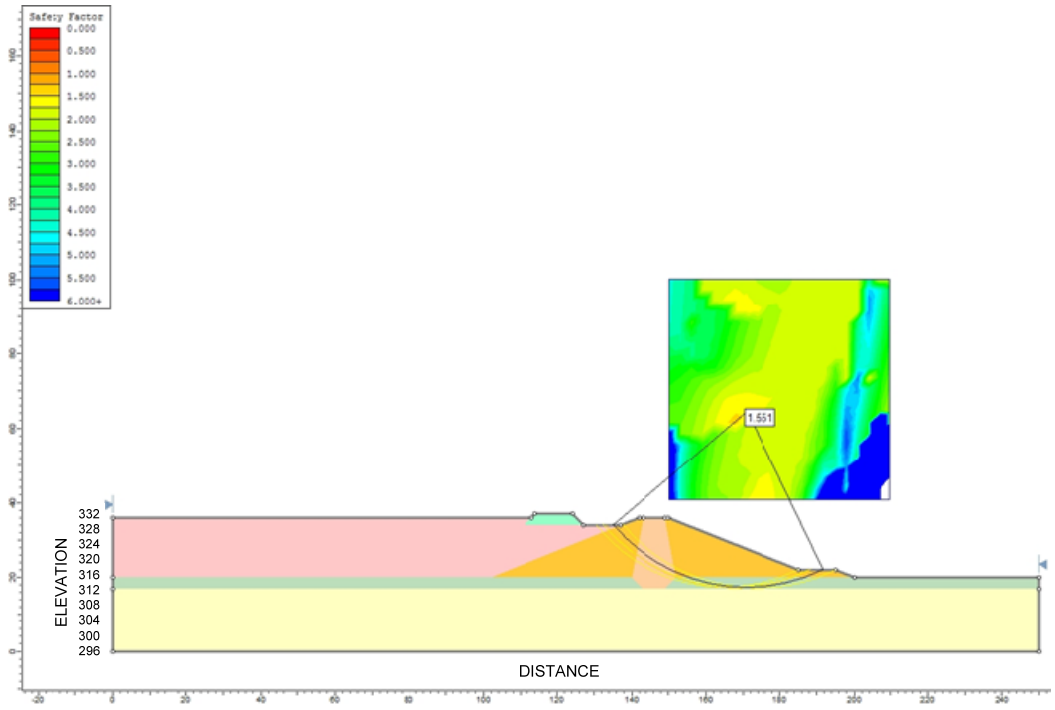

Figure 4-17: Slip surface corresponding to fourth lowest FOS; FOS=1.551

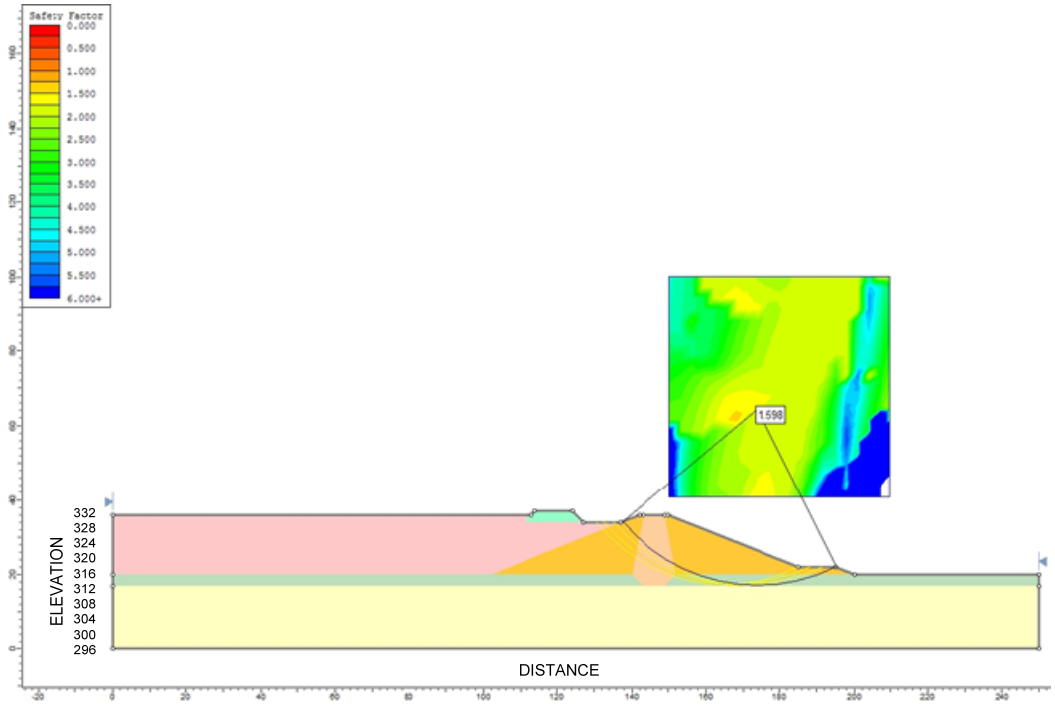

Figure 4-18: Slip surface corresponding to fifth lowest FOS; FOS=1.598

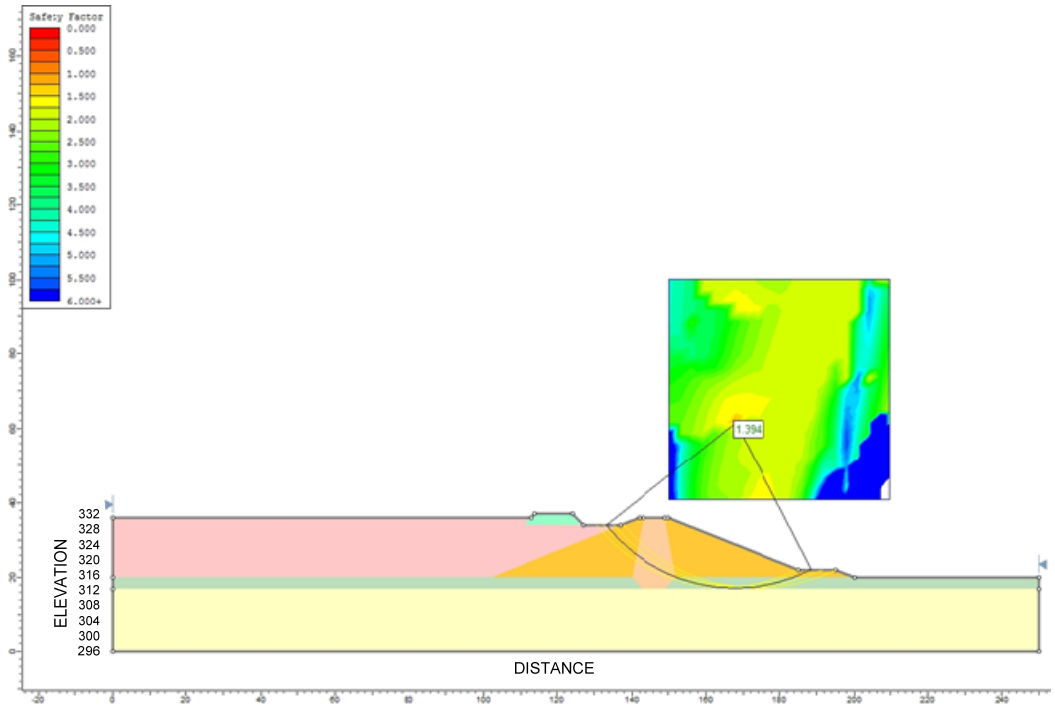

Figure 4-19: Illustration delineating the location of the five lowest FOSs with the lowest highlighted.

4.4 SENSITIVITY ANALYSIS

Another advantage of LEM slope stability tools is that aside from the fact that it can calculate a FOS in a matter of seconds, it can also perform a quick sensitivity analysis on the materials shear strength parameters. As such, the tailings impoundments shear strength parameters were varied ± 20%; and the output is presented in Figure 4-20 in the form of a spider diagram. It is evident from the sensitivity plot that the angle of friction of the core material controls the stability of the tailings impoundment facility. The difference between the FOS corresponding to the +20% variation in the dam's core angle of friction and that corresponding to a -20% variation is approximately 0.14 or a 12% increase from the lower value. As a result, the dam's core angle of friction can be considered the controlling "safety" parameter for this specific tailings impoundment site.

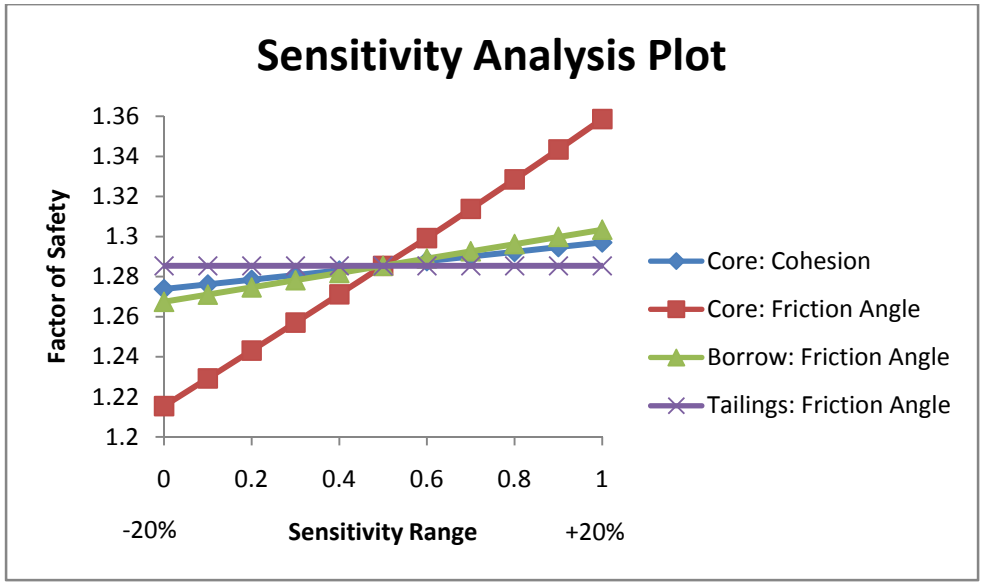

Figure 4-20: Sensitivity analysis for FOS vs. Impoundment's materials shear strength parameters. (Range on x-axis: 0 for -20% and 1 for +20%)

4.5 LIMITATIONS OF LIMIT EQUILIBRIUM METHODS

As illustrated in the previous sections, LEMs are fairly easy-to-use tools; however, it is evident from the analysis presented that the myriad of options available from various software packages will more likely lead to the user achieving close but different results by varying the modeling technique. Moreover, the sheer scale of use of LEM software in the industry and its wide acceptance in regulatory agencies has eroded the attentiveness that "the limit equilibrium method of slices is based purely on the principle of statics; that is, the summation of moments, vertical forces, and horizontal forces. The method says nothing about strains and displacements, and as a result it does not satisfy displacement compatibility. It is this key piece of missing physics that creates many of the difficulties with the limit equilibrium method" (verbatim from (GEO-SLOPE and SLOPE/W 2010) p. 29). One way of overcoming this piece of "missing physics" has been by computing stresses using finite element methods that incorporate a stress-strain constitutive relationship instead of determining the stresses from equation of statics. Then these computed stresses will be used as input in the limit equilibrium method of slices.

Moreover, the issues get compounded when regulations are invoked. The Canadian Dam Association (CDA) specifies a FOS=1.3 as a lower limit for designing "safe" slopes. But, as illustrated earlier, with or without the vast options at hand in LEM tools, the user will get on the one hand a result that is below the limit and on the other hand a result that is above the limit, with both being correctly computed results. Knowing that the LEM is based purely on the principle of statics, engineering judgement has to be exercised extensively when performing these stability studies, let alone when incorporating soil uncertainty.

Judgement is an art; and geotechnical engineering is founded on both art and the advancements of science in the realm of soil mechanics. As such, another goal of this thesis is to provide a novel methodology that shall lessen the burden on judgement in its share of decision making and increase the share of science.

CHAPTER : 5 HYDROMECHANICAL ANALYSIS

5.1 OVERVIEW OF THE FLUID-MECHANICAL INTERACTION

Biot (1941) first introduced the coupling equations for analyzing the three dimensional consolidation process of porous media for the purpose of representing the full soil-fluid interaction. His (Biot 1941) approach has a fundamental advantage over other classical theories whereby the formulations imply that mechanical loads cause flow and an imposed flow causes deformation. In his work, Biot considers the soil skeleton to be incompressible, isotropic elastic and governed by the small displacement theory and the fluid to be incompressible and governed by Darcy's law. Moreover, he considers the total stress to be equal to the summation of the effective stress and the pore water pressure.

In this section, the background theory behind the hydromechanical numerical model setup is presented from the lens of an explicit, finite difference program, namely FLAC: Fast Lagrangian Analysis of Continua, which is developed by the Itasca Consulting Group Inc. (FLAC and ICGInc. 2011). The purpose behind this approach is the fact that there are hundreds of finite difference software available and it would make the utmost sense to limit the presented formulations to those applied in the numerical model setup in FLAC.

Given the highly anticipated "ill-behaviour" of the system, it was justifiable to pursue an explicit time-marching scheme. A comparison between the explicit and implicit solution methods is presented in Table 5-1 where the advantages of the explicit over the implicit scheme are highlighted.

Table 5-1: Comparison of explicit and implicit solution methods (verbatim from (FLAC and ICGInc. 2011) p.1-4)

Explicit	Implicit
Timestep must be smaller than a critical value for stability.	Timestep can be arbitrarily large, with unconditionally stable schemes.
Small amount of computational effort per timestep.	Large amount of computational effort per timestep.
No significant numerical damping introduced for dynamic solution.	Numerical damping dependent on timestep present with unconditionally stable schemes.
No iterations necessary to follow non linear constitutive law.	Iterative procedure necessary to follow non linear constitutive law.
Provided that the timestep criterion is always satisfied, nonlinear laws are always followed in a valid physical way.	Always necessary to demonstrate that the above mentioned procedure is: (a) stable; and (b) follows the physically correct path (for path-sensitive problems).
Matrices are never formed. Memory requirements are always at a minimum. No bandwidth limitations.	Stiffness matrices must be stored. Ways must be found to overcome associated problems such as bandwidth. Memory requirements tend to be large.
Since matrices are never formed, large displacements and strains are accommodated without additional computing effort.	Additional computing effort is needed to follow large displacements and strains.

In this section, the *main* formulations behind the numerical setup of the hydro-mechanical staged construction of the tailings impoundment facility which will also accommodate large-strain deformation are presented *verbatim* from (FLAC and ICGInc. 2011). Furthermore, as will be presented in Chapter 6, this model will be used for pursuing the stochastic analysis.

The continuum expression of the governing equations are presented as follows:

The fluid transport is described by Darcy's law,

$$\boldsymbol{q_i} = -\boldsymbol{k_{ij}}\widehat{\boldsymbol{k}}(\boldsymbol{s})\frac{\boldsymbol{\partial}}{\boldsymbol{\partial x_j}}(\boldsymbol{P} - \boldsymbol{\rho_w g_k x_k}) \tag{5-1}$$

Where q_i is the specific discharge vector, k_{ij} is the mobility coefficient, $\hat{k}(s)$ is the relative permeability (which is a function of the saturation s), P is the fluid pressure, ρ_w is the mass density of the fluid, and g_i , i = 1,2 are the two components of the gravity vector.

The fluid mass balance relation is,

$$\frac{\partial \zeta}{\partial t} = -\frac{\partial q_i}{\partial x_i} + q_v \tag{5-2}$$

Where ζ is the variation of fluid content (variation of fluid volume per unit volume of porous material), and q_v is the volumetric fluid source intensity.

The balance of momentum has the form,

$$\frac{\partial \sigma_{ij}}{\partial x_j} + \rho g_i = \rho \frac{d\dot{u}_i}{dt} \tag{5-3}$$

Where $\rho = (1-n)\rho_s + n\rho_w$ is the solid bulk density; ρ_s and ρ_w are the densities of the solid and fluid phase, respectively, and n is porosity. Note that $(1-n)\ \rho_s$ corresponds to the bulk density of the dry matrix, ρ_d (i.e., $\rho = \rho_d + n\rho_w$).

The response equation for the pore fluid depends on the value of the saturation. At full saturation, $s = 1$ and $k_{ij}^{a}(s) = k_{ij}$ and the response is,

$$\frac{\partial P}{\partial t} = M\left(\frac{\partial \zeta}{\partial t} - \frac{\partial \epsilon}{\partial t}\right) \tag{5-4}$$

Where M is the Biot modulus, α is the Biot coefficient and ε is the volumetric strain. The Biot modulus is related to the drained bulk modulus of the porous medium, K, and the fluid bulk modulus, K_w, via n and α, as follows:

$$M = \frac{K_w}{n + (\alpha - n)(1-\alpha)\frac{K_w}{K}} \tag{5-5}$$

If the compressibility of the grains is neglected compared to that of the drained bulk material (α=1), then,

$$\boldsymbol{M = \frac{K_w}{n}} \tag{5-6}$$

For s< 1, the constitutive response of the pore fluid is described by the saturation equation,

$$\boldsymbol{\frac{\partial s}{\partial t} = \frac{1}{n}\left(\frac{\partial \zeta}{\partial t} - \alpha \frac{\partial \epsilon}{\partial t}\right)} \tag{5-7}$$

And the relation between saturation and pressure (the retention curve), $P = h(s)$, is set to zero in the unsaturated flow, and as such the unsaturated flow is governed only by gravity. And the relation between the relative permeability and saturation is given by the cubic law, $\hat{k}(s) = s^2(3 - 2s)$, where it is equal to 1 at full saturation.

The small-strain constitutive response for the porous solid is described by,

$$\boldsymbol{\frac{d}{dt}\left(\sigma_{ij} + \alpha P \delta_{ij}\right) = H\left(\sigma_{ij}, \dot{\epsilon_{ij}}, k\right)} \tag{5-8}$$

Where H is the functional form of the constitutive law and k is a history parameter.

The elastic relations that relate effective stresses to strains have the form

$$\boldsymbol{\sigma_{ij} - \sigma_{ij}^0 + \alpha(P - P^o)\delta_{ij} = 2G\dot{\epsilon_{ij}} + \left(K - \frac{2}{3}G\right)\dot{\epsilon_{kk}}\delta_{ij}} \tag{5-9}$$

Where the superscript ^{o} refers to the initial state and $\dot{\epsilon_{kk}}$is the volumetric strain increment.

The relation between strain rate and velocity gradient is

$$\boldsymbol{\dot{\epsilon_{ij}} = \frac{1}{2}\left[\frac{\partial \dot{u_i}}{\partial x_j} + \frac{\partial \dot{u_j}}{\partial x_i}\right]} \tag{5-10}$$

In *FLAC*, "starting from a state of mechanical equilibrium, a coupled hydromechanical static simulation using the basic scheme in *FLAC* involves a series of steps. Each step includes one or more flow steps (flow loop), followed by enough mechanical steps (mechanical loop) to maintain a quasi-static

equilibrium. The increment of pore pressure due to fluid flow is evaluated in the flow loop; the contribution from volumetric strain is evaluated in the mechanical loop as a zone value, which is then distributed to the nodes. The total stress correction due to pore pressure change arising from mechanical volume strain is performed in the mechanical loop, and that arising from fluid flow in the flow loop. The total value of the pore pressure is used to evaluate effective stresses and detect failure in plastic materials" (verbatim from (FLAC and ICGInc. 2011) p. 1-10).

The following set of equations will describe the derivation of the Element Stiffness Matrix.

While neglecting gravity for the moment, Darcy's law for an anisotropic porous medium is reduced to

$$\boldsymbol{q_i = -k_{ij}\frac{\partial P}{\partial x_j}} \tag{5-11}$$

And each quadrilateral in a grid is divided into triangles in two different ways (refer to Figure 5-1a). Pore pressure is assumed to vary linearly in a triangle, and the vector q_i is derived for a generic triangle of area A by application of the Gauss divergence theorem. And while referring to Figure 5-1b, we get,

$$\boldsymbol{q_i \cong \frac{k_{ij}}{A}\sum P n_j s} \tag{5-12}$$

where Σ is the summation over the three sides of the triangle, n is the unit normal to the side, and $s$is the length of the side.

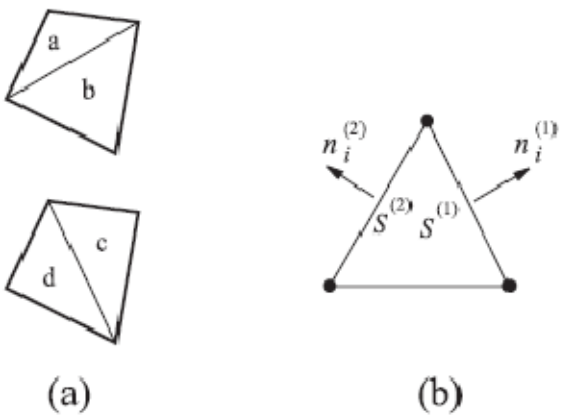

Figure 5-1: (a) *FLAC* zone composed of overlaid triangular elements; (b) typical triangular element.

The two components of q are

$$\boldsymbol{q_1 = \frac{1}{A}\left[k_{11}\sum Pn_1 s + k_{12}\sum Pn_2 s\right]} \quad (5\text{-}13)$$

$$\boldsymbol{q_2 = \frac{1}{A}\left[k_{21}\sum Pn_1 s + k_{22}\sum Pn_2 s\right]} \quad (5\text{-}14)$$

As such, the contribution of side *(ab)* of the triangle to the summations,

$$\boldsymbol{q_1^{(ab)} = \frac{1}{2A}\left[-k_{11}\left(P^{(b)} + P^{(a)}\right)\left(x_2^{(b)} - x_2^{(a)}\right) + k_{12}\left(P^{(b)} + P^{(a)}\right)\left(x_1^{(b)} - x_1^{(a)}\right)\right]} \quad (5\text{-}15)$$

$$\boldsymbol{q_2^{(ab)} = \frac{1}{2A}\left[-k_{21}\left(P^{(b)} + P^{(a)}\right)\left(x_2^{(b)} - x_2^{(a)}\right) + k_{22}\left(P^{(b)} + P^{(a)}\right)\left(x_1^{(b)} - x_1^{(a)}\right)\right]} \quad (5\text{-}16)$$

The other two sides, *(bc)* and *(ca)*, provide similar contributions to q_i. This specific discharge vector contribution is then converted to scalar volumetric flow rates at the nodes by making dot products with the normals to the three sides of the triangle. The general expression is,

$$\boldsymbol{Q = q_i n_i s} \quad (5\text{-}17)$$

And the flow rate into node *(a)* is

$$\boldsymbol{Q^{(a)} = \left\{-q_1\left(x_2^{(b)} - x_2^{(c)}\right) + q_2\left(x_1^{(b)} - x_1^{(c)}\right)\right\}/2} \quad (5\text{-}18)$$

The factor of 2 accounts for the fact that the node only captures half the flow crossing a neighbouring edge (since the other half goes to the other node of the edge). Similar expressions apply to nodes *(b)* and *(c)*. Nodal flow rates are added from the three triangles meeting at the node and divided by 2, since the flow sum comes from two overlaid grids. The "stiffness" matrix [M] of the whole quadrilateral element is defined in terms of the relation between the pressures at the four nodes and the four nodal flow rates, as derived above:

$$\{\boldsymbol{Q}\} = [\boldsymbol{M}]\{\boldsymbol{P}\} \tag{5-19}$$

For the special case of a square zone, aligned with the coordinate axes, the stiffness matrix has the form

$$[\boldsymbol{M}] = -\frac{\boldsymbol{k}}{\boldsymbol{2}}\begin{bmatrix} \boldsymbol{2} & \boldsymbol{-1} & \boldsymbol{0} & \boldsymbol{-1} \\ \boldsymbol{-1} & \boldsymbol{2} & \boldsymbol{-1} & \boldsymbol{0} \\ \boldsymbol{0} & \boldsymbol{-1} & \boldsymbol{2} & \boldsymbol{-1} \\ \boldsymbol{-1} & \boldsymbol{0} & \boldsymbol{-1} & \boldsymbol{2} \end{bmatrix} \tag{5-20}$$

where k is the isotropic mobility coefficient. This matrix is identical to the one that would be obtained in a classical finite difference or finite volume method.

The effect of gravity is incorporated as follows. If the gridpoint pressures around a zone conform to the gradient $\partial P/\partial x_i = g_i \rho_w$, where g_i is the vector of gravitational acceleration, then the nodal flow rates (Babu, Srivastava et al.) should be zero. Hence, Eq. (5-19) is modified as follows:

$$\{\boldsymbol{Q}\} = [\boldsymbol{M}]\left\{\boldsymbol{P} - \left(\boldsymbol{x_i} - \boldsymbol{x_i^{(1)}}\right)\boldsymbol{g_i}\boldsymbol{\rho_w}\right\} \tag{5-21}$$

where $x_i^{(1)}$ is the x-coordinate of one of the corners.

The flow imbalance, $\sum Q$, at a node causes a change in pore pressure at a saturates node as follows:

$$\frac{\boldsymbol{\partial P}}{\boldsymbol{\partial t}} = -\frac{\boldsymbol{M}}{\boldsymbol{V}}\left(\sum \boldsymbol{Q} + \boldsymbol{\alpha}\frac{\boldsymbol{\partial V}}{\boldsymbol{\partial t}}\right) \tag{5-22}$$

Where V is the total volume associated with the node. The term $\sum Q$ includes contributions from the four surrounding zones. In finite difference, the above equation becomes,

$$\boldsymbol{P} \coloneqq \boldsymbol{P} - \frac{\boldsymbol{M}(\sum \boldsymbol{Q}\Delta \boldsymbol{t} + \boldsymbol{\alpha}\Delta \boldsymbol{V_{mech}})}{\boldsymbol{V}} \tag{5-23}$$

Where $\Delta Vmech$ is the equivalent nodal volume increase arising from mechanical deformations of the grid. The term V is computed as the sum of the contributions from all triangular subzones connected to the node. Each triangle contributes a third of its volume, and the resulting sum is divided by two to account for the double overlay scheme in *FLAC*.

There are two aspects of numerical stability associated with the pore-fluid scheme. First, an explicit solution of the fluid flow equations requires that the timestep be less than a critical value. Second, the bulk modulus of the fluid increases the mechanical stiffness of a saturated zone. The effect of increased mechanical stiffness is incorporated in quasi-static analysis in the density-scaling scheme already in *FLAC*; the apparent mechanical bulk modulus of a zone is modified by the presence of fluid as follows:

$$\boldsymbol{K} \coloneqq \boldsymbol{K} + \boldsymbol{\alpha^2 M} \tag{5-24}$$

Where α is the Biot coefficient and M is the Biot modulus.

The explicit fluid timestep can be derived by imagining that one node at the center of four zones is given a pressure of P_0, and knowing that $Q = P_0 \sum M_{kk}$, where $\sum M_{kk}$ is the sum over the 4 zones of the diagonal terms corresponding to the selected node.

The excess nodal flow gives rise to an increment in ΔP, defined as:

$$\Delta \boldsymbol{P} = -\frac{\boldsymbol{MQ}\Delta \boldsymbol{t}}{\boldsymbol{V}} \tag{5-25}$$

The new pressure at the node P_1 is then

$$\boldsymbol{P_1 = P_0 + \Delta P = P_0\left(1 - \frac{M \sum M_{kk} \Delta t}{V}\right)} \quad (5\text{-}26)$$

Where *[M]* is the stiffness matrix relating pore pressure to flow rate.

In *FLAC*, when solving for a coupled steady state analysis after completing consolidation, it is important to calculate the characteristic time of both the mechanical and diffusion processes.

The characteristic time of the mechanical process is given as,

$$t_c^m = \sqrt{\frac{\rho}{K_u + 4G/3}} L_c \quad (5\text{-}27)$$

Where K_u is the undrained bulk modulus, G is the shear modulus, ρ is mass density and L_c is characteristic length (i.e. the average dimension of the medium).

The characteristic time of the diffusion process is given as,

$$\boldsymbol{t_c^f = \frac{L_c^2}{c}} \quad (5\text{-}28)$$

Where L_c is the characteristic length (i.e. the average length of the flow path through the medium) and c is the diffusivity, defined as the mobility coefficient k divided by the storativity S, where:

$$\boldsymbol{c = \frac{k}{S}} \quad (5\text{-}29)$$

$$\boldsymbol{S = \frac{n}{K_w} + \frac{1}{K + 4G/3}} \quad (5\text{-}30)$$

5.2 NUMERICAL MODEL SETUP

5.2.1. STAGING

As was described in the previous section, the fully hydro-mechanical coupled numerical analysis model was completed using the finite difference software *FLAC* (FLAC and ICGInc. 2011). After setting up the grid, which consists of over 2,300 zones (refer to Figure 5-2), the model material groups were defined as illustrated in Figure 5-3. Figure 5-4 shows the grid zones overlaying the model's different groups. All materials were considered to follow the Mohr-Coulomb failure criterion, and were treated as elastic perfectly plastic; refer to Table 4-1. The choice of other soil constitutive models was not possible due to a limitation in FLAC in conjunction with the FOS calculation method, as will be described later in this chapter.

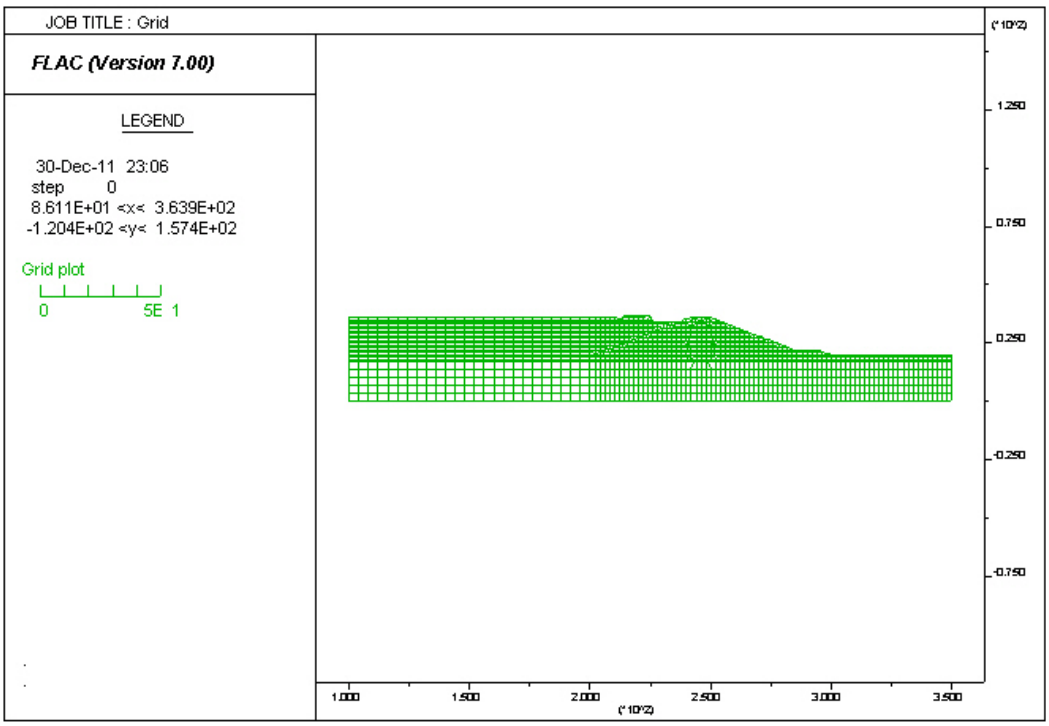

Figure 5-2: Grid zones in numerical model using *FLAC*

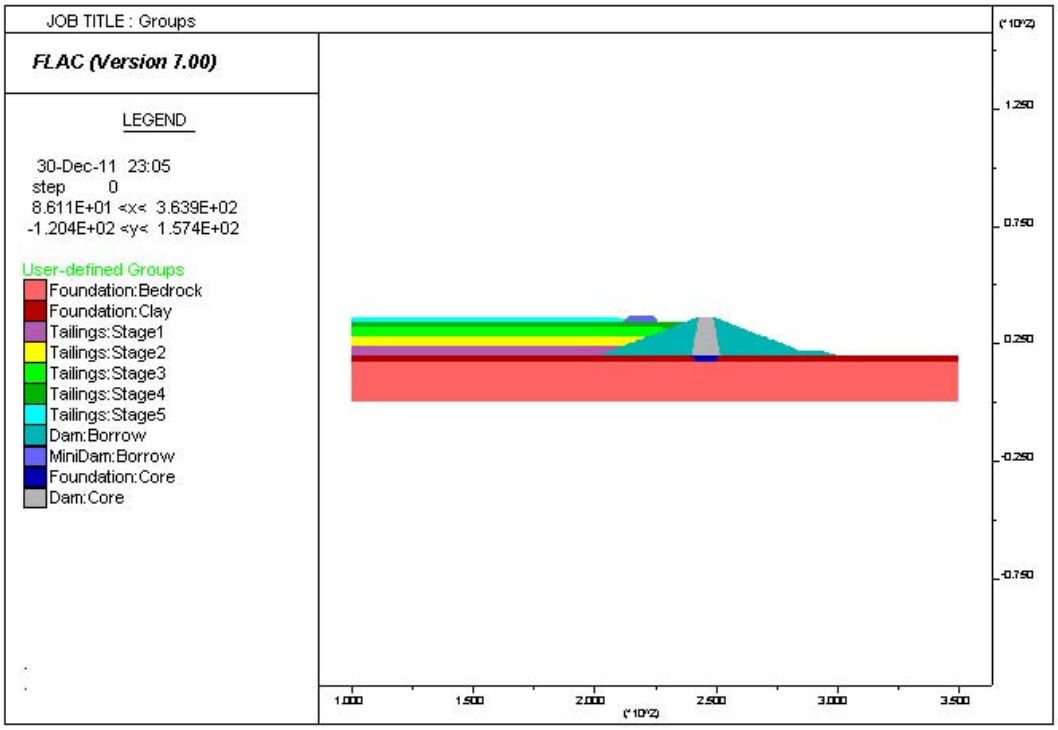

Figure 5-3: Model's material groups

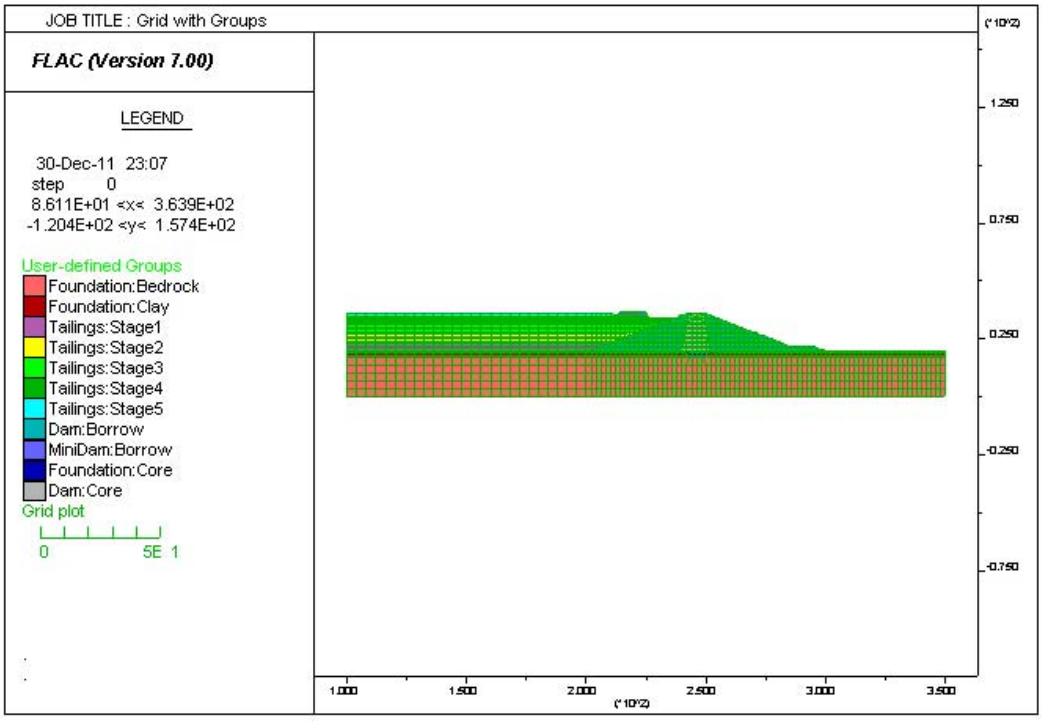

Figure 5-4: Grid overlaying model's material groups

The model was built in stages to represent the staged construction of a tailings impoundment.

1. Foundation (refer to Figure 5-5)
2. Dam (refer to Figure 5-6)
3. Filling up impoundment with 4m of tailings up to El. 320m (refer to Figure 5-7)
4. Filling up impoundment with 4m of tailings up to El. 324m (refer to Figure 5-8)
5. Filling up impoundment with 4m of tailings up to El. 328m (refer to Figure 5-9)
6. Filling up impoundment with 2m of tailings up to El. 330m (refer to Figure 5-10)
7. Dyke (refer to Figure 5-11)
8. Filling up impoundment with 2m of tailings up to El. 332m (refer to Figure 5-12)

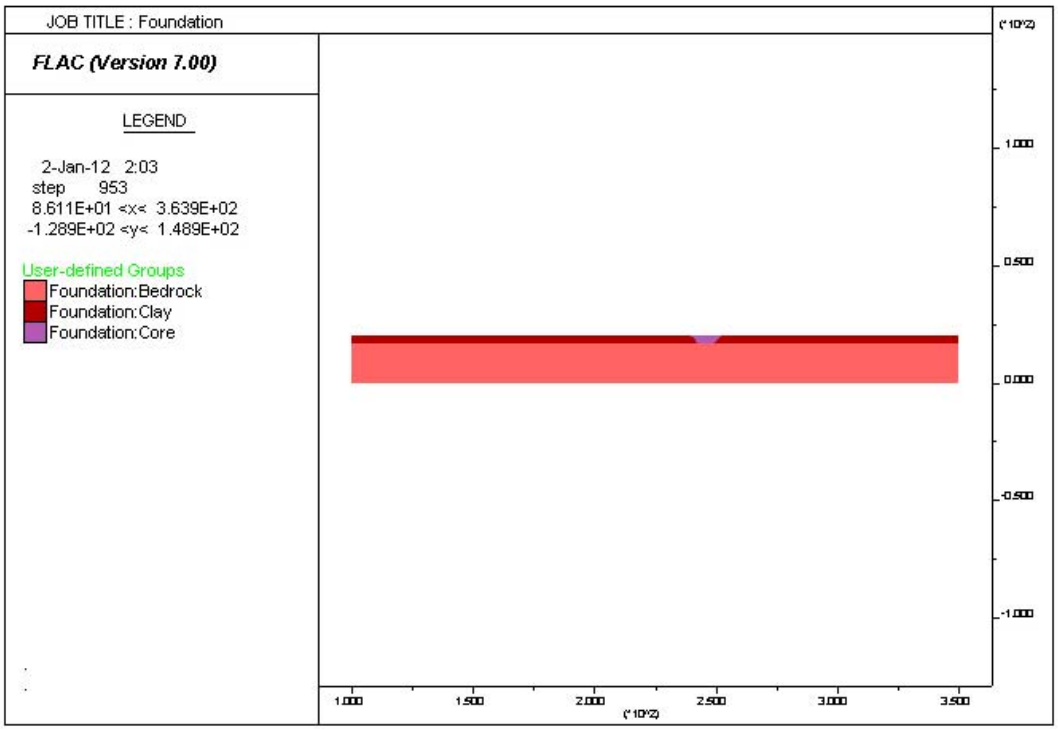

Figure 5-5: Setup equilibrium in foundation

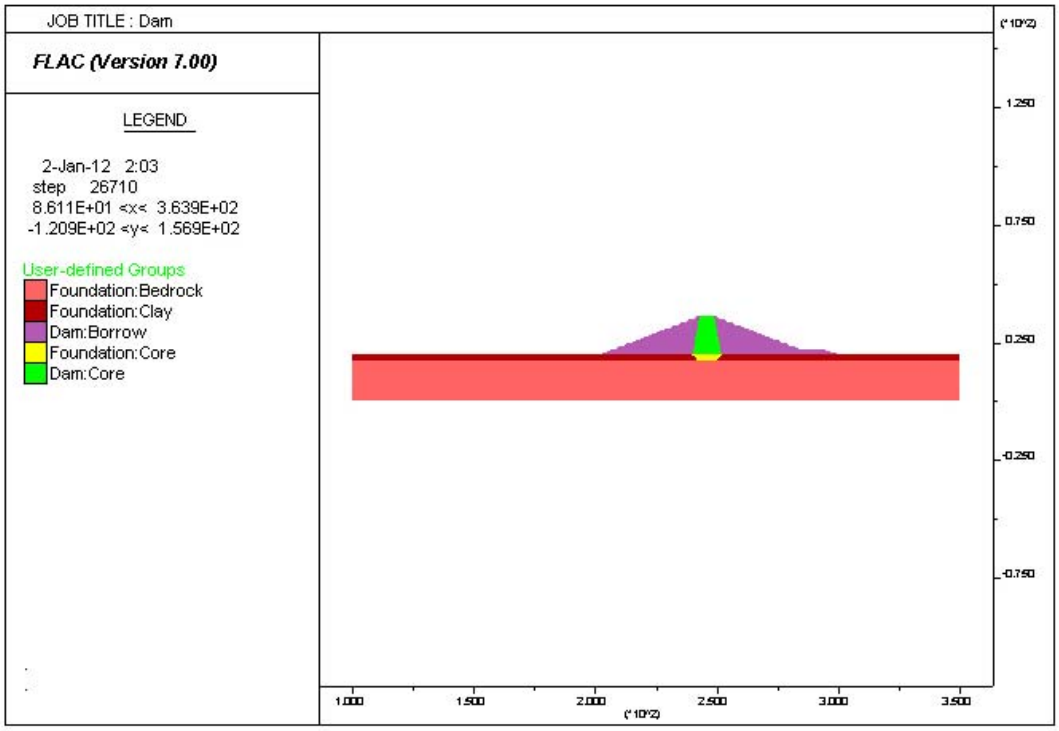

Figure 5-6: Build dam over foundation

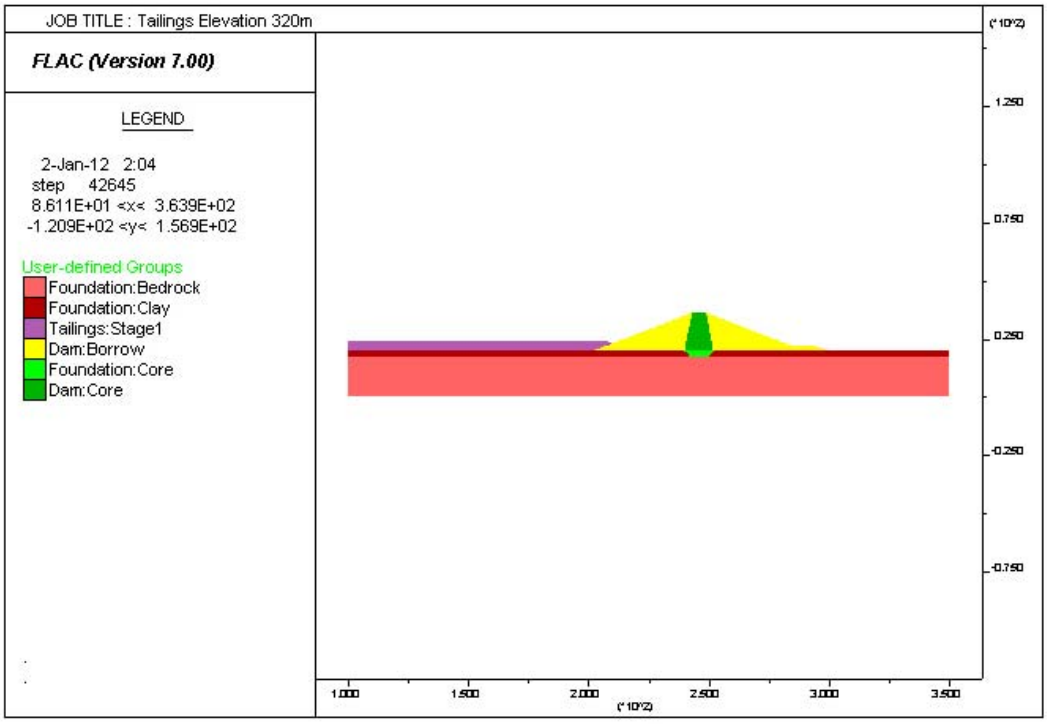

Figure 5-7: Raise tailings impoundment 4m up to El. 320m

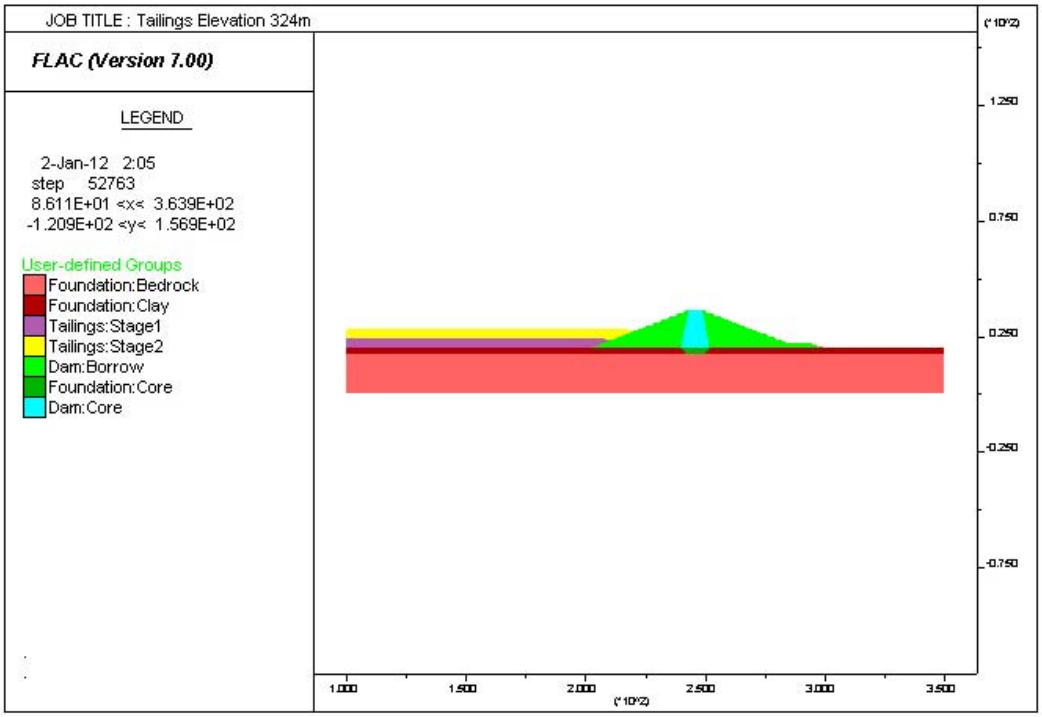

Figure 5-8: Raise tailings impoundment 4m up to El. 324m

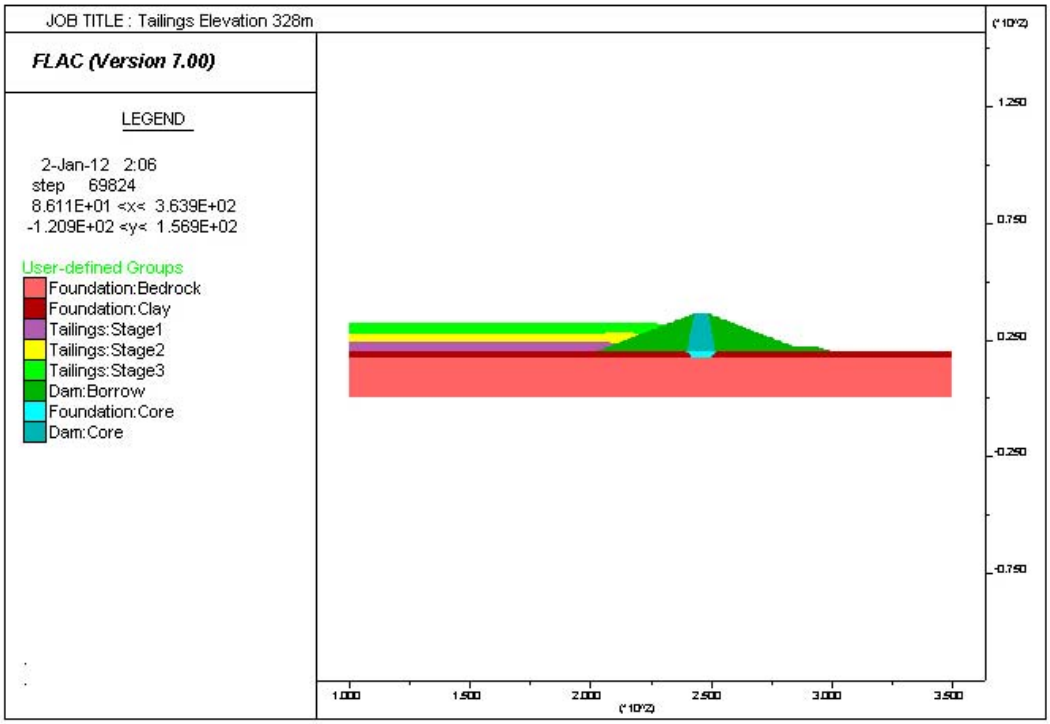

Figure 5-9: Raise tailings impoundment 4m up to El. 328m

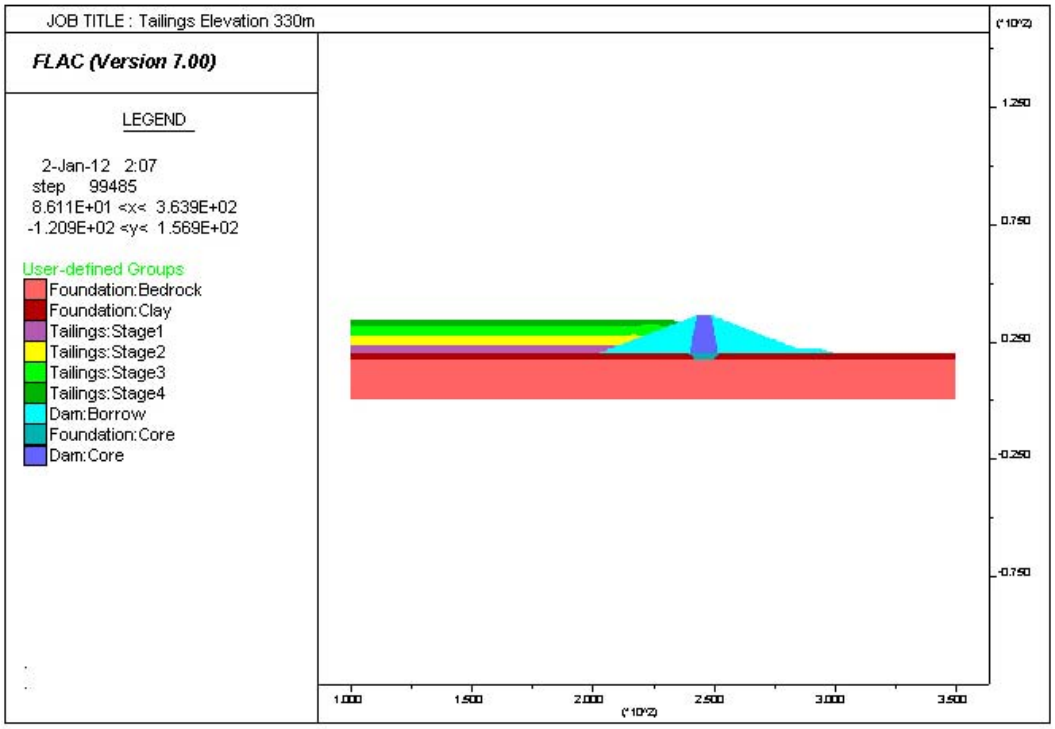

Figure 5-10: Raise tailings impoundment 2m up to El. 330m

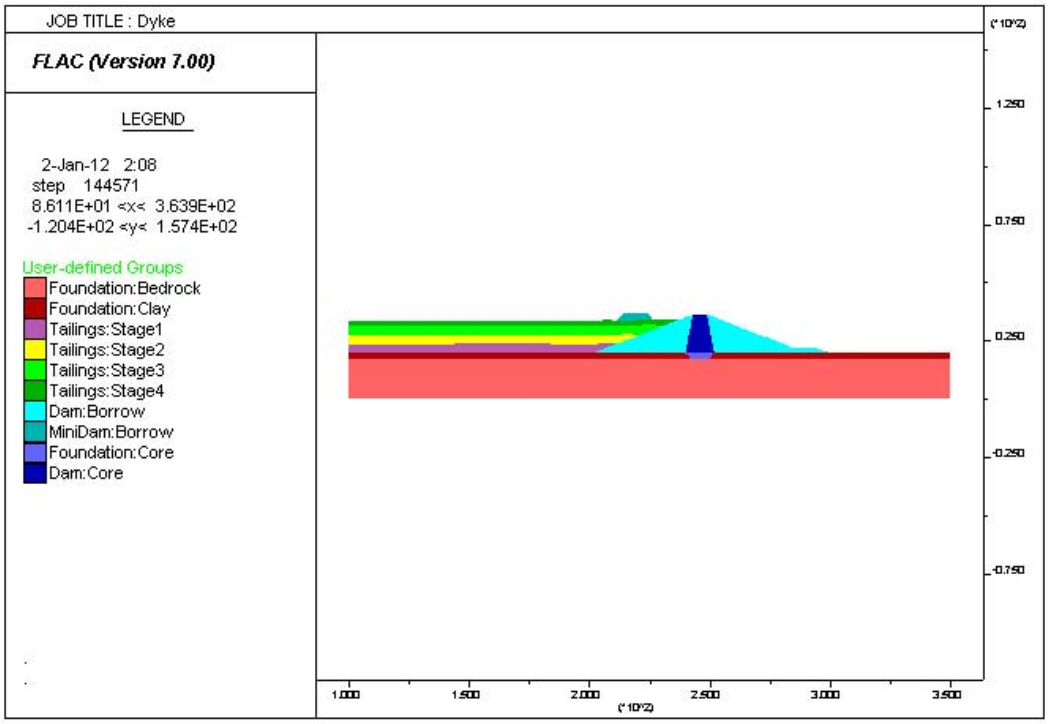

Figure 5-11: Construct upstream dyke

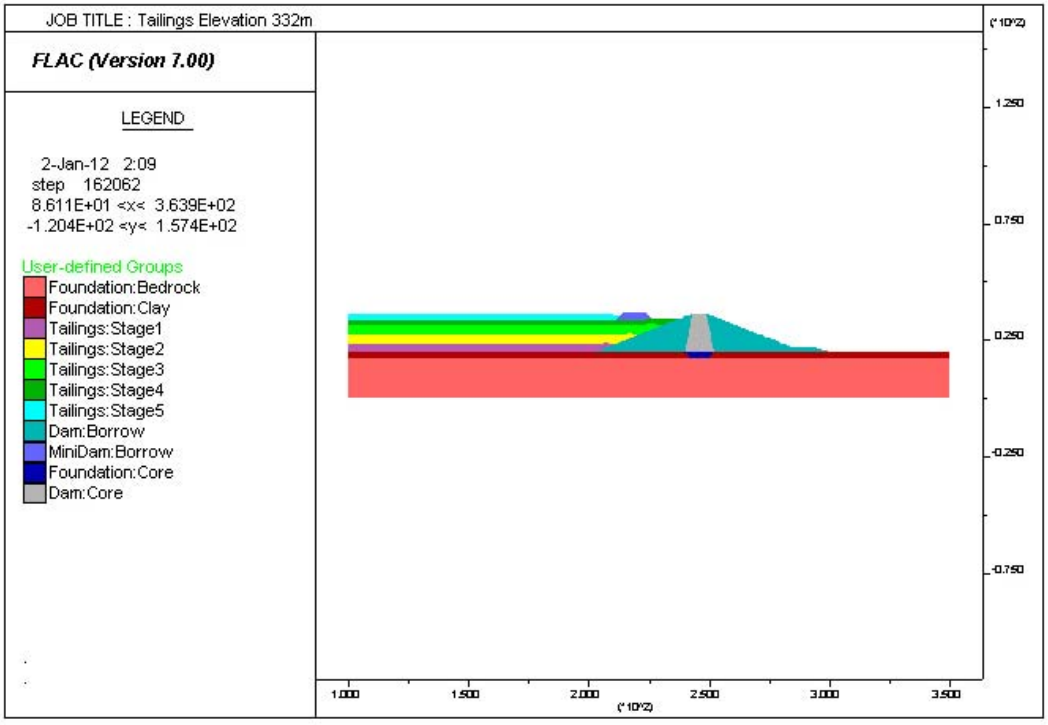

Figure 5-12: Raise tailings impoundment 2m up to El. 332m

5.2.2. MODEL SETUP

After constructing the whole grid and marking the respective material groups, the boundary conditions are defined.

First, all the zones above the foundation are nulled or removed, and the foundation is fixed at the bottom in both the horizontal and vertical directions. The sides of the model are fixed in the horizontal direction. The hydrostatic pressure is then initialized across the foundation layers with the ground surface given a free surface condition, thus allowing fluid to flow to and from the outside world. Since the pore pressure distribution has been defined, the model is allowed to run only mechanical loops to reach equilibrium.

Next, the dam is added on top of the foundation in four stages. To avoid numerical instability, the grid points of the foundation are fixed in both the horizontal and vertical direction, and then the model is allowed to run mechanical

loops. Then the foundation's grid points are released and the model is allowed to run the mandatory elastic step. Next, given that the coupled model is experiencing the sudden change of loading, the undrained (short-term) response is allowed to develop before allowing the flow to take place. Finally the model is allowed to compute the subsequent coupled flow/mechanical response and cycle to equilibrium or the final steady state response. When performing the coupled analysis, several mechanical steps may be done for every fluid timestep, or several fluid timesteps may be done for every mechanical step. Specific keywords are invoked in FLAC to specify the number of these sub-cycles with the number of fluid and mechanical sub-cycles being adjusted automatically to keep the maximum unbalanced force ratio (or unbalanced force) below a preset value.

Then the first 4 meters of tailings are added (up to El. 320m), along with the appropriate boundary conditions, and the model is first allowed to solve for the undrained response and then cycle to equilibrium in the drained coupled response. The same procedure is applied to the subsequent raises to El. 324m, El. 328m, El. 330m, Dyke, and finally the current design capacity of El. 332m. Note that the complete model has been solved in large strain.

The main output that will be presented in this section is the pore pressure at steady state, the vertical displacement and the impoundment's factor of safety after the completion of each stage.

The factor of safety (FOS) will be calculated using the strength reduction technique (SRT) by progressively reducing the shear strength of the material to bring the slope to a state of limiting equilibrium. The SRT was first introduced in the literature by Zienkiewicz et al. in 1975 (Zienkiewicz, Humpheson et al. 1975) and has been applied by a number of researchers including: (Naylor 1981; Donald and Giam 1988; Matsui and San 1992; Dawson and Drescher 1999; Dawson and Roth 1999; Griffiths and Lane 1999).

As a result, the FOS is defined according to the following equations:

$$c^{trial} = \frac{1}{FOS^{trial}} c \quad (5\text{-}31)$$

$$\emptyset^{trial} = arctan\left(\frac{1}{FOS^{trial}} tan\emptyset\right) \quad (5\text{-}32)$$

where the model initiates a systematic search for the value of FOS^{trial} that will just cause the slope to fail. The same FOS^{trial} will be used to reduce the material shear strength parameters.

5.3 NUMERICAL MODEL OUTPUT

As discussed earlier, this hydro-mechanical coupled model takes into account consolidation, seepage and the stress-deformation behaviour of the impoundment at different stages. Moreover, it has the capability of translating the impoundment's performance at the end of each stage to a commonly known parameter, the FOS. The output for the respective stages are as follows:

5.3.1. DAM

After completing the first stage of the analysis, which includes constructing the dam, the results are presented below. The maximum vertical displacement at the crest of the dam is noted to be 15cm (Figure 5-13) and the maximum horizontal displacement is recorded to be 5cm (Figure 5-14). Figure 5-15 presents the output for the FOS calculations using the SRT, with the FOS=1.47. Note that in this analysis, the user does not have to specify in which direction the slope will naturally fail. Given the fact that the downstream face of the dam includes an extended toe, it is conclusive that the failure surface following the maximum shear strain rate will be on the upstream side of the dam. Furthermore, the failure surface starts at the high point of the core and continues outwards. It is important to note that the FOS calculations were made after completing the coupled analysis and the geometry deforming in large strain mode. Moreover, the advantage of using the SRT is that the failure surface corresponds

to the zones corresponding to the maximum shear-strain rate in contrast with LEM's use of predefined failure surfaces.

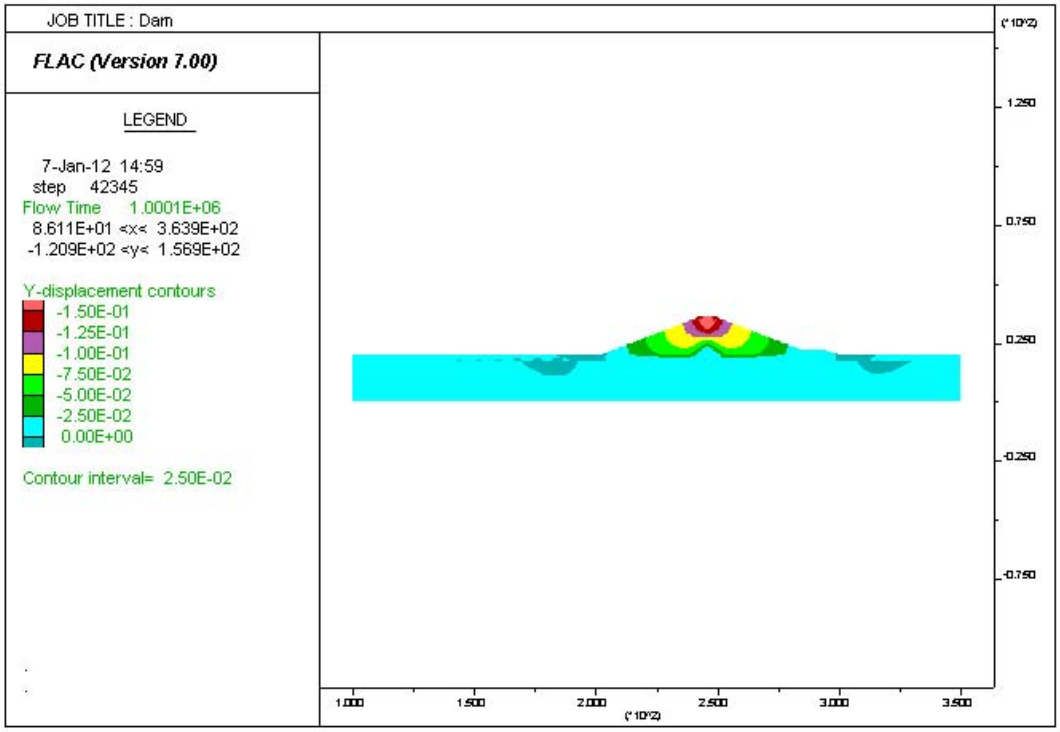

Figure 5-13: Vertical displacement contours after dam construction stage

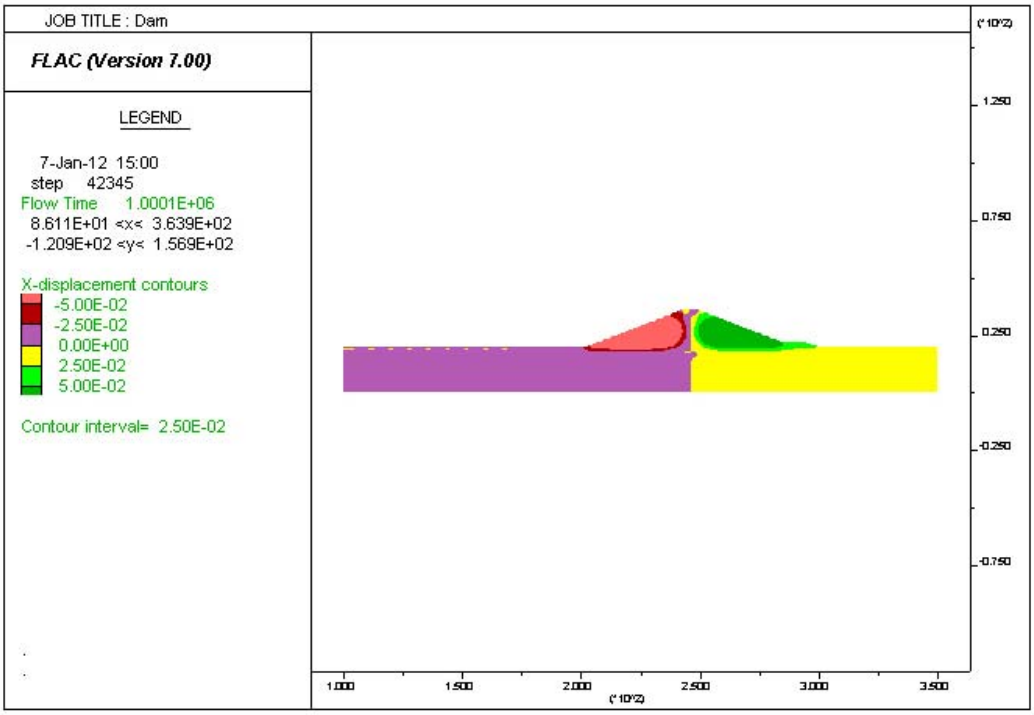

Figure 5-14: Horizontal displacement contours after dam construction stage

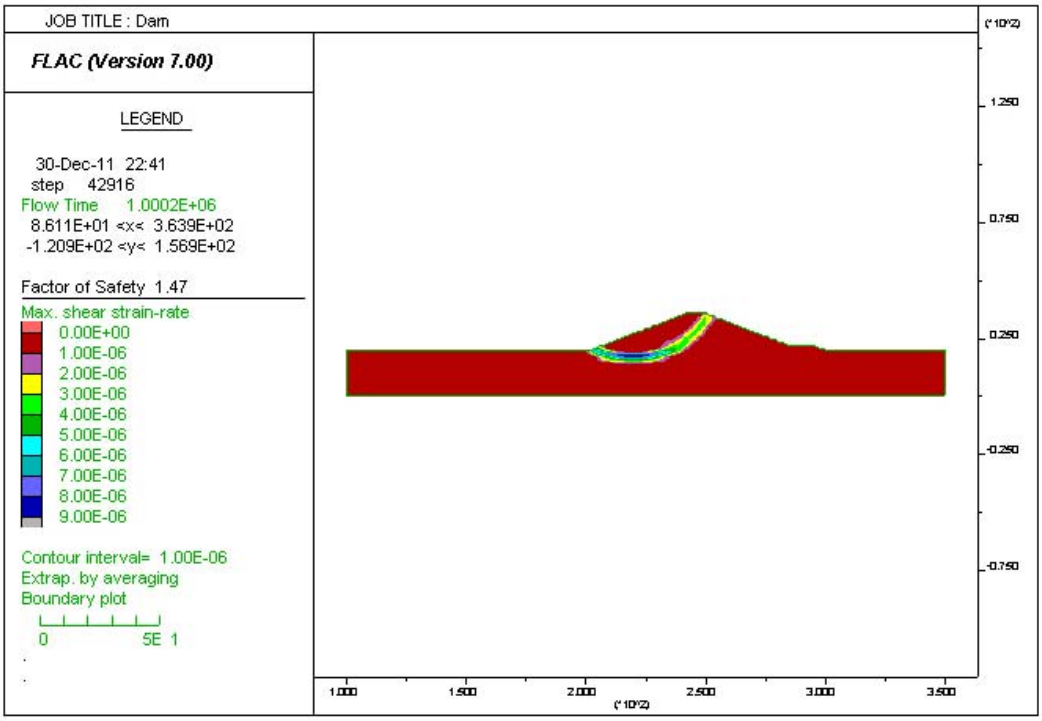

Figure 5-15: Maximum shear strain-rate contours with FOS=1.47

5.3.2. TAILINGS DEPOSITION TO ELEVATION 320M

A 4 meter layer of tailings is added, and after the model reaches equilibrium the output for the pore pressure, vertical displacement and FOS are recorded; see results in Figure 5-16, Figure 5-17, and Figure 5-18, respectively. Note that the model's displacement output values are incremental. This is accomplished by initializing the displacements to zero before the construction of every stage for the purpose of understanding the individual contributions of every stage to the overall displacements of the impoundment after the completion of that particular stage; whereas, the grid points will remain in their new position in the deformed model.

The maximum shear-strain rate contours flip sides and now progress from the left side to the right side, i.e. on the downstream side of the dam. Moreover, the FOS increases due to the added tailings layer that is supporting the dam's upstream side.

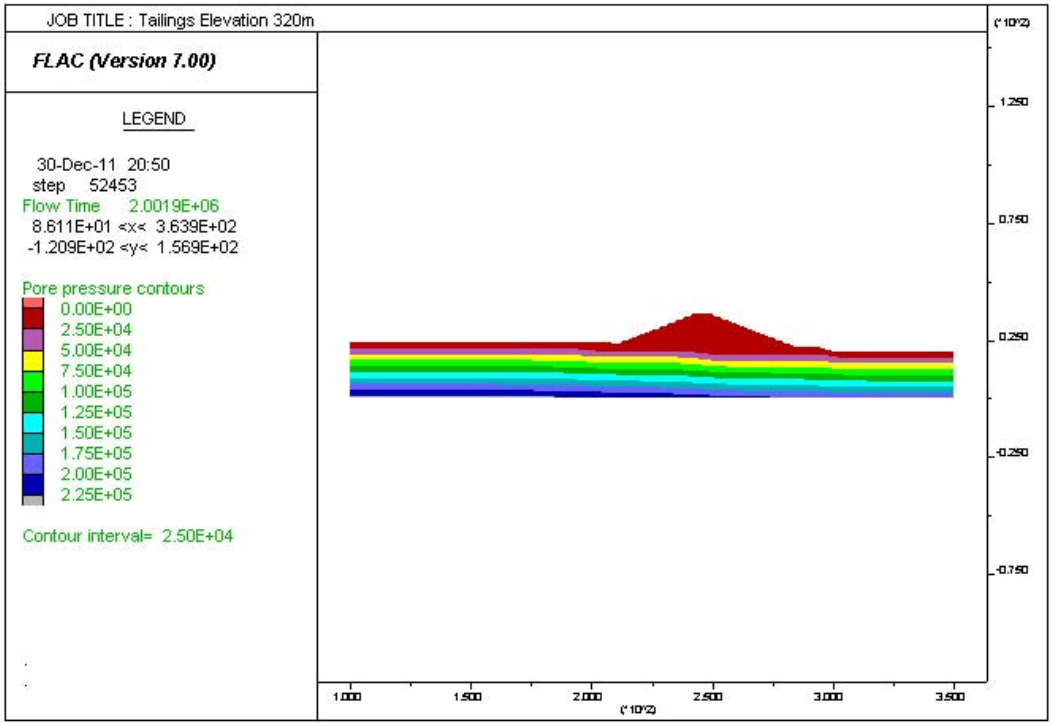

Figure 5-16: Pore pressure distribution at the end of the coupled analysis for tailings El. 320m

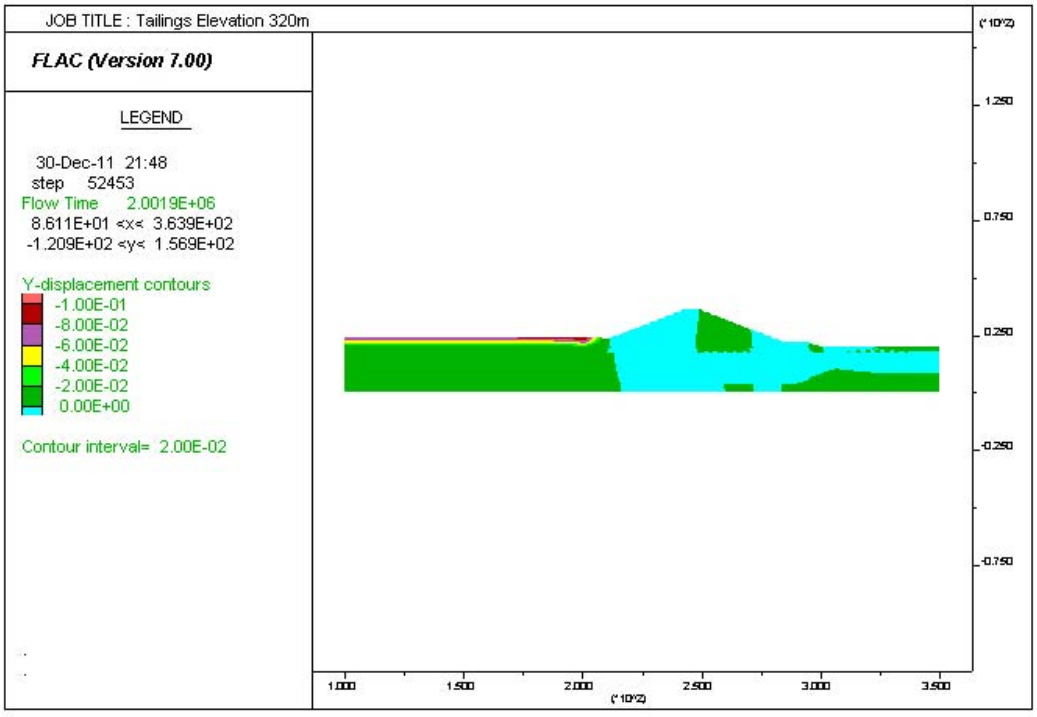

Figure 5-17: Vertical displacement increments at the end of the coupled analysis for tailings El. 320m

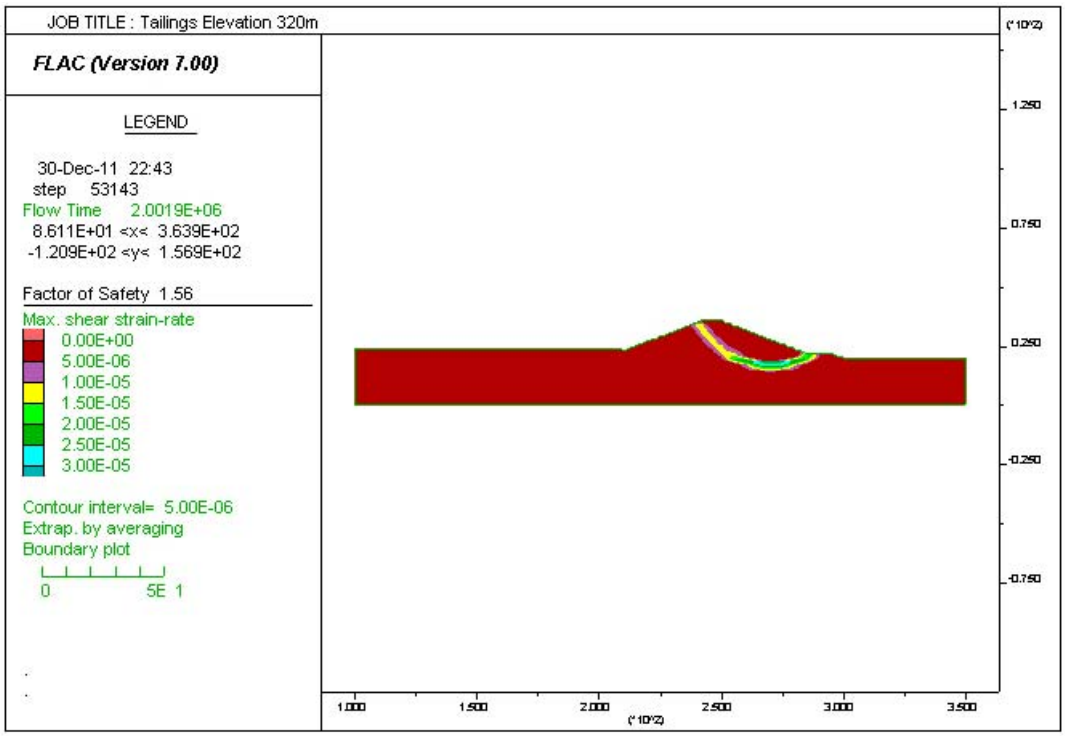

Figure 5-18: Maximum shear strain-rate contours at tailings El. 320m with FOS=1.56

5.3.3. TAILINGS DEPOSITION TO ELEVATION 324M

The output for the pore pressure distribution, vertical displacement increments and the maximum shear-strain contours is illustrated in Figure 5-20, Figure 5-21, and Figure 5-22 respectively. The calculated FOS remained unchanged at 1.56. Moreover, to provide more insight on the undrained response discussed in Section 5.2.2, Figure 5-19 illustrates the pore pressure distribution immediately after the undrained response.

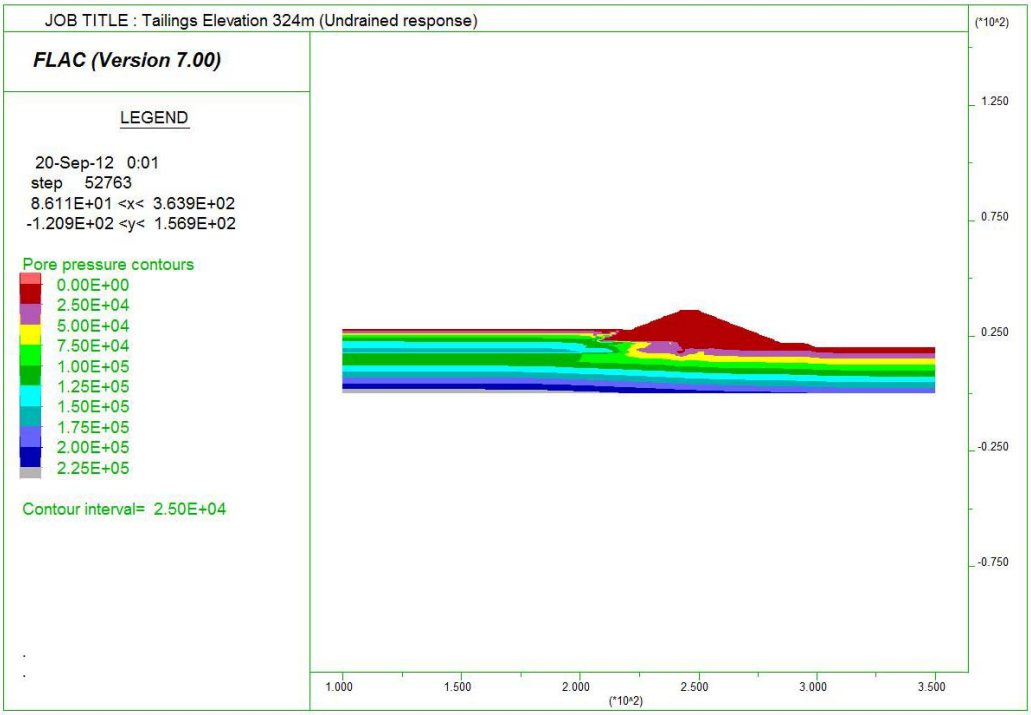

Figure 5-19: Pore pressure distribution immediately after the undrained response for tailings El. 324m

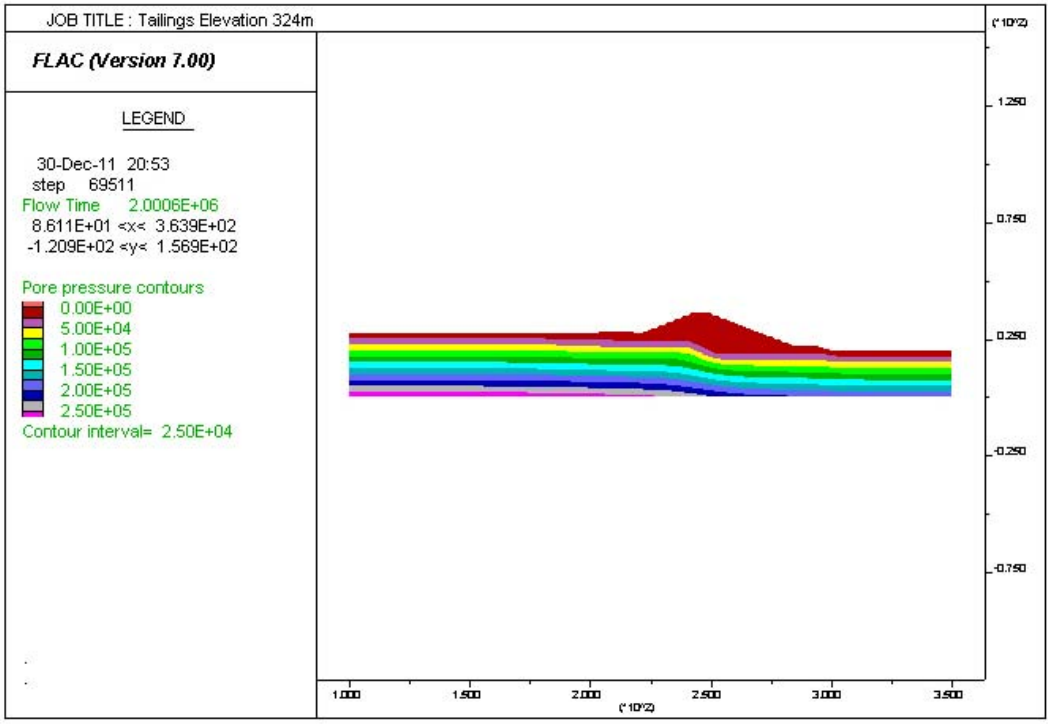

Figure 5-20 : Pore pressure distribution at the end of the coupled analysis for tailings El. 324m

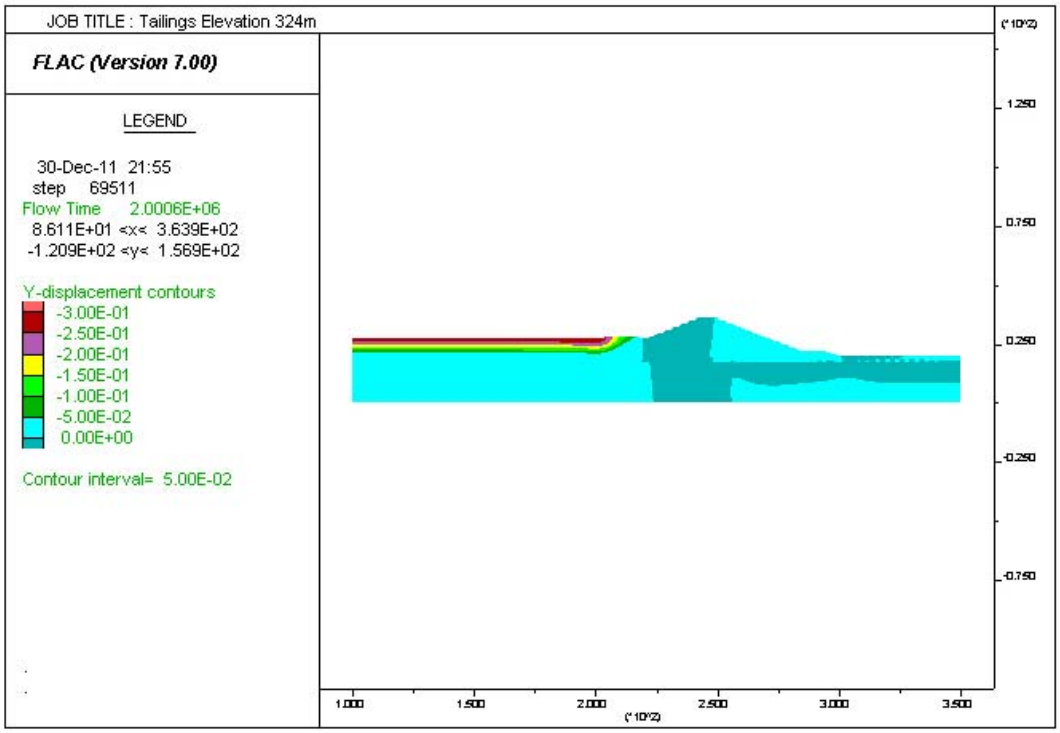

Figure 5-21: Vertical displacement increments at the end of the coupled analysis for tailings El. 324m

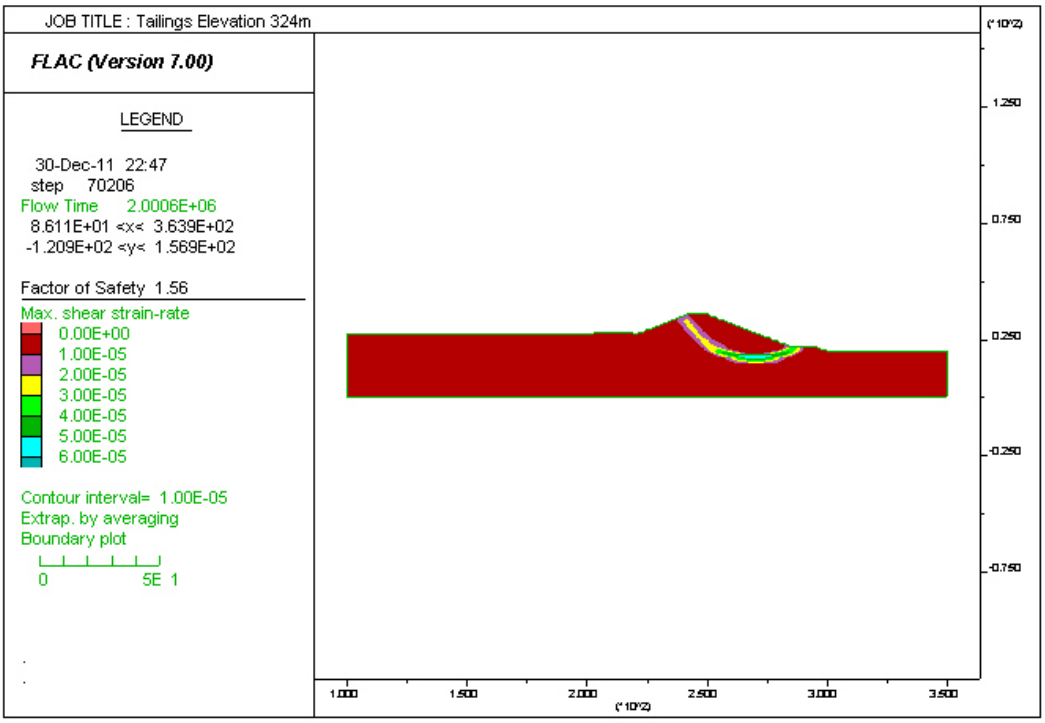

Figure 5-22: Maximum shear strain-rate contours at tailings El. 324m with FOS=1.56

5.3.4. TAILINGS DEPOSITION TO ELEVATION 328M

The output for the pore pressure distribution, vertical displacement and the maximum shear-strain contours is illustrated in Figure 5-23, Figure 5-24, and Figure 5-25, respectively. The FOS drops to 1.49 after raising the tailings impoundment to El. 328m.

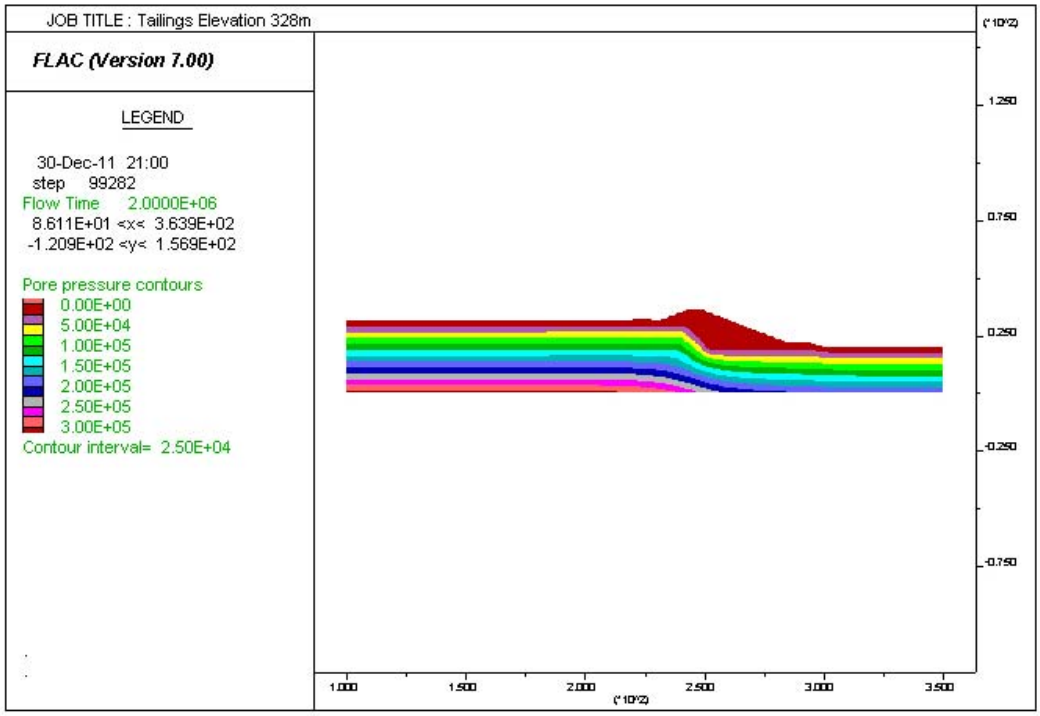

Figure 5-23: Pore pressure distribution at the end of the coupled analysis for tailings El. 328m

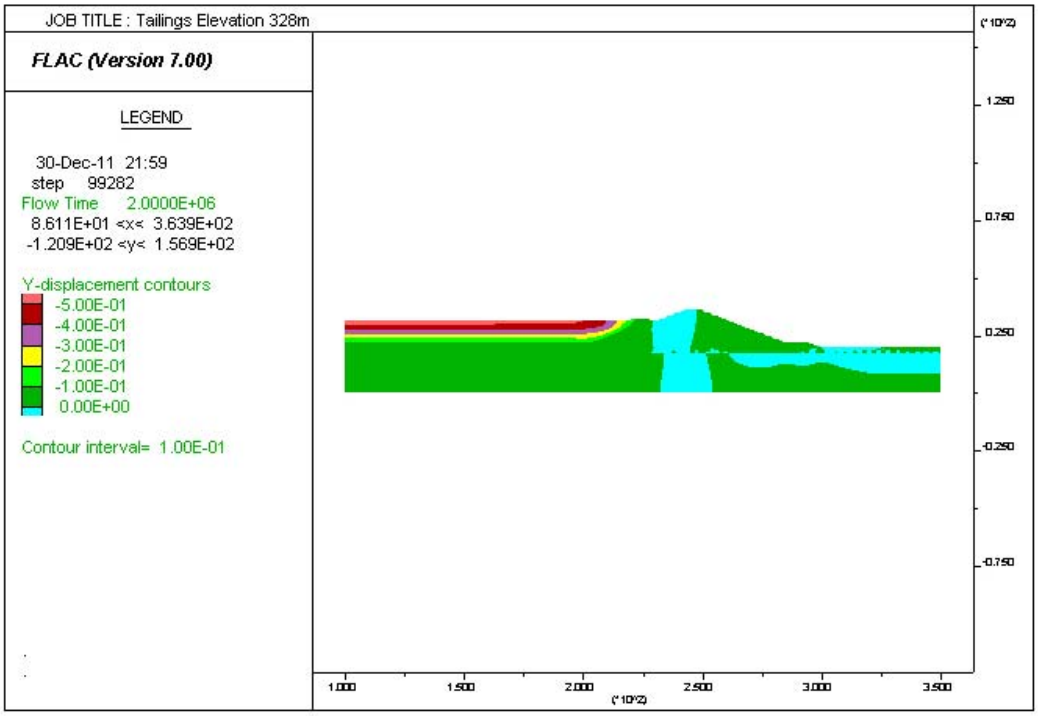

Figure 5-24: Vertical displacement increments at the end of the coupled analysis for tailings El. 328m

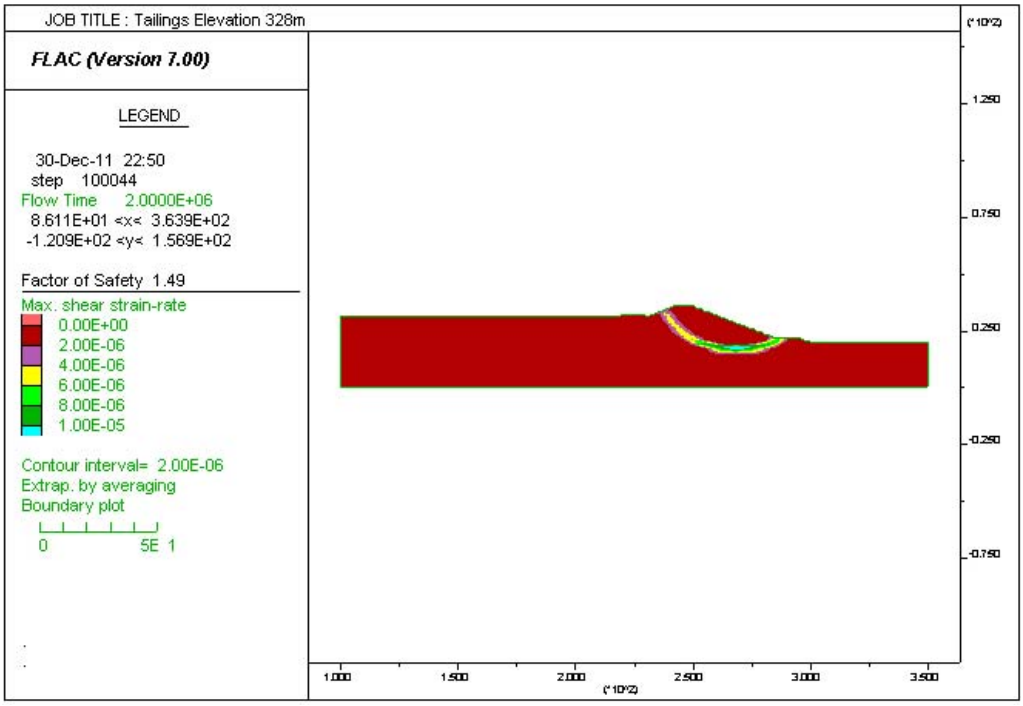

Figure 5-25: Maximum shear strain-rate contours at tailings El. 328m with FOS=1.49

5.3.5. TAILINGS DEPOSITION TO ELEVATION 330M

The output for the pore pressure distribution, vertical displacement and the maximum shear-strain contours is illustrated in Figure 5-26, Figure 5-27, and Figure 5-28, respectively. The FOS drops to 1.41 after raising the tailings impoundment to El. 330m.

It is important to note that raising the impoundment by 2 meters, from El. 328m to El. 330m has resulted in a drop in the FOS from 1.49 to 1.41, which corresponds to a 5.6% decrease.

Moreover, note that the at El. 330, which is the maximum capacity after which a dyke needs to be constructed upstream in order to increase the impoundment's capacity, the dam's core is still functioning as designed and retaining the water.

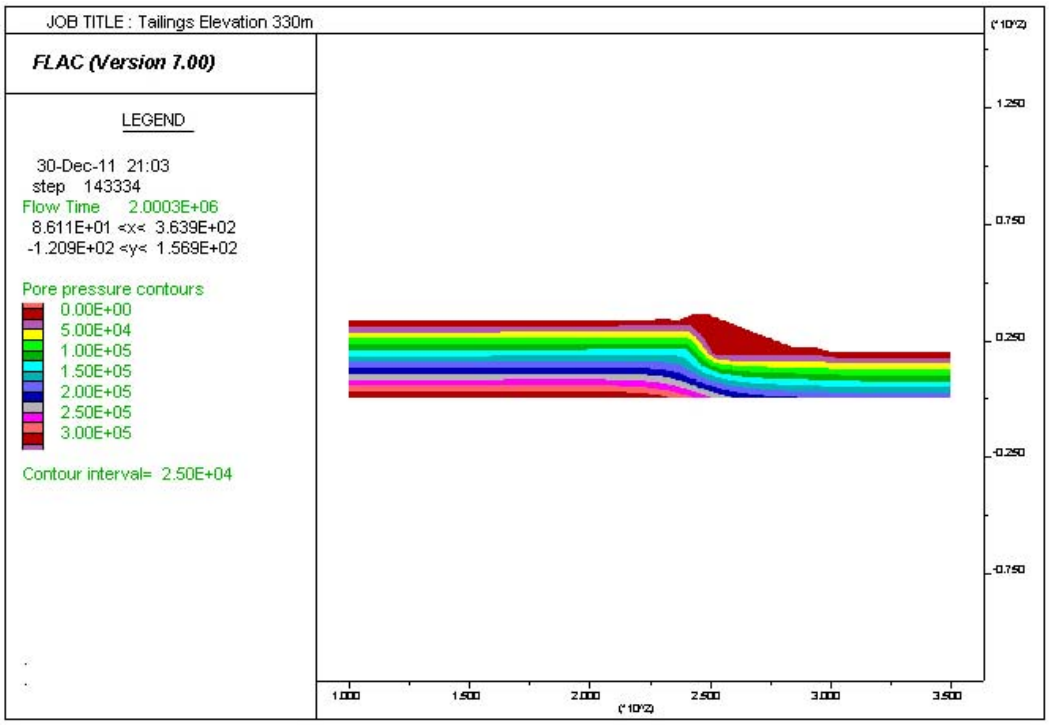

Figure 5-26: Pore pressure distribution at the end of the coupled analysis for tailings El. 330m

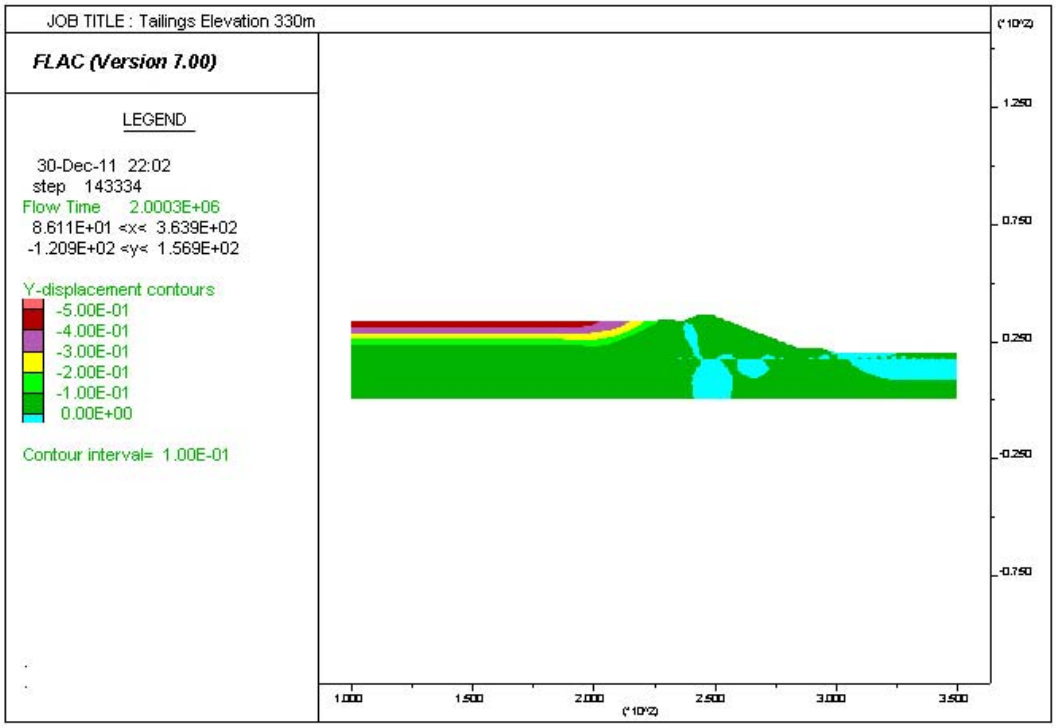

Figure 5-27: Vertical displacement increments at the end of the coupled analysis for tailings El. 330m

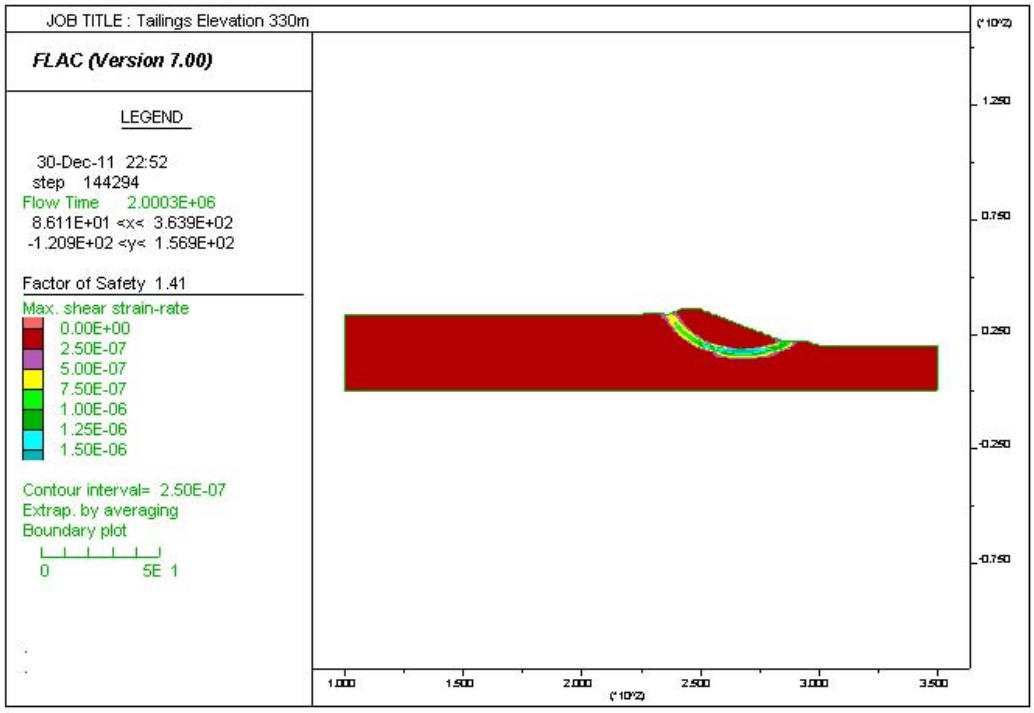

Figure 5-28: Maximum shear strain-rate contours at tailings El. 330m with FOS=1.41

5.3.6. DYKE

The output for the pore pressure distribution, vertical displacement and the maximum shear-strain contours is illustrated in Figure 5-29, Figure 5-30, and Figure 5-31 respectively. The calculated FOS remained unchanged at 1.41.

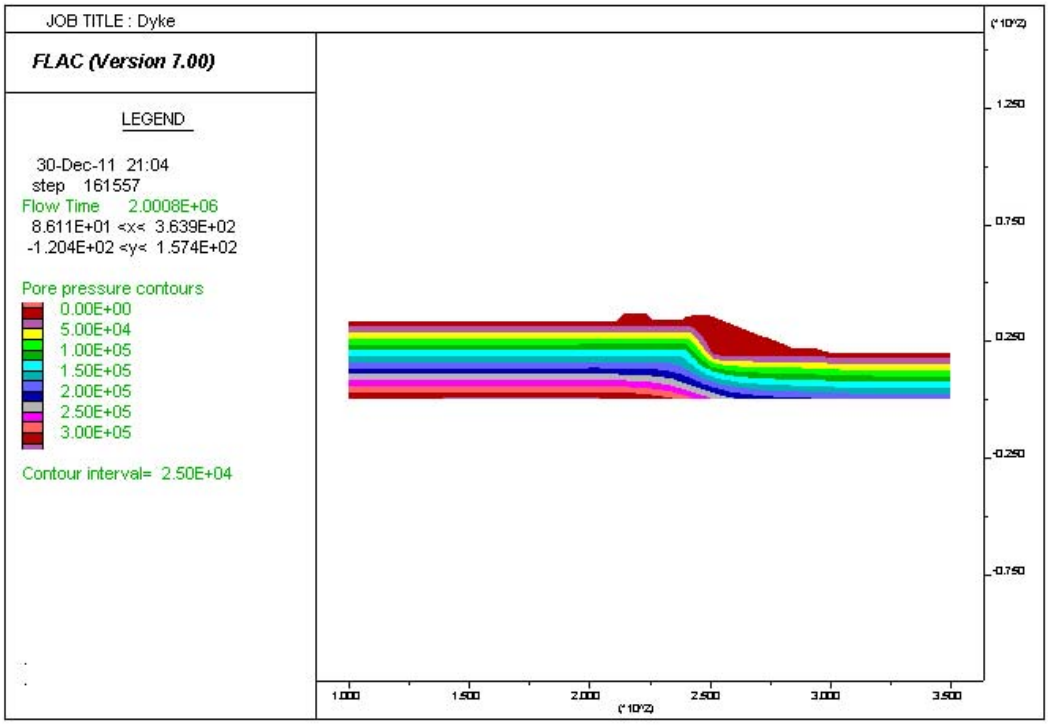

Figure 5-29: Pore pressure distribution at the end of the coupled analysis of dyke construction

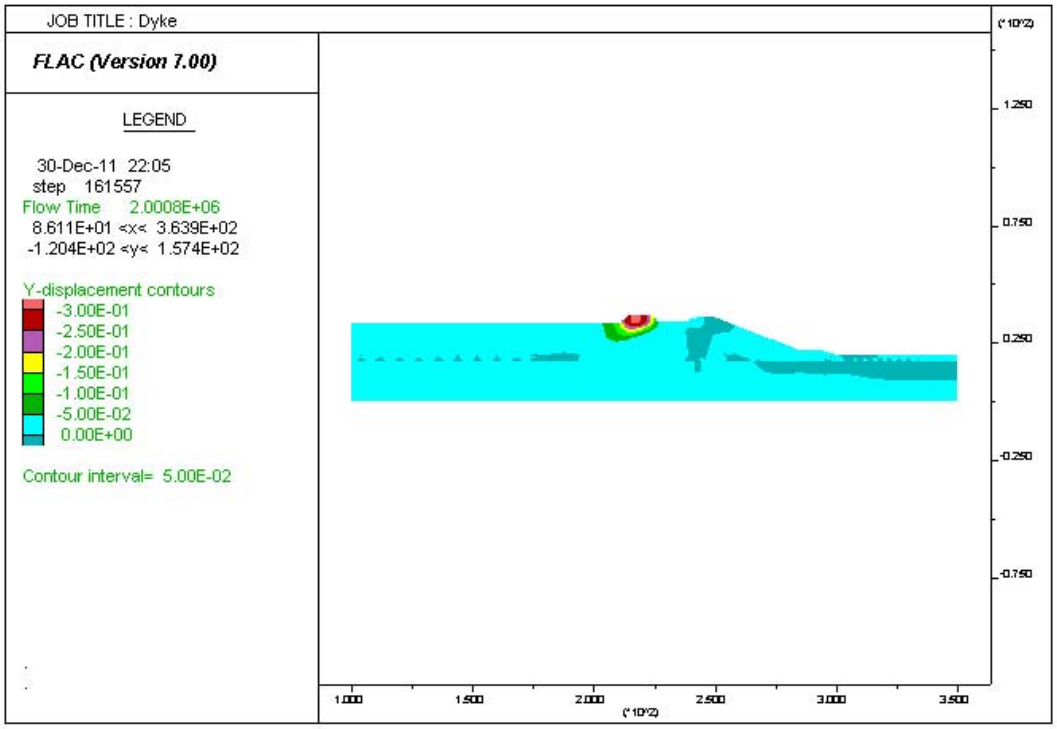

Figure 5-30: Vertical displacement increments at the end of the coupled analysis of dyke construction

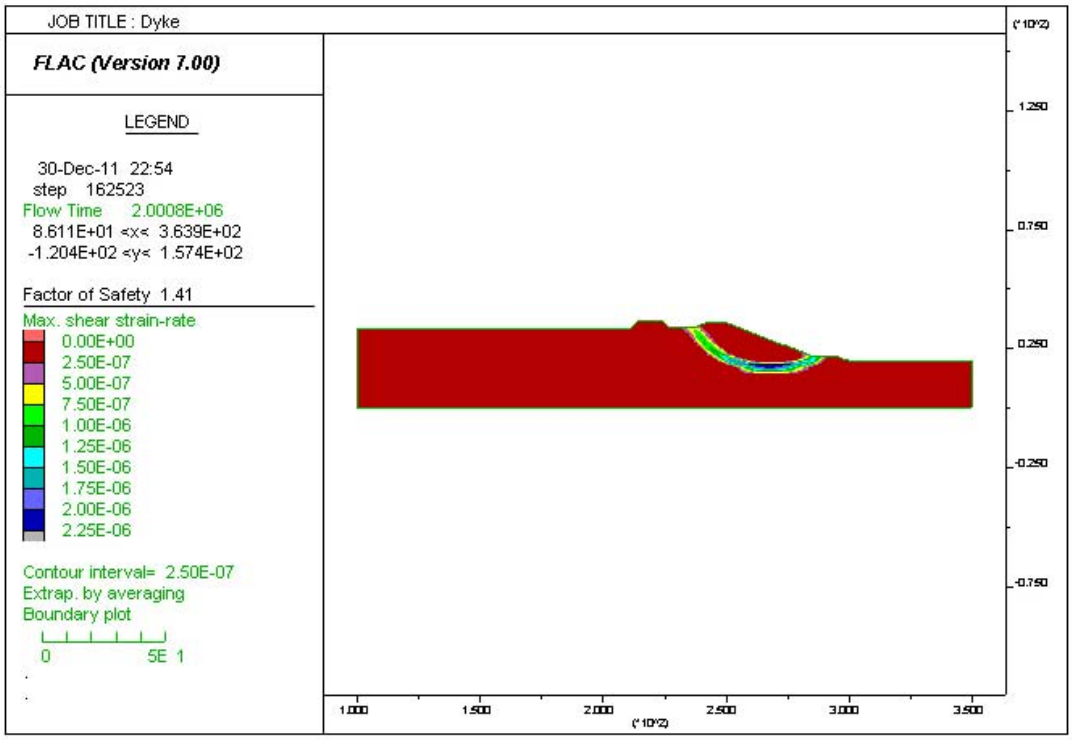

Figure 5-31: Maximum shear strain-rate contours at end of dyke construction with FOS=1.41

5.3.7. TAILINGS DEPOSITION TO ELEVATION 332M

The output for the pore pressure distribution, vertical displacement and the maximum shear-strain contours is illustrated in Figure 5-32, Figure 5-33, and Figure 5-34, respectively. The FOS drops to 1.31 after raising the tailings impoundment to El. 330m.

It is important to note that raising the impoundment by 2 meters, from El. 330m to El. 332m has resulted in a drop in the FOS from 1.41 to 1.31, which corresponds to a 7.1% decrease.

The dam's core continues to function as designed and is retaining the water volume with the impoundment reaching its maximum capacity of El. 332m (refer to Figure 5-32). Furthermore, the extent of the consolidation corresponding to the addition of the final 2m of tailings material is evident in Figure 5-33.

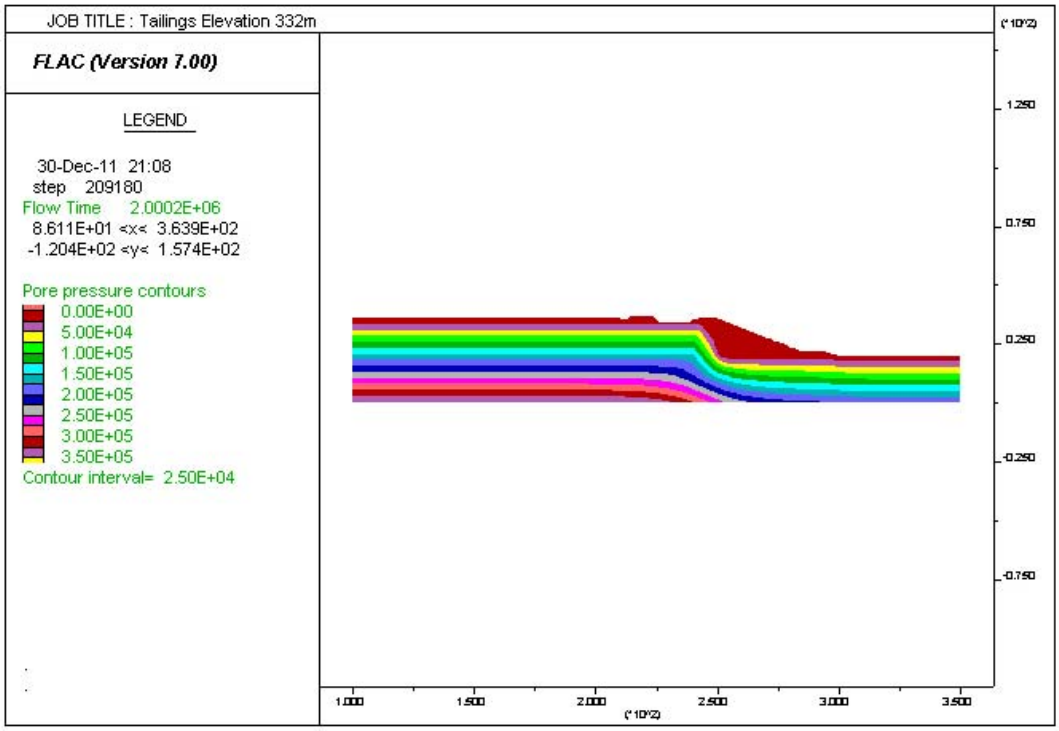

Figure 5-32: Pore pressure distribution at the end of the coupled analysis for tailings El. 332m

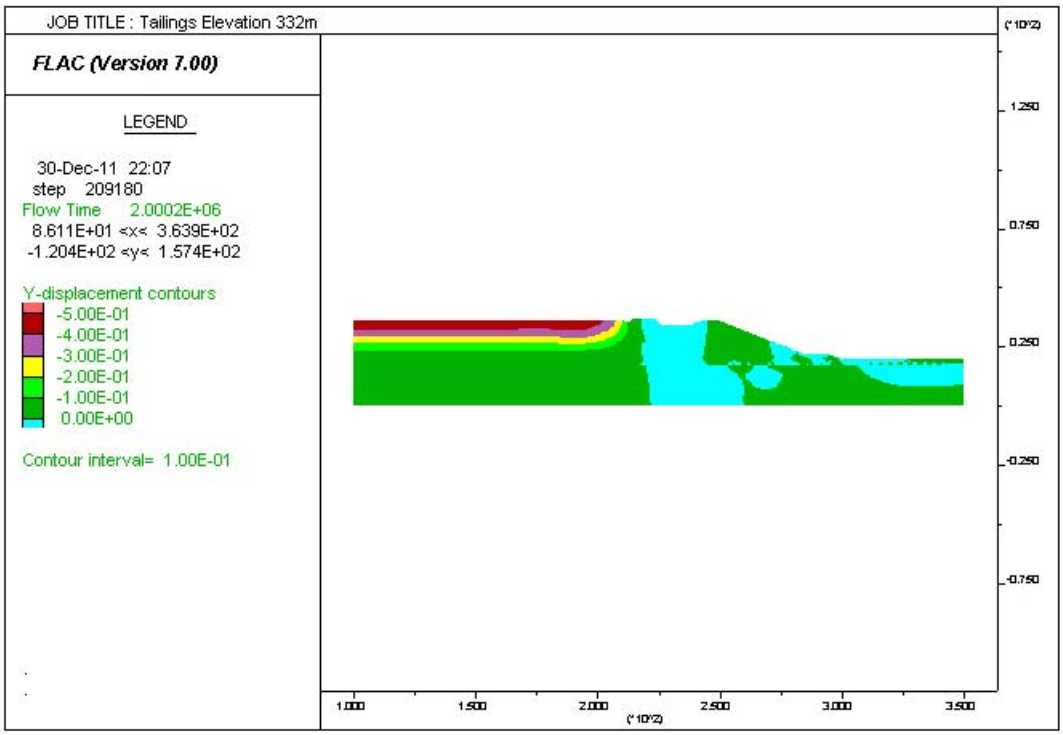

Figure 5-33: Vertical displacement increments at the end of the coupled analysis for tailings El. 332m

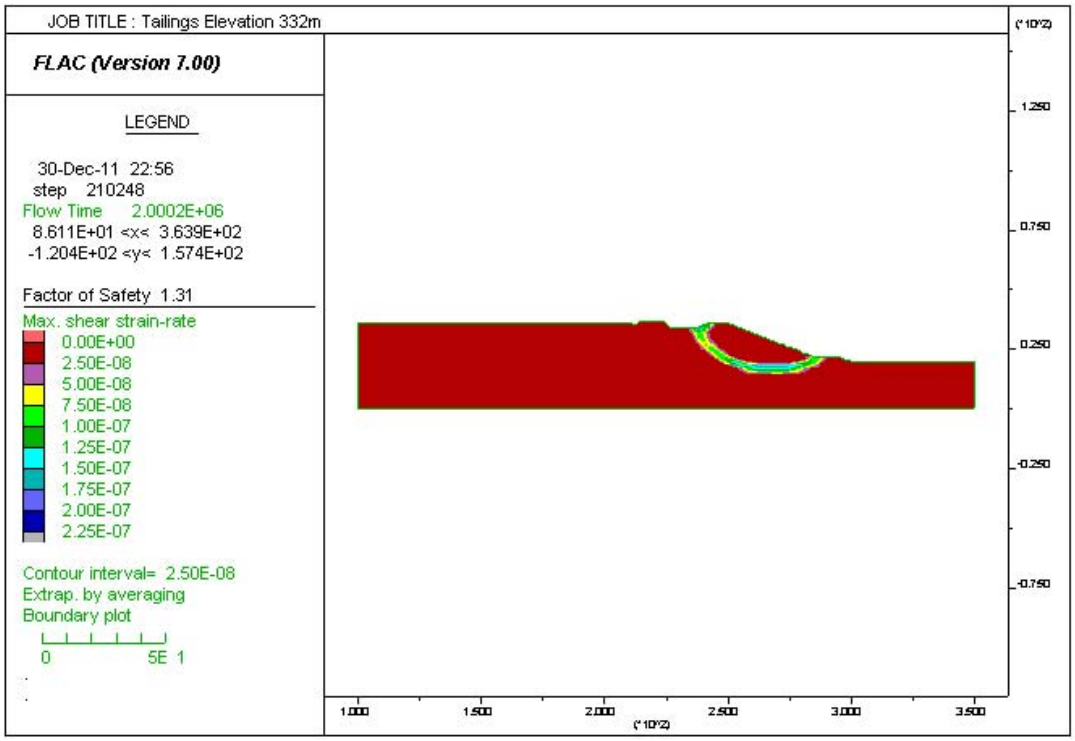

Figure 5-34: Maximum shear strain-rate contours at tailings El. 330m with FOS=1.31

5.3.8. SUMMARY

A summary of the tailings impoundment's FOS evolution over the different stages of construction and filling is presented in Table 5-2 and Figure 5-35. The global FOS for the tailings impoundments changes between 1.56 and 1.31 during its operation.

Table 5-2: Summary of impoundment's FOS at different stages with the percentage change in safety

STAGE	FOS	Percentage Change (%)
Dam	1.47	-
Tailings Elevation 320m	1.56	6.12
Tailings Elevation 324m	1.56	0
Tailings Elevation 328m	1.49	-4.49
Tailings Elevation 330m	1.41	-5.37
Dyke	1.41	0
Tailings Elevation 332m	1.31	-7.09

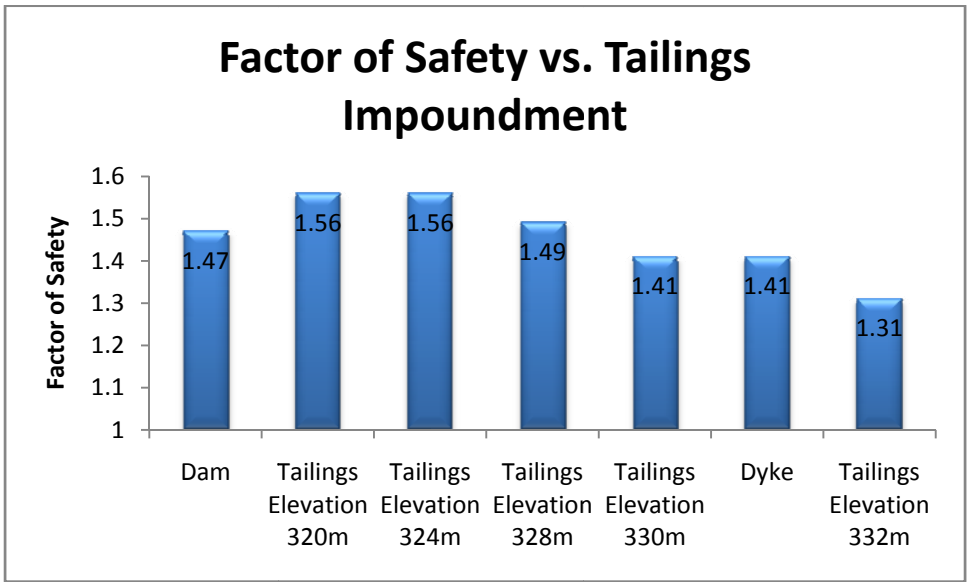

Figure 5-35: Factor of safety versus construction and filling of tailings impoundment

5.4 MODEL CALIBRATION & VALIDATION

All mechanical properties of the materials used in this study have been provided to the mine from a soil mechanics laboratory. Moreover, in the fall of 2010, the impoundment was filled up to elevation 324m and the water level was recorded in the piezometer well in the dam nearest to the cross-section (A-A) under study. This information was used to calibrate the permeability of the core material of the dam in the numerical model. As a result of the calibration, the location of the phreatic surface predicted in the model matches the recorded data on site. The calibrated value of the core permeability of the model is 1E-7 m/s.

The numerical model results correlate very well with those obtained from the work done by Saad and Mitri (2011) whereby minimal horizontal displacements was reported in their modelling of a gold tailings impoundment, which was constructed higher than the one modelled in this study.

5.5 LIMITATIONS OF HYDRO-MECHANICAL COUPLED MODEL

In this model, the filling of the tailings impoundment was done in stages; whereby, the first three lifts were 4 meters each and the last two lifts were 2 meters each for a total filling height of 16 meters. In reality, an impoundment is filled up gradually in increments that are smaller than 1 cm; however, modelling such gradient is computationally expensive. The current model run time averaged between one and two hours for each simulation. Modelling smaller lifts would naturally require more computation time; hence the choice for the 4m lift. Moreover, the smaller 2 meter lifts were left to the last two layers as this is when the height of the tailings impoundment becomes critical to the overall stability of the dam.

Furthermore, it was presented in this study that the shear strength parameters of the dam's core were the most influencing the impoundment's stability. And in the subsequent chapters, these shear strength parameters will be

considered as the stochastic variables for the probabilistic analysis. As such, the analysis is based on the assumption of isotropic strength parameters. However, it should be noted that anisotropy in the shear strength parameters influences the resulting factor of safety (Al-Karni and Al-Shamrani 2000). Moreover, the results of anisotropic analyses become increasingly significant relative to the isotropic results as the strength anisotropy increases (Dong, Tu et al. 2012).

CHAPTER : 6 CASE STUDY: MINE TAILINGS IMPOUNDMENT EXPANSION PROJECT – STOCHASTIC ANALYSIS

In the previous chapter, the deterministic stability analysis of a water retention tailings impoundment was demonstrated using the classical LEM approach as well as the advanced hydro-mechanical coupled approach with the FOS calculated using the SRT. In this chapter, different stochastic analysis techniques will be used to analyse the stability of the tailings impoundment by incorporating uncertainty in critical material input parameters.

First a brief overview of the classical statistical characteristics of soil properties is made. Then the Point Estimate Method (PEM) application to the case study tailings impoundment is presented, followed by an extensive Mont-Carlo (MC) analysis.

6.1 STATISTICAL CHARACTERISTICS OF SOIL PROPERTIES

In any deterministic analysis, every input parameter takes on a single value; however, in a stochastic analysis, stochastic variables take on a range of values defined by their respective probability density function (PDF). As such, stochastic or random variables are described by the following properties: Mean, variance, standard deviation, coefficient of variation, correlation factor and the PDF.

Considering the random variable denoted as *X*, then:

The mean is $E[X] = \mu_X = \int_{-\infty}^{+\infty} xf(x)dx$ and; (6-1)

The variance is $Var[X] = \sigma_X^2 = E[(X - \mu_X)^2] = \int_{-\infty}^{+\infty} (X - \mu_X)^2 f(x)dx$ (6-2)

The standard deviation is $\sigma_X = \sqrt{Var[X]}$ (6-3)

The coefficient of variation is $COV = \frac{\sigma_X}{\mu_X}$ (6-4)

If two random variables, *X* and *Y*, are correlated, then their correlation is described as follows:

The covariance of *X* and *Y* is $Cov[X,Y] = E[(X - \mu_X)(Y - \mu_Y)]$ (6-5)

The coefficient of correlation is $\rho_{XY} = \frac{Cov[X,Y]}{\sigma_X \sigma_Y}$, (6-6)

where $-1 \leq \rho_{XY} \leq +1$, and $\rho_{XY} = \pm 1$ indicating a positive or negative perfect correlation and $\rho_{XY} = 0$ reflecting their independence.

The most commonly used PDFs to describe random variables in geotechnical applications are the Normal and Lognormal distributions (Baecher and Christian 2003).

The PDF of a normal distribution with mean, μ, and standard deviation, σ, is:

$$f(x) = \frac{1}{\sigma\sqrt{2\pi}} \exp\left[-\frac{1}{2}\left(\frac{x-\mu}{\sigma}\right)^2\right] \quad (6\text{-}7)$$

It is important to note that although the limits of normal distribution are $-\infty$ to $+\infty$, 99.7% of the values will be distributed between -3σ and $+3\sigma$.

The PDF of a lognormal distribution with a mean, μ_X, and a standard deviation, σ_X, is:

$$f(x) = \frac{1}{x\sigma_{lnX}\sqrt{2\pi}} exp\left[-\frac{1}{2}\left(\frac{\ln(x)-\mu_{lnX}}{\sigma_{lnX}}\right)^2\right] \quad (6\text{-}8)$$

Where the natural logarithm, ln(*X*), is normally distributed and;

$\mu_{lnX} = ln\mu_X - \frac{1}{2}\sigma_{lnX}^2$ and $\sigma_{lnX} = \sqrt{\ln\,(1 + COV_X^2)}$

The main parameter that describes the extent of variability of a parameter in a soil system is the Coefficient of Variation (COV). The literature reports a range of COVs for different geotechnical parameters (Hoede-Keyser 1970; Singh 1971; Lumb 1974; Schultze 1975; Lee, White et al. 1983; Lacasse and Nadim 1996). The COV for both the angle of friction and the cohesion ranges from 10 to 50% with the choice of PDF varying between Normal or Lognormal. However, the soil's permeability is known to vary in orders of magnitude. Lumb (1974) reported permeability's COV of 200 to 300%. In a study that involved 57 sites, Benson (Benson 1993) reported values for the permeability's COV reaching over 700% with half the sites having a COV greater than 150%. The permeability's PDF is typically the Lognormal (Baecher and Christian 2003).

6.2 STOCHASTIC MODEL SETUP

In the previous chapter, the output of the deterministic analysis for the hydro-mechanical coupled model setup in *FLAC* was presented. In order to conduct a stochastic analysis, be it for the PEM or MC approach, it was imperative to develop computer codes that will automate the input and output process. The flow chart of this process is illustrated in Figure 6-1.

First a spreadsheet including the combinations of the pre-defined stochastic variables was created. As an example, if one were to run a MC simulation consisting of 1,000 simulations with the purpose of studying the effect of the dam's core angle of friction as a stochastic variable on the FOS output of the tailings impoundment at each stage, then this spreadsheet would consist of two columns, with the first identifying the run id and the second including the 1,000 randomly generated values for the dam's core angle of friction. Then a MATLAB code was developed that reads each row in this spreadsheet as an input and generates a data file including the new value for the dam's core angle of friction. As such, the MATLAB code would have generated 1,000 data files with each including a unique value for the dam's core angle of friction. Next, a FLAC FISH code (FLAC's programming language) was developed that will automatically pull

in each data file for simulation in *FLAC*. Furthermore, a FISH code was also embedded in the data file that will enable *FLAC* to record the FOS output at each stage and for every input data file into a log file. Then another computer code was developed using the programming language RUBY that will process the *FLAC* log file and tabulate the output in a spread sheet format. Finally @RISK is used to fit the PDFs for the FOS histogram outputs at every stage and for every run.

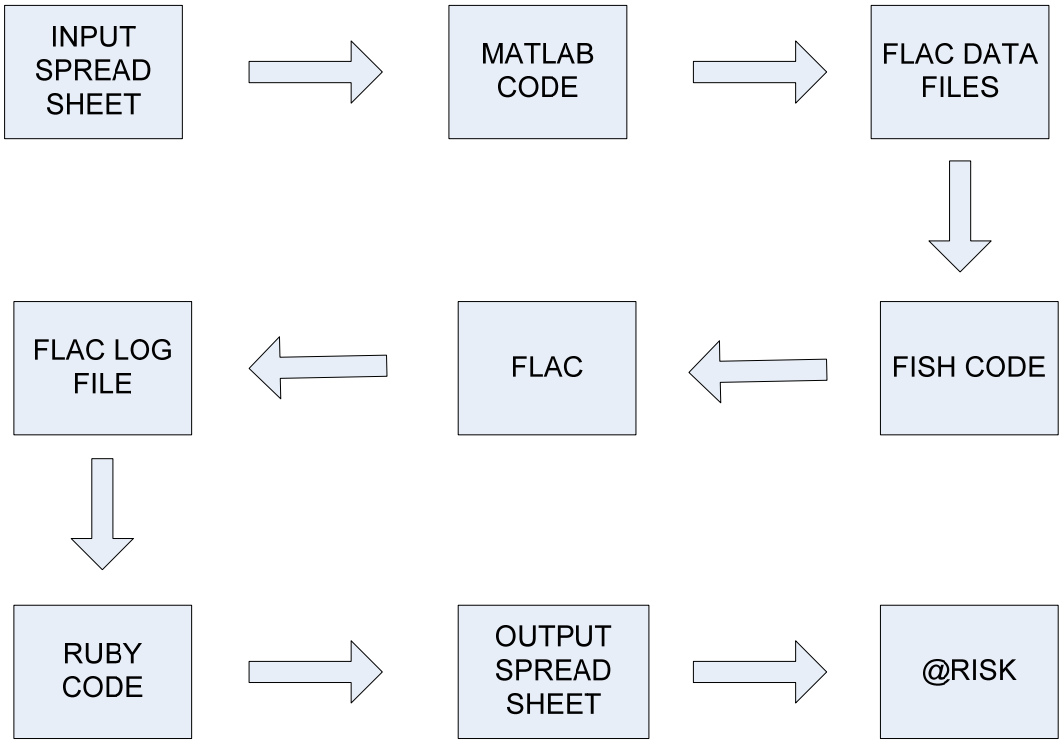

Figure 6-1: Stochastic model setup

6.3 THE POINT ESTIMATE METHOD (PEM)

The PEM is considered a first step in a complete stochastic analysis study given the minimal number of runs required relative to computationally exhaustive Monte-Carlo approach. A detailed overview of the PEM has been provided in Chapter 3. Moreover, the sensitivity analysis performed earlier showed that the dam's core angle of friction is the parameter most influencing the stability of the tailings impoundment. As a result, the dam's core shear strength parameters, the

angle of friction and the cohesion, and its permeability were chosen as stochastic variables for applying the PEM. It is important to note that the PEM does not factor in the type of PDF or Cumulative Density Function (CDF) for each stochastic variable.

Three sets of PEM analysis were performed according to the following input Table 6-1:

Table 6-1: COV combinations for each set of PEM analysis

	∅-COV (%)	c-COV (%)	k-COV (%)
PEM-1	15	15	50
PEM-2	30	30	50
PEM-3	45	45	50

6.3.1. PEM-1

In PEM-1, the following values for the COVs were considered: ∅-COV = c-COV = 15% and k-COV = 50%. As such, each variable was varied between its ±σ limits and the combination sets were defined as per Zhou and Nowak (Zhou and Nowak 1988).

The factor of safety histogram output at every stage was fitted with a Normal PDF and the individual output is presented in the Appendix A.

Figure 6-2 and Figure 6-3 illustrate the fitted Normal CDFs and PDFs at every stage for the output of the simulations, respectively. Furthermore, in Figure 6-3 the mean and standard deviation of the Normal PDF is presented.

Figure 6-4summarizes the PDFs at every stage by highlighting the mean, +/- standard deviation limits and the 5% - 95% boundary lines. Figure 6-5 replaces the 5% - 95% boundary lines with the whole range of Min - Max output. Note that Figure 6-5 does not factor in the frequency of the output; i.e. the range extends to a minimum FOS=1.18 with a frequency of 0.0001.The reliability and

Probability of Unsatisfactory Performance corresponding to FOS < 1 are presented in Table 6-2.

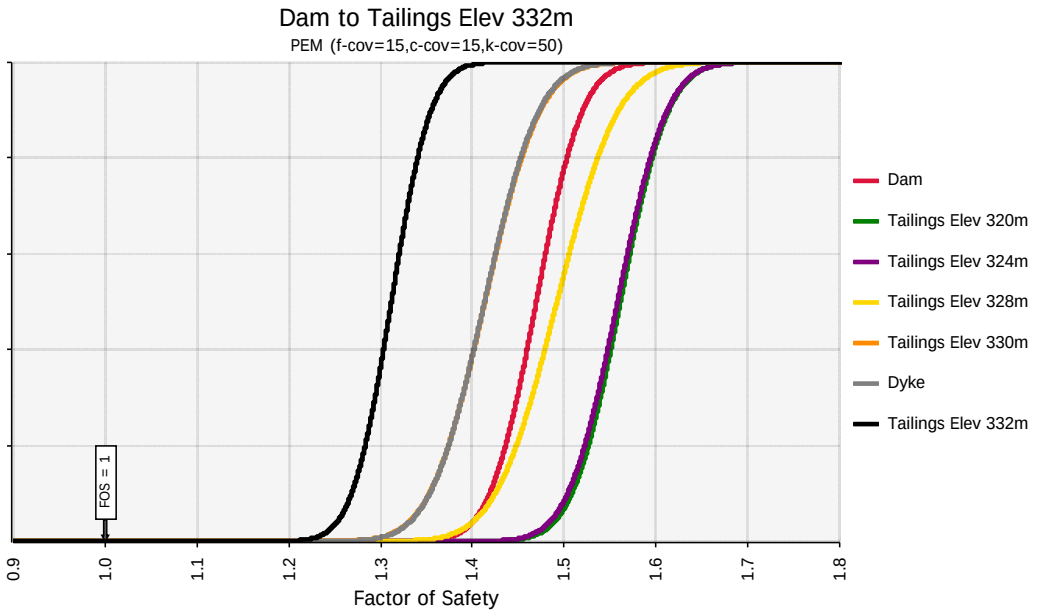

Figure 6-2: CDFs for all stages of PEM-1

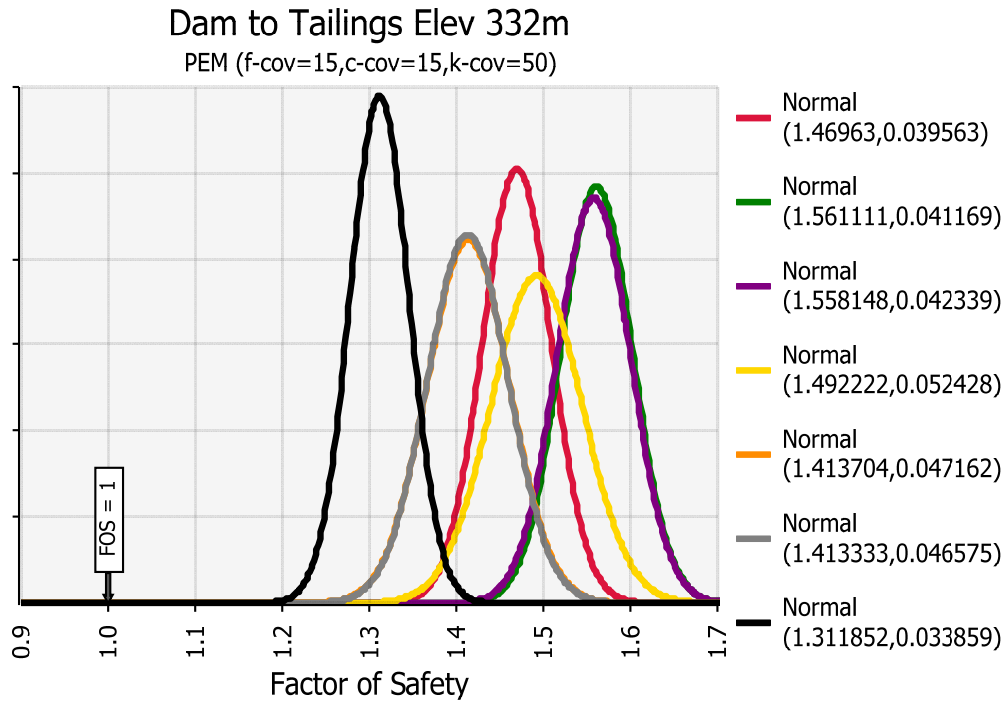

Figure 6-3: PDFs for all stages of PEM-1

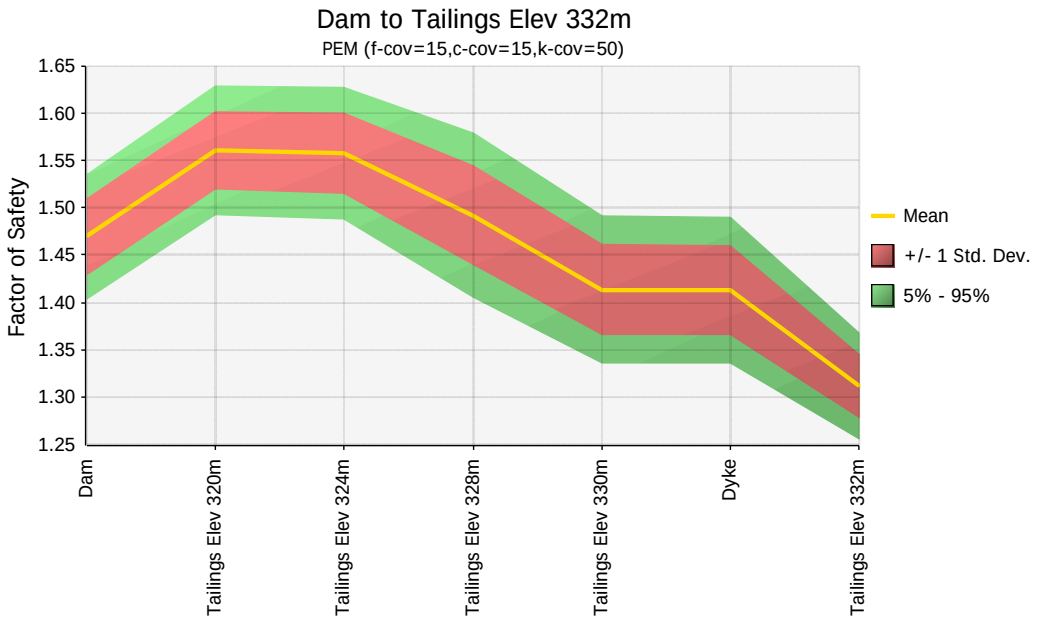

Figure 6-4: PEM-1 summary showing the Mean, +/- Std. Dev. and the 5% - 95% range

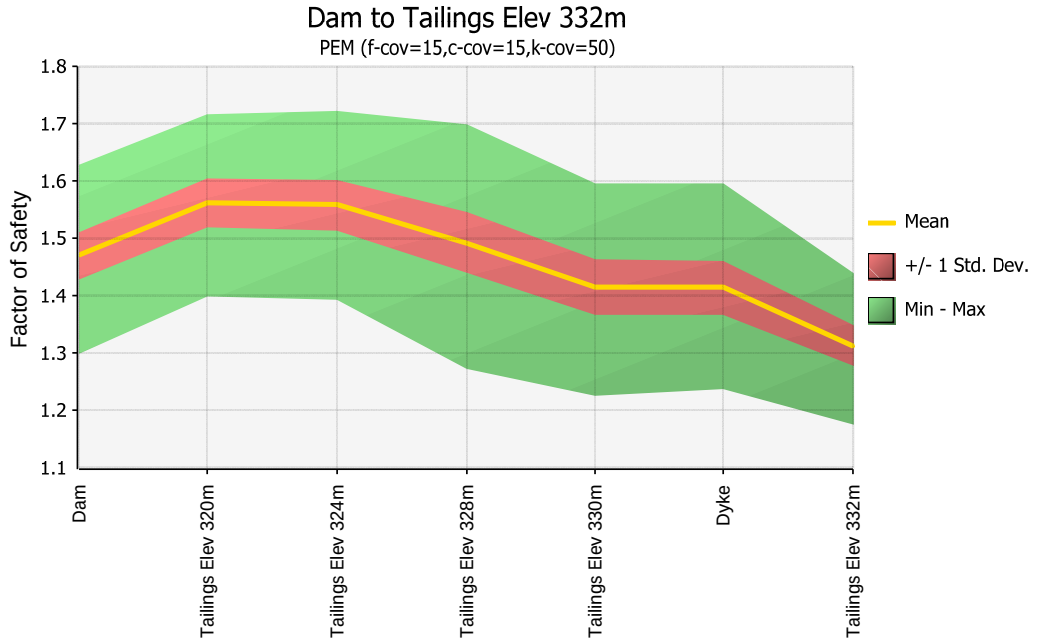

Figure 6-5: PEM-1 summary showing the Mean, +/- Std. Dev. and the Min - Max range of output

Table 6-2: PEM-1 Summary of the Reliability and Probability of Unsatisfactory Performance

PEM-1	MEAN	STDEV	Reliability	Probability of Unsatisfactory Performance
Dam	1.4696	0.0396	11.8704	0
Tailings Elev 320m	1.5611	0.0412	13.6295	0
Tailings Elev 324m	1.5581	0.0423	13.1828	0
Tailings Elev 328m	1.4922	0.0524	9.3885	0
Tailings Elev 330m	1.4137	0.0472	8.7720	0
Dyke	1.4133	0.0466	8.8746	0
Tailings Elev 332m	1.3119	0.0339	9.2103	0

6.3.2. PEM-2

In PEM-2, the following values for the COVs were considered: Ø-COV = c-COV = 30% and k-COV = 50%; and similarly each variable was varied between its ±σ limits and the combination sets were defined per Zhou and Nowak (Zhou and Nowak 1988).

The factor of safety histogram output at every stage was fitted with a Normal PDF and the individual output is presented in the Appendix A.

Figure 6-6 and Figure 6-7 illustrate the fitted Normal CDFs and PDFs at every stage for the output of the simulations, respectively.

Figure 6-8 summarizes the PDFs at every stage by highlighting the mean, +/- standard deviation limits and the 5% - 95% boundary lines. Figure 6-9 replaces the 5% - 95% boundary lines with the whole range of Min - Max output. The reliability and Probability of Unsatisfactory Performance results corresponding to FOS < 1 are presented in Table 6-3.

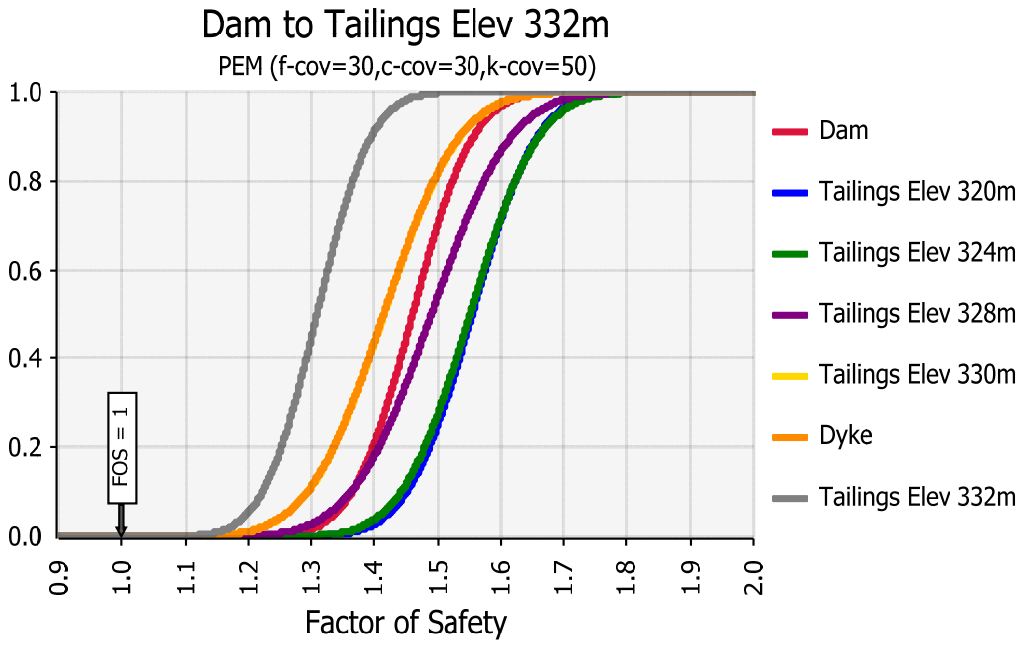

Figure 6-6: CDFs for all stages of PEM-2

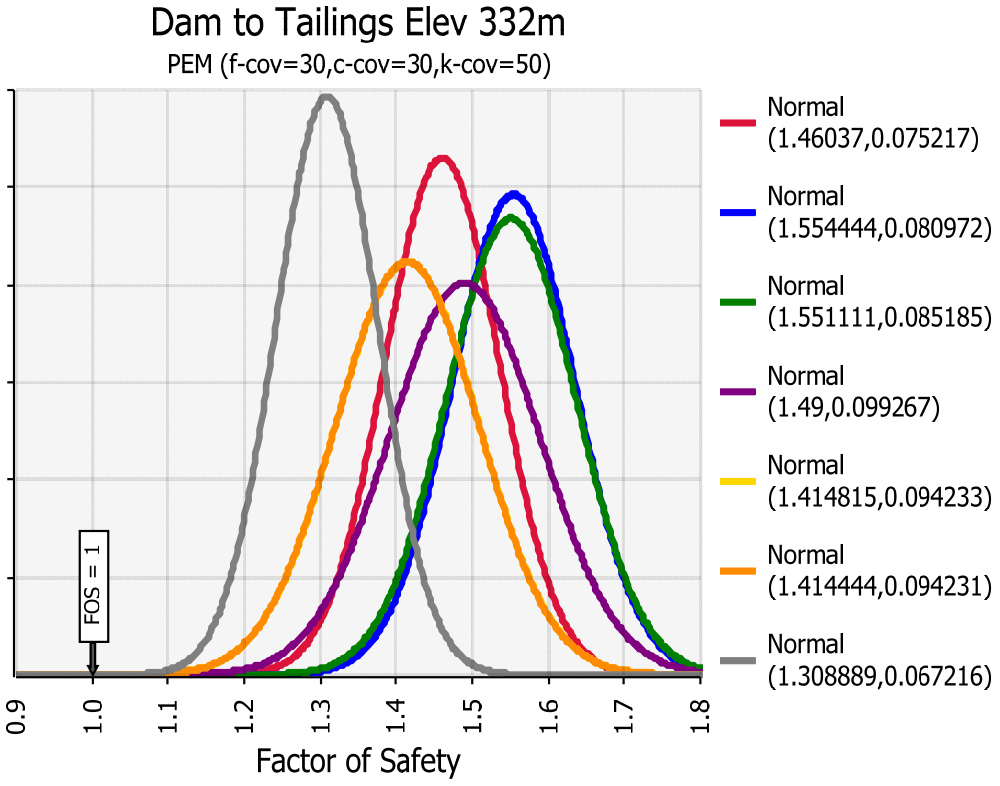

Figure 6-7: PDFs for all stages of PEM-2

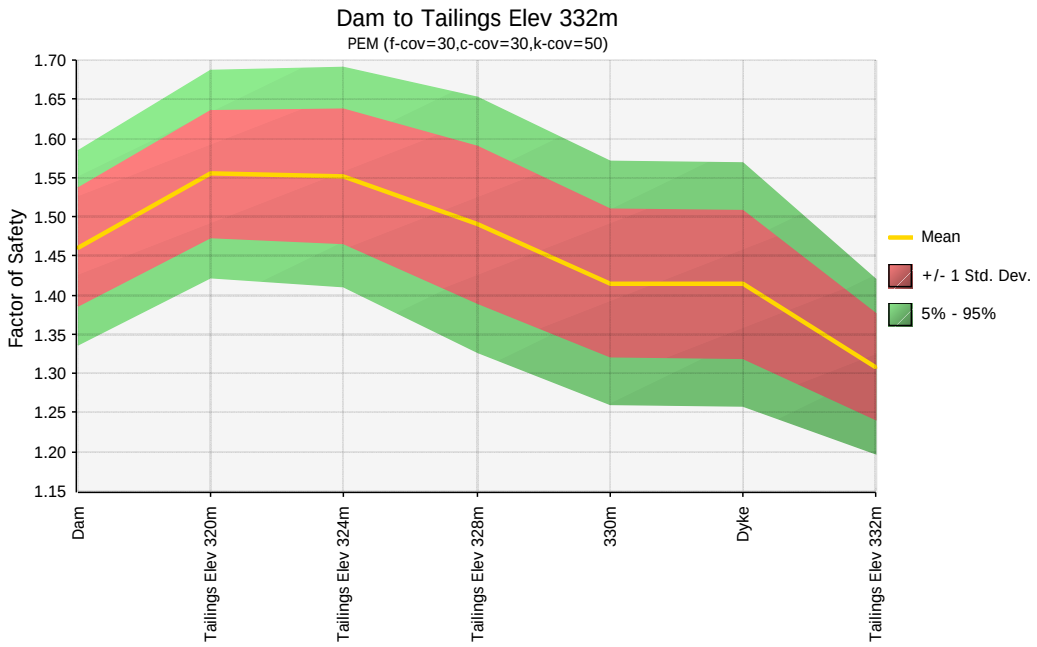

Figure 6-8: PEM-2 summary showing the Mean, +/- Std. Dev. and the 5% - 95% range

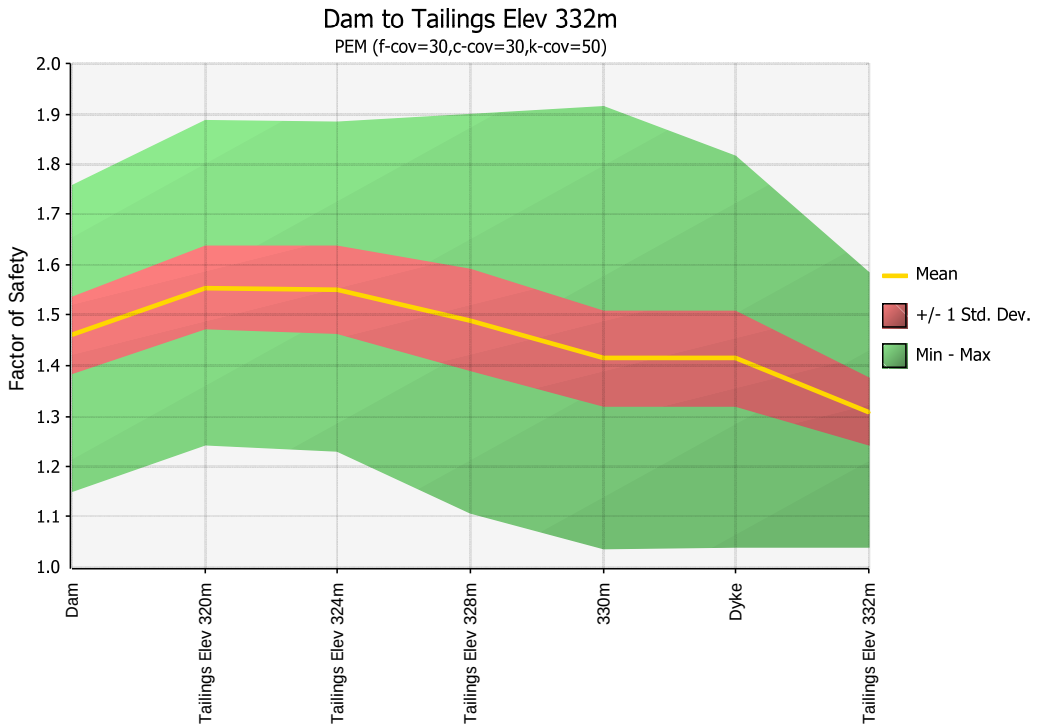

Figure 6-9: PEM-2 summary showing the Mean, +/- Std. Dev. and the Min - Max range of output

Table 6-3: PEM-2 summary of the Reliability and Probability of Unsatisfactory Performance

PEM-2	MEAN	STDEV	Reliability	Probability of Unsatisfactory Performance
Dam	1.460	0.075	6.121	0
Tailings Elev 320m	1.554	0.081	6.847	0
Tailings Elev 324m	1.551	0.085	6.470	0
Tailings Elev 328m	1.490	0.099	4.936	0
Tailings Elev 330m	1.415	0.094	4.402	0
Dyke	1.414	0.094	4.398	0
Tailings Elev 332m	1.309	0.067	4.595	0

6.3.3. PEM-3

In PEM-3, the following values for the COVs were considered: Ø-COV = c-COV = 45% and k-COV = 50% and similarly each variable was varied between its ±σ limits and the combination sets were defined per the propositions by Zhou and Nowak (Zhou and Nowak 1988).

The factor of safety histogram output at every stage was fitted with a Normal PDF and the individual output is presented in the Appendix A.

Figure 6-10 and Figure 6-11illustrate the fitted Normal CDFs and PDFs at every stage for the output of the simulations, respectively.

Figure 6-12 summarizes the PDFs at every stage by highlighting the mean, +/- standard deviation limits and the 5% - 95% boundary lines. Figure 6-13 replaces the 5% - 95% boundary line with the whole range of Min - Max output. The reliability and Probability of Unsatisfactory Performance results corresponding to FOS < 1 are presented in Table 6-4.

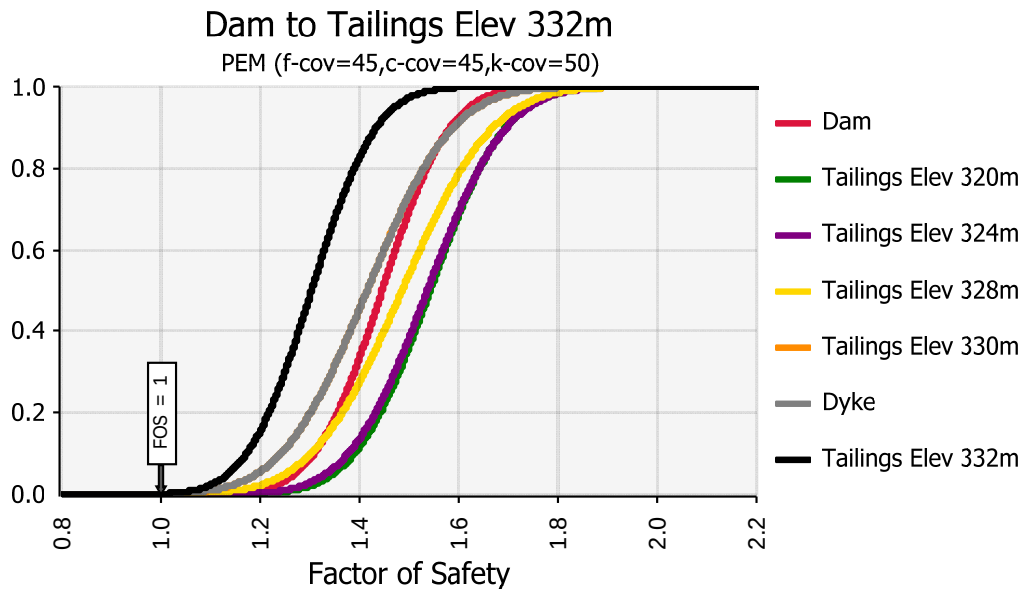

Figure 6-10: CDFs for all stages of PEM-3

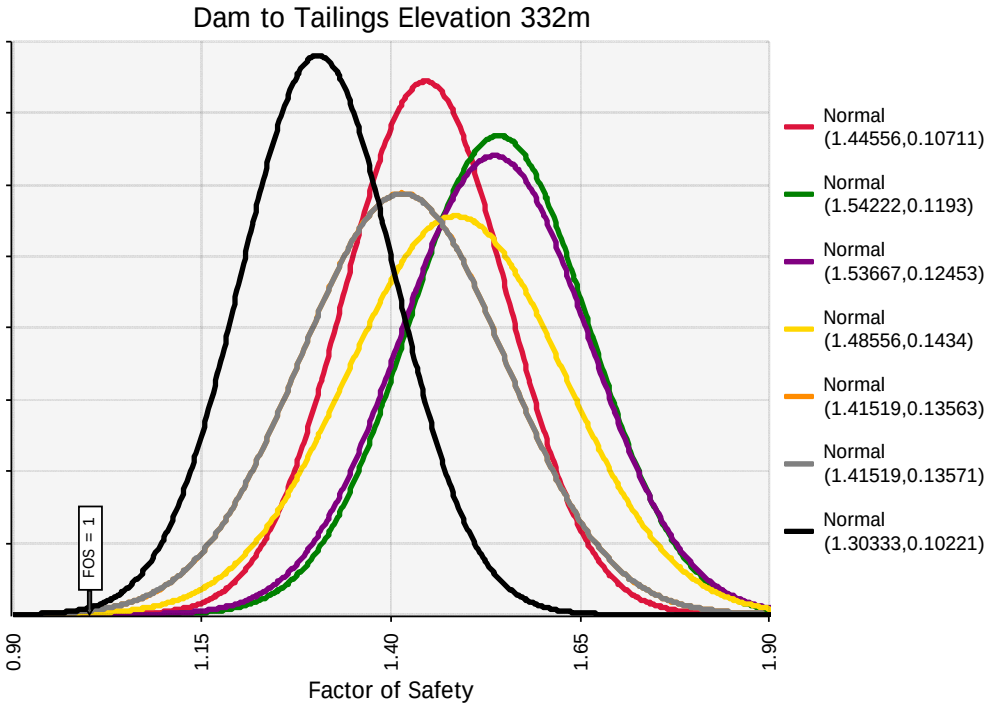

Figure 6-11: PDFs for all stages of PEM-3

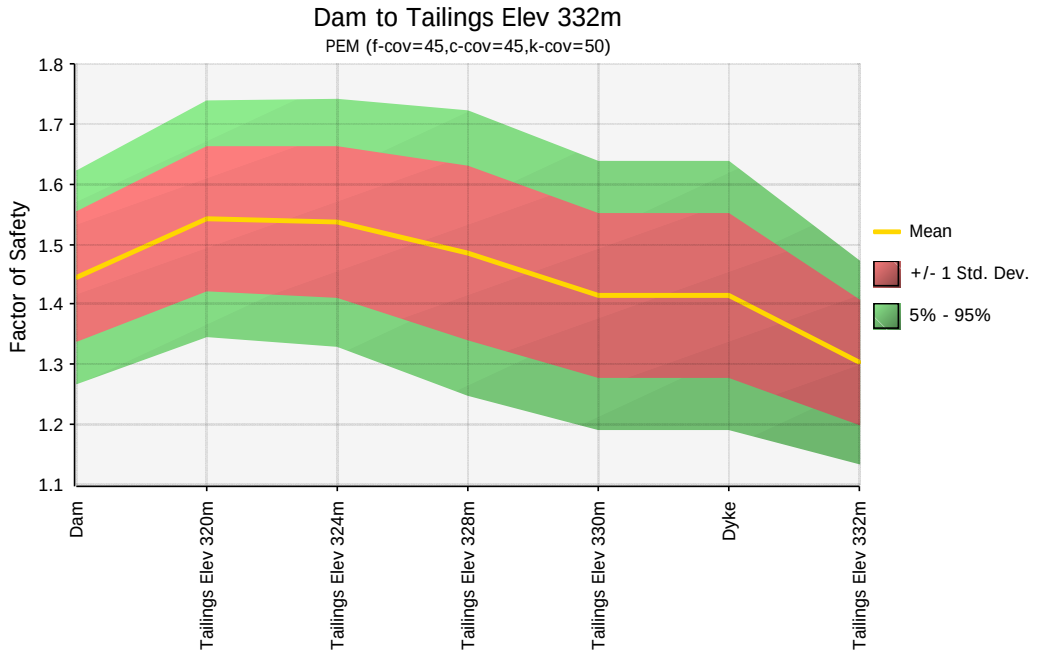

Figure 6-12: PEM-3 summary showing the Mean, +/- Std. Dev. and the 5% - 95% range

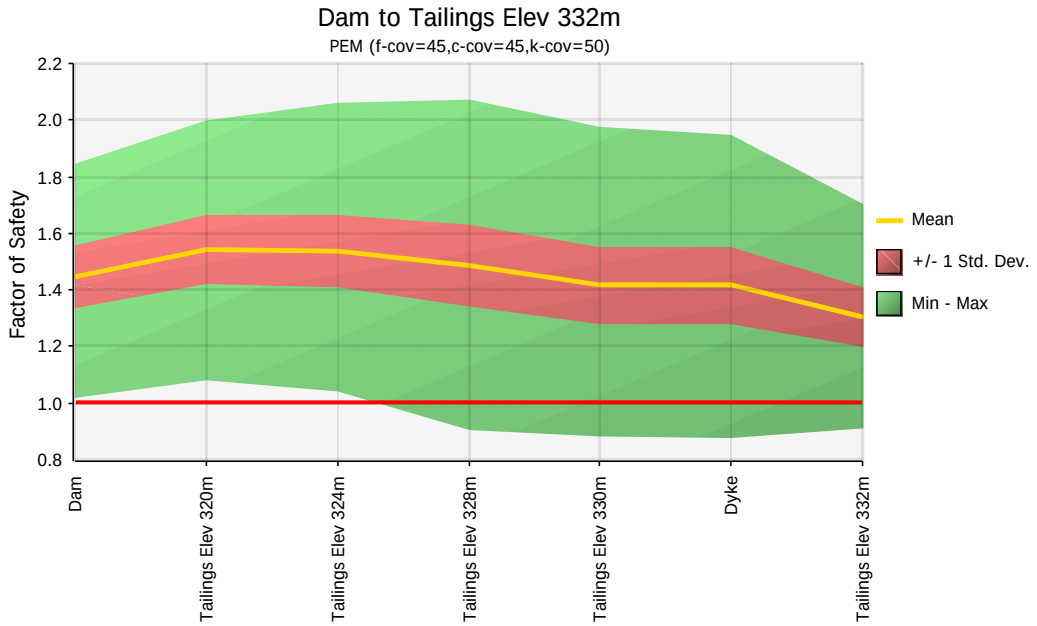

Figure 6-13: PEM-3 summary showing the Mean, +/- Std. Dev. and the Min - Max range of output

Table 6-4: PEM-3 summary of the Reliability and Probability of Unsatisfactory Performance

PEM-3	MEAN	STDEV	Reliability	Probability of Unsatisfactory Performance
Dam	1.446	0.107	4.160	0
Tailings Elev 320m	1.542	0.119	4.545	0
Tailings Elev 324m	1.537	0.125	4.310	0
Tailings Elev 328m	1.486	0.143	3.386	0.0004
Tailings Elev 330m	1.415	0.136	3.061	0.0011
Dyke	1.415	0.136	3.059	0.0011
Tailings Elev 332m	1.303	0.102	2.968	0.0015

6.3.4. PEM SUMMARY

Figure 6-14 presents the mean of the FOS PDFs for all the PEMs. It is evident that the mean barely changes across the PEMS for every stage. However, observing the standard deviations in Figure 6-15 shows that the maximum increase in the standard deviation takes place in PEM-3. Moreover, the trend in the standard deviation increases from the Dam stage to Tailings Elevation 328m and then decreases to Tailings Elevation 332m. This is a very important finding, since the influence of a higher variability in the input parameter diminished at the maximum capacity of the impoundment relative to the filling stages.

Furthermore, as would have been expected, the reliability index is the lowest for PEM-3, which has the highest probability of unsatisfactory performance. However, such values for the reliability index correspond to an above average expected performance level as defined by the U.S. Army Corps of Engineers (USACE 1997).

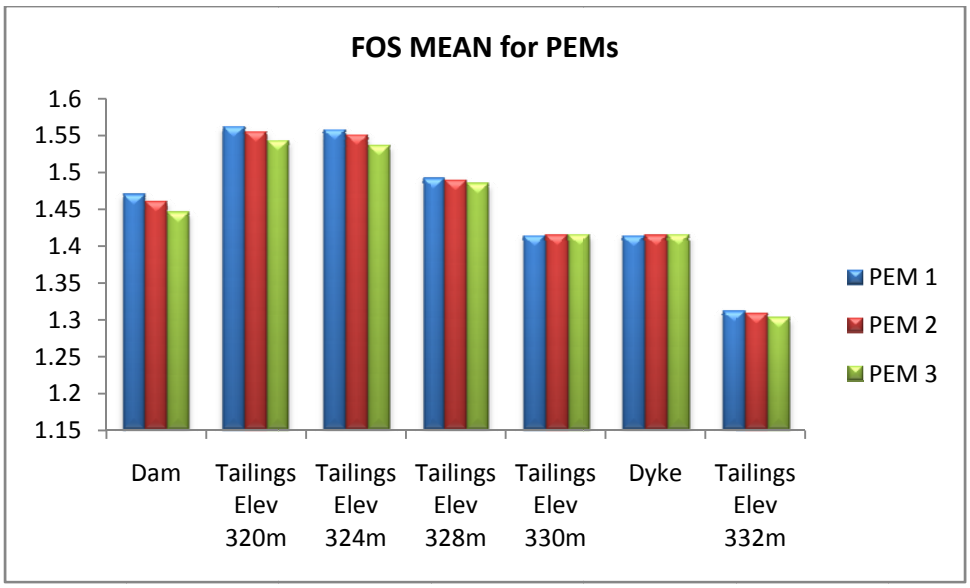

Figure 6-14: Mean of the FOS PDFs at every stage for all PEMs

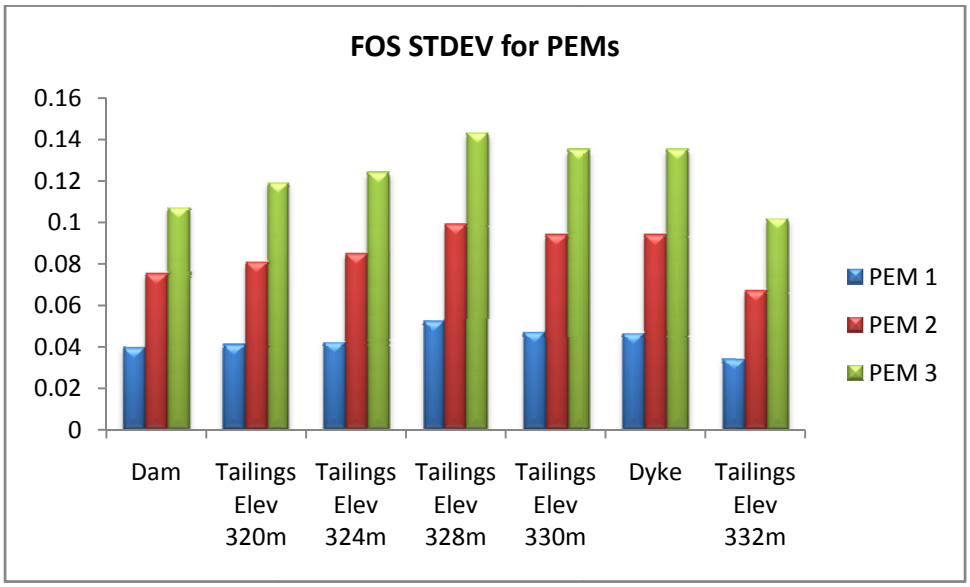

Figure 6-15: Standard deviation of the FOS PDFs at every stage for all PEMs

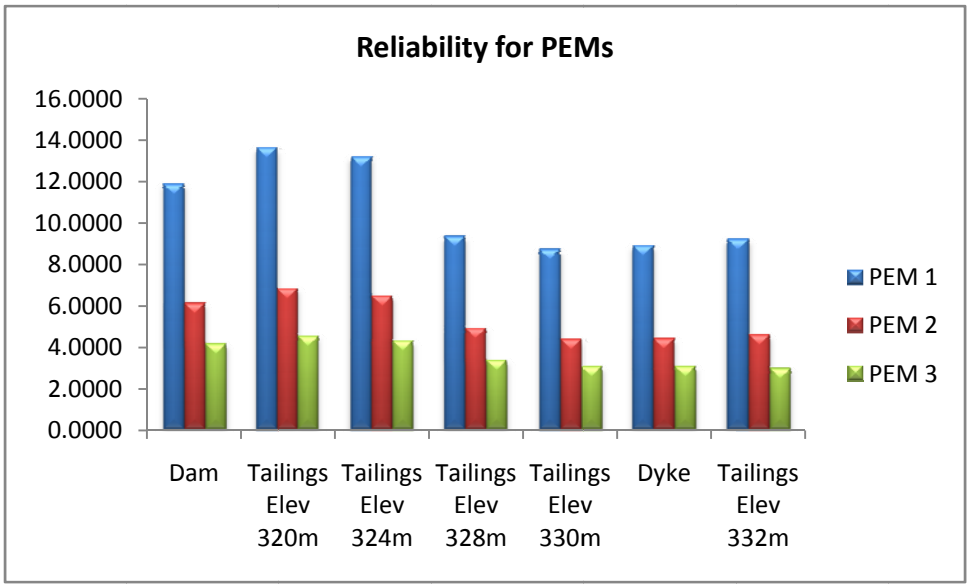

Figure 6-16: Reliability values at every stage for all PEMs

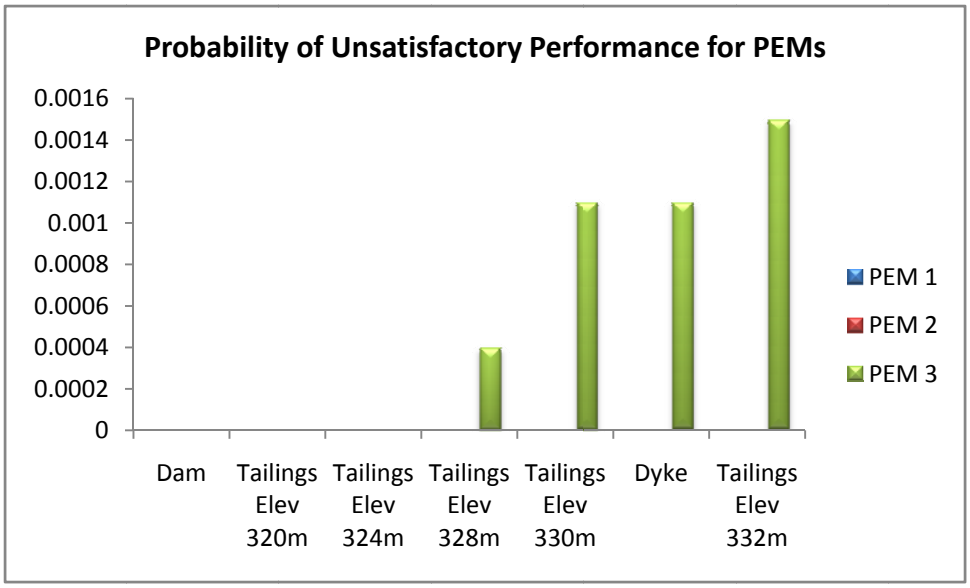

Figure 6-17: Probability of Unsatisfactory Performance at every stage for all PEMs

6.4 MONTE-CARLO (MC) AND RANDOM MONTE-CARLO (RMC) METHODS

In this section, the stochastic analysis is taken a few steps further by exploring the use of both the MC and RMC methods in analyzing the stability of this specific case study.

6.4.1. NORMAL VERSUS LOGNORMAL PDF FOR DAM'S CORE ∅

Before one undertakes an extensive analysis, it is crucial to explore the influence of the input stochastic variable's PDF on the FOS PDF output. Moreover, it is known that the more MC runs performed the more accurate are the results; however, for the purpose of this complex coupled analysis, it is imperative that one establishes a threshold for the number of runs that will not compromise the accuracy of the output while being sufficient enough to reflect the behaviour of the model.

In this section the output of the analysis from assuming the dam's core angle of friction taking on a Normal and Lognormal PDF is compared. Based on the simulation time and the output obtained from the PEM, it was decided that 1,000 runs should serve as an upper bound for the future MC simulations. Furthermore, a Φ-COV=30% was used for this comparative analysis.

6.4.1.1 Normal PDF for Dam's core ∅

The factor of safety histogram output at every stage was fitted with a Normal PDF and the individual output is presented in the Appendix A. Figure 6-18 and Figure 6-19 illustrate the fitted Normal CDFs and PDFs at every stage for the output of the simulations, respectively. Figure 6-20 summarizes the PDFs at every stage by highlighting the mean, +/- standard deviation bracket and the 5% - 95% range. Figure 6-21 replaces the 5% - 95% range with the whole range of Min - Max output. The reliability and Probability of Unsatisfactory Performance results corresponding to FOS < 1 are presented in Table 6-5.

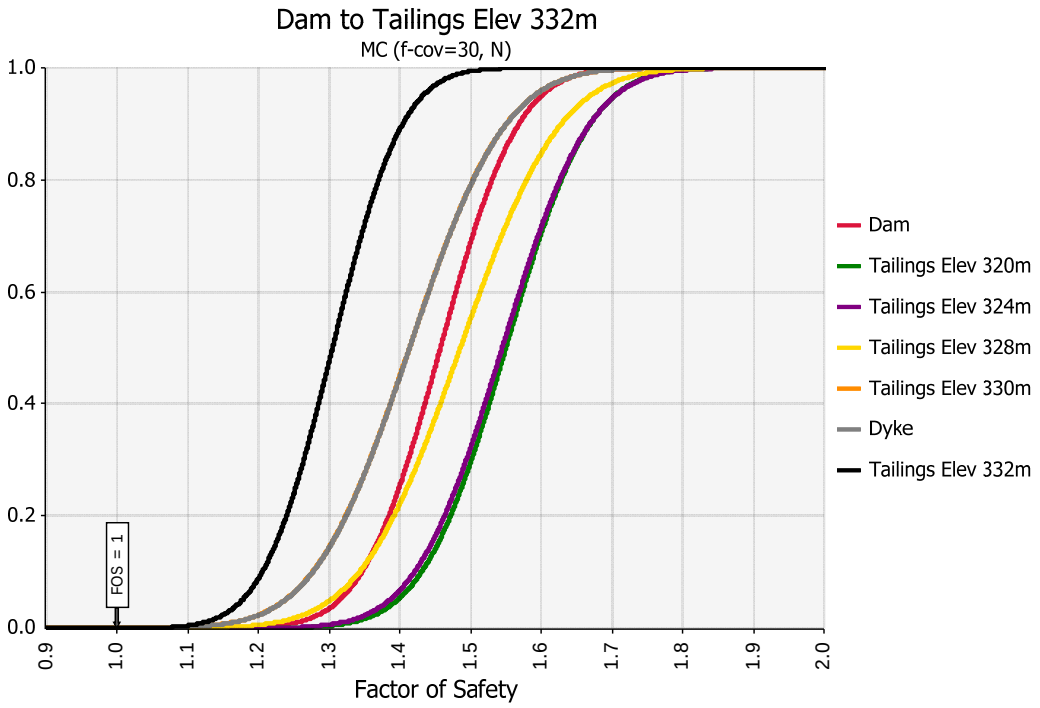

Figure 6-18:CDFs of all stages given a Normal PDF input for ∅

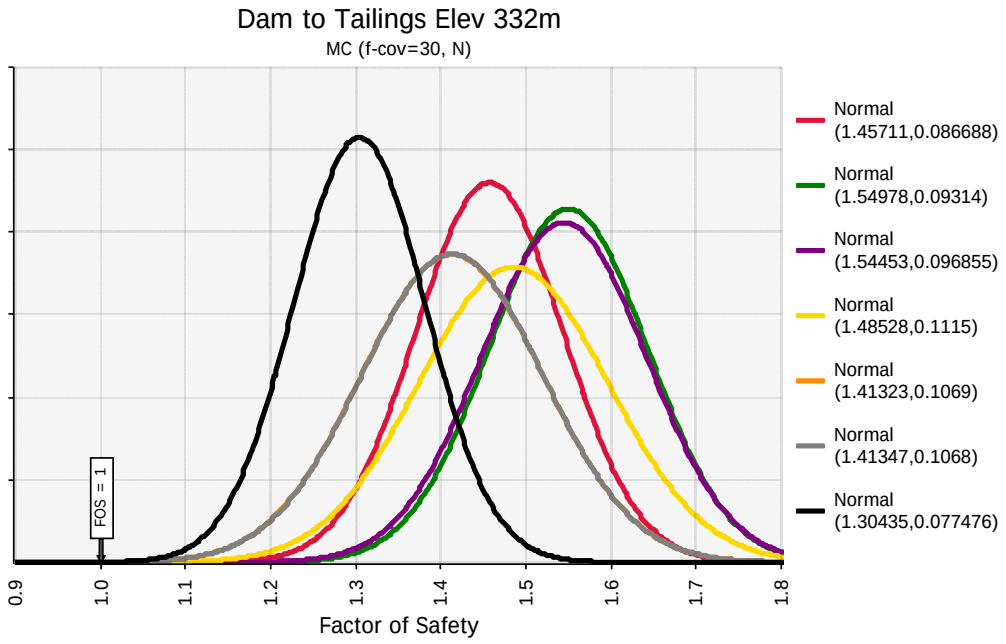

Figure 6-19: PDFs for all stages given a Normal PDF input for ∅

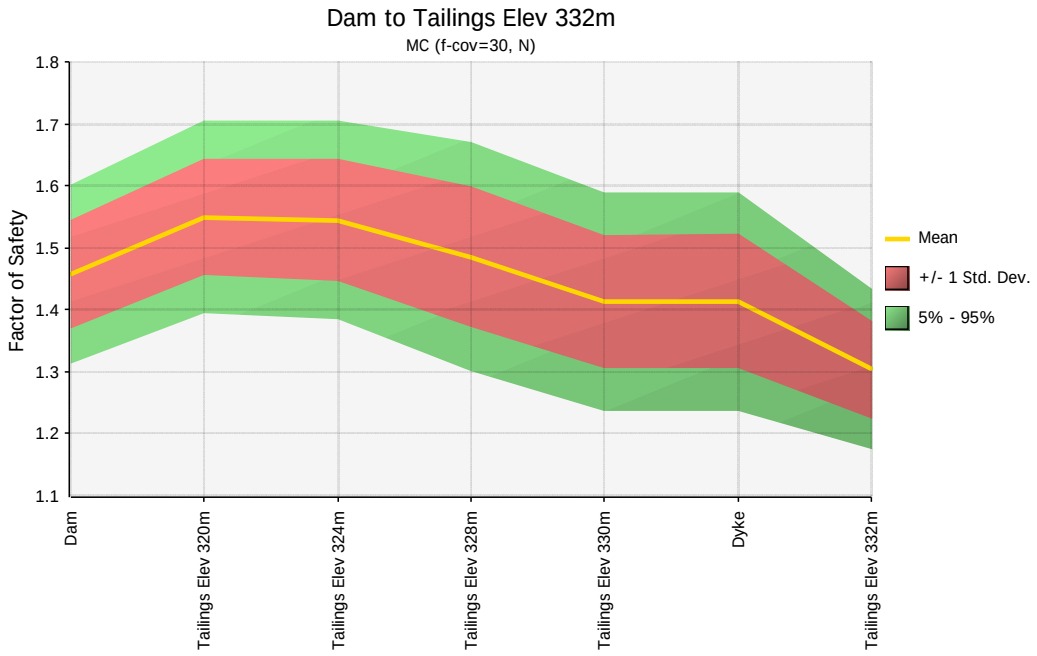

Figure 6-20: Summary showing the Mean, +/- Std. Dev. and the 5% - 95% range given a Normal PDF input for Ø

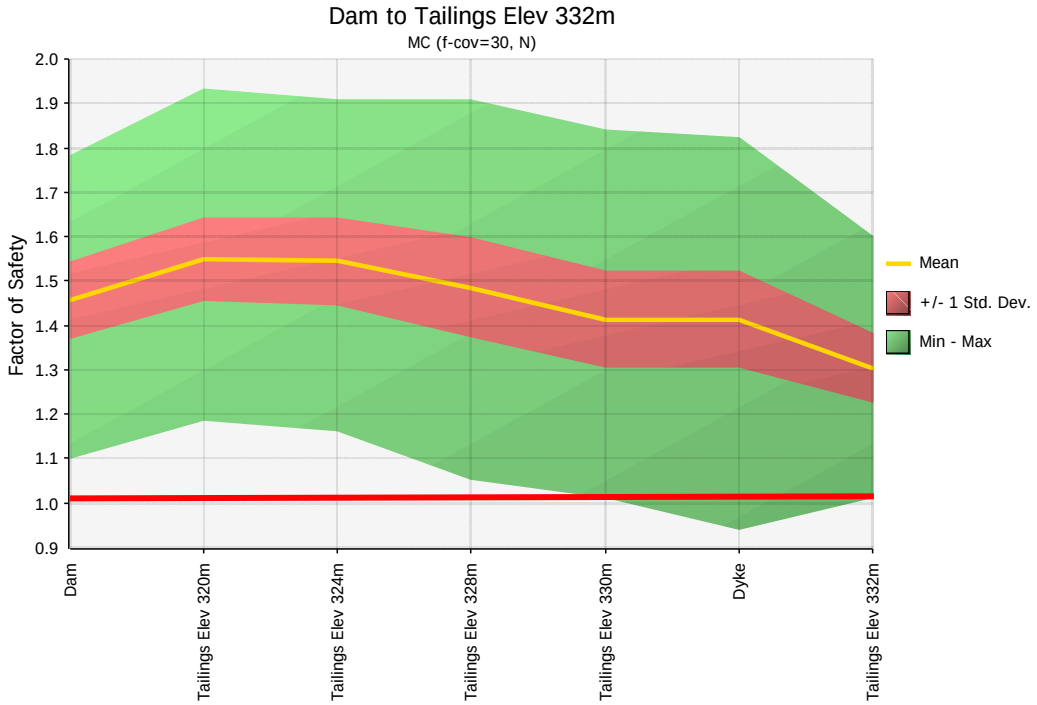

Figure 6-21: Summary showing the Mean, +/- Std. Dev. and the Min - Max range of output given a Normal PDF input for Ø

Table 6-5: Summary of the Reliability and Probability of Unsatisfactory Performance given a Normal PDF input for Φ

MC Normal PDF ∅ 1,000 runs	MEAN	STDEV	Reliability	Probability of Unsatisfactory Performance
Dam	1.457	0.087	5.273	0
Tailings Elev 320m	1.550	0.093	5.903	0
Tailings Elev 324m	1.545	0.097	5.622	0
Tailings Elev 328m	1.485	0.112	4.352	0
Tailings Elev 330m	1.413	0.107	3.866	0.000055
Dyke	1.413	0.107	3.871	0.00005
Tailings Elev 332m	1.304	0.077	3.928	0.00004

6.4.1.2 LogNormal PDF for Dam's core ∅

The factor of safety histogram output at every stage was fitted with a LogNormal PDF and the individual output is presented in the Appendix A. Figure 6-22 and Figure 6-23 illustrate the fitted Normal CDFs and PDFs at every stage for the output of the simulations, respectively. Figure 6-24 summarizes the PDFs at every stage by highlighting the mean, +/- standard deviation limits and the 5% - 95% boundary lines. Figure 6-25 replaces the 5% - 95% boundary line with the whole range of Min - Max output. The reliability and Probability of Unsatisfactory Performance results corresponding to FOS < 1 are presented in Table 6-6.

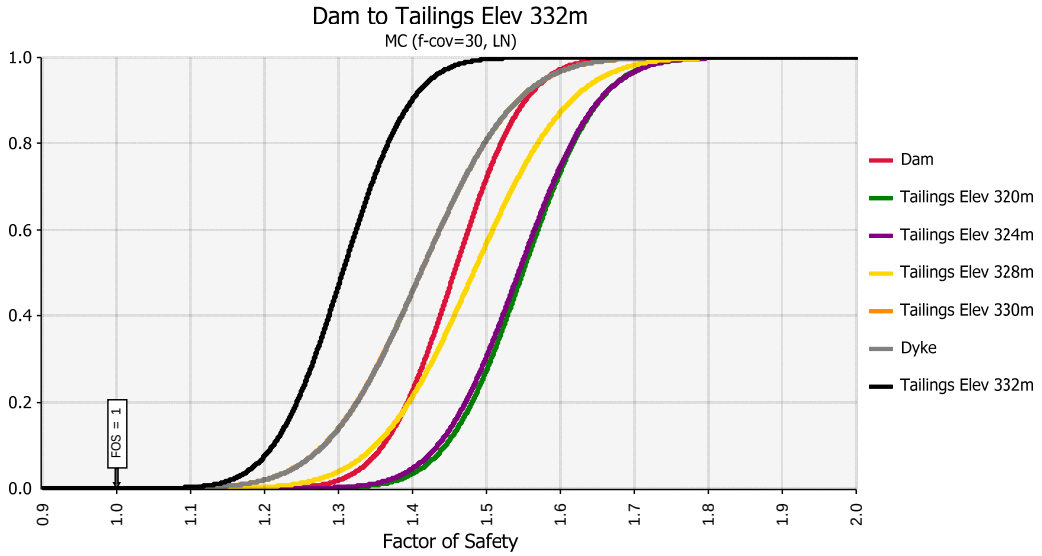

Figure 6-22: CDFs for all stages given a LogNormal PDF input for Ø

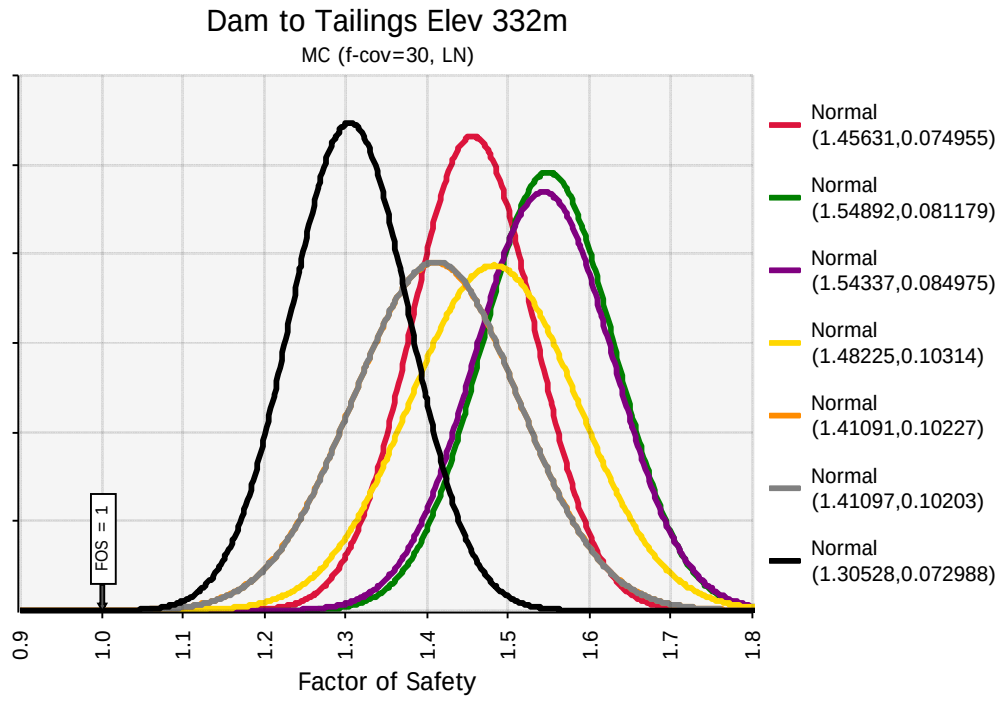

Figure 6-23: PDFs for all stages given a LogNormal PDF input for Ø

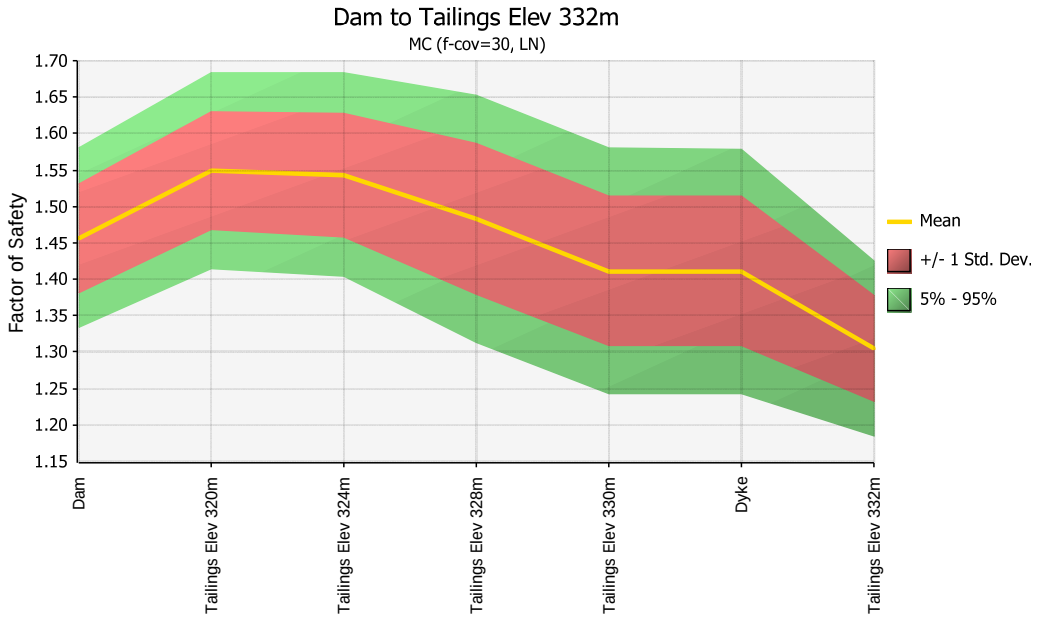

Figure 6-24: Summary showing the Mean, +/- Std. Dev. and the 5% - 95% range given a LogNormal PDF input for Ø

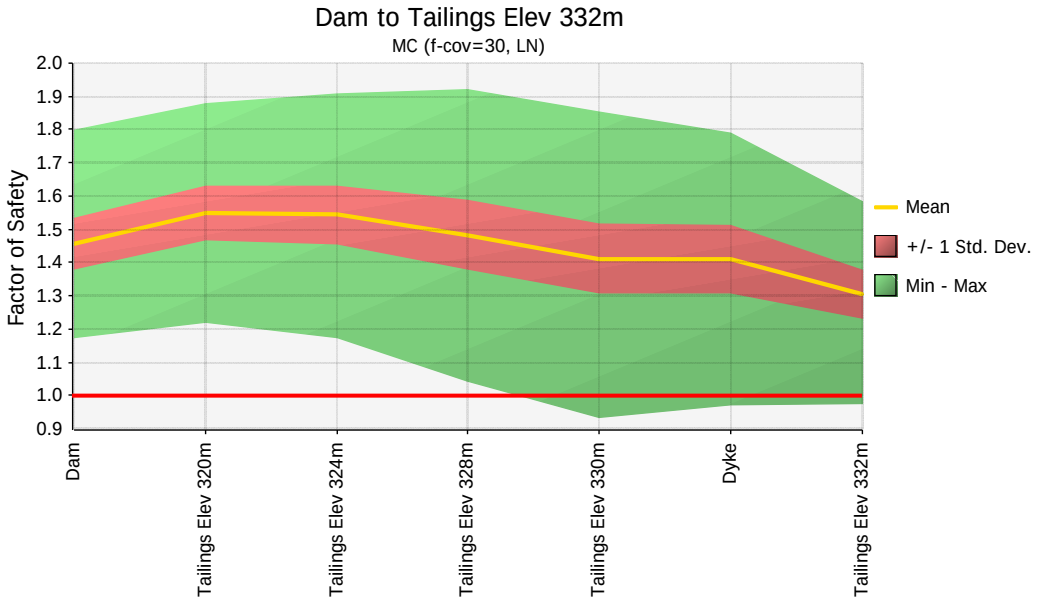

Figure 6-25: Summary showing the Mean, +/- Std. Dev. and the Min - Max range of output given a LogNormal PDF input for Ø

Table 6-6: Summary of the Reliability and Probability of Unsatisfactory Performance given a LogNormal PDF input for Ø

MC LogNormal PDF Ø 1,000 runs	MEAN	STDEV	Reliability	Probability of Unsatisfactory Performance
Dam	1.456	0.075	6.088	0
Tailings Elev 320m	1.549	0.081	6.762	0
Tailings Elev 324m	1.543	0.085	6.394	0
Tailings Elev 328m	1.482	0.103	4.676	0
Tailings Elev 330m	1.411	0.102	4.018	0
Dyke	1.411	0.102	4.028	0
Tailings Elev 332m	1.305	0.073	4.183	0

6.4.1.3 Summary

Comparing the data presented in Table 6-5 and Table 6-6, it is evident that output from the LogNormal (LN) PDF of the dam's core angle of friction generated a higher reliability index and lower probability of unsatisfactory performance than that of the Normal PDF. This is also reflected in whereby the FOS output for the LogNormal input has a lower standard deviation than that of the Normal (Figure 6-26 and Figure 6-27). As a result, it was concluded to be more conservative and pursue the Normal (N) PDF for the dam's core angle of friction.

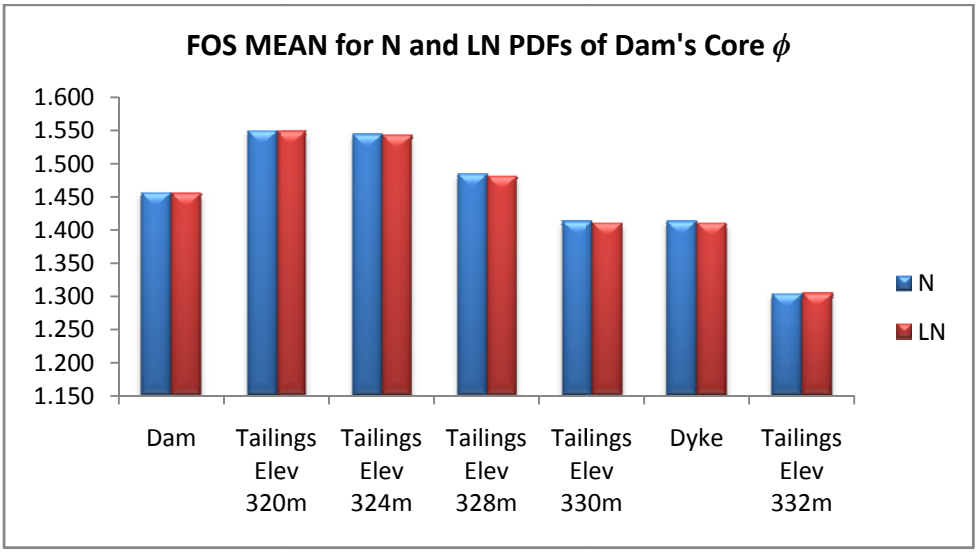

Figure 6-26: Mean of the FOS PDFs at every stage for input N vs. LN for Dam's CoreØ

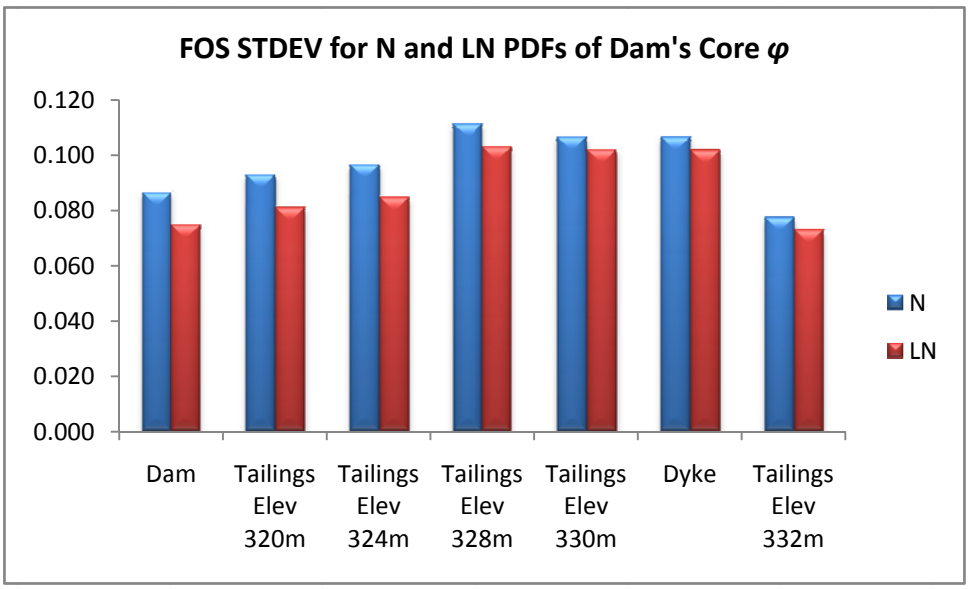

Figure 6-27: STDEV of the FOS PDFs at every stagefor input N vs. LN PDF Dam's CoreØ

6.4.2. MC VERSUS RMC FOR NORMAL PDF OF DAM'S CORE Φ

In the previous sections, the dam's core angle of friction was kept constant throughout the mesh in every simulation; however, in this section the uncertainty in the dam's core is taken at the local level by introducing the spatial variability of the material property. The material property assigned at the local level will be chosen randomly from a normal (Gaussian) distribution of a specific standard deviation and mean. In every run, the seed will be changed and a new mapping of the spatial variability will be generated for every simulation. Similar to the previous work, after each run the FOS is calculated using the SRT and then the FOS probability density function is constructed. It is important to note that there is no spatial correlation between the property values.

For illustrative purposes, the left side of the dam's core in Figure 6-28 shows the variation in the material property at the local level, with the right side showing the overall spatial variability.

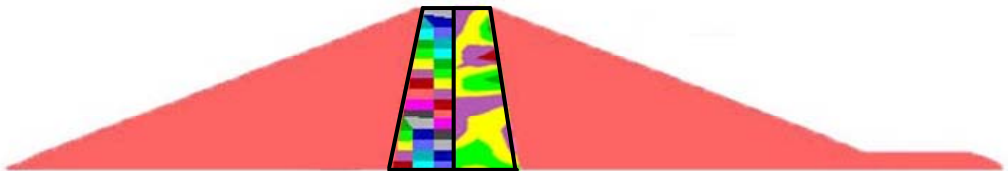

Figure 6-28: Material uncertainty in the core's angle of friction represented at the local level

A total of 1,000 simulations were conducted. Furthermore, a Ø-COV=30% was used for this comparative analysis. The factor of safety histogram output at every stage was fitted with a Normal PDF and the individual output is presented in the Appendix A. Figure 6-29 and Figure 6-30 illustrate the fitted Normal CDFs and PDFs at every stage for the output of the simulations, respectively. Figure 6-31 summarizes the PDFs at every stage by highlighting the mean, +/- standard deviation limits and the 5% - 95% boundary lines. Figure 6-32 replaces the 5% - 95% boundary lines with the whole range of Min - Max output. The reliability and Probability of Unsatisfactory Performance results corresponding to FOS < 1 are presented inTable 6-7.

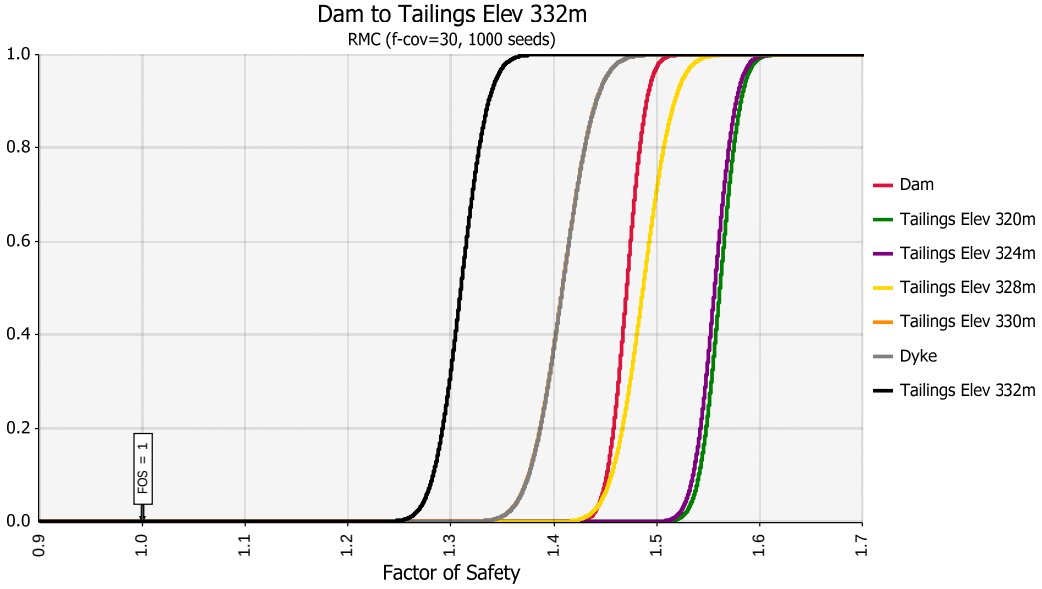

Figure 6-29: CDFs for all stages given a Normal PDF input for Øin the RMC

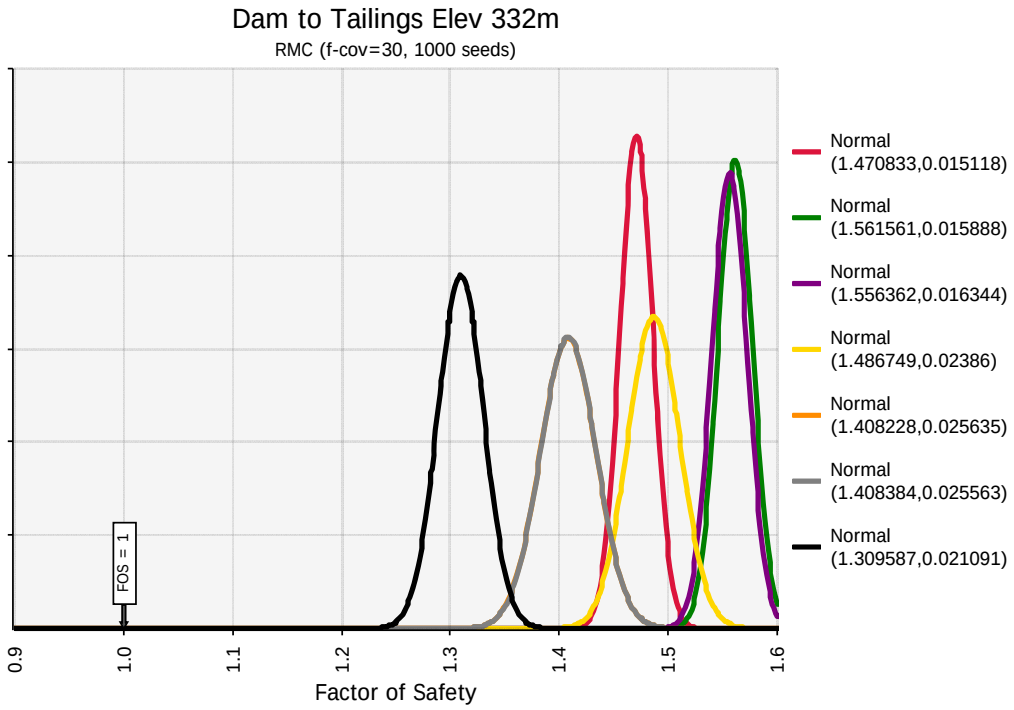

Figure 6-30: PDFs for all stages given a Normal PDF input for Ø in the RMC

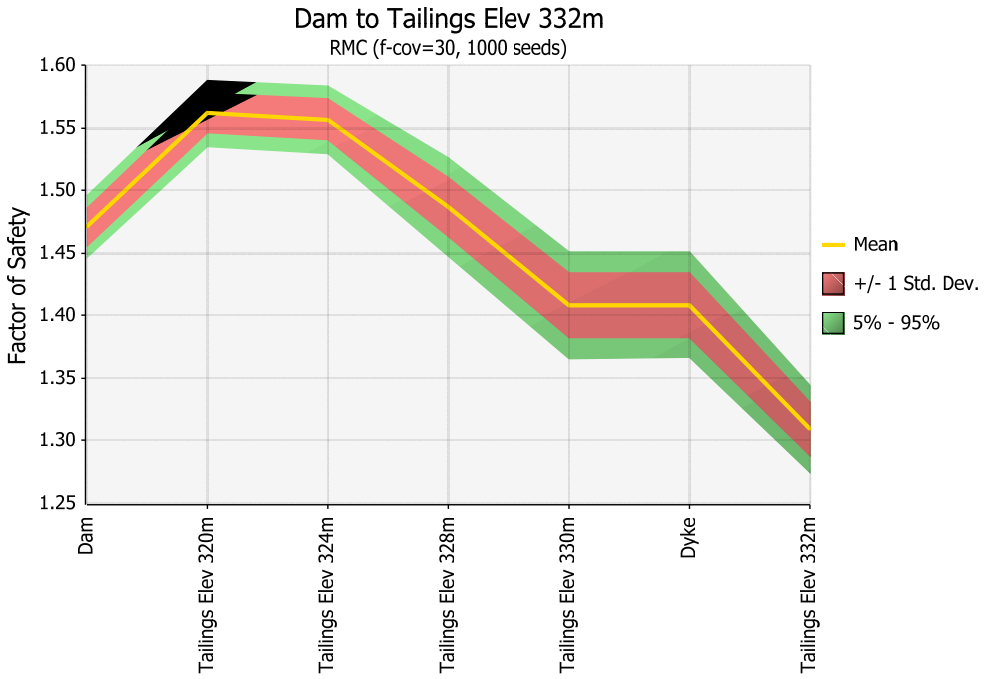

Figure 6-31: Summary showing the Mean, +/- Std. Dev. and the 5% - 95% range given a Normal PDF input for Ø in the RMC

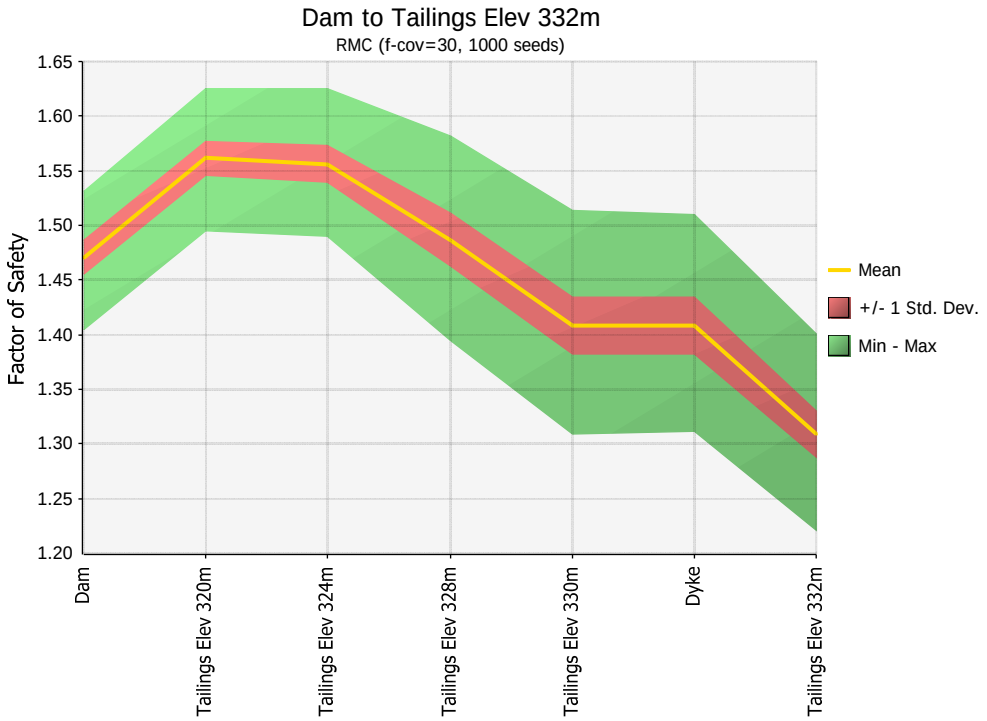

Figure 6-32:Summary showing the Mean, +/- Std. Dev. and the Min - Max range of output given a Normal PDF input for Øin the RMC

Table 6-7: Summary of the Reliability and Probability of Unsatisfactory Performance given a Normal PDF input for Ø in the RMC

RMC Normal PDF Ø 1,000 seeds	MEAN	STDEV	Reliability	Probability of Unsatisfactory Performance
Dam	1.471	0.015	31.144	0
Tailings Elev 320m	1.562	0.016	35.345	0
Tailings Elev 324m	1.556	0.016	34.041	0
Tailings Elev 328m	1.487	0.024	20.400	0
Tailings Elev 330m	1.408	0.026	15.925	0
Dyke	1.408	0.026	15.976	0
Tailings Elev 332m	1.310	0.021	14.679	0

From the analysis above, and the comparison presented in Figure 6-33 and Figure 6-34 it is evident that the variance generated from fitting the Normal PDF to the output at every stage is extremely narrow in the RMC approach when compared to the output of that of the MC approach. This conclusion is similar to that observed by El-Ramly (El-Ramly 2001). For the purpose of this research in illustrating the powerful use of the hydro-mechanical coupled analysis of the

staged construction of the impoundment is along with calculating the FOS using the SRT, it was decided to pursue the MC in the extensive analysis discussed in the following chapter.

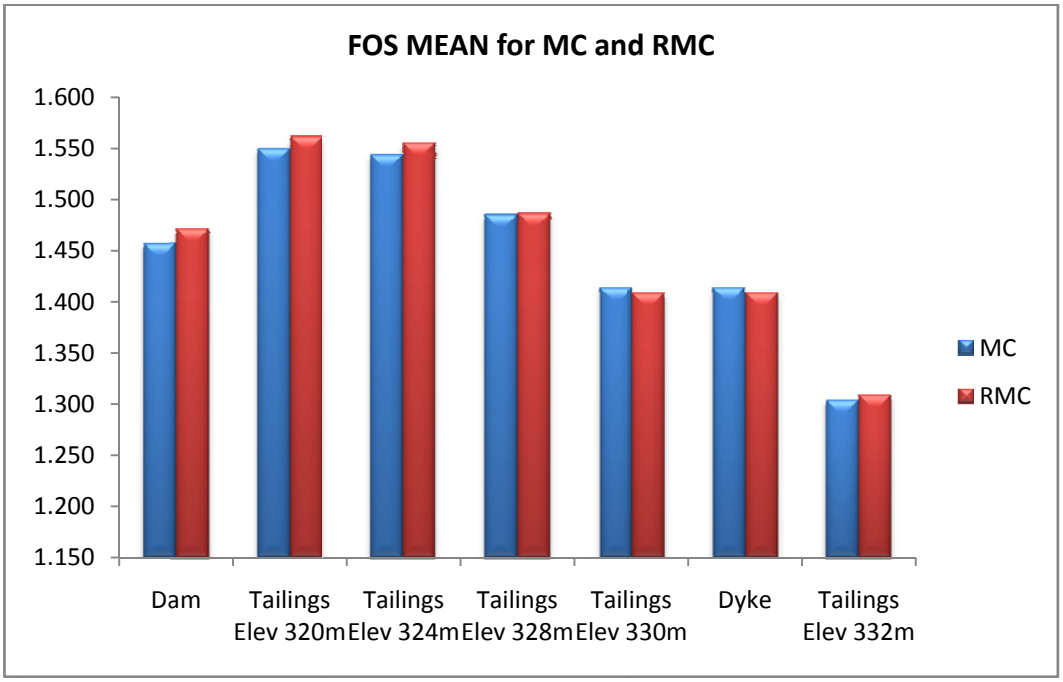

Figure 6-33: Mean of the FOS PDFs at every stage for MC vs. RMC

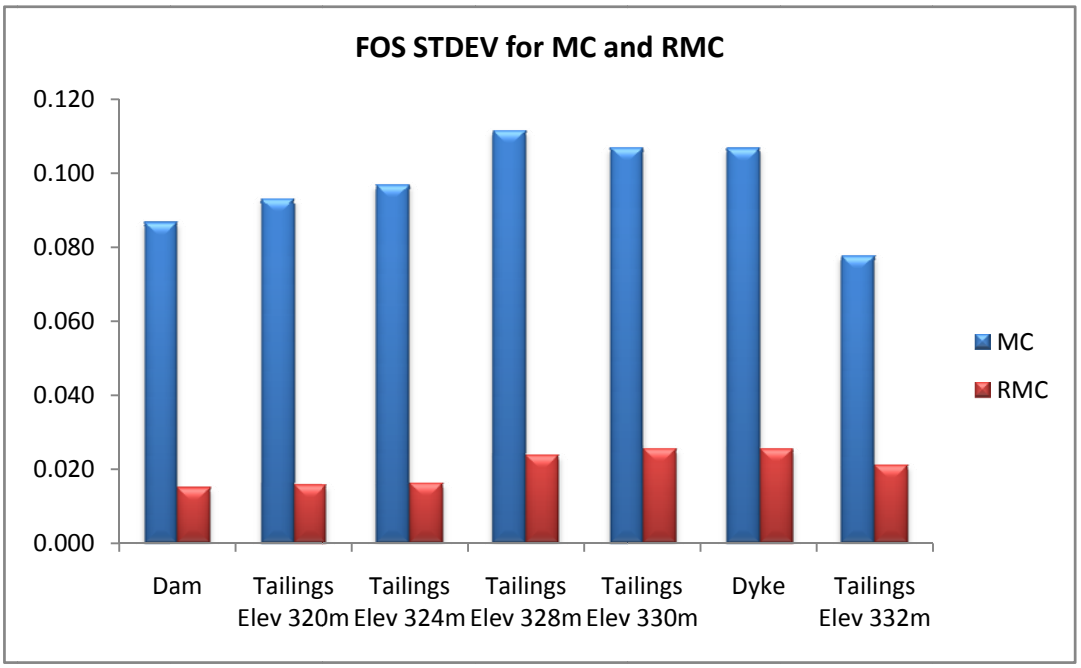

Figure 6-34: Standard deviation of the FOS PDFs at every stage for MC vs. RMC

6.4.3. FROM 1,000 TO 200 MC SIMULATIONS

The factor of safety histogram output at every stage was fitted with a Normal PDF and the individual output is presented in the Appendix A. Figure 6-35 and Figure 6-36 illustrate the fitted Normal CDFs and PDFs at every stage for the output of the simulations, respectively. Figure 6-37 summarizes the PDFs at every stage by highlighting the mean, +/- standard deviation limits and the 5% - 95% boundary lines. Figure 6-38 replaces the 5% - 95% boundary line with the whole range of Min - Max output. The reliability and Probability of Unsatisfactory Performance results corresponding to FOS < 1 are presented in Table 6-8.

Comparing the results tabulated in Table 6-5 for the 1,000 MC runs with the output for the 200 runs in Table 6-8 shows them to be extremely close to each other. As such, it is imperative that the number of MC runs to be lowered to 200 for the extensive analysis to be conducted in the next chapter, given the long computational time involved in every run.

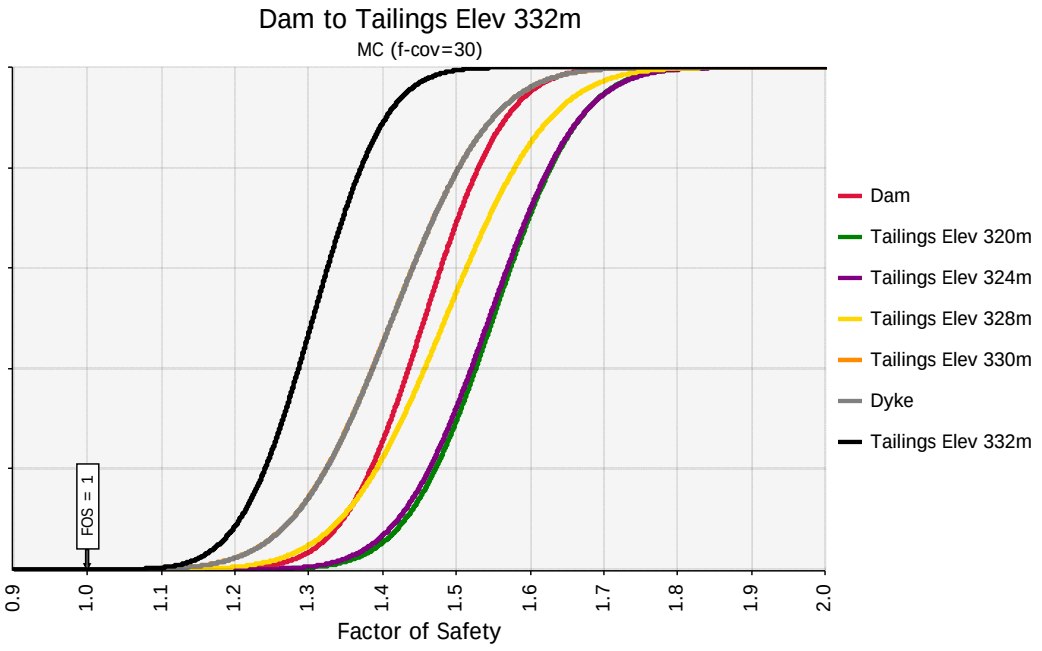

Figure 6-35: CDFs for all stages given a Normal PDF input for Ø (200 runs)

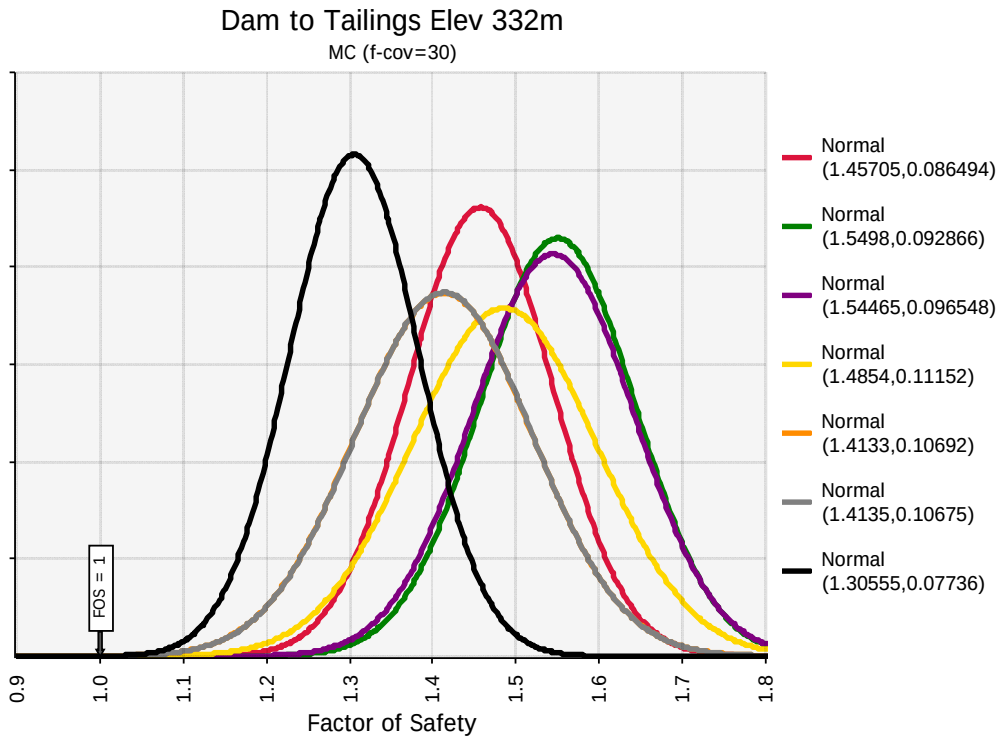

Figure 6-36: PDFs for all stages given a Normal PDF input for ∅ (200 runs)

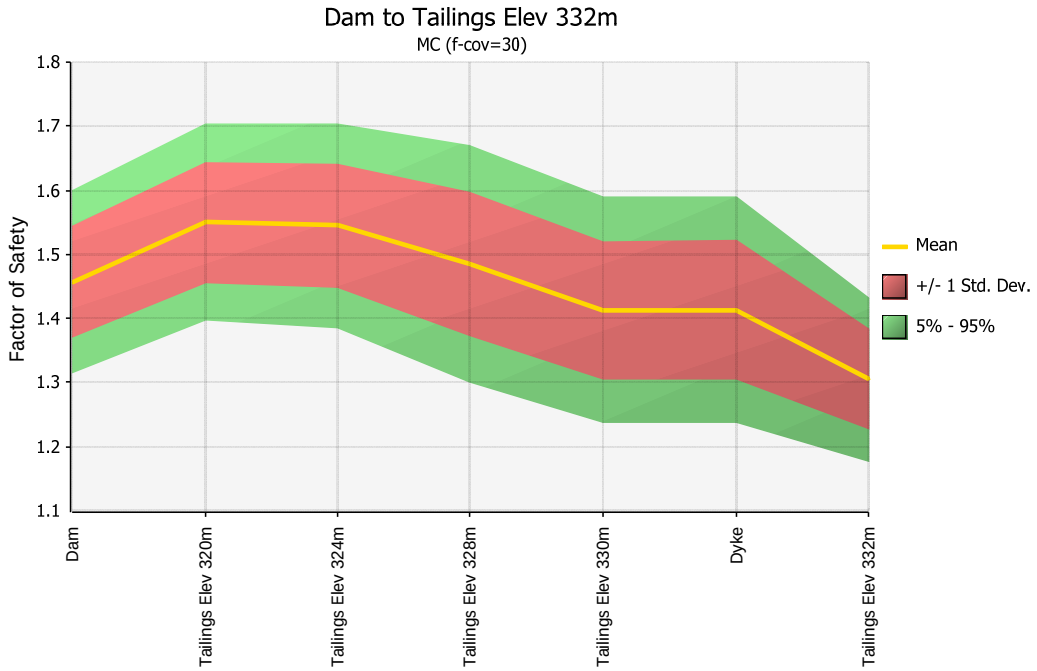

Figure 6-37: Summary showing the Mean, +/- Std. Dev. and the 5% - 95% range given a Normal PDF input for Ø (200 runs)

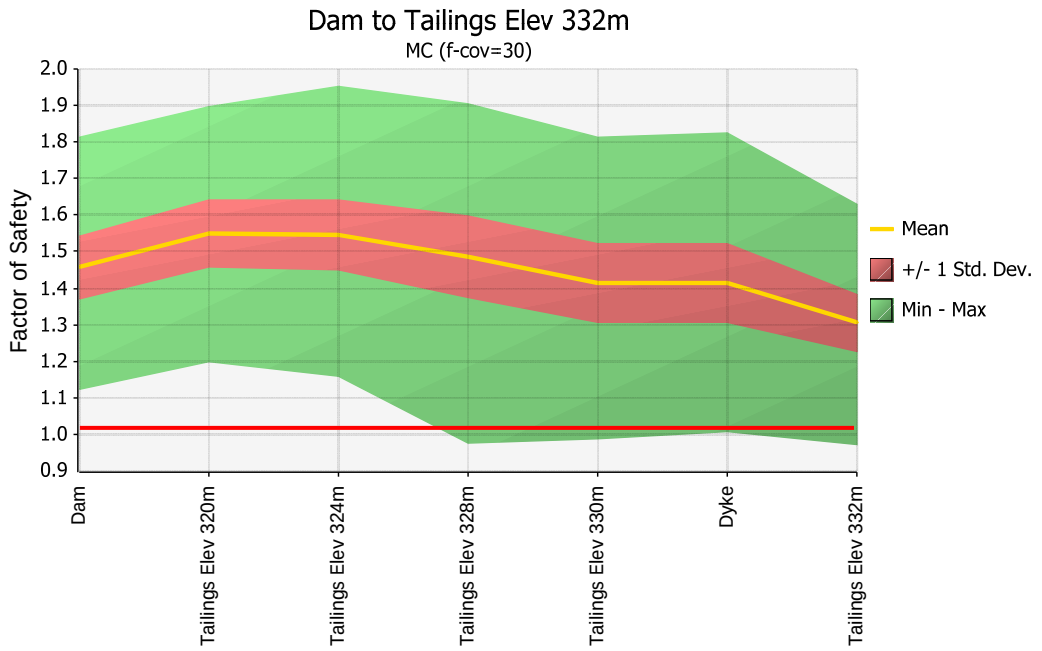

Figure 6-38: Summary showing the Mean, +/- Std. Dev. and the Min - Max range of output given a Normal PDF input for Ø (200 runs)

Table 6-8: Summary of the Reliability and Probability of Unsatisfactory Performance given a Normal PDF input for Ø (200 runs)

MC Normal PDF Ø 200 runs	MEAN	STDEV	Reliability	Probability of Unsatisfactory Performance
Dam	1.457	0.086	5.284	0
Tailings Elev 320m	1.550	0.093	5.920	0
Tailings Elev 324m	1.545	0.097	5.641	0
Tailings Elev 328m	1.485	0.112	4.353	0
Tailings Elev 330m	1.413	0.107	3.866	0.0001
Dyke	1.414	0.107	3.874	0.0001
Tailings Elev 332m	1.306	0.077	3.950	0.00001

6.5 SUMMARY

First, the stochastic model setup was presented which showed the nine components involved in producing the reliability and probability of unsatisfactory performance for a tailings impoundments by incorporating a hydro-mechanical coupled analysis and the different stochastic approaches.

Second, the PEM, which is the least exhaustive stochastic method, was applied by varying the coefficient variation of the dam's core angle of friction; COV (Ø) = 15%, 30% and 45%. As was shown, the reliability was the lowest and the probability of unsatisfactory performance was highest with a COV=45%, which corresponded to higher variability in the stochastic input parameter.

Third, the MC and RMC methods were adopted. It was shown that a lower reliability and higher probability of unsatisfactory performance was obtained when defining a Normal versus a LogNormal PDF for the stochastic input variable which was the dam's core angle of friction. Moreover, the results obtained from the RMC showed high reliability values due to the narrow standard deviation recorded in the output when compared to that of the MC.

Lastly, it was shown using the MC method that the output generated from 200 runs was almost identical to that generated using 1000 runs. As a result, the MC analysis using 200 runs will be adopted for the extensive stochastic analysis presented in the following chapter.

It is important to note that this stochastic hydro-mechanical coupled analysis is presented as a design approach for integration into future tailings dam design and must not be considered alone and by itself; i.e. it shall remain complementary to the developed deterministic approaches and the advanced deterministic modelling presented as part of this thesis as well.

6.6 LIMITATIONS OF STOCHASTIC APPROACH

In this section a number of limitations of the above-mentioned results are discussed. First, it should be noted that the shape of the FOS histogram during the filling period (up to elevation 328m) dam suggests that distributions other than Normal could provide better fit than the adopted Normal distribution; refer to Appendix A. However, since the FOS histogram results during the last four meters of filling up the impoundment as well as constructing the dyke on the upstream side show better fit with the Normal Distribution PDF, it was decided to adopt it.

Secondly, a simplified approach accounting for spatial variability through the RMC method implemented in FLAC has been used. It should be noted that other, more sophisticated techniques for modelling spatial variability of the random variable such as the Local Area Subdivision (Fenton and Griffiths 2008) have been developed. However, these methods are limited to simplified model geometries and cannot be suited to the more complex design of a tailings dam.

Moreover, the results obtained from 200 MC simulations appear to give nearly identical results to those obtained from 1000 MC simulations. Nevertheless, these results are limited to the present case study and cannot be warranted for other case studies of dams with different geometries.

Finally, the SRT only allows for the simultaneous reduction of the shear material properties (c & Φ) by the same trial factor of safety for every iteration to calculate the final FOS. One limiting factor in this technique is that it doesn't allow for arbitrary and independent reduction of the shear material properties using various combinations of trail FOSs at every iteration.

CHAPTER : 7 **CASE STUDY: MINE TAILINGS IMPOUNDMENT EXPANSION PROJECT – RELIABILITY ANALYSIS**

7.1 PERFORMANCE CRITERIA

In the previous chapter, the analysis presented narrowed down the choices for the stochastic analysis to the Monte-Carlo approach consisting of 200 simulations. In this chapter, the performance criteria are first defined. Following that, a second stochastic variable is introduced, the dam's core cohesion based on correlation coefficients. Lastly, a third stochastic variable is included, the dam's core permeability.

As defined in Chapter 3, the relationship between the probability of unsatisfactory performance and the reliability index for Normal Probability density functions is $P_u = \phi(-\beta)$, where $\phi(\,)$ is the CDF. The reliability index is included as another factor in the performance criteria, as it is more stable than the probability of unsatisfactory performance when estimating small probabilities (El-Ramly 2001).Table 7-1, from the US Army Corps of Engineers provides target reliability indices as a function of the expected performance level.

Table 7-1: Target reliability indices table (*verbatim* from (USACE 1997)

Target Reliability Indices		
Expected Performance Level	**Beta - Reliability Index**	**Probability of Unsatisfactory Performance**
High	5	0.0000003
Good	4	0.00003
Above average	3	0.001
Below average	2.5	0.006
Poor	2.0	0.023
Unsatisfactory	1.5	0.07
Hazardous	1.0	0.16
Note: Probability of unsatisfactory performance is the probability that the value of the performance function will approach the limit state, or that an unsatisfactory event will occur. For example, if the performance function is defined in terms of slope instability, and the probability of unsatisfactory performance is 0.023, then 23 of every 1,000 instabilities will result in damage, which causes a safety hazard.		

7.2 RELIABILITY ANALYSIS WITH TWO VARIABLES: C AND Φ

The analysis in this section will consist of analyzing the influence of the COV and the correlation coefficient (ρ) between the shear strength parameters on the stability of the impoundment.

A review of the literature shows that the *c* and ∅ are usually negatively correlated with the correlation coefficient ranging between -0.7 and 0.5 (Lumb 1970; Grivas 1981; Wolff 1985; Cho 2010).

As a result, in this section combinations of COVs and correlation coefficients for both the *c* and ∅ will be examined. Table 7-2 summarizes the simulation matrix. The next section presents the results for each COV with the three different correlation coefficients.

Table 7-2: MC simulation matrix for different COV and correlation coefficient values

MC Simulation ID (200 runs each)	c-cov = ∅-cov	ρ (*c* and ∅)
1	15	0.5
2	15	0
3	15	-0.5
4	30	0.5
5	30	0
6	30	-0.5
7	45	0.5
8	45	0
9	45	-0.5

7.2.1. RESULTS FOR MC-1, MC-2 & MC-3

Figure 7-1 illustrates that for a Φ-cov = c-cov = 15%, the mean FOS does not vary with different correlation coefficients for every stage. Moreover, the mean FOS output is very close to the one generated by the deterministic analysis. However, comparing the standard deviation output in Figure 7-2, it can be observed that the output corresponding to a correlation coefficient of 0.5 experiences a higher variance than that which corresponds to a ρ equal to 0 and -0.5.

Figure 7-3 reflects the fact that smaller variability correspond to higher reliability in the model, as the reliability for the output corresponding to a ρ equal to -0.5 is the highest, followed by ρ=0 and lastly ρ=0.5. Lastly, as was illustrated in Table 7-1, the higher the beta-reliability index, the lower the probability of unsatisfactory performance. The results for MC-1, MC-2 & MC-3 show that the reliability exceeds 5, thus corresponding to a virtually zero probability of unsatisfactory performance and reflecting a high performance level for the tailings impoundment.

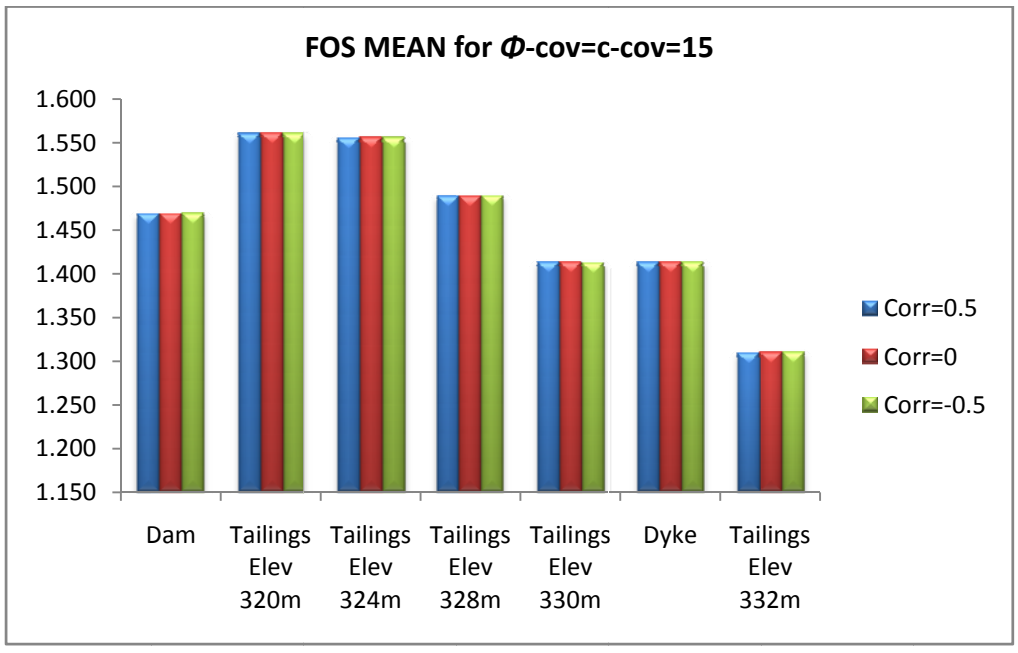

Figure 7-1: FOS Mean for Φ-cov=c-cov=15 (MC-1, MC-2 & MC-3)

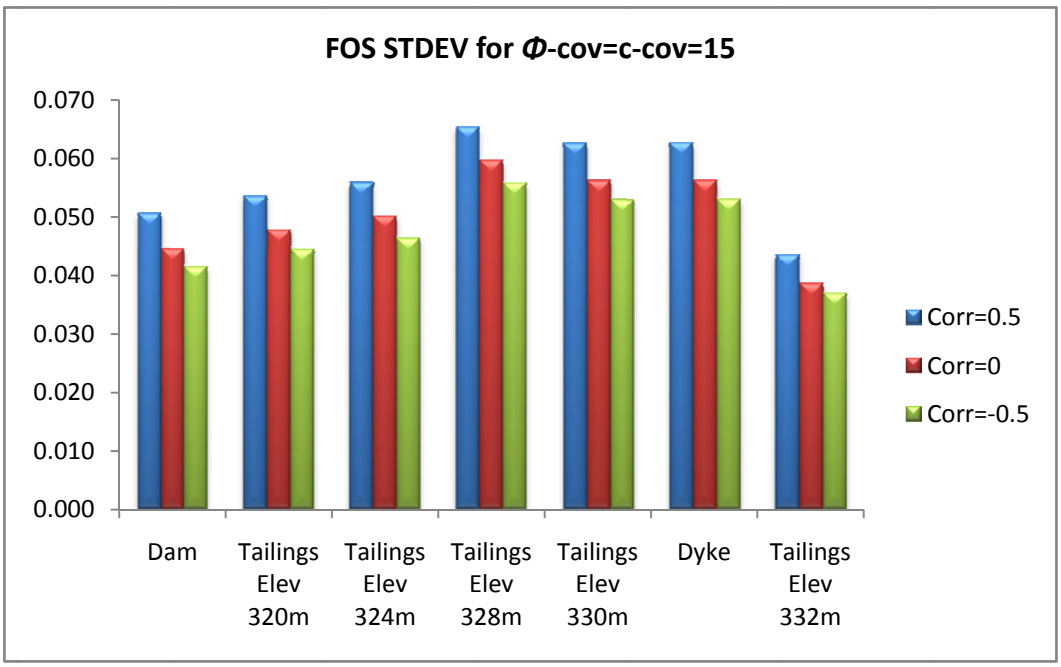

Figure 7-2: FOS Stdev for Φ-cov=c-cov=15 (MC-1, MC-2 & MC-3)

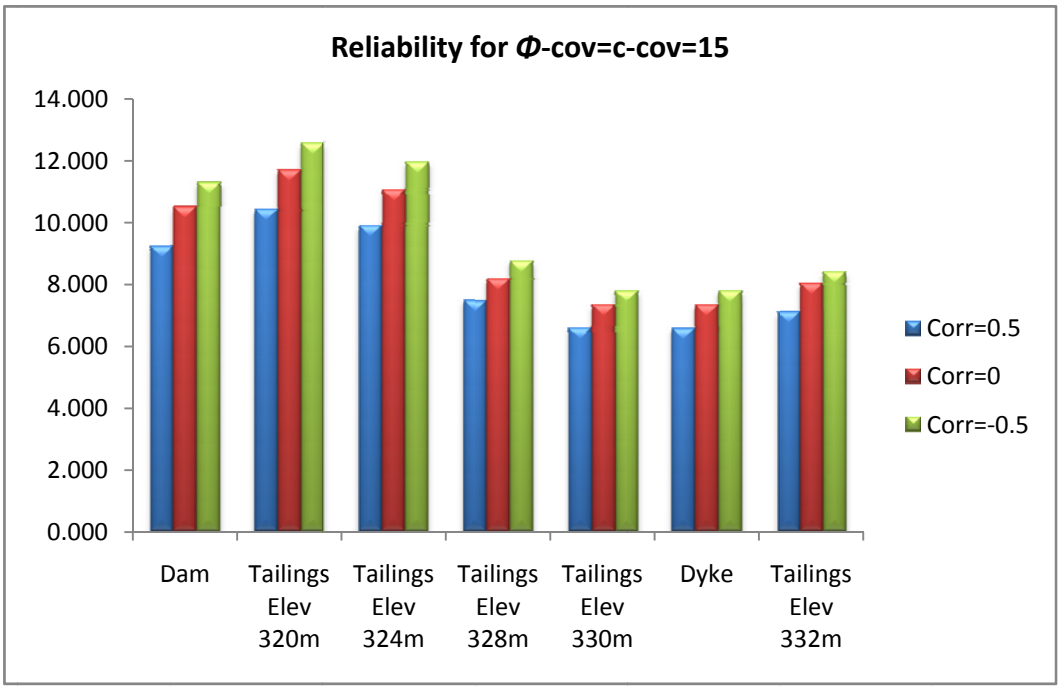

Figure 7-3: Reliability for Φ-cov=c-cov=15 (MC-1, MC-2 & MC-3)

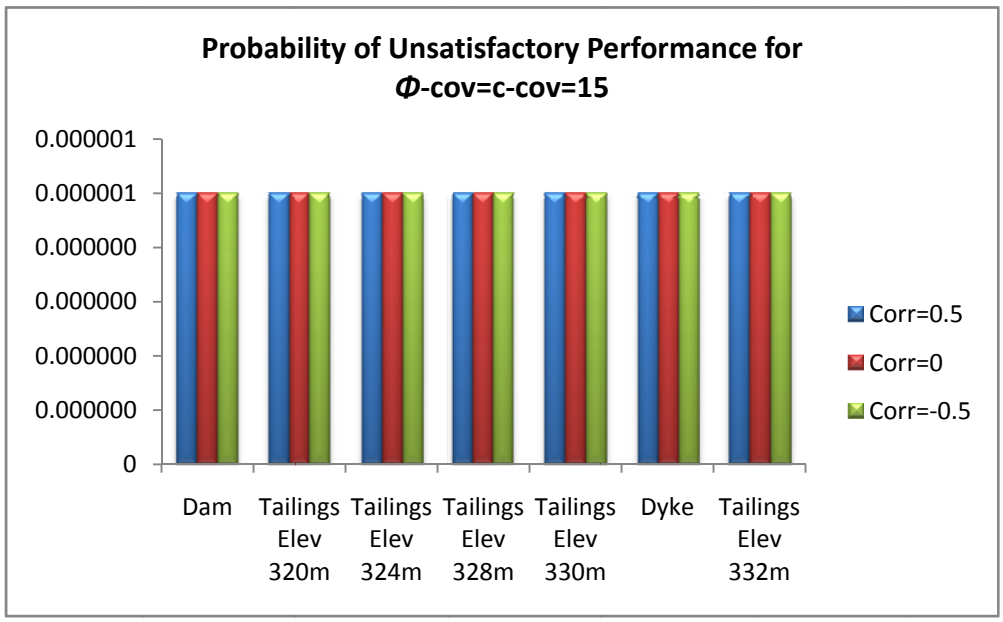

Figure 7-4: Probability of Unsatisfactory Performance for Φ-cov=c-cov=15 (MC-1, MC-2 & MC-3)

7.2.2. RESULTS FOR MC-4, MC-5 & MC-6

Similarly, Figure 7-5 illustrates that for a Φ-cov = c-cov = 30%, the mean FOS does not vary with different correlation coefficients for every stage and the mean FOS output is very close to the one generated by the deterministic analysis. Moreover, again comparing the standard deviation output in Figure 7-6 shows the output corresponding to a correlation coefficient of 0.5 experience a higher variance than that corresponding to a ρ equal to 0 and -0.5.

Figure 7-7 reflects that the reliability for the output corresponding to a ρ equal to -0.5 is the highest, followed by ρ =0 and lastly ρ =0.5. However, the output for MC-4 now corresponds to a probability of unsatisfactory performance exceeding 0.0002 which according to Table 7-1 reflects an above average to good performance level for the tailings impoundment.

It is noteworthy that these results for the reliability are significantly lower than those obtained from MC-1 to MC-3. Thus, it can be concluded that the COV

plays an important role in the assessment of the geotechnical performance of the tailings impoundment. In practice, a higher COV of 30% reflects wider variation of mechanical properties of the core material which could be attributed to a number of site conditions including but not limited to, e.g. placement methods.

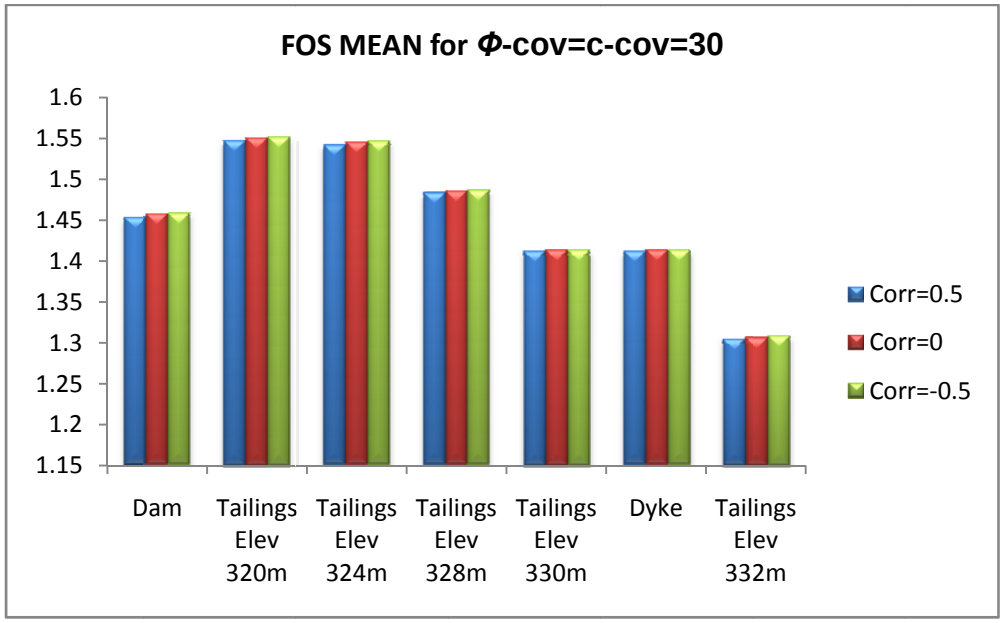

Figure 7-5: FOS Mean for Φ-cov=c-cov=30 (MC-4, MC-5& MC-6)

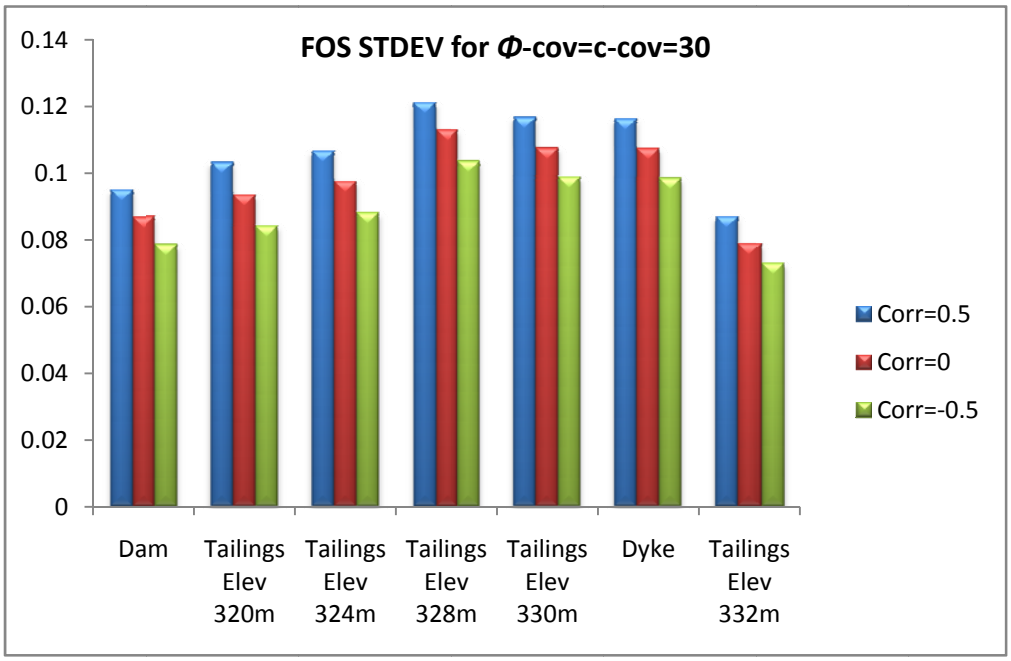

Figure 7-6: FOS Stdev for Φ-cov=c-cov=30 (MC-4, MC-5& MC-6)

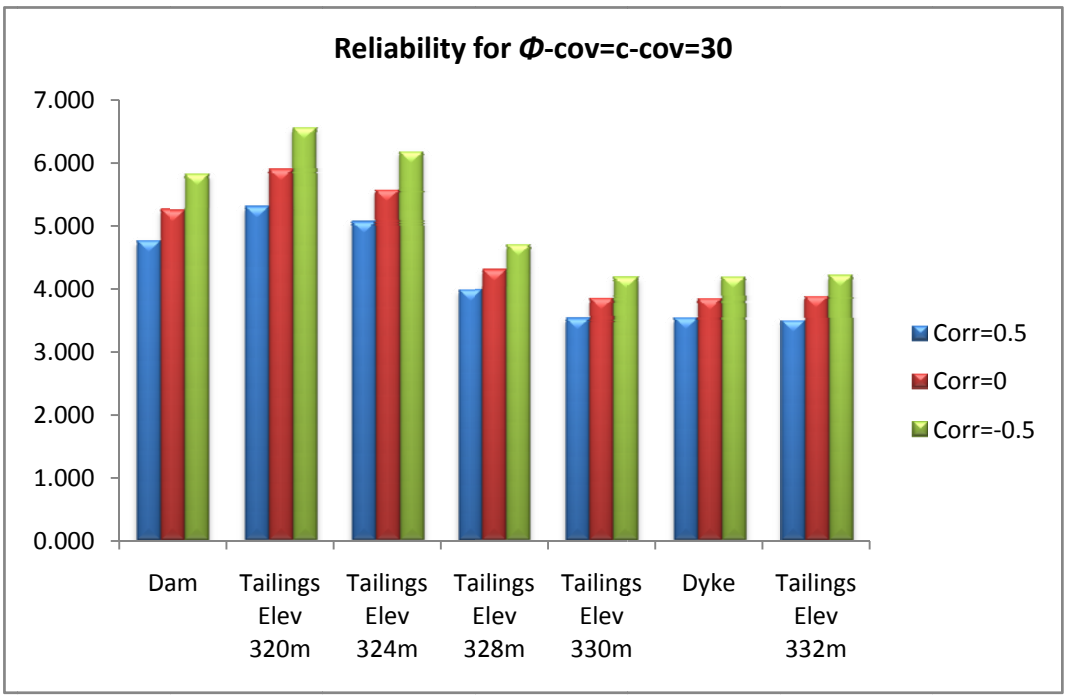

Figure 7-7: Reliability for Φ-cov=c-cov=30 (MC-4, MC-5& MC-6)

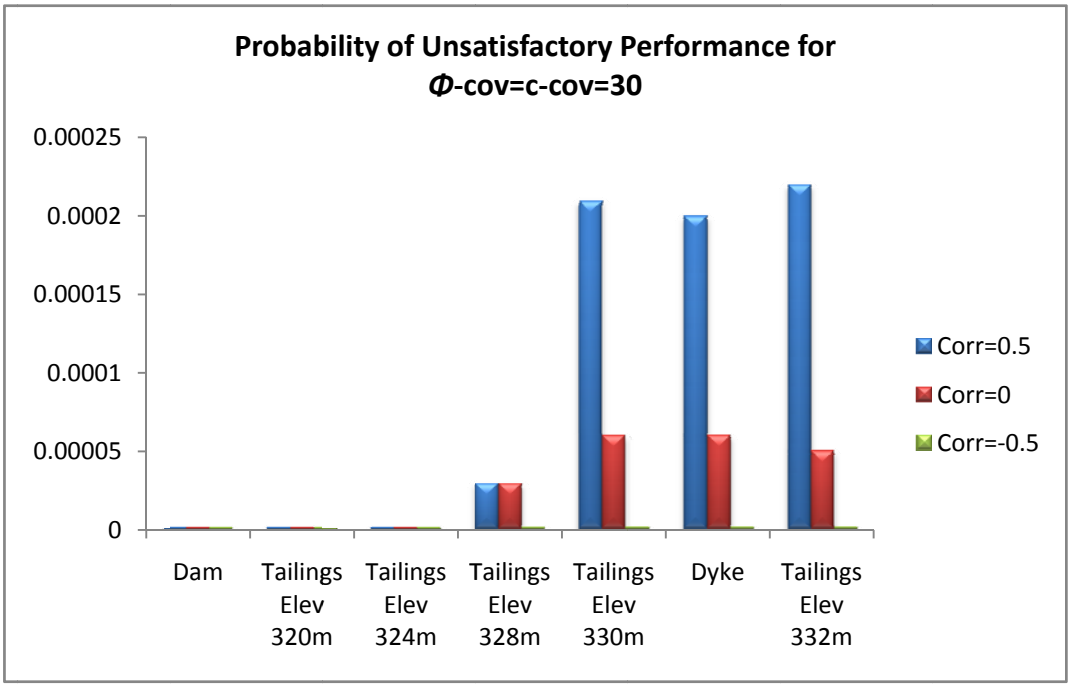

Figure 7-8: Probability of Unsatisfactory Performance for Φ-cov=c-cov=30 (MC-4, MC-5& MC-6)

7.2.3. RESULTS FOR MC-7, MC-8 & MC-9

Similarly, Figure 7-9 illustrates that for a Φ-cov = c-cov = 45%, the mean FOS does not vary with different correlation coefficients for every stage; and the mean FOS output is very close to the one generated by the deterministic analysis. Moreover, again comparing the standard deviation output in Figure 7-10 shows the output corresponding to a correlation coefficient ρ of 0.5 experiences a higher variance than that corresponding to a ρ equal to 0 or -0.5.

Figure 7-11 reflects that the reliability for the output corresponding to a ρ equal to -0.5 is the highest, followed by ρ=0 then ρ=0.5. The output for MC-7 corresponds to a probability of unsatisfactory performance exceeding 0.006, which is more than one order of magnitude higher than the probability calculated in the previous section. According to Table 7-1, now the tailings impoundment reflects a below average performance level.

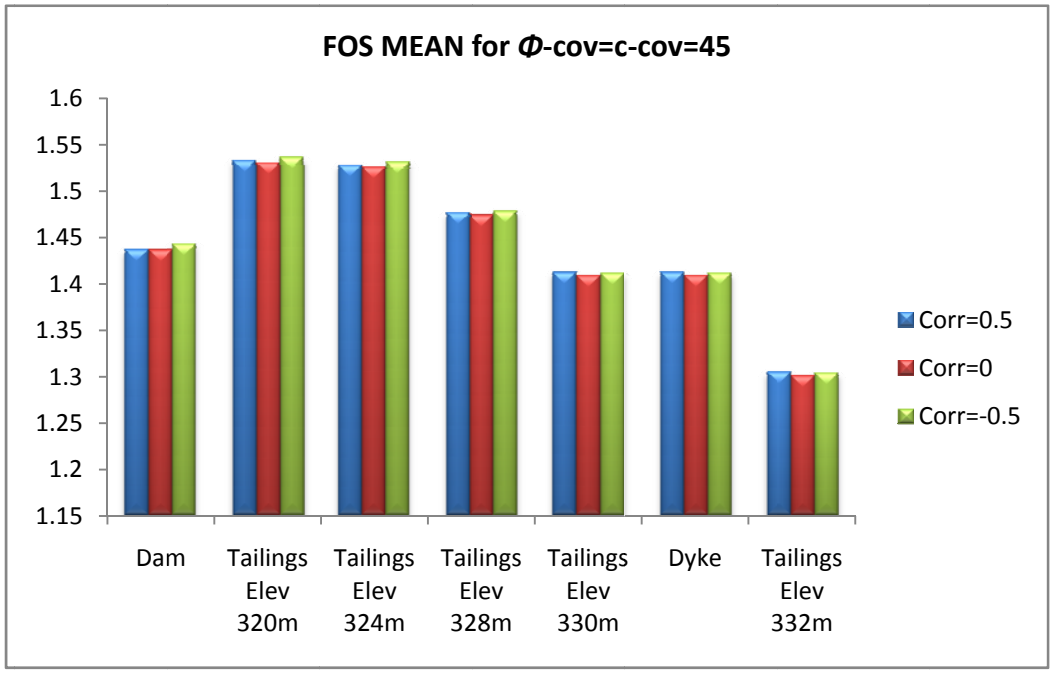

Figure 7-9: FOS Mean for Φ-cov=c-cov=45 (MC-7, MC-8& MC-9)

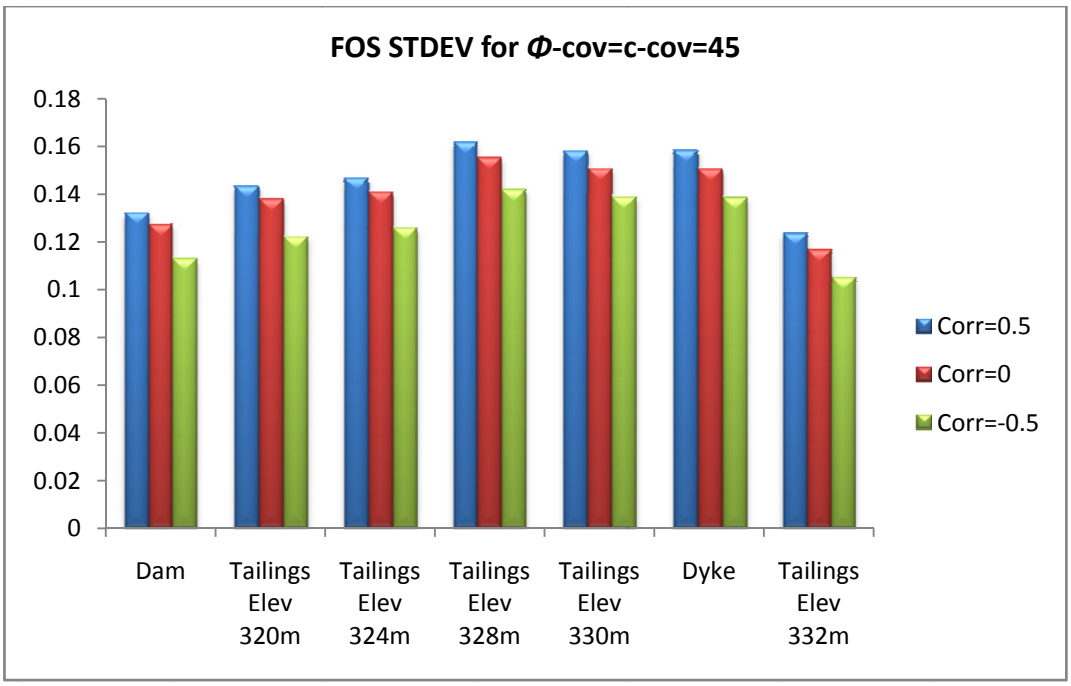

Figure 7-10: FOS Stdev for Φ-cov=c-cov=45 (MC-7, MC-8& MC-9)

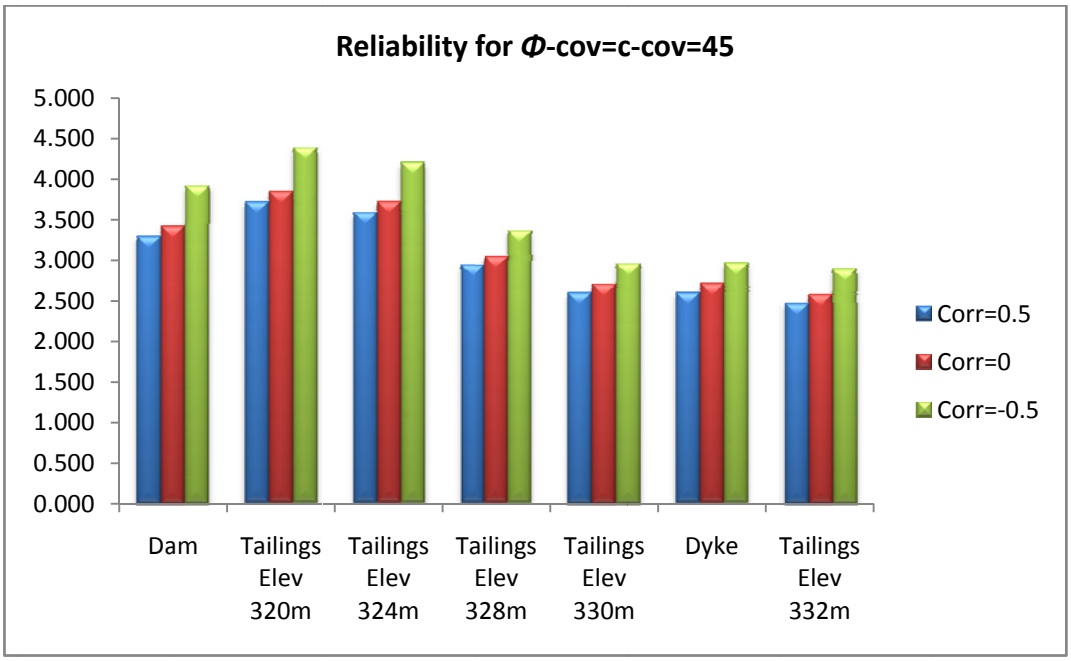

Figure 7-11: Reliability for Φ-cov=c-cov=45 (MC-7, MC-8& MC-9)

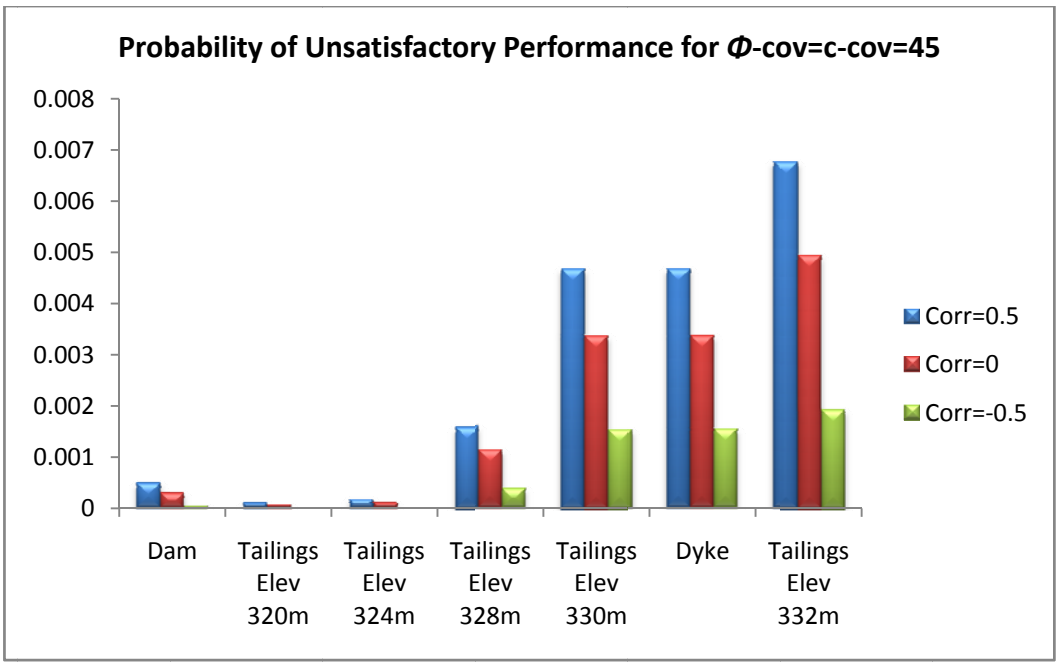

Figure 7-12: Probability of Unsatisfactory Performance for Φ-cov=c-cov=45 (MC-7, MC-8& MC-9)

7.2.4. SUMMARY FOR MC-1 THROUGH MC-9

A summary of the results for MC-1 through MC-9 for both the reliability and the probability of unsatisfactory performance are presented in Figure 7-13and Figure 7-14, respectively.

Similar to the conclusion presented by Cho (2010), the results will illustrate that the uncertainty in the calculated shear strength, represented by the FOS, is smaller than the combined uncertainty in both the c and ∅ for negative correlations. Moreover, Fenton and Griffiths (2003), add that this observation "arises from the fact that the variance of the shear strength is reduced if there is a negative correlation" (Fenton and Griffiths 2003; Cho 2010). From Figure 7-14 it is evident that MC-7 which corresponds to c-COV=Φ-COV=45 and ρ=0.5 results in the highest Probability of Unsatisfactory Performance for the tailings impoundment, which is over 250% higher than the probability corresponding to a ρ=-0.5 for the same COV. This shows the significant influence of the coefficient of correlation on the output results.

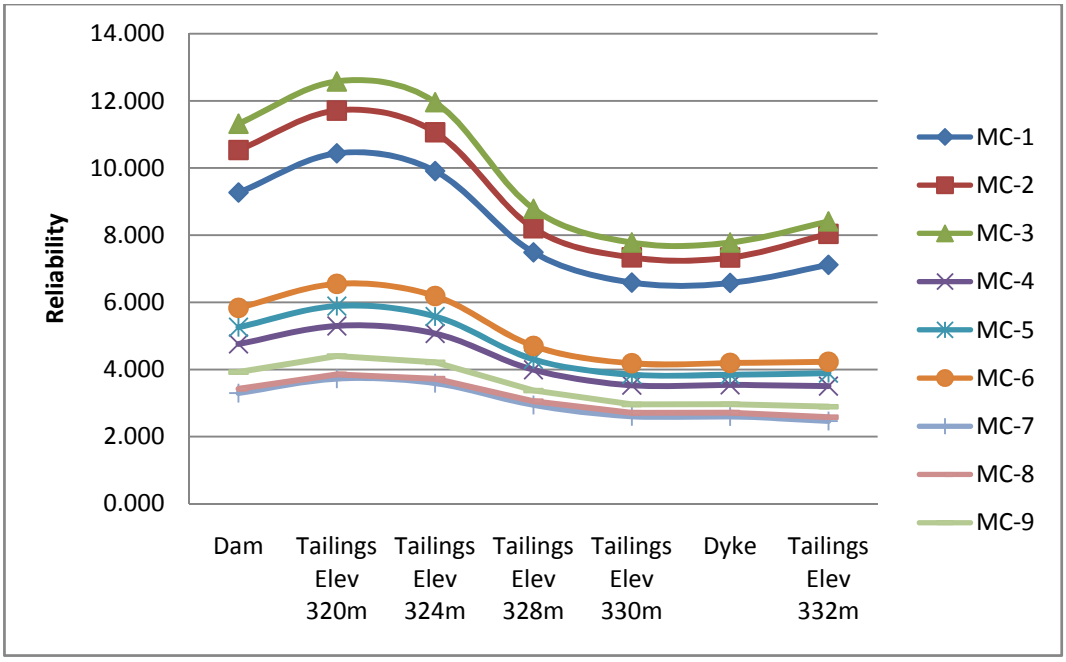

Figure 7-13: Reliability results for MC-1 through MC-9

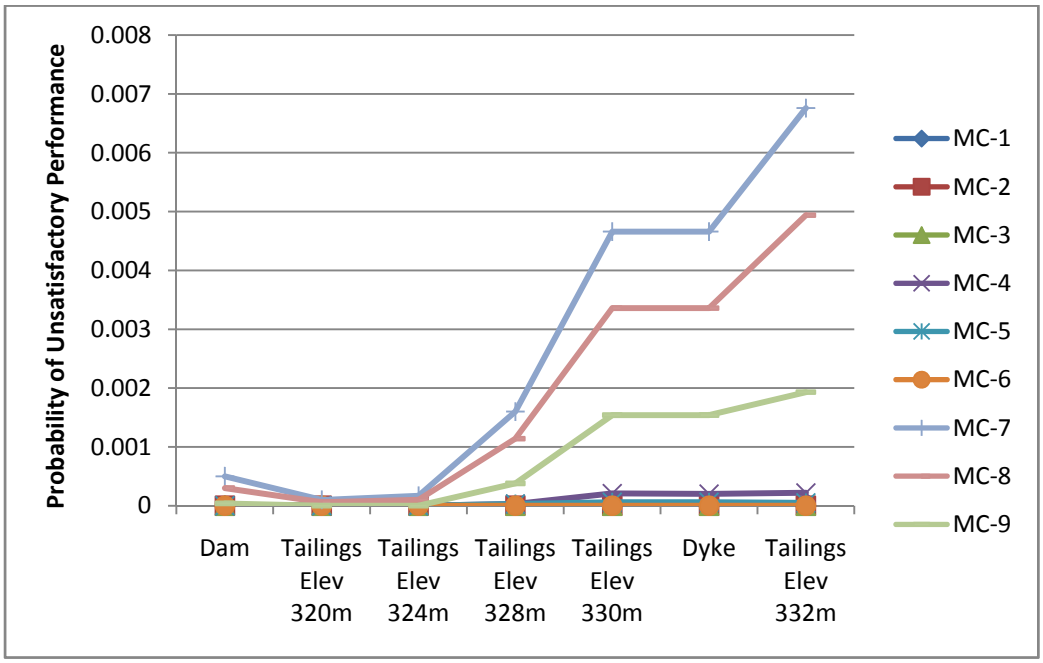

Figure 7-14: Probability of Unsatisfactory Performance for MC-1 through MC-9

7.3 RELIABILITY ANALYSIS WITH THREE VARIABLES: C, Φ AND K

In this section, a third stochastic variable is included in the probabilistic modelling. The purpose of the third dimension is to investigate how a hydraulic parameter influences the shear properties of the tailings impoundment through a hydro-mechanical coupled analysis. The hydraulic conductivity (k) has been considered to follow a LogNormal distribution (Baecher and Christian 2003). In this study a COV=150% was chosen for the core's hydraulic conductivity (recall k=1E-7 m/s), as it corresponded to the median value for 57 sites investigated by Benson (1993). This illustrates the high variability that is inherent in hydraulic conductivity material property as was recorded by Benson (1993).

Table 7-3: MC simulation matrix for different COV and correlation coefficient values

MC Simulation ID (200 runs each)	k-cov = 150 c-cov = ∅-cov	ρ (*c* and ∅)
10	15	0.5
11	15	0
12	15	-0.5
13	30	0.5
14	30	0
15	30	-0.5
16	45	0.5
17	45	0
18	45	-0.5

7.3.1. RESULTS FOR MC-10, MC-11 & MC-12

Figure 7-15 illustrates that for a ∅-cov = c-cov = 15%, the mean FOS does not vary with different correlation coefficients for every stage. Moreover, the mean FOS output is very close to the one generated by the deterministic analysis. However, comparing the standard deviation output in Figure 7-16, it can be observed that the output corresponding to a correlation coefficient of 0.5 experiences a higher variance than that which corresponds to a ρ equal to 0 and -0.5.

Similarly, Figure 7-17 reflects the fact that smaller variability correspond to higher reliability in the model, as the reliability for the output corresponding to a ρ equal to -0.5 is the highest, followed by ρ =0 and lastly ρ =0.5. Lastly, as was illustrated in Table 7-1, the higher the beta-reliability index, the lower the probability of unsatisfactory performance. The results for MC-10, MC-11 & MC-12 show that the reliability is significantly lower than those presented in MC-1, MC-2 & MC-3; and this is mainly due to the fact of introducing the hydraulic conductivity as a stochastic variable. Figure 7-18 presents the probability of unsatisfactory performance which is slightly higher than the virtual zero figure; thus, corresponding to a virtually zero probability of unsatisfactory performance and reflecting a high performance level for the tailings impoundment.

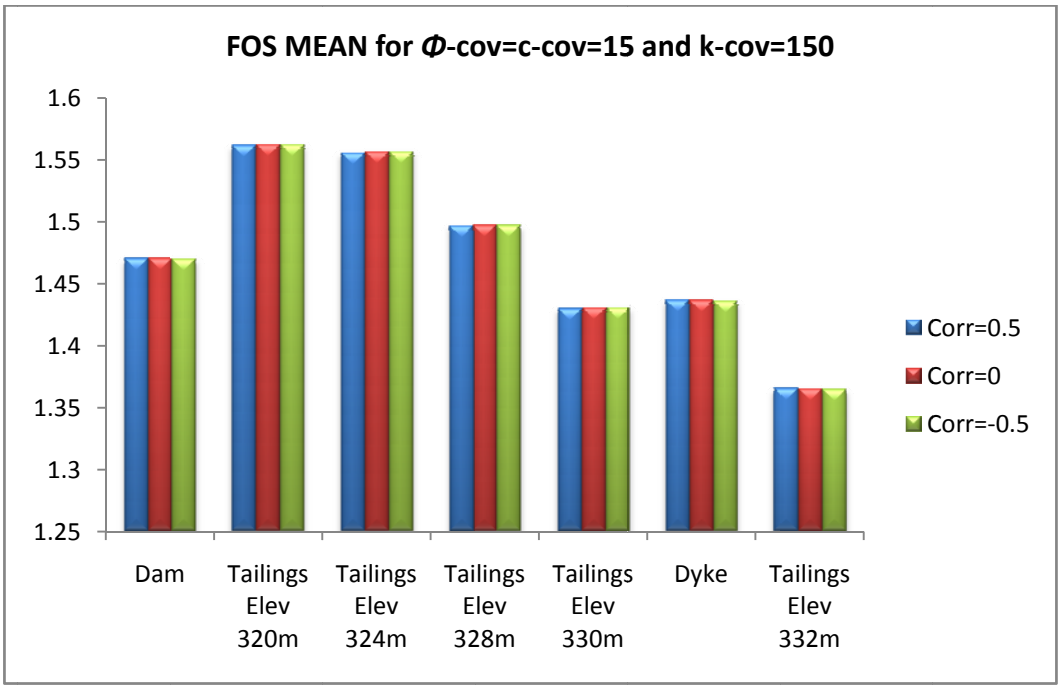

Figure 7-15: FOS Mean for Φ-cov=c-cov=15 and k-cov=150 (MC-10, MC-11& MC-12)

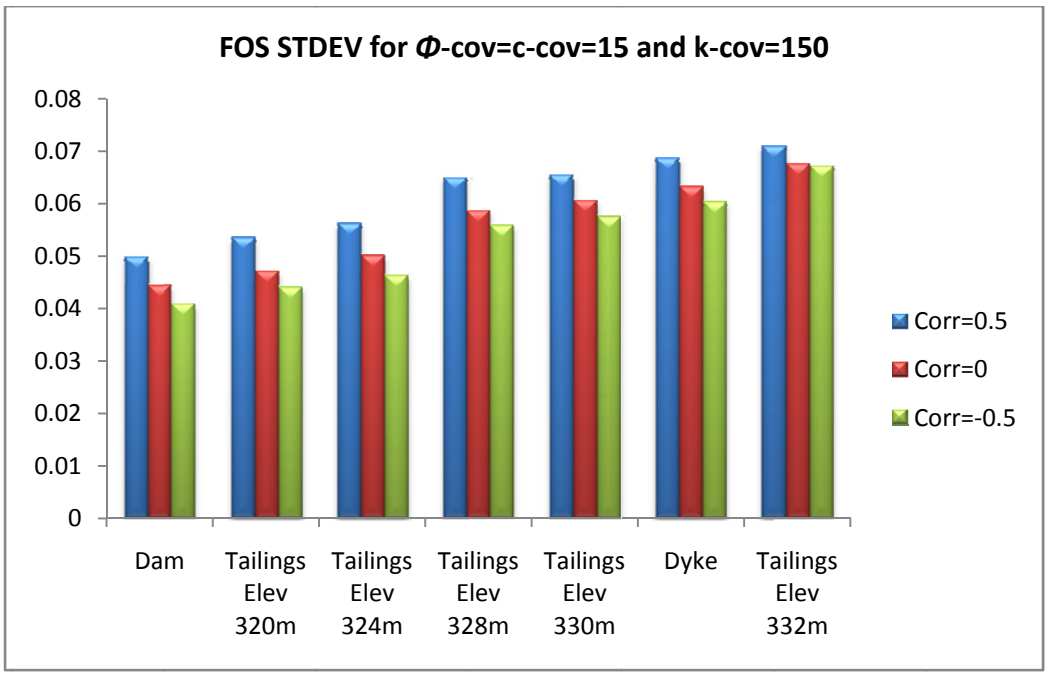

Figure 7-16: FOS Stdev for Φ-cov=c-cov=15 and k-cov=150 (MC-10, MC-11& MC-12)

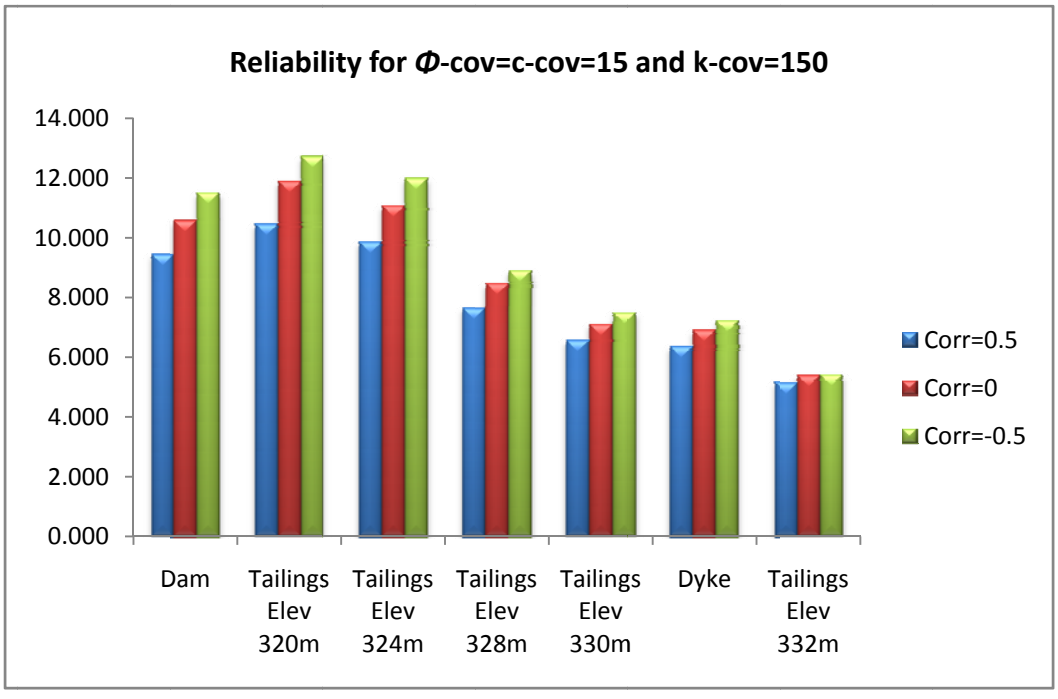

Figure 7-17: Reliability for Φ-cov=c-cov=15 and k-cov=150 (MC-10, MC-11& MC-12)

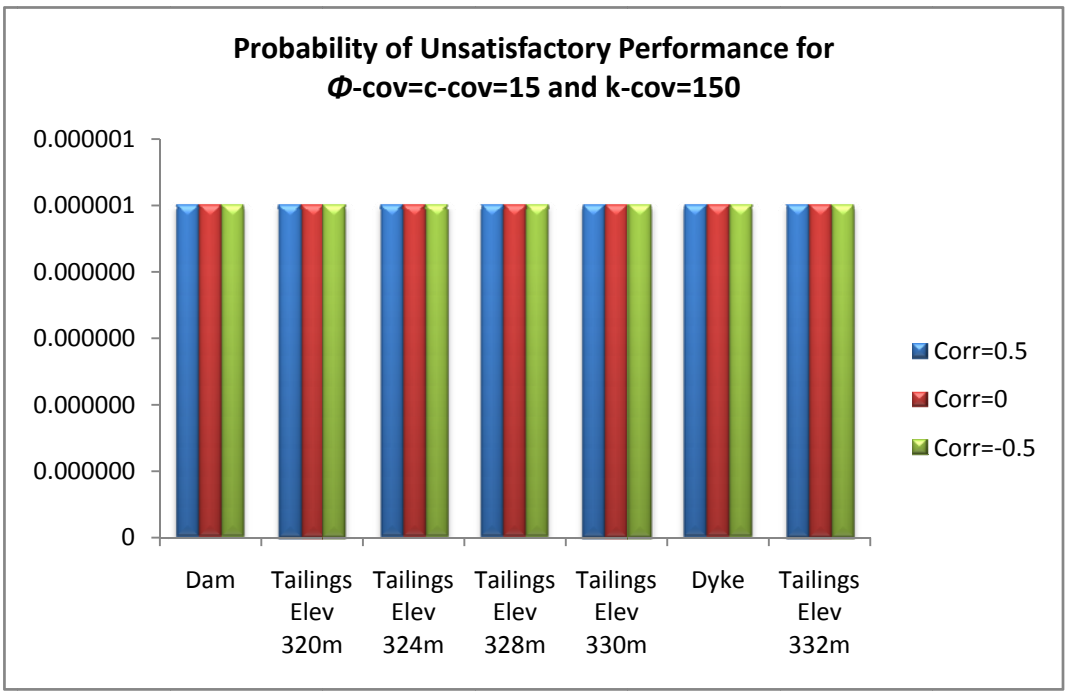

Figure 7-18: Probability of Unsatisfactory Performance for Φ-cov=c-cov=15 and k-cov=150 (MC-10, MC-11& MC-12)

7.3.2. RESULTS FOR MC-13, MC-14 AND MC-15

Similarly, Figure 7-19 illustrates that for a Φ-cov = c-cov = 30%, the mean FOS does not vary with different correlation coefficients for every stage and the mean FOS output is very close to the one generated by the deterministic analysis. Moreover, again comparing the standard deviation output in Figure 7-20 shows the output corresponding to a correlation coefficient of 0.5 experiences a higher variance than that corresponding to a ρ equal to 0 and -0.5.

Figure 7-21 reflects that the reliability for the output corresponding to a ρ equal to -0.5 is the highest, followed by ρ=0 and lastly ρ=0.5. However, the output for MC-13 now corresponds to a probability of unsatisfactory performance exceeding 0.0006 (Figure 7-22) which according to Table 7-1 reflects an above average to good performance level for the tailings impoundment. Again, the probability of unsatisfactory increases after introducing *k* as a stochastic variable.

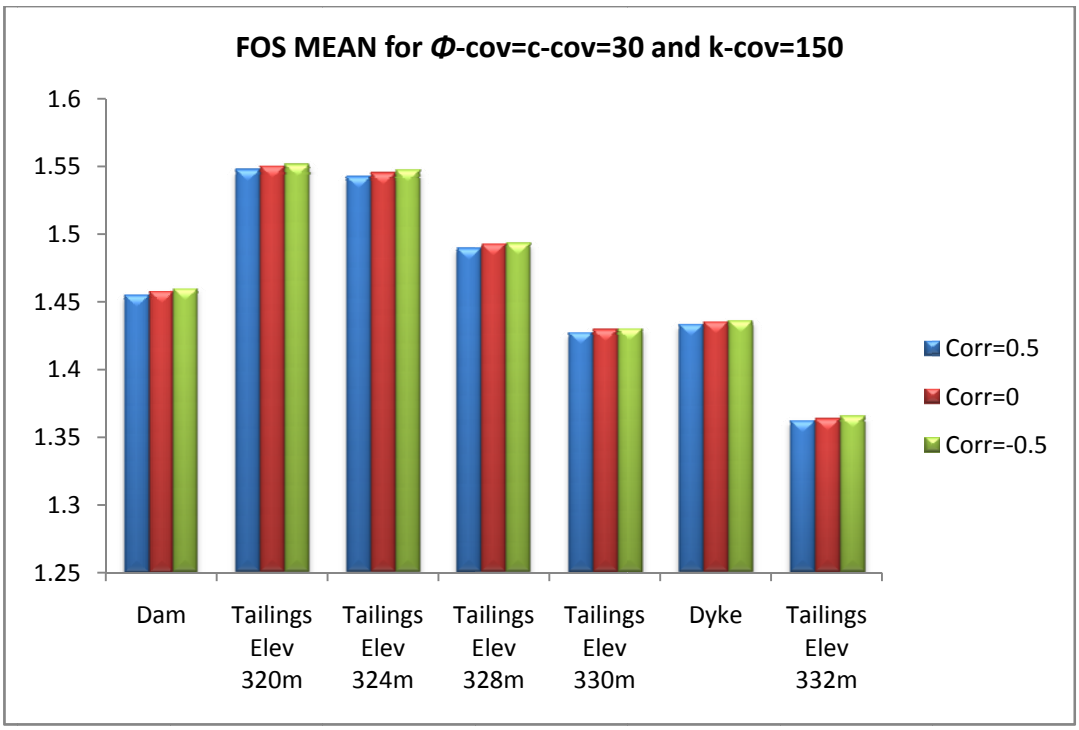

Figure 7-19: FOS Mean for Φ-cov=c-cov=30 and k-cov=150 (MC-13, MC-14& MC-15)

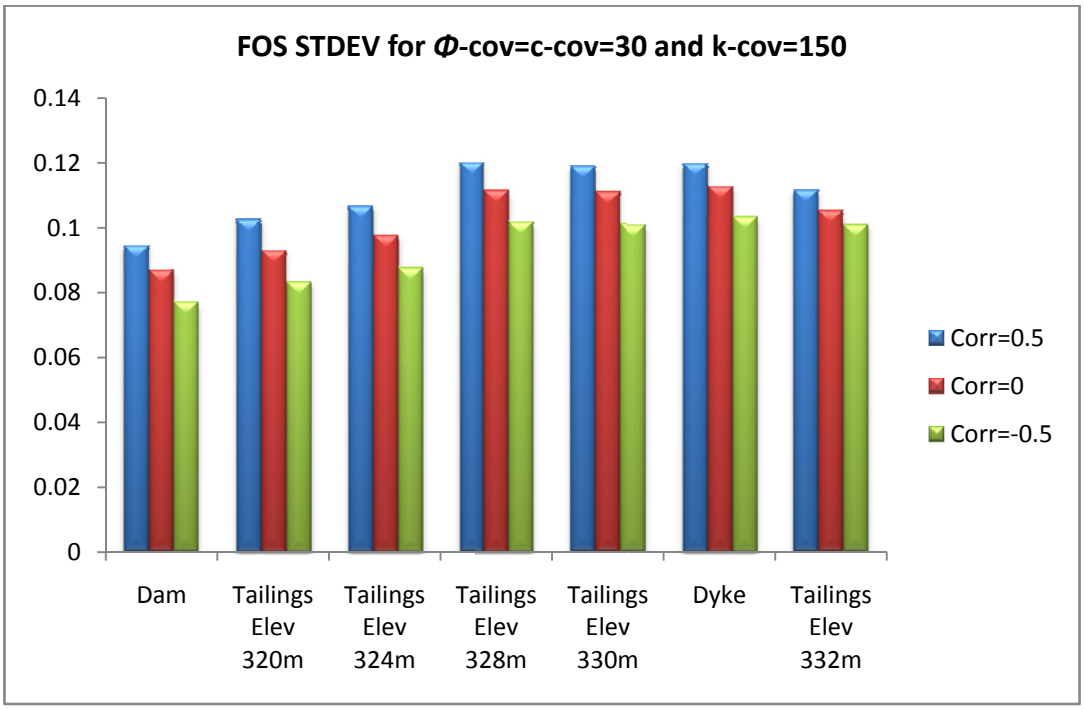

Figure 7-20: FOS Stdev for Φ-cov=c-cov=30 and k-cov=150 (MC-13, MC-14& MC-15)

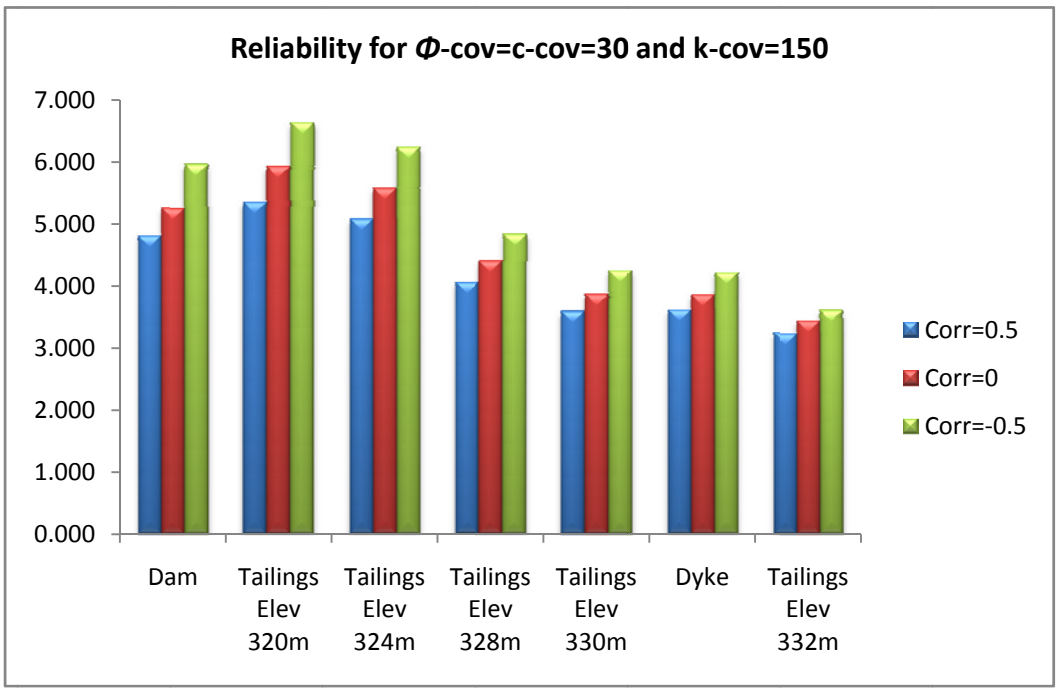

Figure 7-21: Reliability for Φ-cov=c-cov=30 and k-cov=150 (MC-13, MC-14& MC-15)

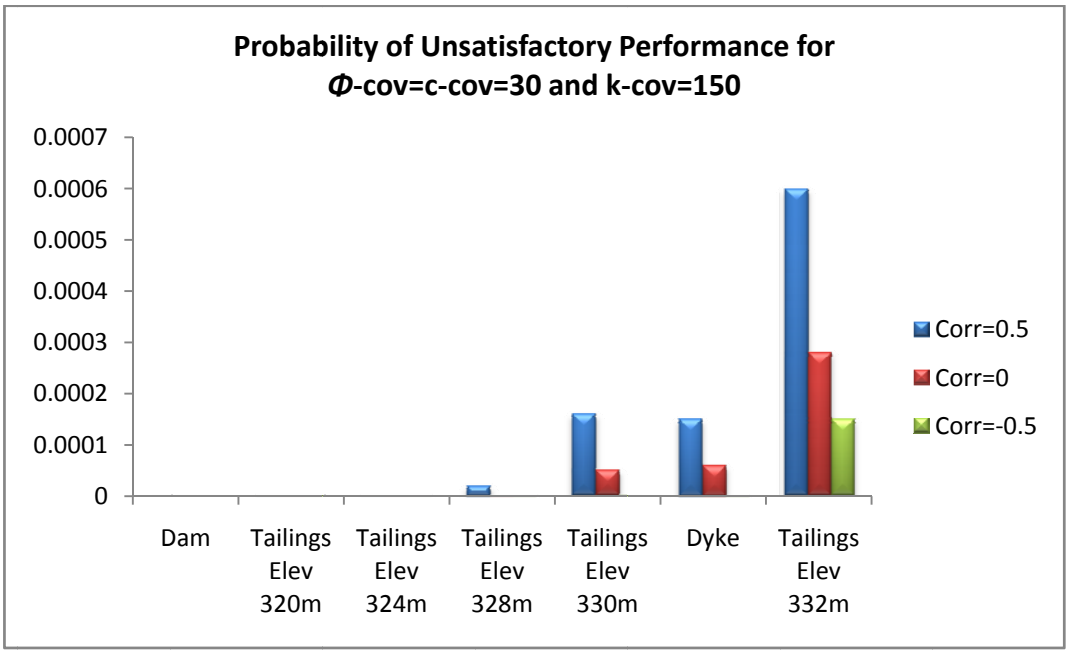

Figure 7-22: Probability of Unsatisfactory Performance for Φ-cov=c-cov=30 and k-cov=150 (MC-13, MC-14& MC-15)

7.3.3. RESULTS FOR MC-16, MC-17 AND MC-18

Similarly, Figure 7-23 illustrates that for a Φ-cov = c-cov = 45%, the mean FOS does not vary with different correlation coefficients for every stage; and the mean FOS output is very close to the one generated by the deterministic analysis. Moreover, again comparing the standard deviation output in Figure 7-24 shows the output corresponding to a correlation coefficient ρ of 0.5 experiences a higher variance than that corresponding to a ρ equal to 0 or -0.5.

Figure 7-25 reflects that the reliability for the output corresponding to a ρ equal to -0.5 is the highest, followed by ρ =0 then ρ =0.5. The output for MC-16 corresponds to a probability of unsatisfactory performance exceeding 0.007 (Figure 7-26), which is more than one order of magnitude higher than the probability calculated in the previous section. According to Table 7-1, now the tailings impoundment reflects a below average performance level.

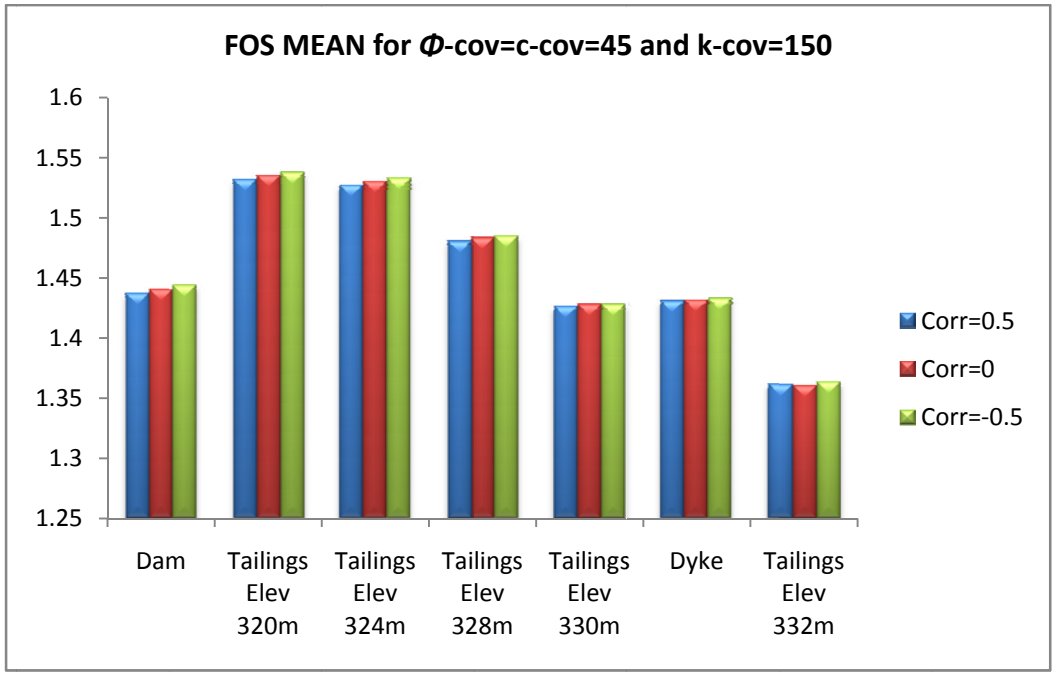

Figure 7-23: FOS Mean for Φ-cov=c-cov=45 and k-cov=150 (MC-16, MC-17& MC-18)

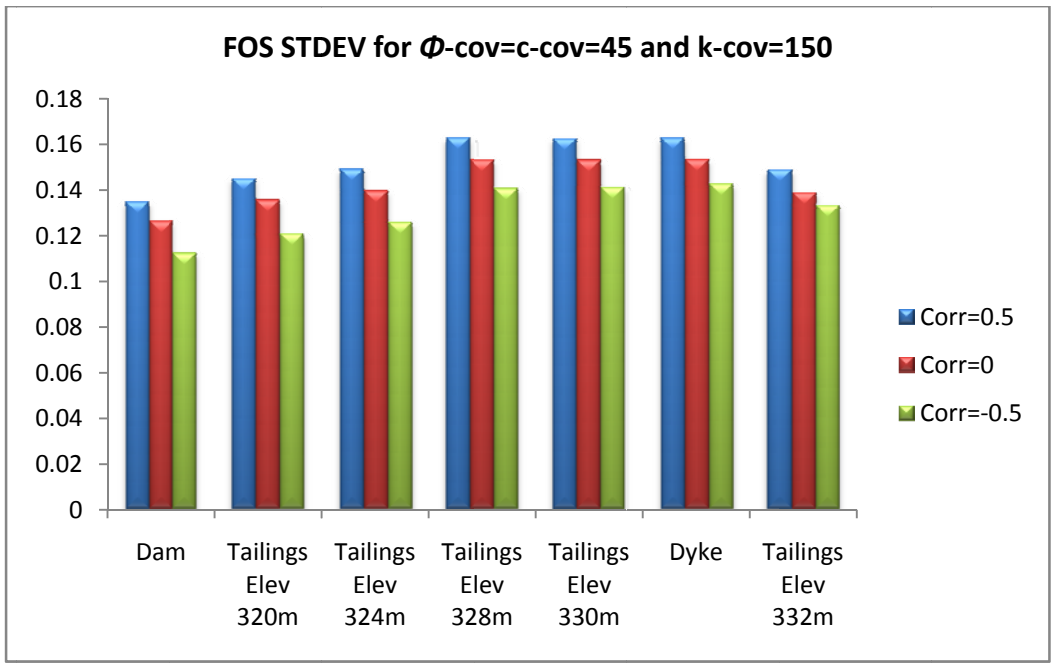

Figure 7-24: FOS Stdev for Φ-cov=c-cov=45 and k-cov=150 (MC-16, MC-17& MC-18)

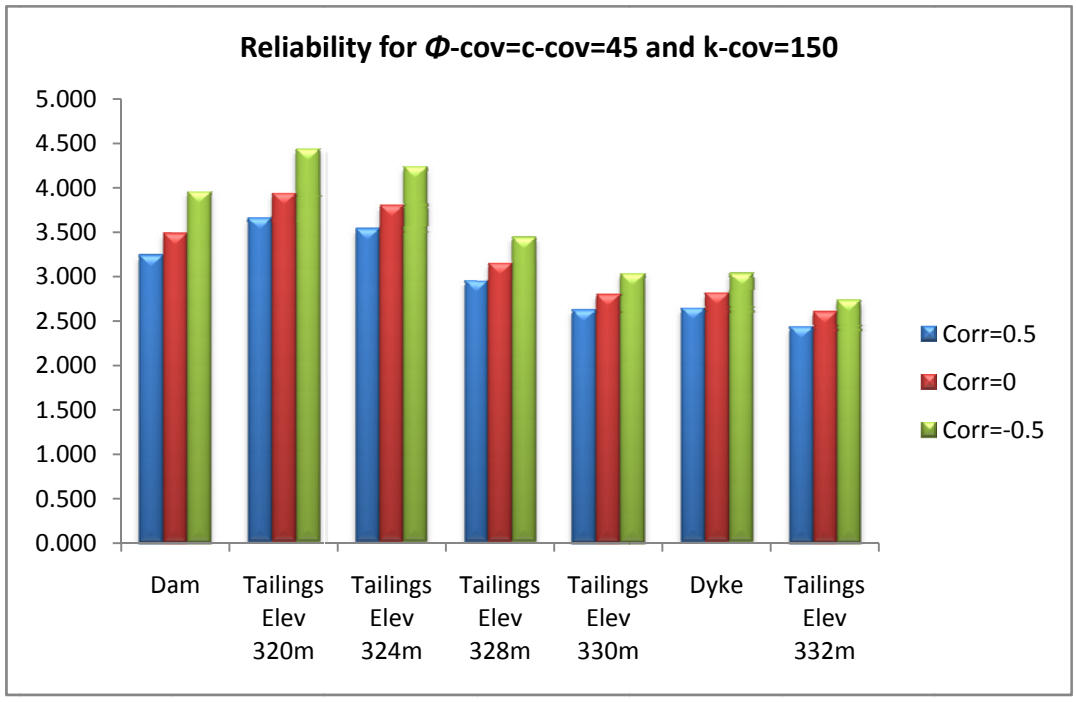

Figure 7-25: Reliability for Φ-cov=c-cov=45 and k-cov=150 (MC-16, MC-17& MC-18)

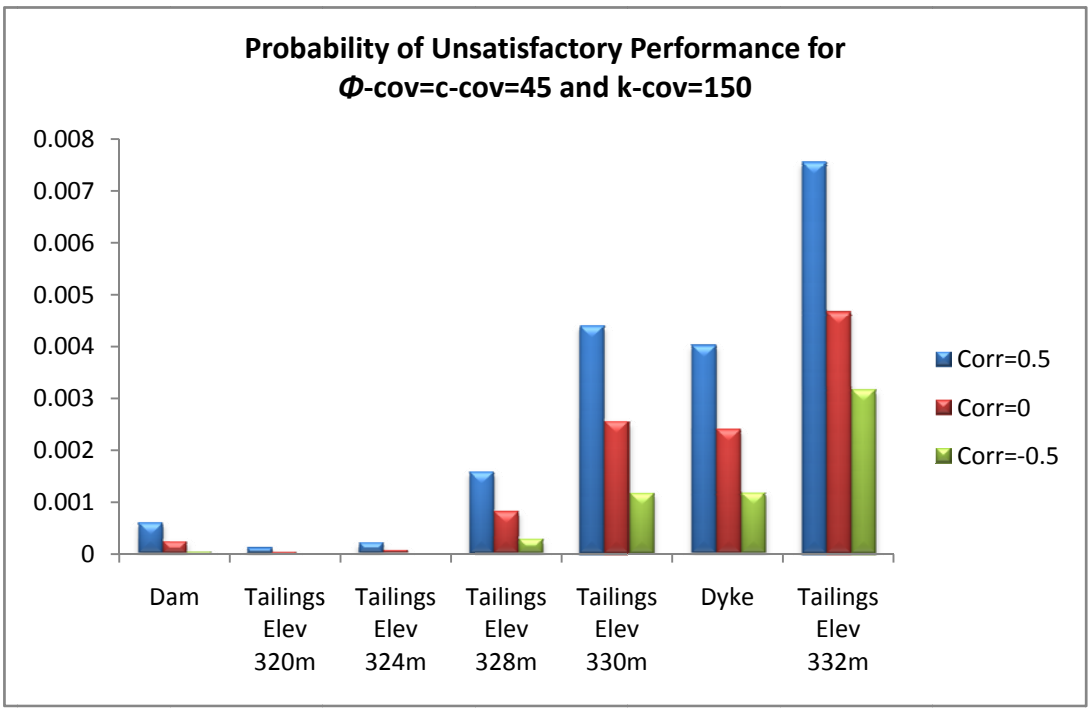

Figure 7-26: Probability of Unsatisfactory Performance for Φ-cov=c-cov=45 and k-cov=150 (MC-16, MC-17& MC-18)

7.3.4. SUMMARY FOR MC-10 THROUGH MC-18

A summary of the results for MC-10 through MC-18 for both the reliability and the probability of unsatisfactory performance are presented in Figure 7-27 and Figure 7-28, respectively.

From Figure 7-28, it is evident that MC-16 which corresponds to c-COV=Φ-COV=45, k-COV=150 and ρ=0.5 results in the highest Probability of Unsatisfactory Performance for the tailings impoundment, which is over 138% higher than the probability corresponding to a ρ=-0.5 for the same COVs. This shows the significant influence of the coefficient of correlation on the output results. Moreover, adding the *k* as a third stochastic variable increased the probability of unsatisfactory performance of the tailings impoundment.

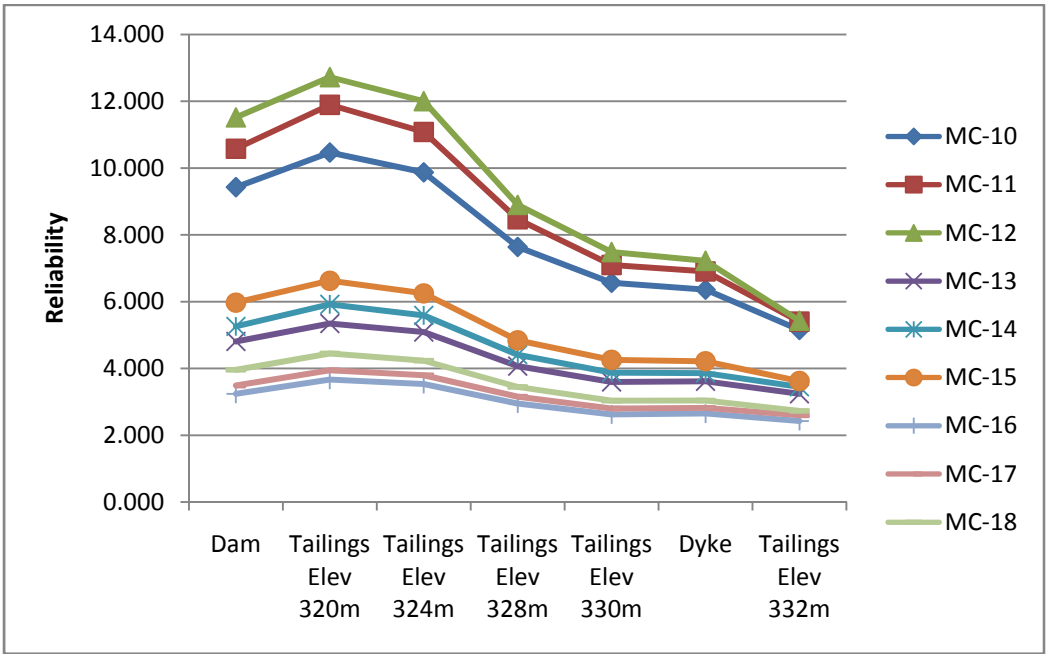

Figure 7-27: Reliability results for MC-10 through MC-18

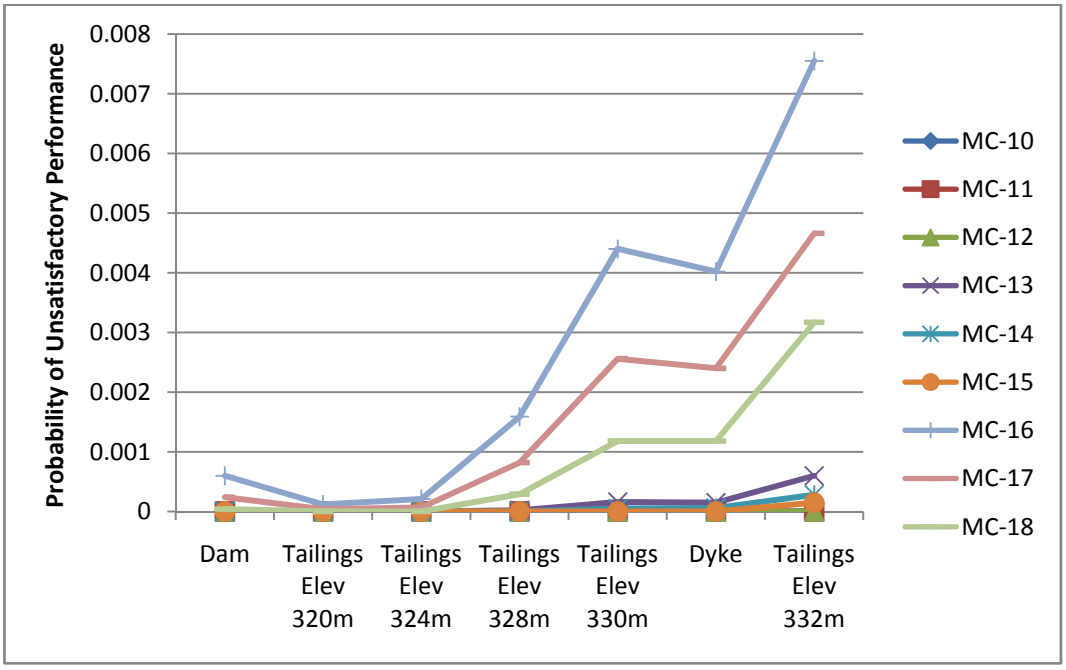

Figure 7-28: Probability of Unsatisfactory Performance results for MC-10 through 18

7.4 DISCUSSION OF RESULTS

In this section a comparison of the results with and without the permeability of the core material as a stochastic variable is presented.

In Figure 7-29, the output for Ø-cov=c-cov=30 with and without k-cov=150 is illustrated; where it is clear that systematically for all correlation values, the probability of unsatisfactory performance is higher at the end of the staged construction of the impoundment when the permeability is introduced as a stochastic variable. A similar trend is observed in Figure 7-30 corresponding to Ø-cov=c-cov=45 with and without k-cov=150. This clearly highlights the practical importance of the hydromechanical coupled analysis approach. It is evident from both figures, that as the impoundment is built over time, the influence of the uncertainty in the hydraulic parameter influence is felt at an increasing rate.

Furthermore, increasing the coefficient of variation from 15% to 45% appears to cause a significant reduction in the reliability index of the tailings dam from 8.41 to 2.47 without *k* and from 5.43 to 2.43 with *k* at an elevation of 332 meters when the dam construction is complete and under full operational load.

These results highlight the importance and need for quality control on site; e.g. use of correct placement methods and adequate equipment as well as the quality of the core material.

Introducing permeability as a stochastic variable has resulted in further deterioration of the reliability index to as low as 2.43 for a COV=45%. The influence of *k* on the reliability could only be reached using the presented hydr-mechanical coupled analysis.

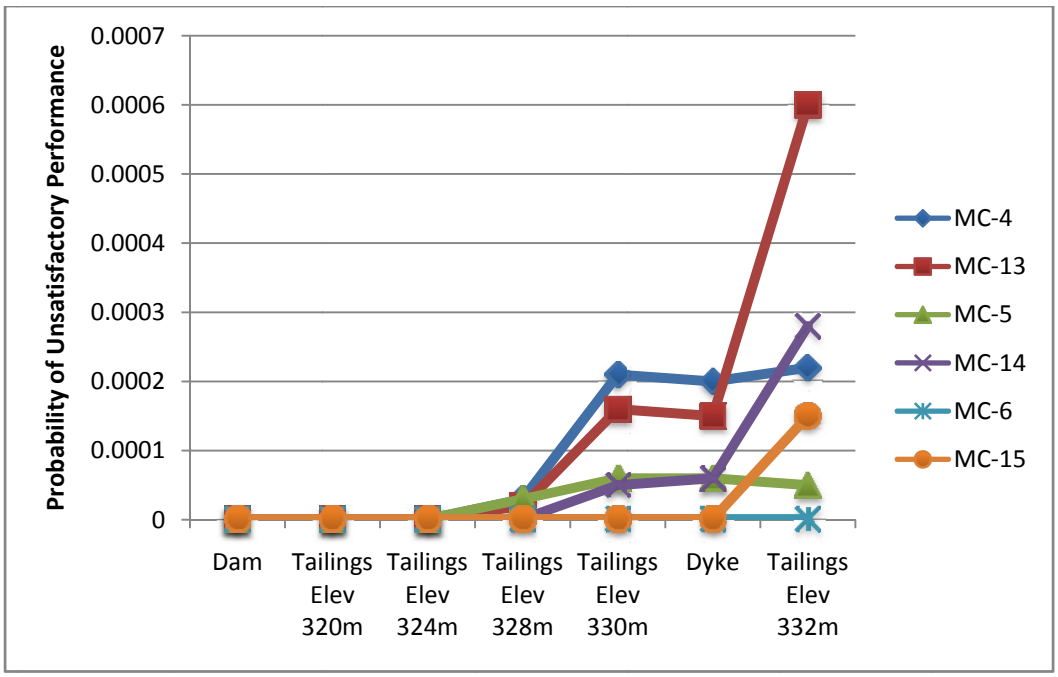

Figure 7-29: Probability of Unsatisfactory Performance for Φ-cov=c-cov=30 with and without k-cov=150 including all correlation coefficients

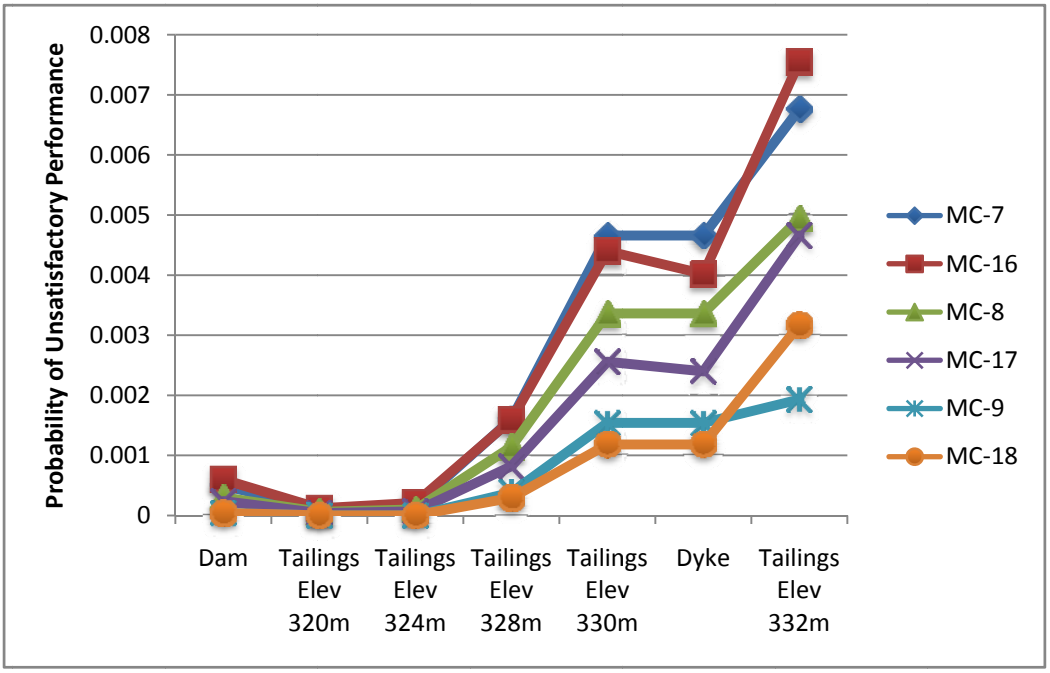

Figure 7-30: Probability of Unsatisfactory Performance for Φ-cov=c-cov=45 with and without k-cov=150 including all correlation coefficients

CHAPTER : 8 **CONCLUSION**

8.1 RESEARCH SUMMARY

Chapter 1 defined the problem as well as the scope and objectives of this work which focuses on applying novel techniques to calculate the reliability and probability of unsatisfactory performance of a water retention tailings dam integral to the tailings impoundment. The graphs presented in this Chapter highlighted the fact that slope instability remains the highest cause of incidents that may lead to dam failure.

Chapter 2 presented a literature review, highlighting the different characteristics of tailings materials and the different impoundment layouts. The chapter ended by presenting the various emerging construction practices in the management of tailings basins.

In Chapter 3 a thorough overview of the different deterministic and stochastic approaches for analyzing the stability of tailings dams was presented. An overview of the different failure modes was illustrated followed by presenting the classical stability analysis approaches and the non-linear transient coupled analysis approach. Then, the concept of uncertainty within a soil structure was presented and lastly a literature review on the probabilistic methods in geotechnical engineering was illustrated, including the Point Estimate Method (PEM), Monte Carlo (MC) and Random Monte Carlo (RMC) methods.

Next, in Chapter 4 the case study was presented and a thorough deterministic analysis study on the stability of the tailings impoundment was undertaken using the Limit Equilibrium Method (LEM). Towards the end of the chapter a sensitivity analysis was completed identifying the dam's critical shear strength parameter. The chapter ended with a section highlighting the limitations of the LEM.

In Chapter 5, the hydro-mechanical coupled approach was adopted to study the stability of the tailings impoundment using a finite difference tool, namely: the Fast Lagrangian Analysis of Continua (FLAC). The Factors of Safety (FOS) were calculated at different construction stages of the tailings basin after completing the hydro-mechanical coupled analysis at every stage. The FOS calculation at the end of every stage was done using the Strength Reduction Technique (SRT) which highlighted the maximum shear strain rate in the dam.

In Chapter 6, different probabilistic approaches were adopted for the case study leading to the choice for the extensive analysis in Chapter 7. In summary, three variations for the coefficient of variation were chosen (COV=15%, 30% & 45%) and applied on the stochastic variable: the dam's core angle of friction. The PEM was next adopted for the three scenarios followed by a comparative study between a Normal versus LogNormal PDF for the angle of friction in the MC analysis. Next, another comparative study was presented highlighting the RMC analysis versus the MC. Lastly, a final study was conducted to justify lowering the number of simulations for the MC analysis from 1,000 to 200. In all the above methods, the FOS was calculated at the end of every construction stage for all simulations and then a Normal PDF was fitted in the histogram; and following the PDF fitting the reliability and probability of unsatisfactory performance were calculated and compared.

In Chapter 7, an extensive reliability analysis was conducted that took into account two and three stochastic variables while incorporating the correlation factor between the dam`s core angle of friction and cohesion (ρ = -0.5, 0 & 0.5).It showed the reliability corresponding to a ρ = 0.5 was lower than that of 0 and -0.5. The third stochastic variable included in the study was the dam's core hydraulic conductivity that was given a COV=150% to highlight the wide variability and uncertainty associated with this parameter as was recorded in the literature. Including the permeability as a third stochastic variable resulted in an even lower reliability for the tailings impoundment.

8.2 RESEARCH CONCLUSIONS

In this research, a stochastic hydro-mechanical coupled analysis approach was presented to analyze the stability of a tailings impoundment during its staged construction over its lifetime. It was shown that such a coupled stochastic analysis approach leads the way in its capability to analyze the stability as well as the serviceability of the tailings impoundment. It can address serviceability by observing the deformations in the embankments after each stage and the stability by calculating factors of safety based on the SRT that produce failure surfaces following the maximum shear-strain rate.

It is evident from the above research, that adopting a probabilistic approach to a hydromechanical coupled model is bound to generate a probability of unsatisfactory performance with high confidence that can then be used in an extensive quantitative risk analysis exercise.

It was further shown, that by considering stochastic properties to both the mechanical and hydraulic material properties of the dam`s core, the probability of unsatisfactory performance increased at the end of the staged construction of the tailings impoundment. This highlights the importance of incorporating both the mechanical and the hydraulic properties as stochastic variables for the purpose of studying the geotechnical performance of the tailings impoundment.

In conclusion, experienced engineers could use the results of this study along with their observations in the field and with their judgement be able to solidify their confidence in the design and construction of the tailings impoundment. The approach proposed in this thesis allows the engineer to better understand the performance of the impoundment under different conditions and as such pre-empt against their existence by relating the findings to the tailings management practices currently being followed on the site.

8.3 RECOMMENDATIONS FOR FURTHER RESEARCH

This research contributed to advancing the application of stochastic methods to tailings impoundments; nevertheless, recommendations for future studies are noted below.

1. Analyzing the same model in the pseudo-static case as well as in the dynamic case.

2. Look into correlating output results with the impoundments susceptibility to liquefaction.

3. Utilize the surface response method to exploit the results of a limited number of MC simulations, e.g. 200, as an alternative approach to assess the reliability index

4. Look into the possibility with future versions of FLAC to use alternative constitutive models while applying the SRT to calculate the FOS.

5. Perform a quantitative risk analysis using the output of this study to calculate risk matrices and measure risk tolerance.

6. Explore the coupled influence of the hydraulic conductivity anisotropy and strength anisotropy on the tailings impoundment slope stability; and consider them as stochastic variables in a future research.

STATEMENT OF CONTRIBUTIONS

This study is the first to adopt multiple stochastic methods to a tailings impoundment for the purpose of analyzing its geotechnical performance. The specific contributions are:

1. Provided a methodological approach for the application of the stochastic analysis on a tailings impoundment. As a result the designer will be able to know how to telescope his stochastic analysis from a broader approach (PEM) to a more rigorous one (MC).

2. Applied a stochastic hydro-mechanical coupled analysis for the purpose of analyzing the stability of the tailings impoundment at different construction stages; i.e. different stages in its life.

3. Considered both mechanical and hydraulic parameters as stochastic variables in the hydro-mechanical coupled stochastic analysis.

4. Performed an extensive reliability analysis on a tailings impoundment using the calculated FOS from the probabilistic approach.

REFERENCES

Al-Karni, A. A. and M. A. Al-Shamrani (2000). "Study of the effect of soil anisotropy on slope stability using method of slices." Computers and Geotechnics **26**(2): 83-103.

Archibald, J. F. Beneficial impacts of Paste Tailings on Environmental Hazard Mitigation and Engineering Performance Improvement. Kingston, Ontario, Department of Mining Engineering, Queen's University.

Auvinet, G. and J. L. González (2000). "Three-dimensional reliability analysis of earth slopes." Computers and Geotechnics **26**(3-4): 247-261.

Babu, G. L. S., A. Srivastava, et al. (2006). "Reliability Analysis of the Bearing Capacity of a Shallow Foundation Resting on Cohesive Soil." Canadian Geotechnical Journal **43**: 217-223.

Babu, G. L. S., A. Srivastava, et al. (2007). "Analysis of Stability of Earthen Dams in Kachchh Region, Gujarat, India." Engineering Geology **94**: 123-136.

Baecher, G. B. and J. T. Christian (2003). Reliability and Statistics in Geotechnical Engineering. The Atrium, Southern Gate, Chichester, West Sussex, England, John Wiley & Sons Ltd.

Benson, C. H. (1993). "Probability Distributions for Hydraulic Conductivity of Compacted Soil Liners." Journal of Geotechnical and Geoenvironmental Engineering, ASCE **119**(3): 471-486.

Biot, M. A. (1941). "General Theory of Three-Dimensional Consolidation." Journal of Applied Physics **12**(2): 155-164.

Bjelkevik, A. (2005). Water Cover Closure Design for Tailings Dams: State of the Art Report. Sweden, Lulea University of Technology**:** 103.

Bowles, D. S., L. R. Anderson, et al. (1996). Risk Assessment Approach to Dam Safety Criteria: Uncertainty in Geologic Environment, from Theory to Practice. Proceedings of ASCE, STP.

Bussiere, B. (2007). "Colloquium 2004: Hygrogeotechnical Properties of Hard Rock Tailings from Metal Mines and Emerging Geoenvironmental Disposal Approaches." Canadian Geotechnical Journal **44**: 1019-1052.

Calderon, A., A. Catalan, et al. (2003). Modelo de Riesgo Geotecnico y Bases Geotecnicas, Plan Minero CBV-2003, Mina Chiquicamata, CODELCO, Chile.

Cho, S. E. (2007). "Effects of spatial variability of soil properties on slope stability." Engineering Geology **92**(3-4): 97-109.

Cho, S. E. (2010). "Probabilistic Assessment of Slope Stability That Considers the Spatial Variability of Soil Properties." Journal of Geotechnical and Geoenvironmental Engineering **136**(7): 975-984.

Christian, J. T. (2004). "Geotechnical Engineering Reliability: How Well Do We Know What We Are Doing?" Journal of Geotechnical and Geoenvironmental Engineering **130**(10): 985-1003.

Christian, J. T. and G. B. Baecher (1999). "Point-Estimate Method as Numerical Quadrature." Journal of Geotechnical and Geoenvironmental Engineering **125**(9): 779-786.

Christian, J. T., C. C. Ladd, et al. (1994). "Reliability Applied to Slope Stability Analysis." Journal of Geotechnical Engineering **120**(12): 2180-2207.

Davies, M. P., P. C. Lighthall, et al. (2002). Design of Tailings Dams and Impoundments. Phoenix, Tailings and Mine Waste Practices, SME, AGM.

Davis, R. O. and A. P. S. Selvadurai (2002). Plasticity and geomechanics. Cambridge, UK ; New York, Cambridge University Press.

Dawson, E. M. and W. H. Drescher (1999). "Slope stability analysis by strength reduction." Geotechnique **49**(6): 835-840.

Dawson, E. M. and W. H. Roth (1999). "Slope stability analysis with FLAC." Flac and Numerical Modeling in Geomechanics: 3-9.

Donald, I. B. and S. K. Giam (1988). Application of the nodal displacement method to slope stability analysis. Proceedings of the 5th Australia-New Zealand Conference on Geomechanics, Sydney, Australia.

Dong, J.-J., C.-H. Tu, et al. (2012). "Effects of hydraulic conductivity/strength anisotropy on the stability of stratified, poorly cemented rock slopes." Computers and Geotechnics **40**(0): 147-159.

Duncan, J. M. (2000). "Factors of Safety and Reliability in Geotechnical Engineering." Journal of Geotechnical and Geoenvironmental Engineering **126**(4): 307-316.

Duncan, J. M. and S. G. Wright (2005). Soil strength and slope stability. Hoboken, N.J., John Wiley & Sons.

El-Ramly, H. (2001). Probabilistic Analyses of Landslide Hazards and Risks: Bridging Theory and Practice. PhD, University of Alberta.

El-Ramly, H., N. R. Morgenstern, et al. (2002). "Probabilistic Slope Stability Analysis for Practice." Canadian Geotechnical Journal **39**: 665-683.

Elkateb, T., R. Chalatumyk, et al. (2003). "An Overview of Soil Heterogeniety: Quantification and Implications on Geotechnical Field Problems." Canadian Geotechnical Journal **40**: 1-15.

Engels, J. (2005). Tailings Info Web Site: Upstream Design, http://www.tailings.info/upstream.htm.

Fenton, G. A. and D. V. Griffiths (2003). "Bearing Capacity Prediction of Spatially Random c - φ Soils." Canadian Geotechnical Journal **40**(1): 54-65.

Fenton, G. A. and D. V. Griffiths (2005). A Slope Stability Reliability Model. Proceedings of the K.Y. Lo Symposium (on CD). London, Ontario, Canada.

Fenton, G. A. and D. V. Griffiths (2008). Risk Assessment in Geotechnical Engineering, John Wiley & Sons, Inc., Hoboken, New Jersey.

Fishman, G. S. (1995). Monte Carlo: Concepts, Algorithms, and Applications, Springer, New York.

FLAC and ICGInc. (2011). FLAC: Fast Lagrangian Analysis of Continua User's Guide. Itasca Consulting Group Inc., Minneapolis.

Fredlund, D. G. and J. Krahn (1977). "Comparison of Slope Stability Methods of Analysis." Canadian Geotechnical Journal **14**(3): 429-439.

GEO-SLOPE and SLOPE/W (2010). Stability Modeling with SLOPE/W 2007 Version. Calgary, Alberta, Canada T2P 2Y5, GEO-SLOPE International Ltd.

Griffiths, D. V. and G. A. Fenton (1998). "Probabilistic Analysis of Exit Gradients Due to Steady Seepage." Journal of Geotechnical and Geoenvironmental Engineering **124**(9): 789-797.

Griffiths, D. V. and G. A. Fenton (2004). "Probabilistic Slope Stability Analysis by Finite Elements." Journal of Geotechnical and Geoenvironmental Engineering **130**(5): 507-518.

Griffiths, D. V. and G. A. Fenton (2007). Probabilistic Methods In geotechnical Engineering. International Centre for Mechanical Sciences -CISM courses and lectures. Udine, Italy, CISM. **491:** 149.

Griffiths, D. V., G. A. Fenton, et al. (2002). "Probabilistic Analysis of Underground Pillar Stability." International Journal for Numerical and Analytical Methods in Geomechanics **26**: 775-791.

Griffiths, D. V., G. A. Fenton, et al. (2002). "Bearing Capacity of Rough Rigid Strip Footing on Cohesive Soil: Probabilistic Study." Journal of Geotechnical and Geoenvironmental Engineering **128**(9): 743-755.

Griffiths, D. V., G. A. Fenton, et al. (2006). "Undrained Bearing Capacity of Two-Strip Footings on Spatially Random Soil." International Journal of Geomechanics **6**(6): 421-427.

Griffiths, D. V. and P. A. Lane (1999). "Slope stability analysis by finite elements." Geotechnique **49**(3): 387-403.

Grivas, D. A. (1981). How Reliable are the Present Slope Failure Prediction Methods? Proceedings of the Tenth International Conference of Soil Mechanics and Foundation Engineering, Stockholm, Sweden.

Haldar, A. and S. Mahadevan (2000). Probability, Reliability, and Statistical Methods in Engineering Design. New York, NY, John Wiley & Sons, Inc.

Hammah, R. E., T. E. Yacoub, et al. (2009). Probabilistic Slope Analysis with the Finite Element Method. American Rock Mechanics Association, Asheville 2009.

HKS (2004). "Hibbit, Karlsson and Sorensen, Inc., ABAQUS Theory and Analysis Users Manual."

Hoede-Keyser, J. (1970). Design, specification, control and performance survey: a quality entity. Symposium on Quality Control of Road Works, Centre d'Etudes Techniques de l'Equipement.

Hoek, E. (1998). Rock engineering: The application of modern techniques to underground design, Brazilian Rock Mechanics Committee (CBMR),

Brazilian Tunneling Committee (CBT), Brazilian Society for Soil Mechanics and Geotechnical Engineering (ABMS), Sao Paulo, Brazil.

Hsu, Y.-C., J.-S. Lin, et al. (2007). "Projection Method for Validating Reliability Analysis of Soil Slopes." Journal of Geotechnical and Geoenvironmental Engineering **133**(6): 753-756.

ICOLD (2001). Tailings Dams - Risk of Dangerous Occurrences: Lessons Learnt from Practical Experiences. Paris, Commission Internationale des grands Barrages. **Bulletin 121:** 145.

Kealy, C. and R. Busch (1971). Determining Seepage Characteristics of Mill-Tailings Dams by the Finite-Element method. RI 7477, U.S. Bureau of Mines.

Lacasse, S. and F. Nadim (1996). Uncertainties in characterizing soil properties. Uncertainty in the Geologic Environment, Madison, ASCE.

Lambe, T. W. and R. V. Whitman (1969). Soil mechanics. New York,, Wiley.

Lee, I. K., W. White, et al. (1983). Geotechnical Engineering. Boston, Pitman.

Lumb, P. (1970). "Safety factors and the probability distribution of soil strength." Canadian Geotechnical Journal **7**(3): 225-242.

Lumb, P. (1974). Applications of statistics in soil mechanics. Soil Mechanics: New Horizons, London, Newnes-Butterworth.

MAC (2011). A Guide to the Management of Tailings Facilities. Ottawa, Ontario, The Mining Association of Canada, www.mining.ca**:** 68.

Matsui, T. and K.-C. San (1992). "Finite element slope stability analysis by shear strength reduction technique." Soils Found **32**(1): 59-70.

Morgenst.Nr and V. E. Price (1967). "A Numerical Method for Solving Equations of Stability of General Slip Surfaces." Computer Journal **9**(4): 388-&.

Morgenstern, N. R. (2000). "Common Ground." from http://lib.hpu.edu.cn/comp_meeting/ICGGE%E5%9B%BD%E9%99%85%E5%9C%B0%E8%B4%A8%E5%B7%A5%E7%A8%8B%E4%BC%9A%E8%AE%AE%E8%AE%BA%E6%96%87%E6%95%B0%E6%8D%AE%E5%BA%93/PAPERS/INVITED/MORGEN.PDF.

Naylor, D. J. (1981). Finite elements and slope stability. Numerical methods in geomechanics, Proceedings of the NATO Advanced Study Institute, Lisbon, Portugal.

Newmark, N. M. (1965). "Effects of Earthquakes on Dams and Embankments." Geotechnique **15**(2): 139-160.

Phoon, K.-K. and F. H. Kulhawy (1999). "Characterization of Geotechnical Variability." Canadian Geotechnical Journal **36**: 612-624.

Riela, J., A. Urzua, et al. (1999). Sliding Rock Wedge Reliability Analysis of Chuquicamata Mine Slopes. Proceedings of the 11th Pan-American Conference on Soil Mechanics and Geotechnical Engineering, Foz do Iguacu, brazil.

RocScience and Slide (2011). Slide: 2D Limit Equilibrium Slope Stability Analysis. 31 Balsam Avenue, Toronto, Ontario M4E 3B5, Rocscience Inc. .

Rosenblueth, E. (1975). "Point Estimates for Probability Moments." Proceedings of the National Academy of Sciences **72**(10): 3812-3814.

Rosenblueth, E. (1981). "Two-point estimates in probabilities." Applied Mathematical Modelling **5**(5): 329-335.

Saad, B. (2008). Transient Coupled Analysis of Upstream Tailings Disposal Facilities Construction. PhD, McGill University.

Saad, B. and H. Mitri (2010). "Staged Construction Analysis of Surface Tailings Disposal Facilities." International Journal of Mining, Reclamation and Environment **24**(1): 44-63.

Saad, B. and H. Mitri (2011). "Hydromechanical Analysis of upstream Tailings Disposal Facilities." Journal of Geotechnical and Geoenvironmental Engineering **137**(1): 27-42.

Schultze, E. (1975). Some aspects concerning the application of statistics and probability to foundation structures. Second International Conference on Applications of Statistics and Probability in Soil and Structural Engineering, Aachen.

Seed, H. B. (1979). "19th Rankine Lecture - Considerations in the Earthquake Resistant Design of Earth and Rockfill Dams." Geotechnique **29**(3): 213-263.

Singh, A. (1971). How reliable is the factor of safety in foundation engineering? First International Conference on Applications of Statistics and Probability in Soil and Structural Engineering, Hong Kong, Hong Kong University Press.

USACE (1997). Introduction to probability and reliability methods for use in geotechnical engineering. Washington, D.C., U.S. Army Corps of Engineers. **ETL 1110-2-547**.

USACE (1997). Risk-Based Analysis in Geotechnical Engineering for Support of Planning Studies, Engineering and Design. Washington, D.C., U.S. Army Corps of Engineers, Department of Army**:** p. 20314-20100.

USACE (1998). Risk-Based Analysis in Geotechnical Engineering for Support of Planning Studies. Engineering Circular No. 1110-2-554. Washington, D.C., U.S. Army Corps of Engineers, Department of the Army.

Vick, S. G. (1983). Planning, Design, and Analysis of Tailings Dams. New York John Wiley & Sons.

Vick, S. G. (1990). Planning, Design and Analysis of Tailings Dams, BiTech Publishers Ltd.

Whitman, R. V. (2000). "Organizing and Evaluating Uncertainty in Geotechnical Engineering." Journal of Geotechnical and Geoenvironmental Engineering **126**(7): 583-593.

Wolff, T. H. (1985). Analysis and design of embankment dam slopes: A probabilistic approach. PhD Thesis, Purdue University.

Zhou, J. and A. S. Nowak (1988). "Integration formulas to evaluate functions of random variables." Structural safety **5**: 267-284.

Zienkiewicz, O. C., A. H. C. Chan, et al. (1999). Computational Geomechanics with Special Reference to Earthquake Engineering, John Wiley and Sons Ltd., England

Zienkiewicz, O. C., C. Humpheson, et al. (1975). "Associated and non-associated viscoplasticity and plasticity in soil mechanics." Geotechnique **25**: 671-689.

APPENDIX A – PDF FITTING FOR STOCHASTIC OUTPUT

MC (f-cov=15,c-cov=15,corr(f,c)=0.5)

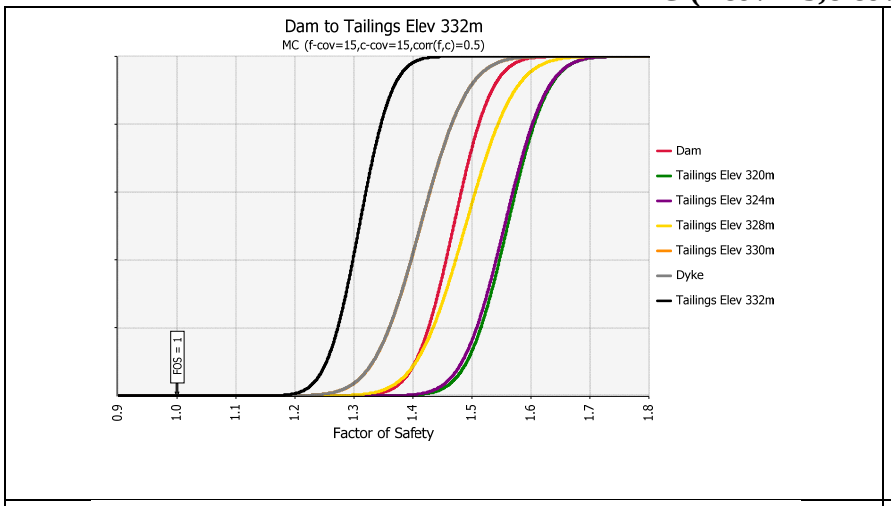

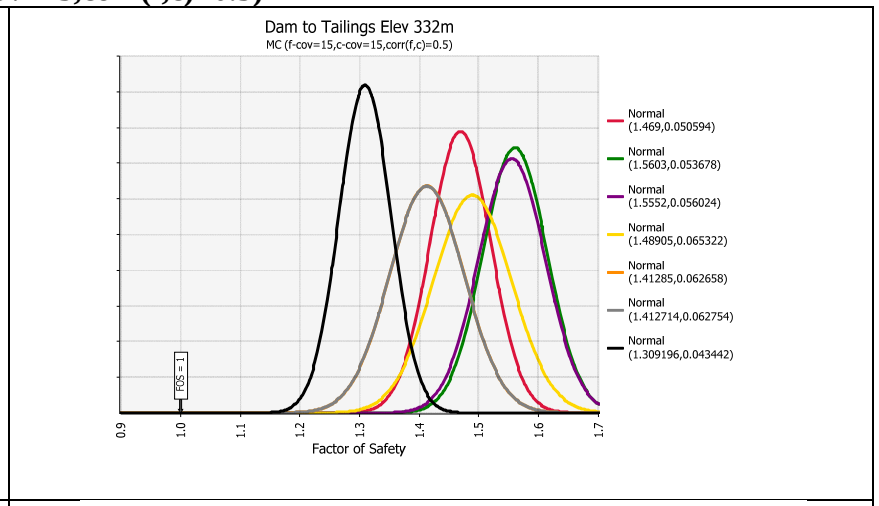

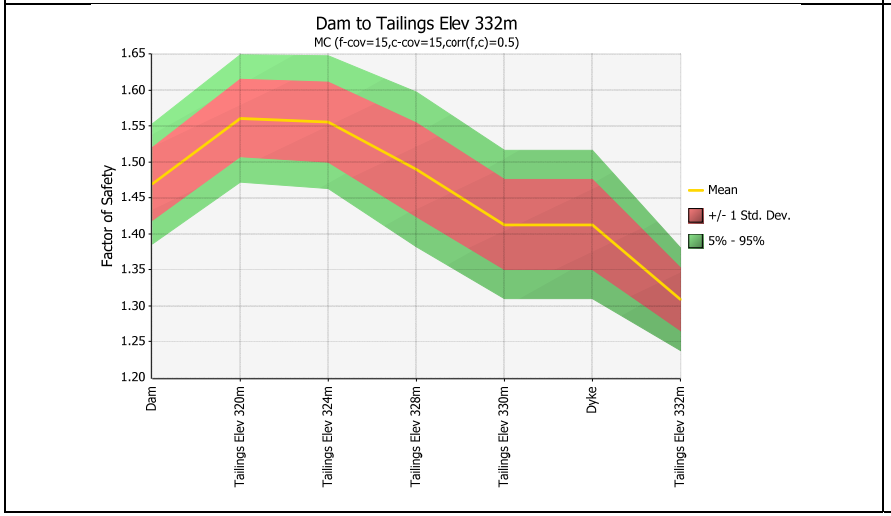

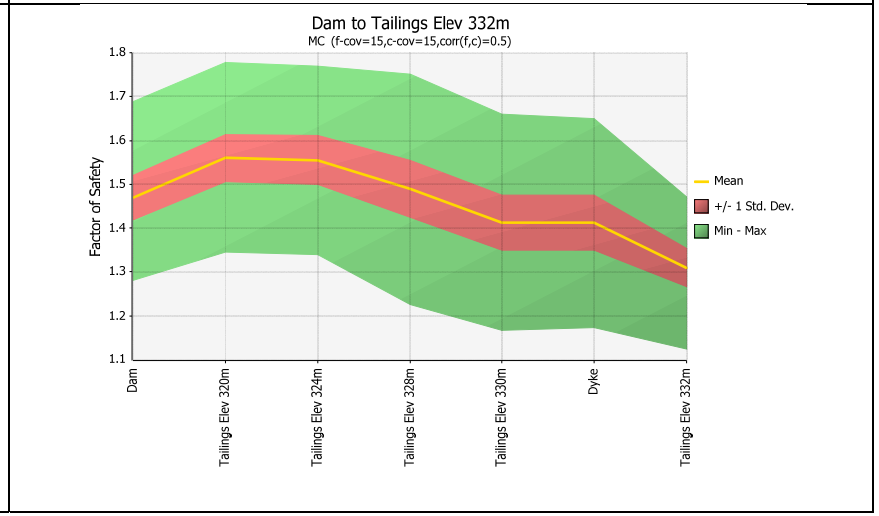

MC (f-cov=15,c-cov=15,corr(f,c)=0.5)

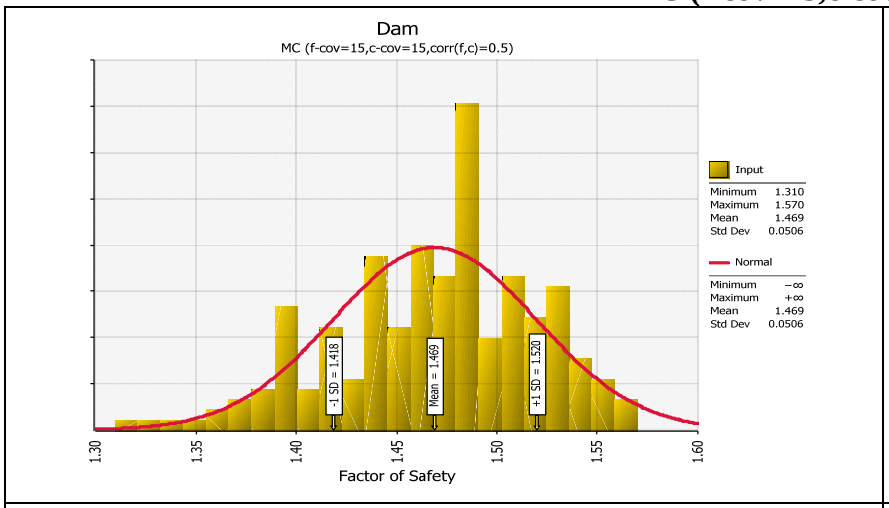

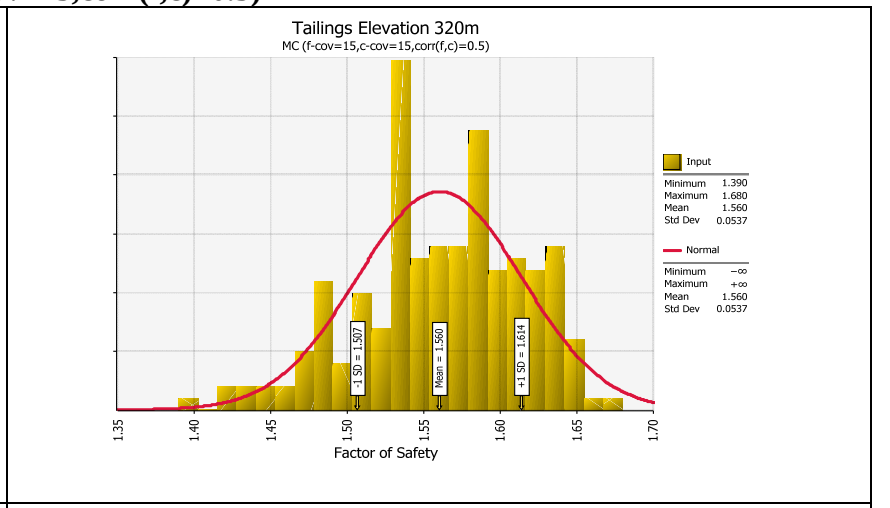

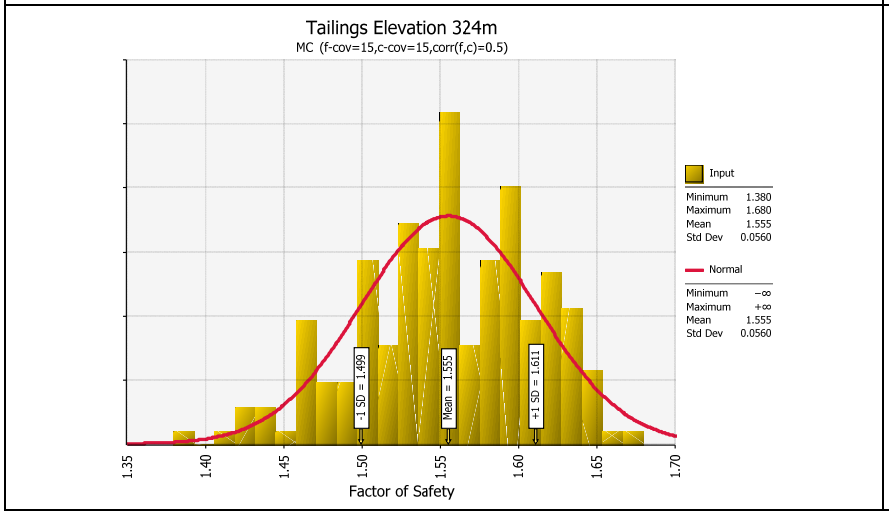

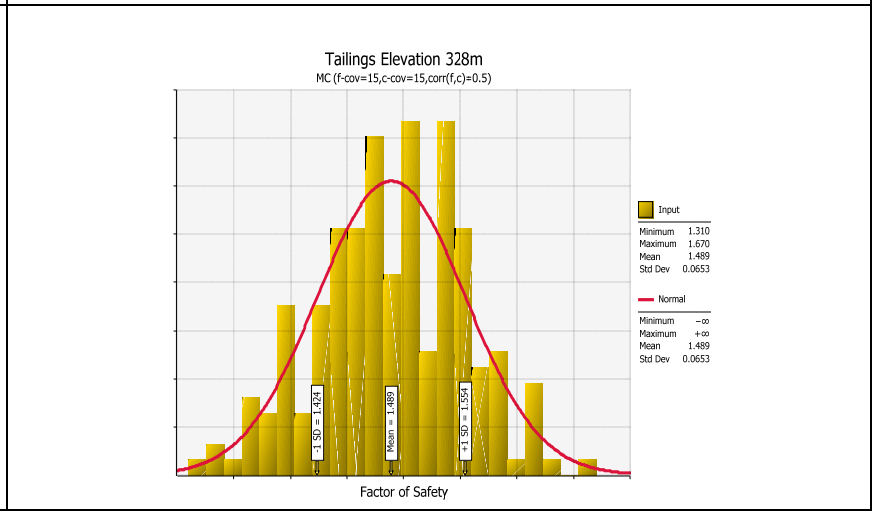

MC (f-cov=15,c-cov=15,corr(f,c)=0.5)

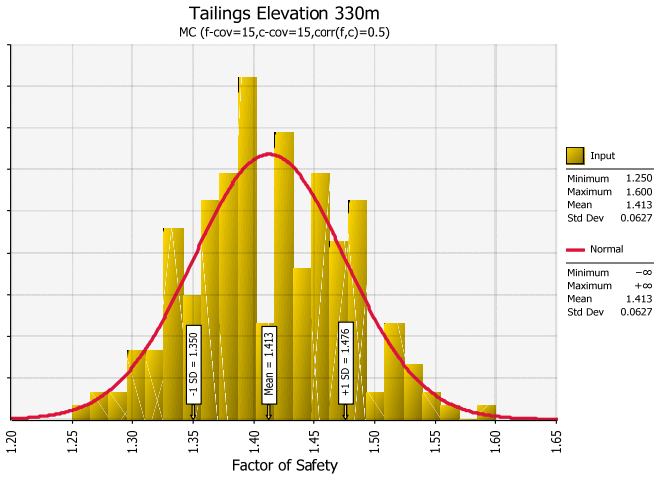

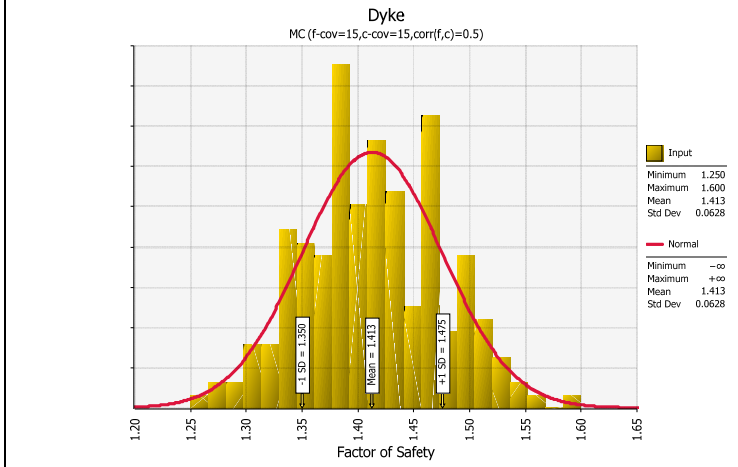

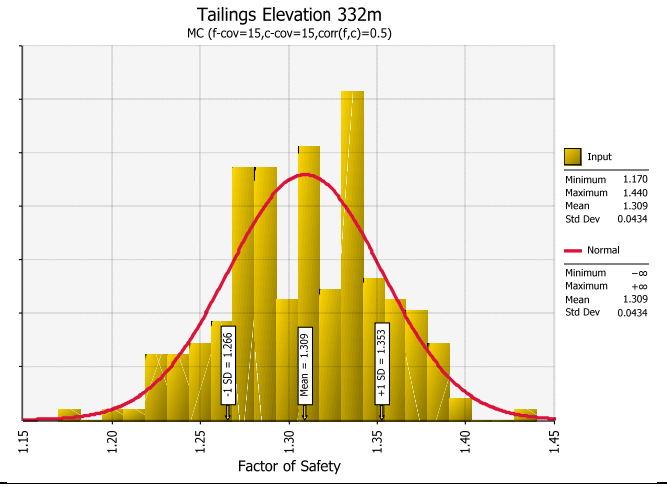

MC (f-cov=15,c-cov=15, corr(f,c)=0.5)	MEAN	STDEV	Reliability	Probability of Unsatisfactory Performance
Dam	1.469	0.050594	9.269874	0
Tailings Elev 320m	1.5603	0.053678	10.43817	0
Tailings Elev 324m	1.5552	0.056024	9.910039	0
Tailings Elev 328m	1.48905	0.065322	7.486758	0
Tailings Elev 330m	1.41285	0.062658	6.588943	0
Dyke	1.412714	0.062754	6.576696	0
Tailings Elev 332m	1.309196	0.043442	7.117444	0

MC (f-cov=15,c-cov=15,corr(f,c)=0)

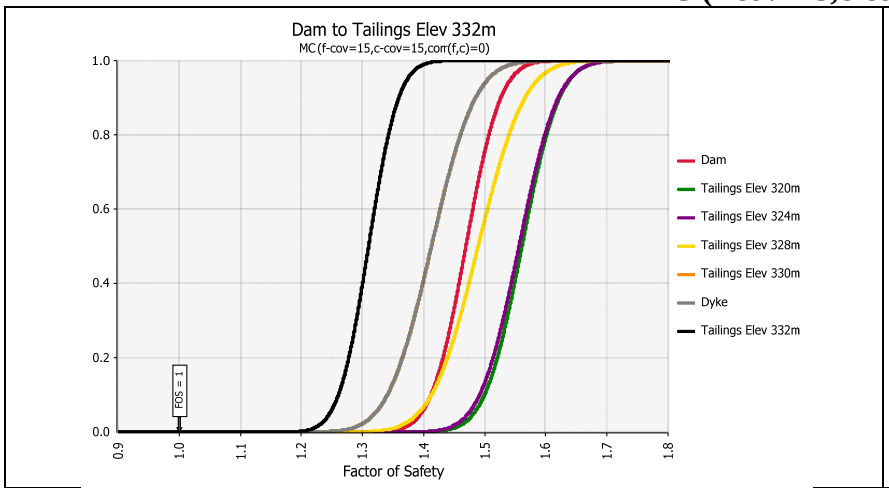

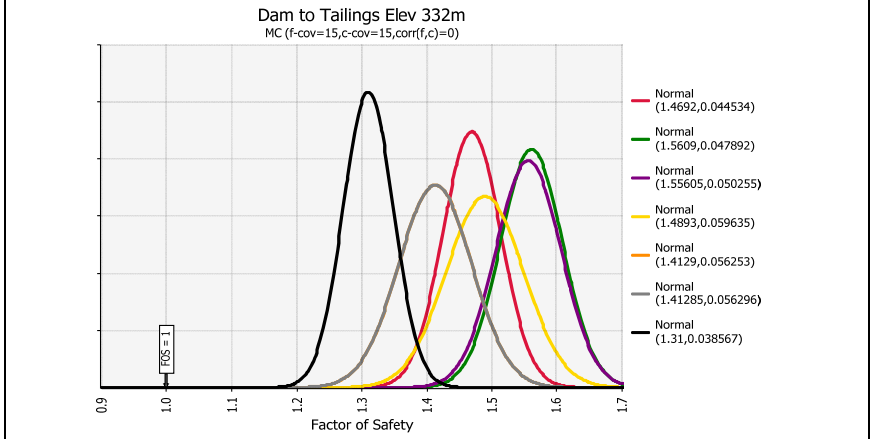

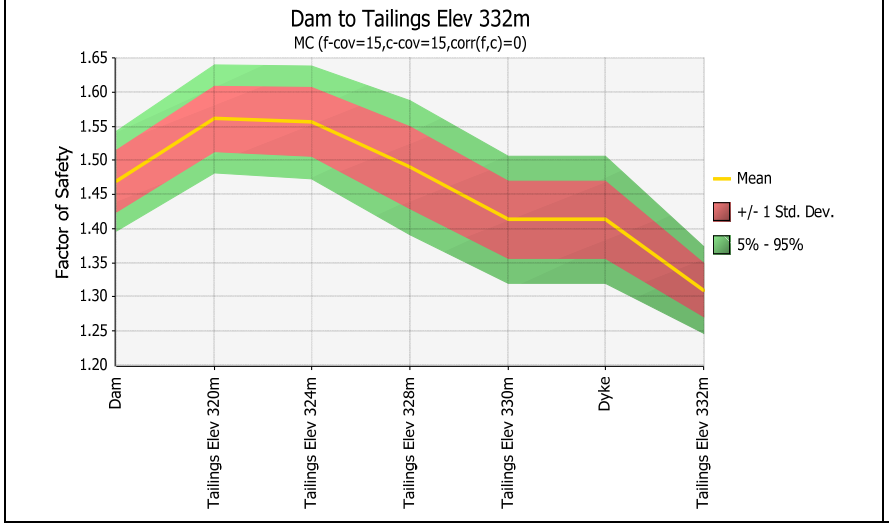

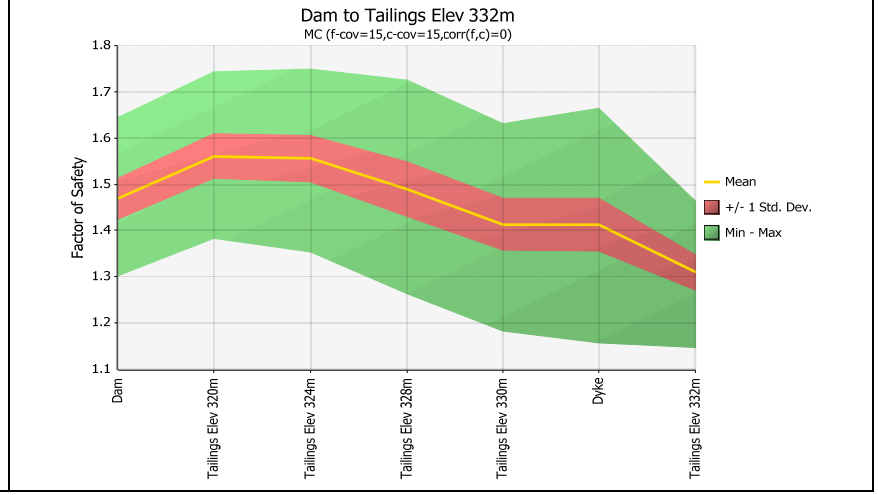

MC (f-cov=15,c-cov=15,corr(f,c)=0)

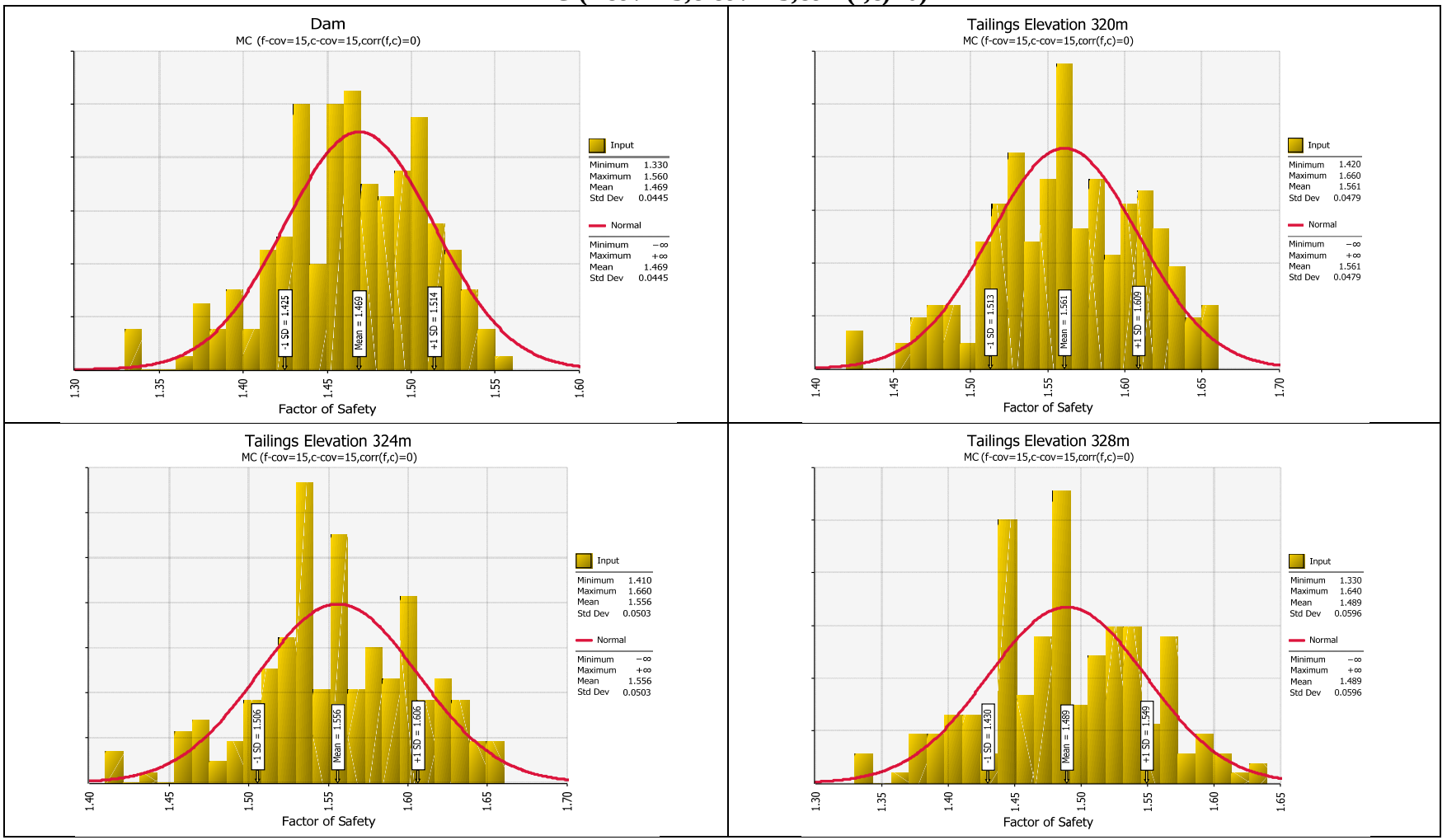

MC (f-cov=15,c-cov=15,corr(f,c)=0)

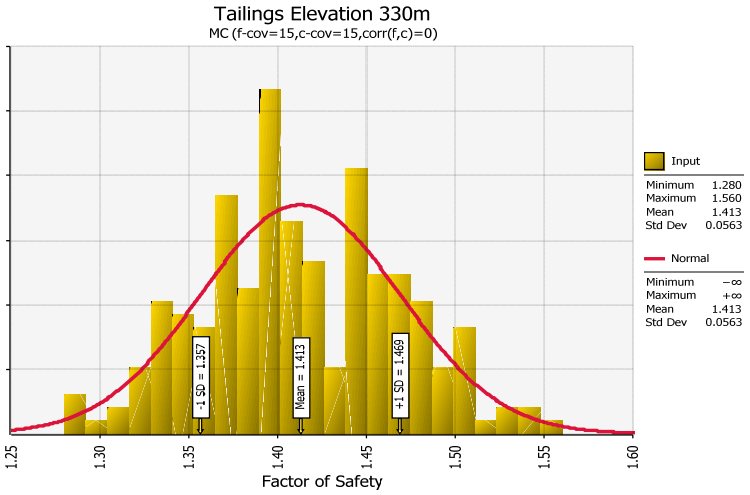

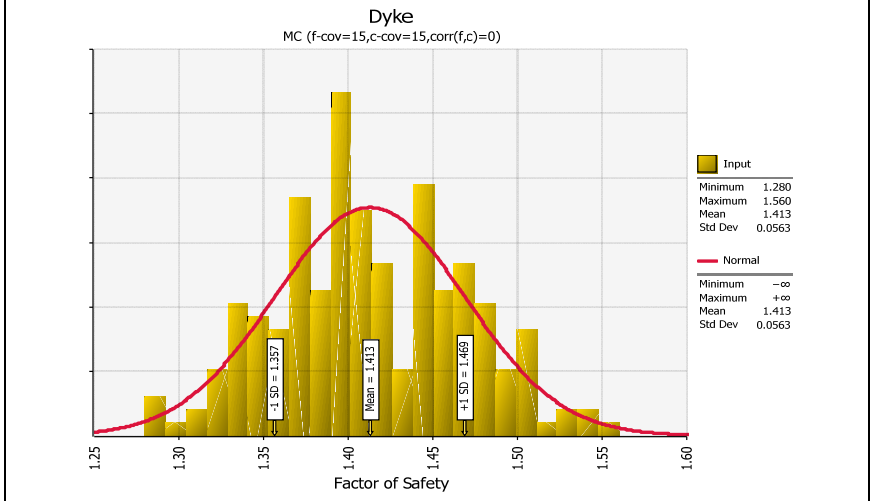

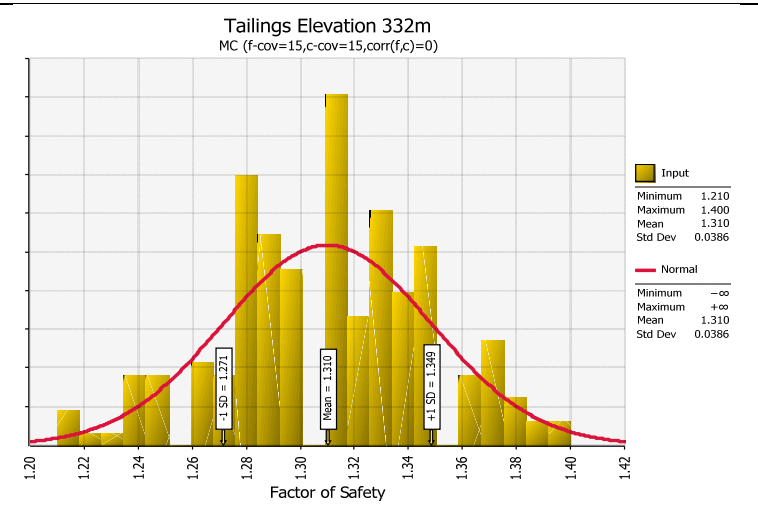

MC (f-cov=15,c-cov=15,corr(f,c)=0)	MEAN	STDEV	Reliability	Probability of Unsatisfactory Performance
Dam	1.4692	0.044534	10.5358	0
Tailings Elev 320m	1.5609	0.047892	11.7118	0
Tailings Elev 324m	1.55605	0.050255	11.0646	0
Tailings Elev 328m	1.4893	0.059635	8.2049	0
Tailings Elev 330m	1.4129	0.056253	7.3401	0
Dyke	1.41285	0.056296	7.3336	0
Tailings Elev 332m	1.31	0.038567	8.0380	0

MC (f-cov=15,c-cov=15,corr(f,c)=-0.5)

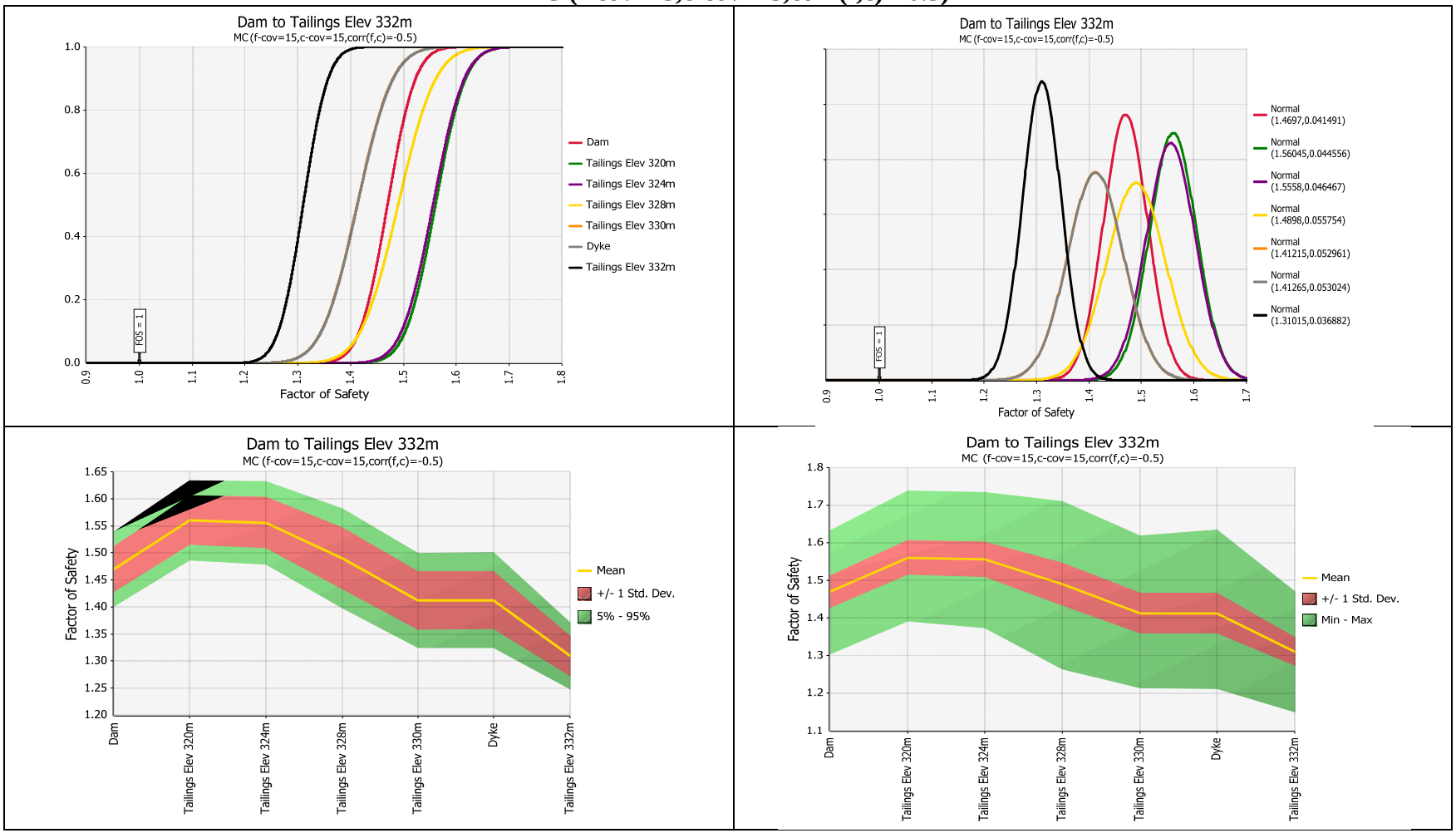

MC (f-cov=15,c-cov=15,corr(f,c)=-0.5)

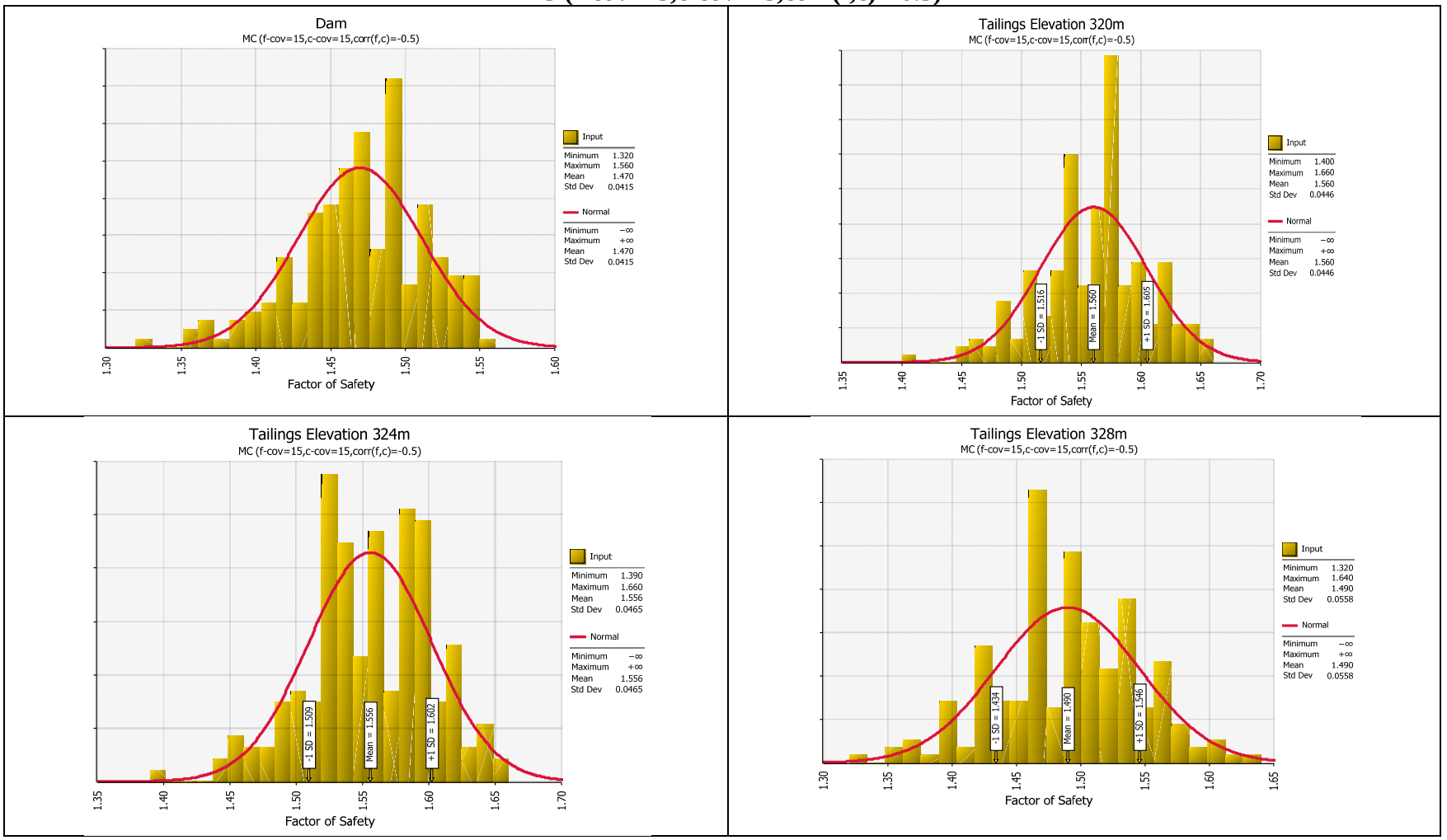

MC (f-cov=15,c-cov=15,corr(f,c)=-0.5)

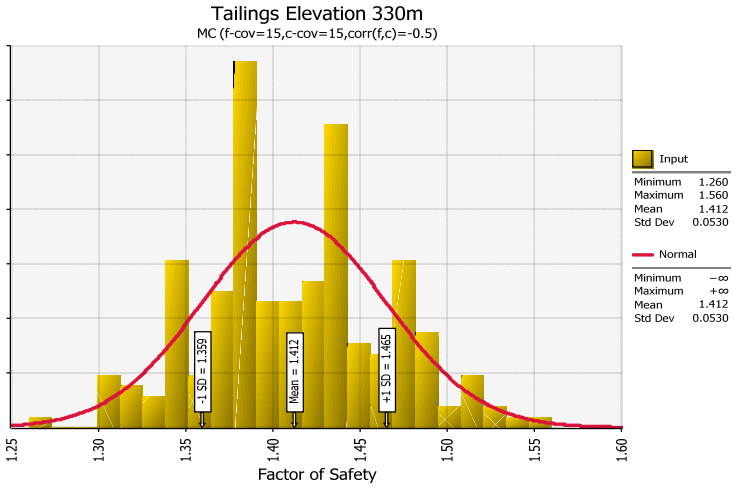

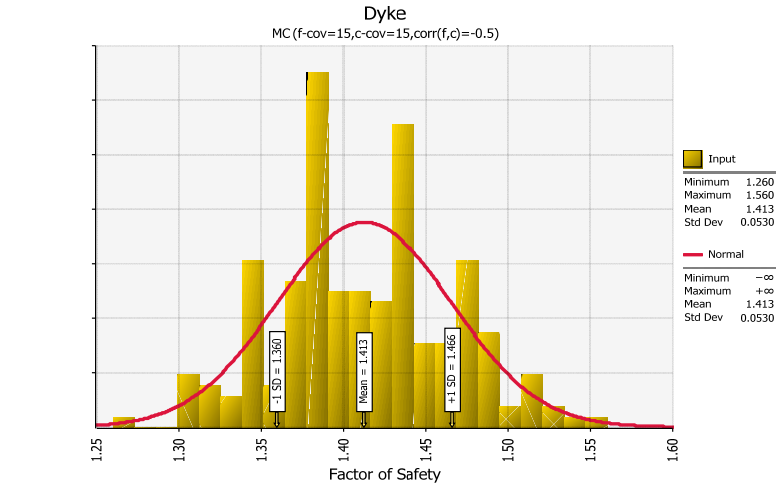

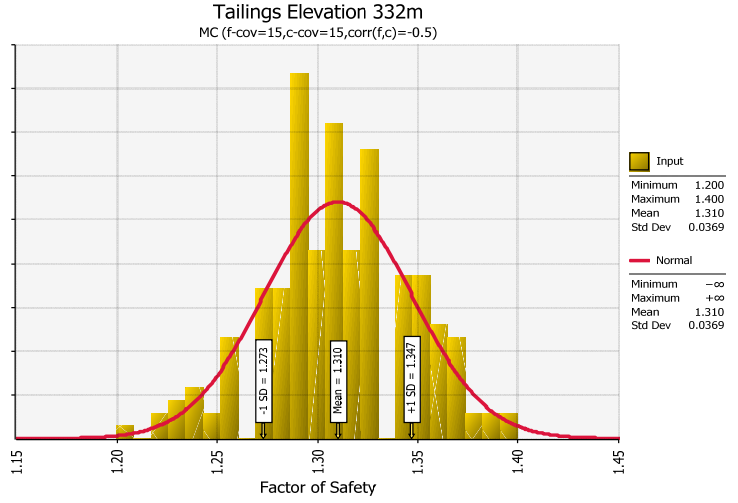

MC (f-cov=15,c-cov=15,corr(f,c)=-0.5)	MEAN	STDEV	Reliability	Probability of Unsatisfactory Performance
Dam	1.4697	0.041491	11.32053	0
Tailings Elev 320m	1.56045	0.044556	12.57855	0
Tailings Elev 324m	1.5558	0.046467	11.96118	0
Tailings Elev 328m	1.4898	0.055754	8.78502	0
Tailings Elev 330m	1.41215	0.052961	7.78214	0
Dyke	1.41265	0.053024	7.78232	0
Tailings Elev 332m	1.31015	0.036882	8.40925	0

MC (f-cov=30,c-cov=30,corr(f,c)=0.5)

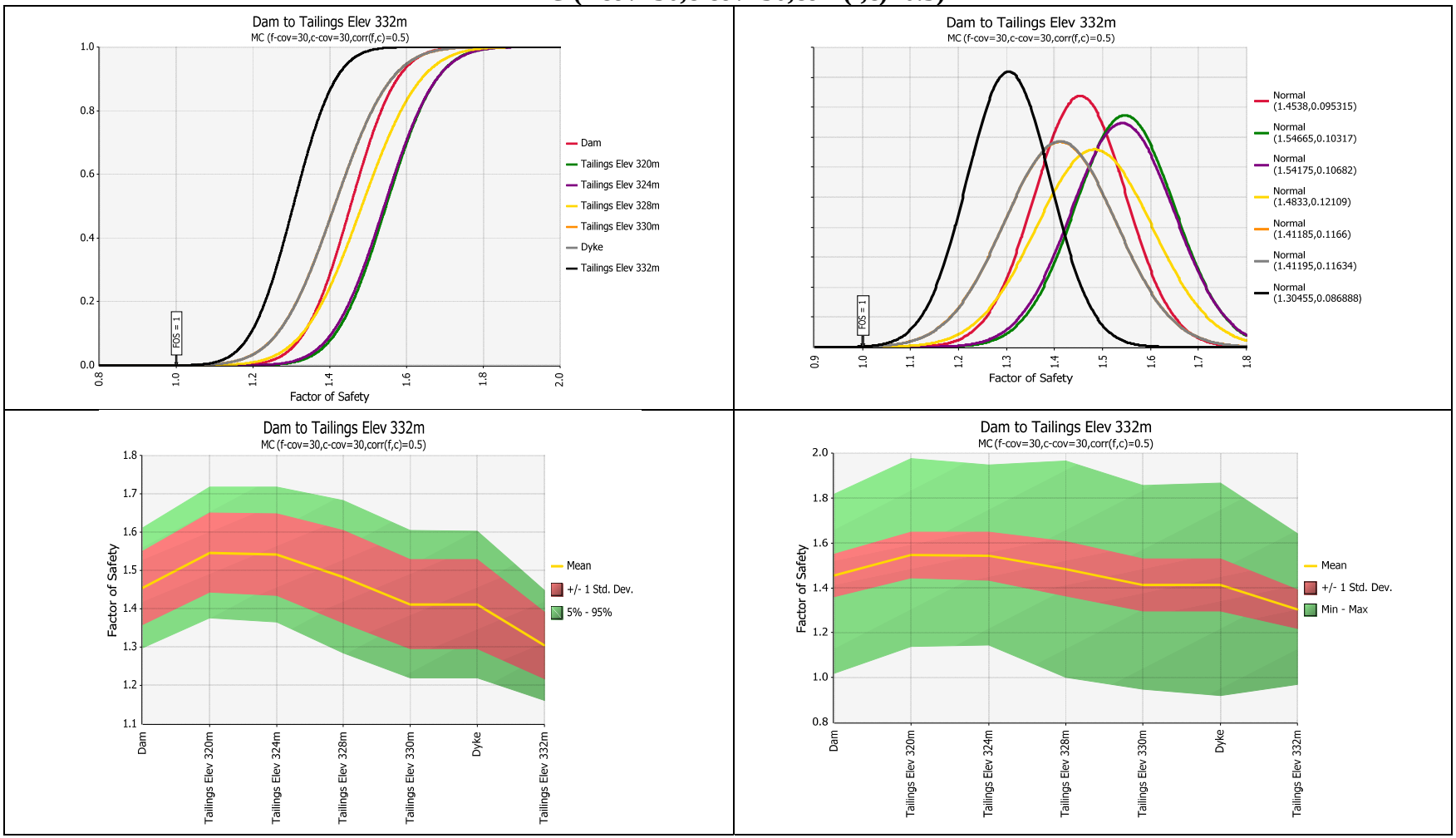

MC (f-cov=30,c-cov=30,corr(f,c)=0.5)

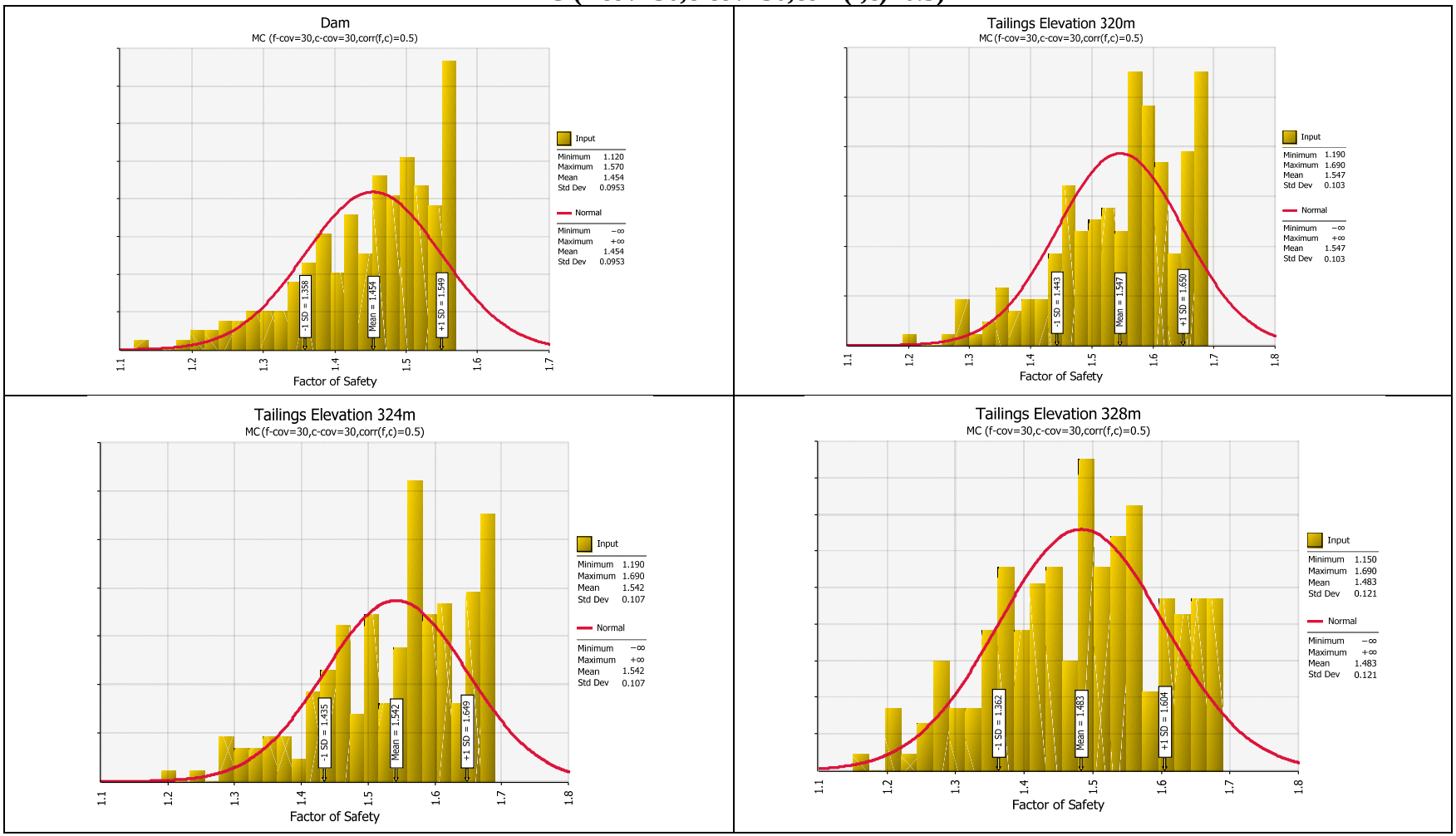

MC (f-cov=30,c-cov=30,corr(f,c)=0.5)

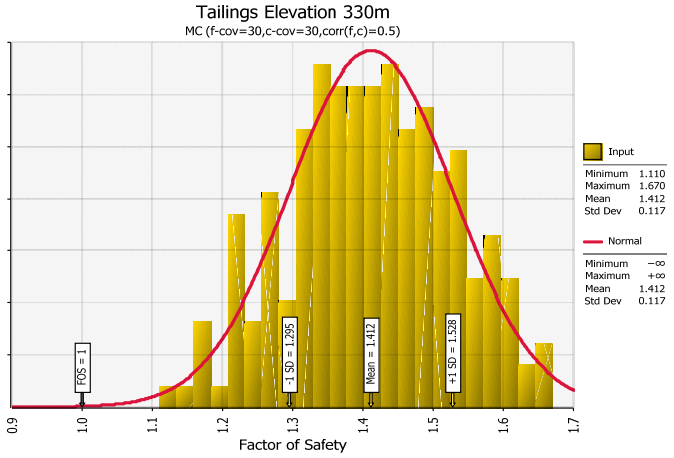

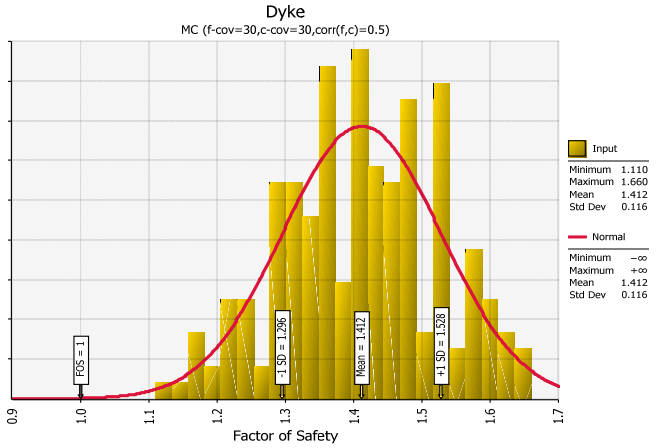

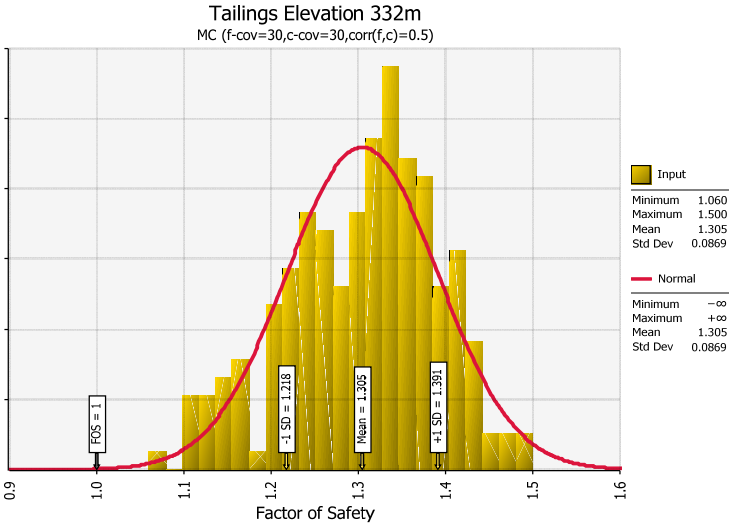

MC (f-cov=30, c-cov=30, corr(f,c)=0.5)	MEAN	STDEV	Reliability	Probability of Unsatisfactory Performance
Dam	1.4538	0.095315	4.761	0
Tailings Elev 320m	1.54665	0.10317	5.299	0
Tailings Elev 324m	1.54175	0.10682	5.072	0
Tailings Elev 328m	1.4833	0.12109	3.991	0.00003
Tailings Elev 330m	1.41185	0.1166	3.532	0.00021
Dyke	1.41195	0.11634	3.541	0.00020
Tailings Elev 332m	1.30455	0.086888	3.505	0.00022

MC (f-cov=30,c-cov=30,corr(f,c)=0)

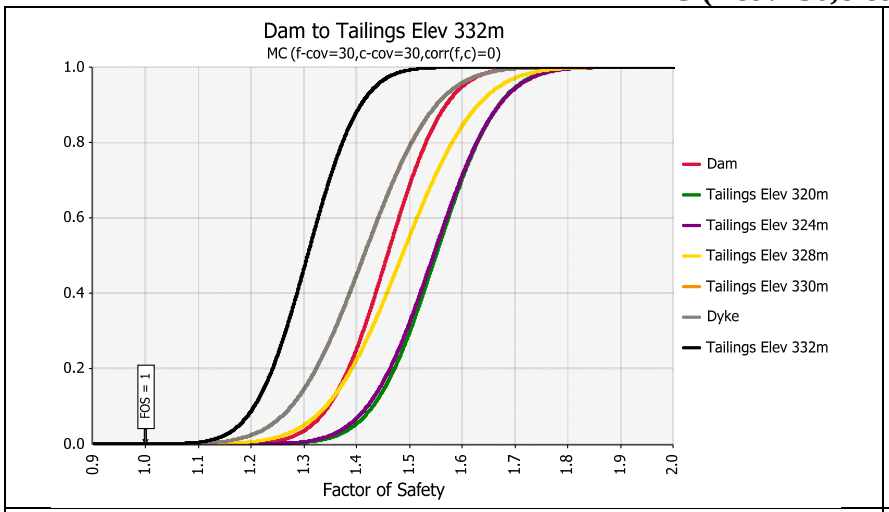

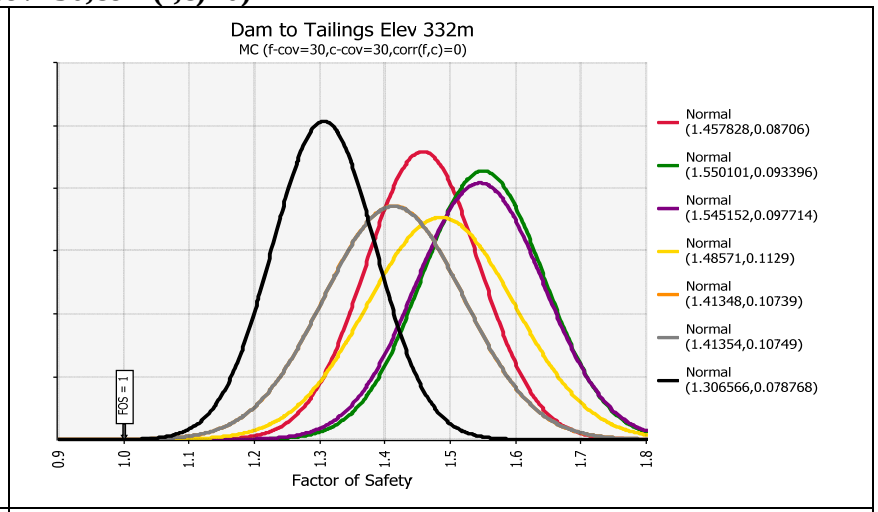

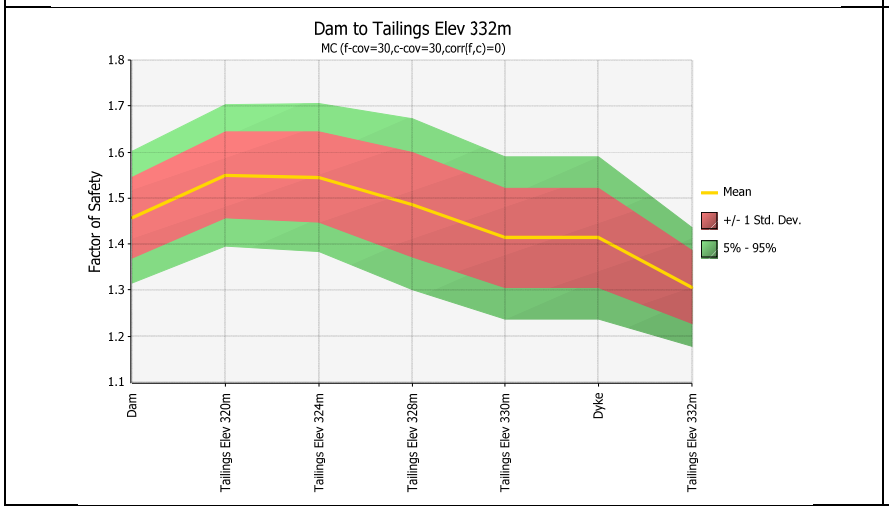

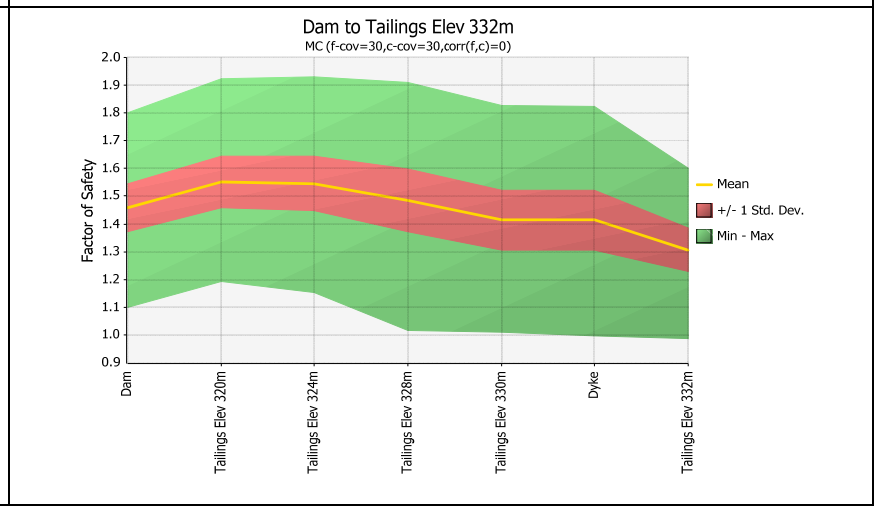

MC (f-cov=30,c-cov=30,corr(f,c)=0)

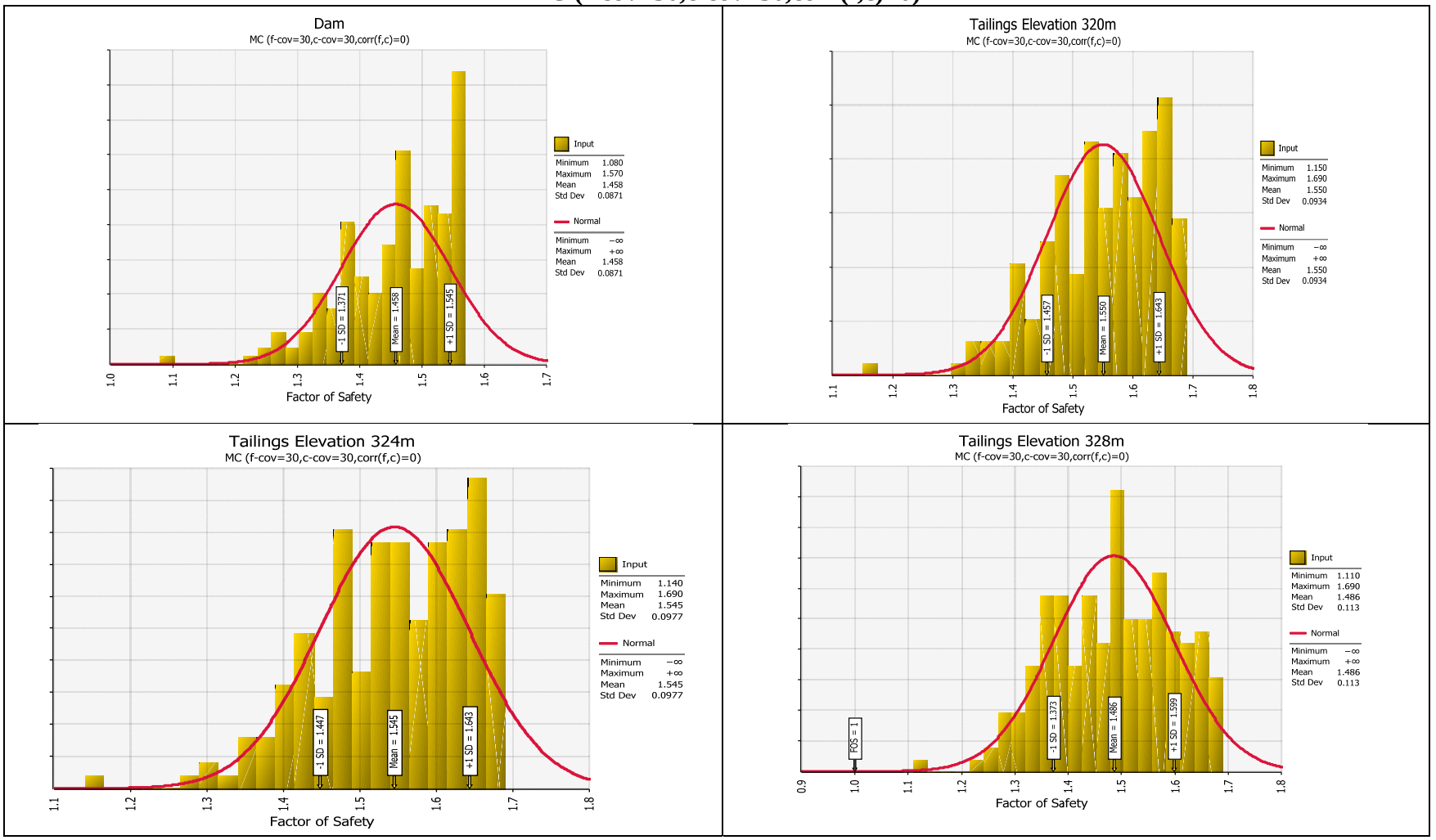

MC (f-cov=30,c-cov=30,corr(f,c)=0)

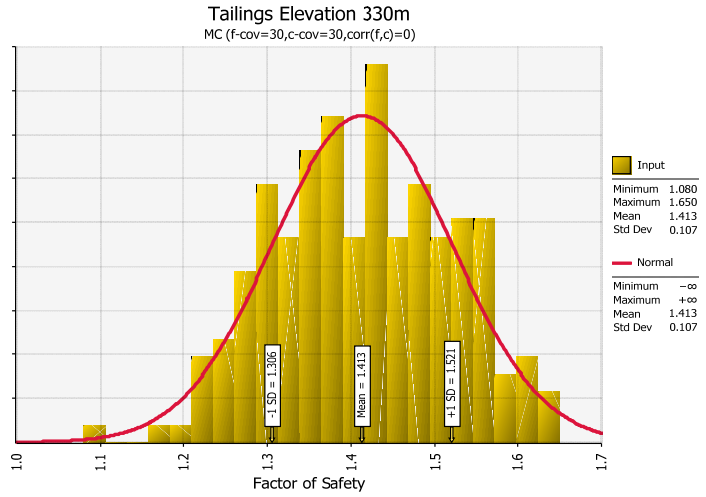

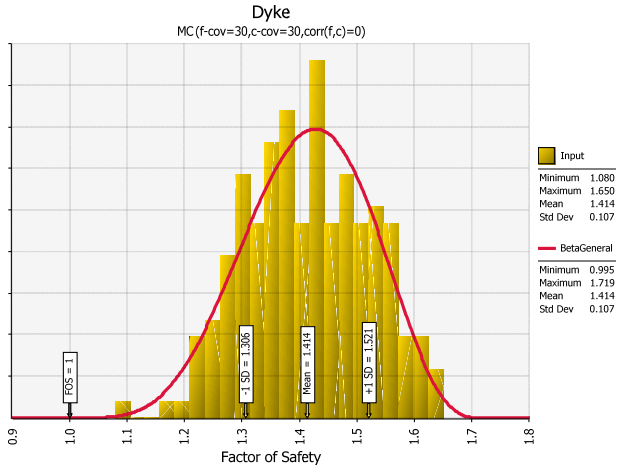

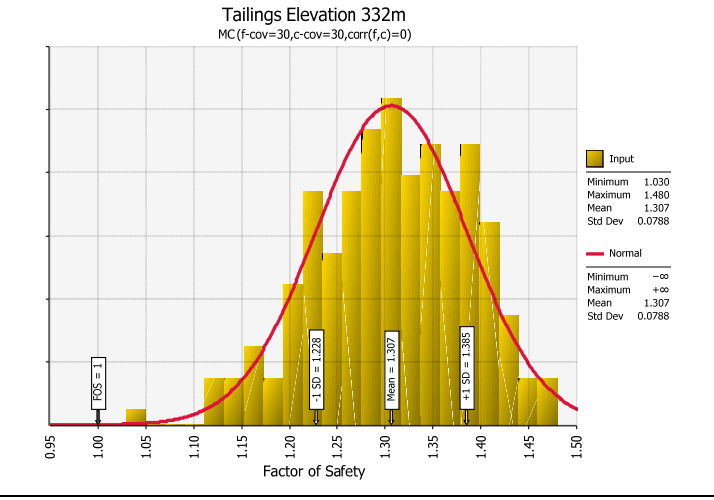

MC(f-cov=30, c-cov=30, corr(f,c)=0)	MEAN	STDEV	Reliability	Probability of Unsatisfactory Performance
Dam	1.457828	0.08706	5.259	0
Tailings Elev 320m	1.550101	0.093396	5.890	0
Tailings Elev 324m	1.545152	0.097714	5.579	0
Tailings Elev 328m	1.48571	0.1129	4.302	0.00003
Tailings Elev 330m	1.41348	0.10739	3.850	0.00006
Dyke	1.41354	0.10749	3.847	0.00006
Tailings Elev 332m	1.306566	0.078768	3.892	0.00005

MC (f-cov=30,c-cov=30,corr(f,c)=-0.5)

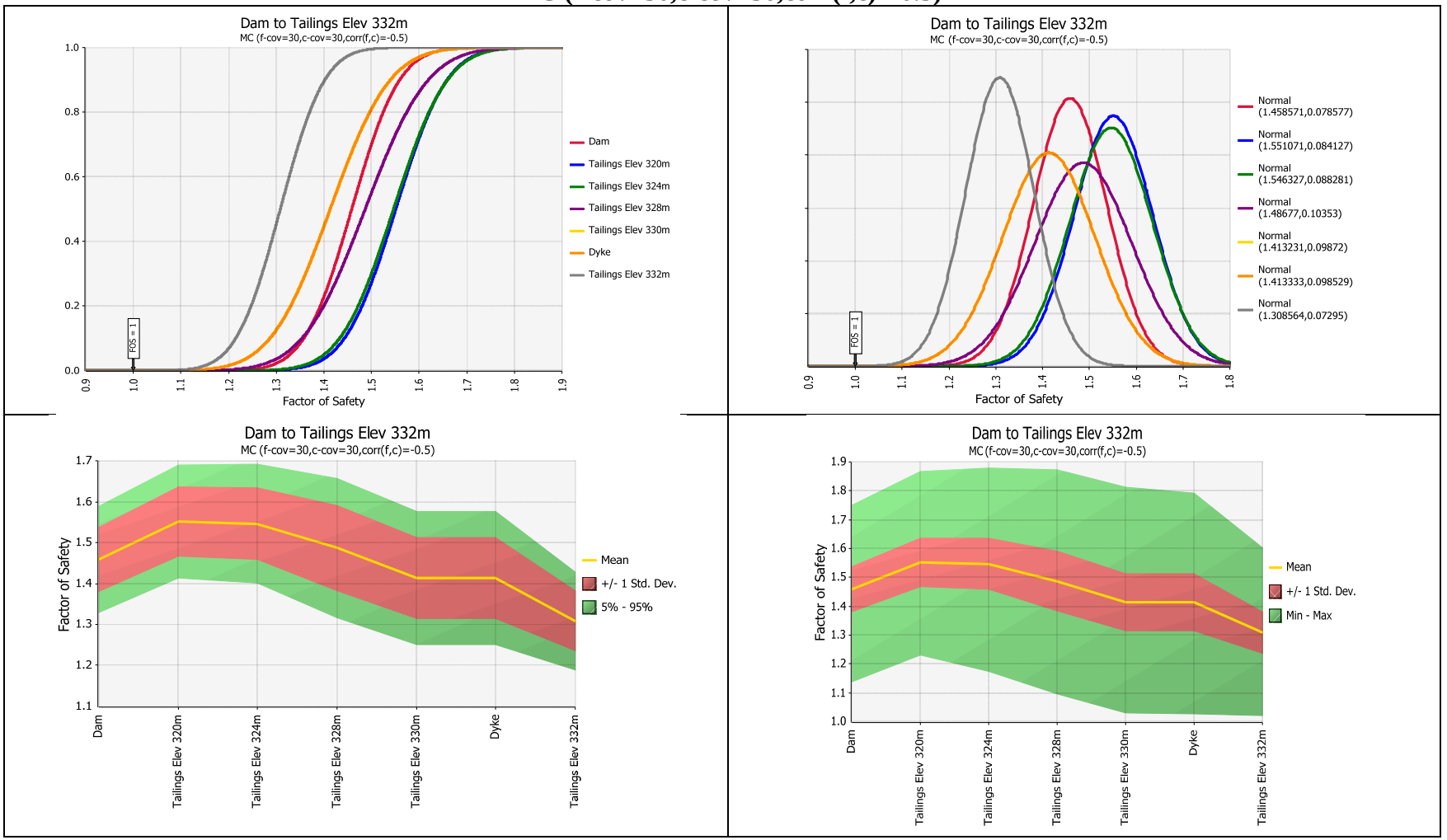

MC (f-cov=30,c-cov=30,corr(f,c)=-0.5)

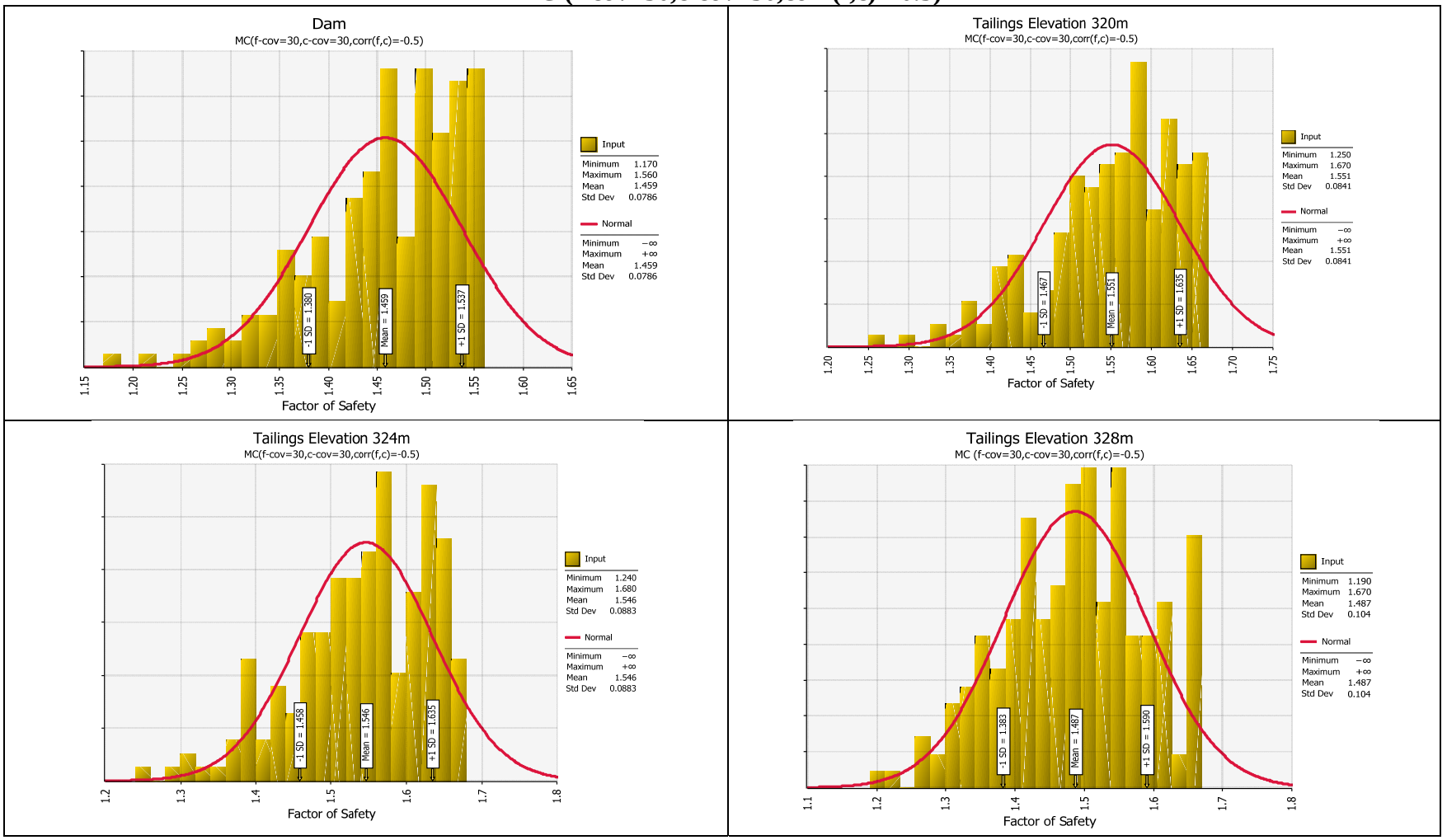

MC (f-cov=30,c-cov=30,corr(f,c)=-0.5)

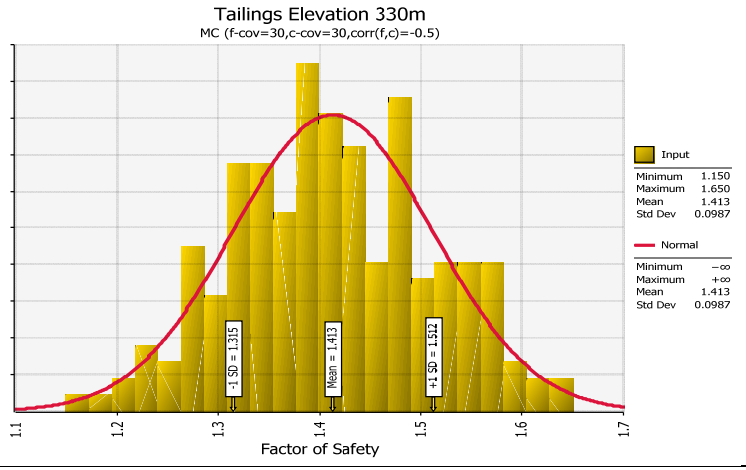

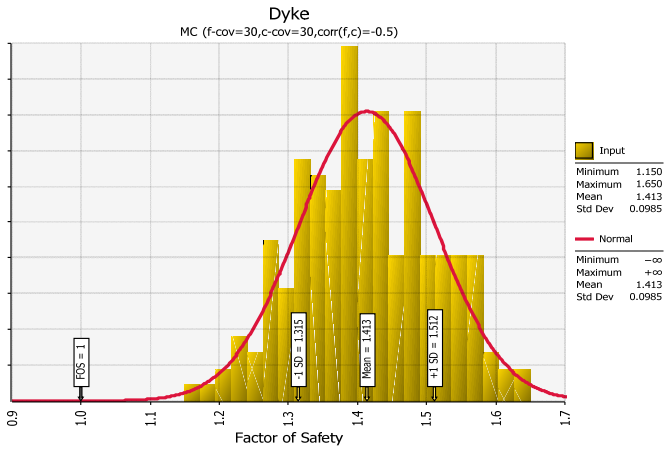

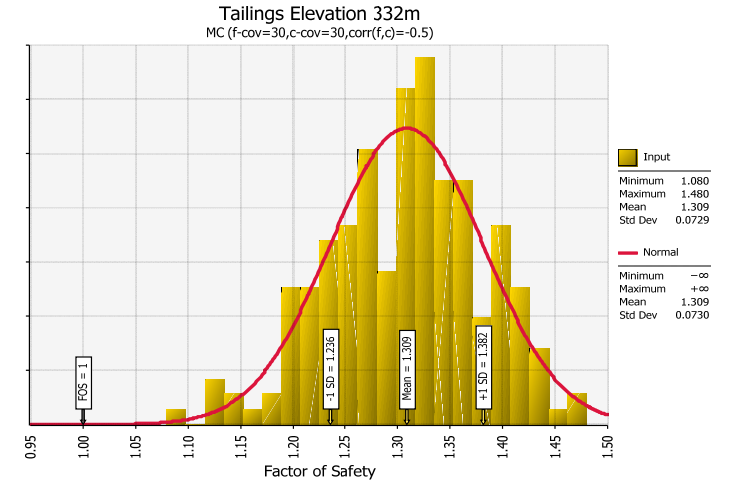

MC (f-cov=30,c-cov=30,corr(f,c)=0)	MEAN	STDEV	Reliability	Probability of Unsatisfactory Performance
Dam	1.458571	0.078577	5.836	0
Tailings Elev 320m	1.551071	0.084127	6.550	0
Tailings Elev 324m	1.546327	0.088281	6.189	0
Tailings Elev 328m	1.48677	0.10353	4.702	0
Tailings Elev 330m	1.413231	0.09872	4.186	0
Dyke	1.413333	0.098529	4.195	0
Tailings Elev 332m	1.308564	0.07295	4.230	0

MC (f-cov=45,c-cov=45,corr(f,c)=0.5)

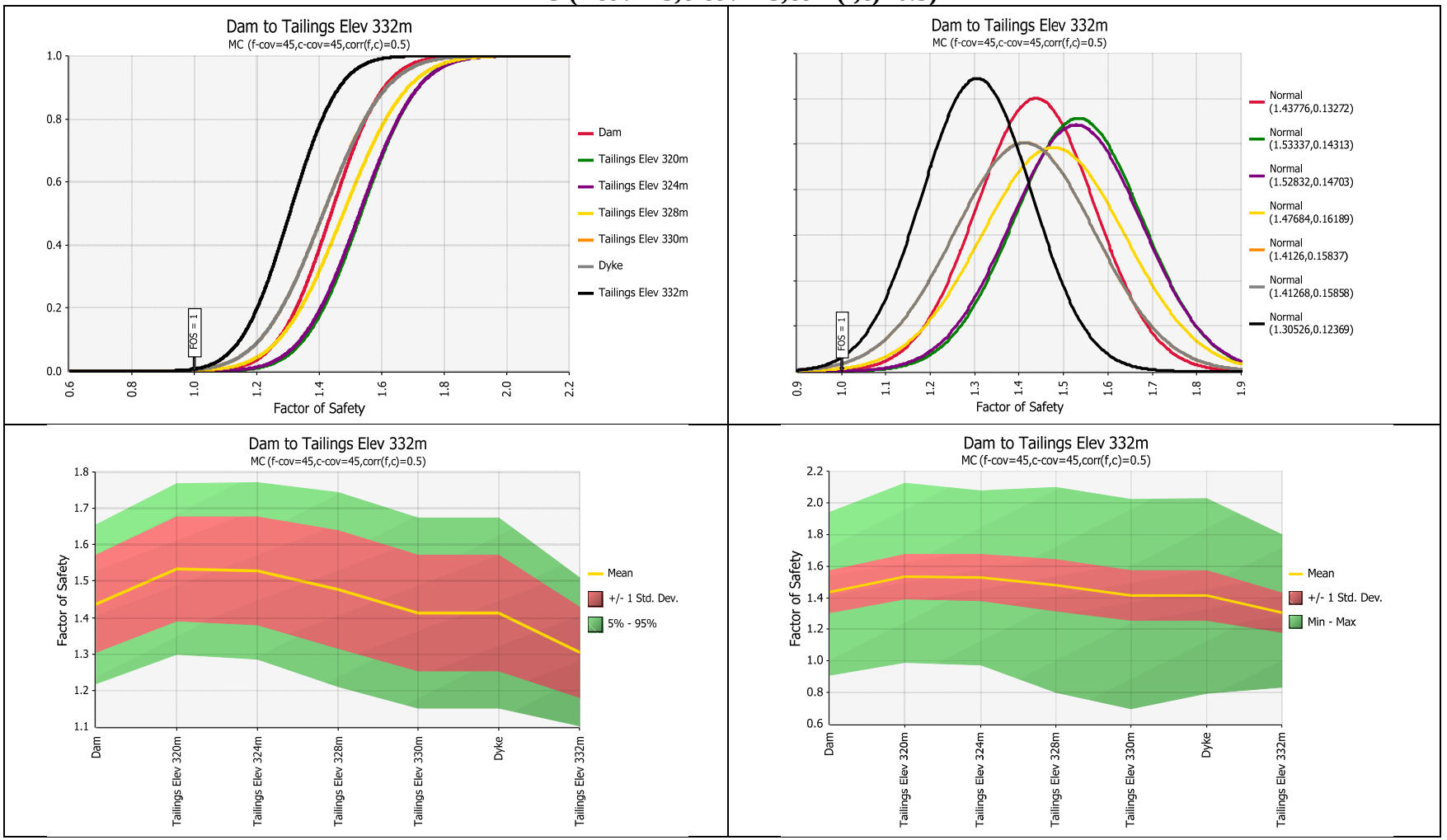

MC (f-cov=45,c-cov=45,corr(f,c)=0.5)

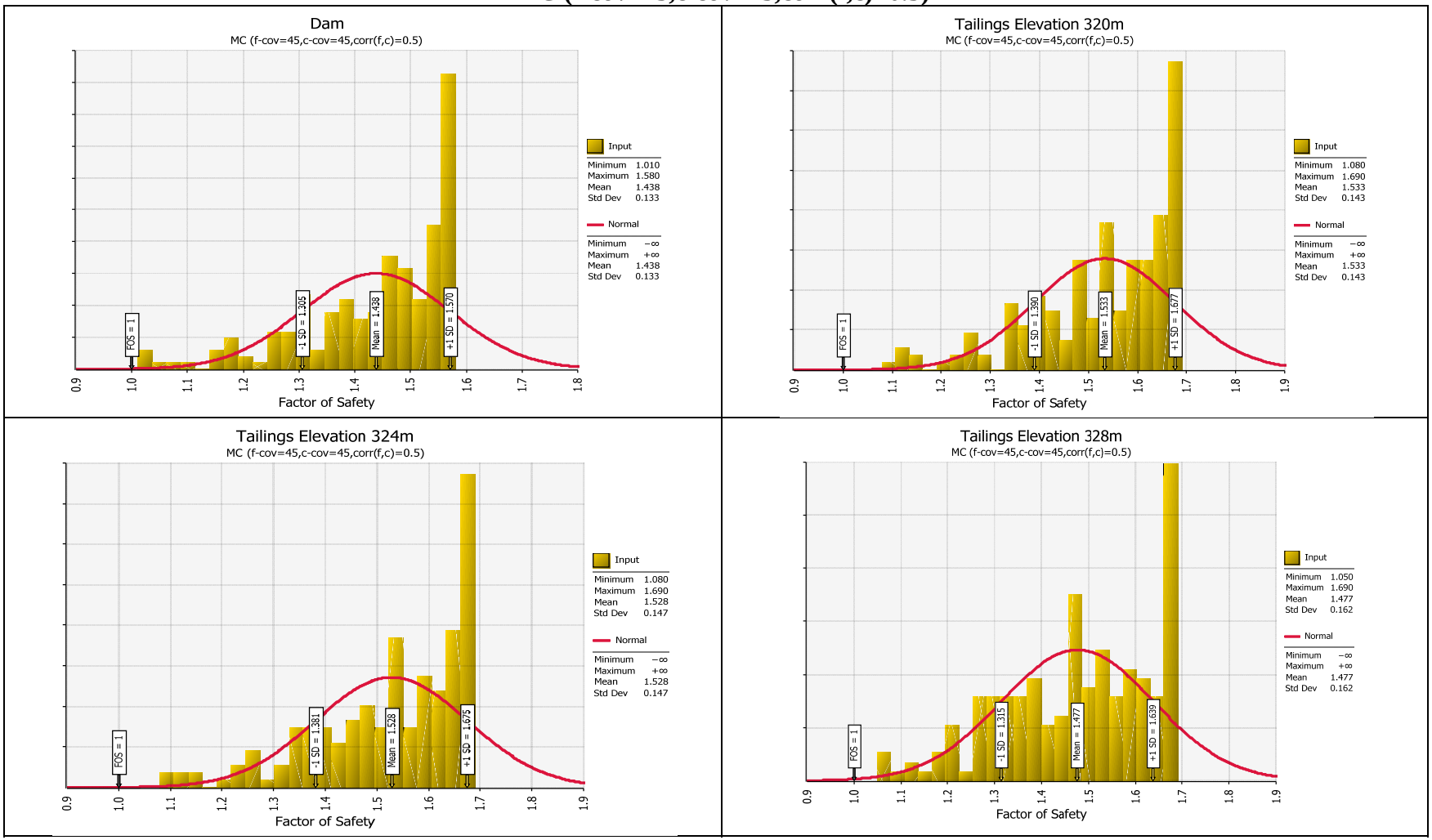

MC (f-cov=45,c-cov=45,corr(f,c)=0.5)

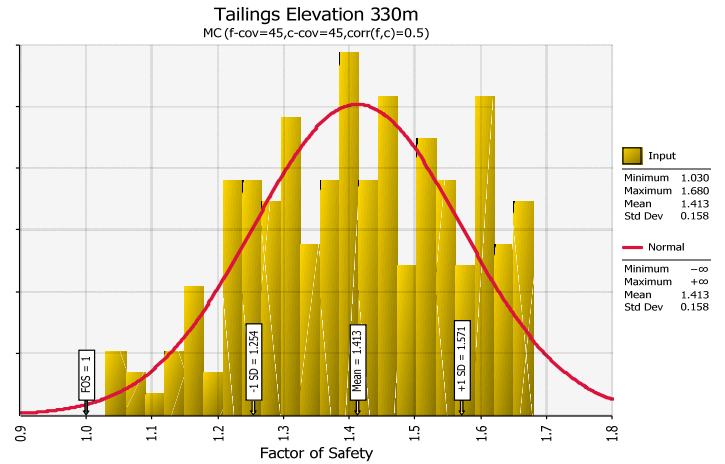

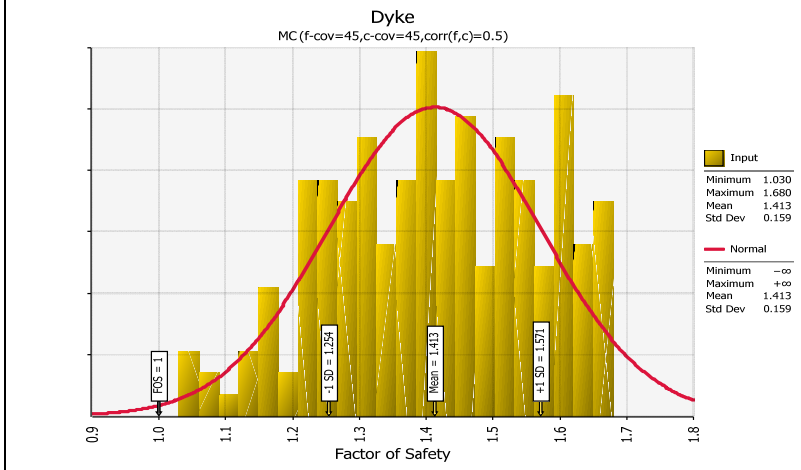

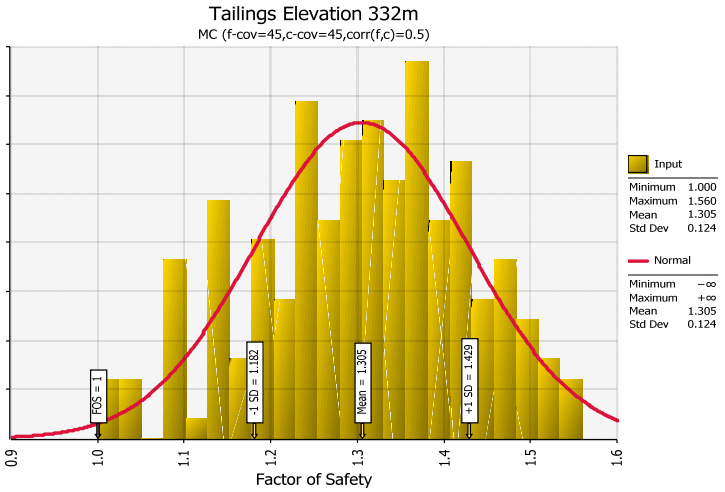

MC(f-cov=45, c-cov=45, corr(f,c)=0.5)	MEAN	STDEV	Reliability	Probability of Unsatisfactory Performance
Dam	1.43776	0.13272	3.298	0.0005
Tailings Elev 320m	1.53337	0.14313	3.726	0.0001
Tailings Elev 324m	1.52832	0.14703	3.593	0.00017
Tailings Elev 328m	1.47684	0.16189	2.945	0.0016
Tailings Elev 330m	1.4126	0.15837	2.605	0.00466
Dyke	1.41268	0.15858	2.602	0.00466
Tailings Elev 332m	1.30526	0.12369	2.468	0.00676

MC (f-cov=45,c-cov=45,corr(f,c)=0)

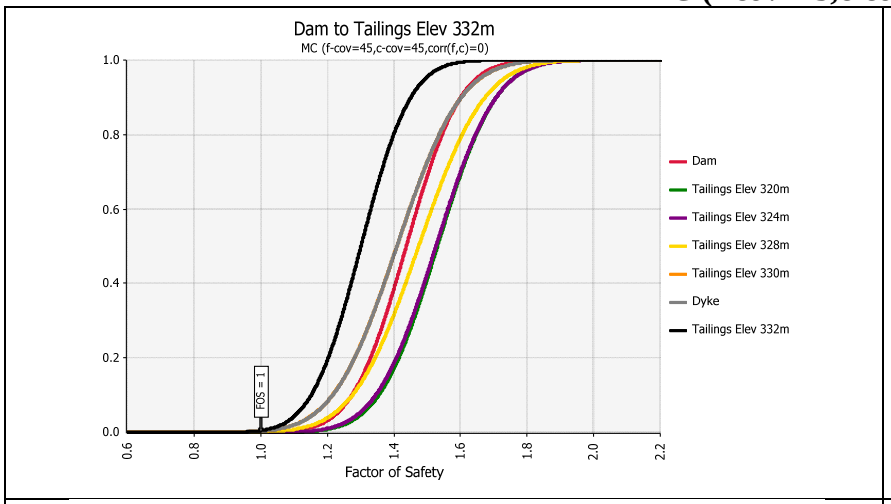

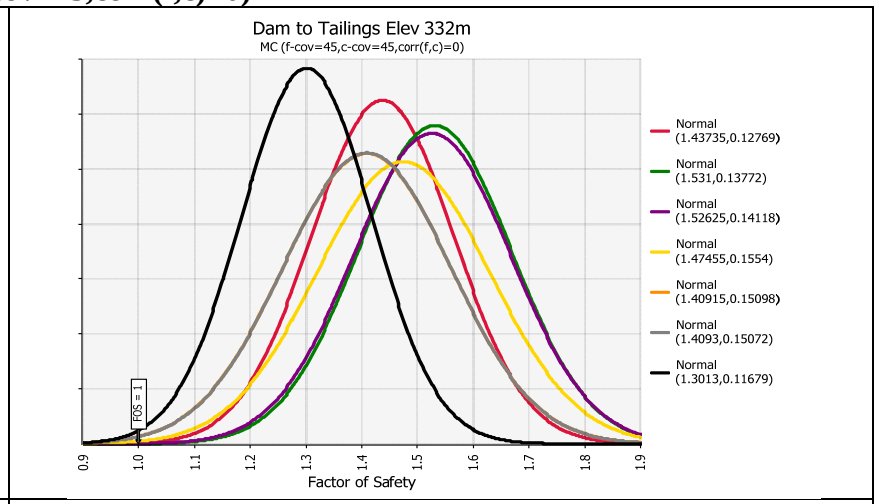

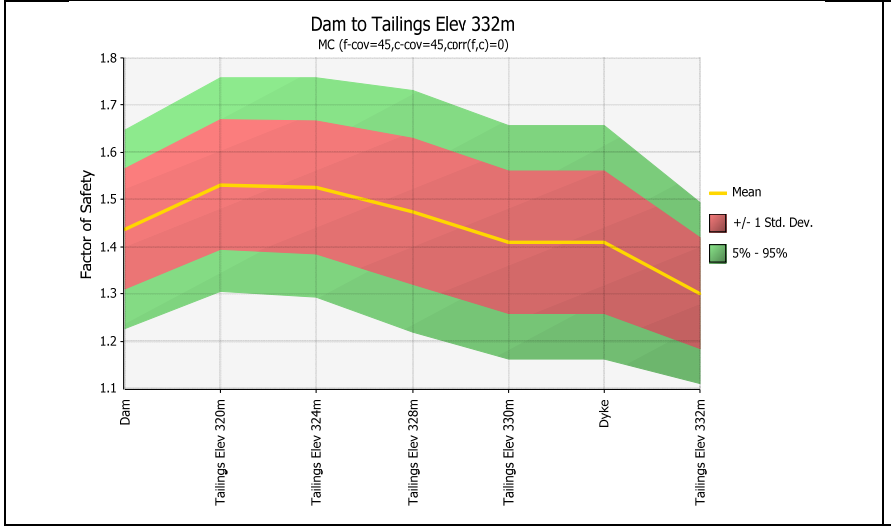

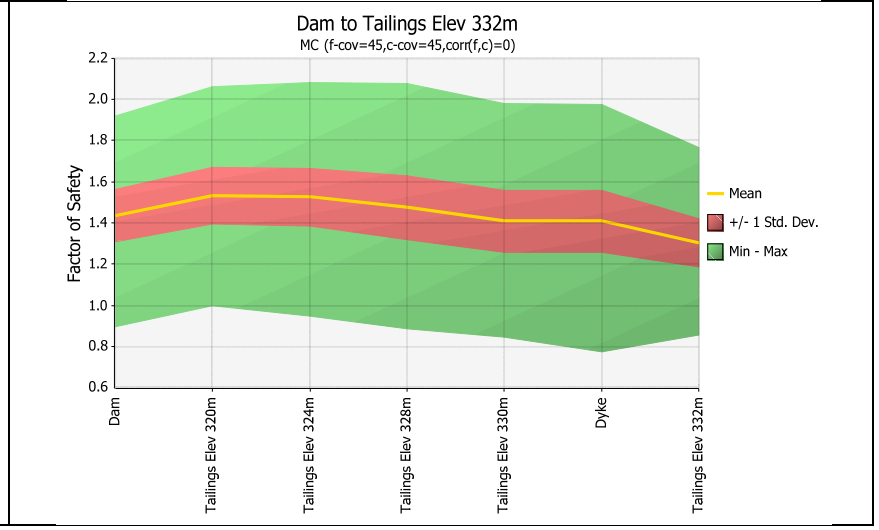

MC (f-cov=45,c-cov=45,corr(f,c)=0)

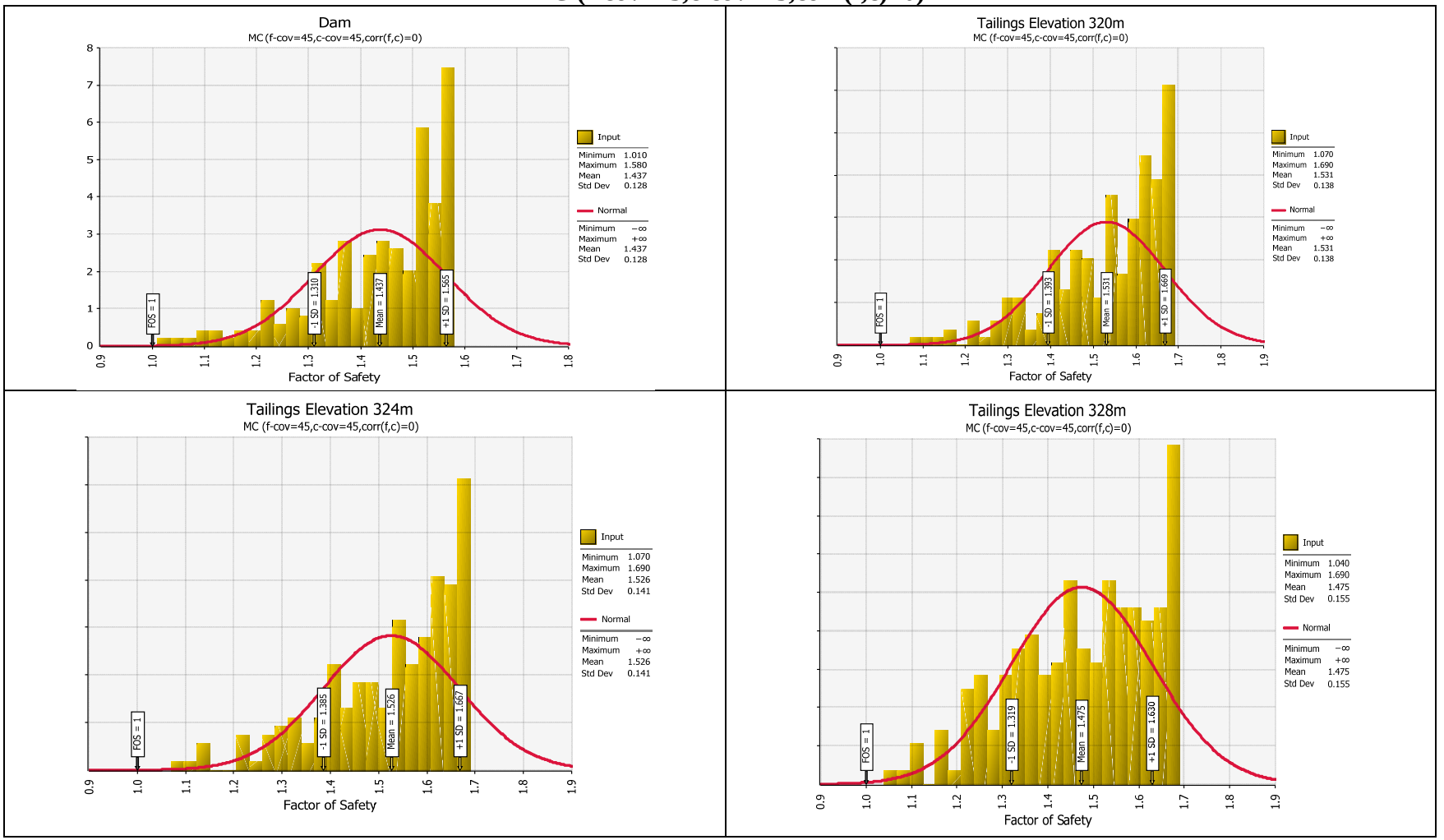

MC (f-cov=45,c-cov=45,corr(f,c)=0)

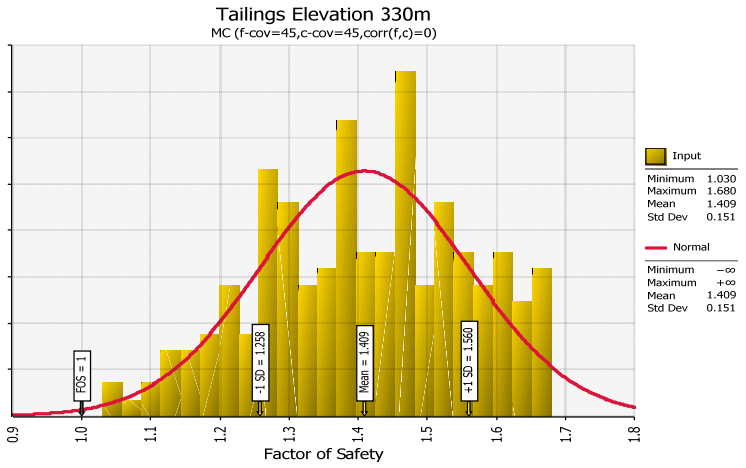

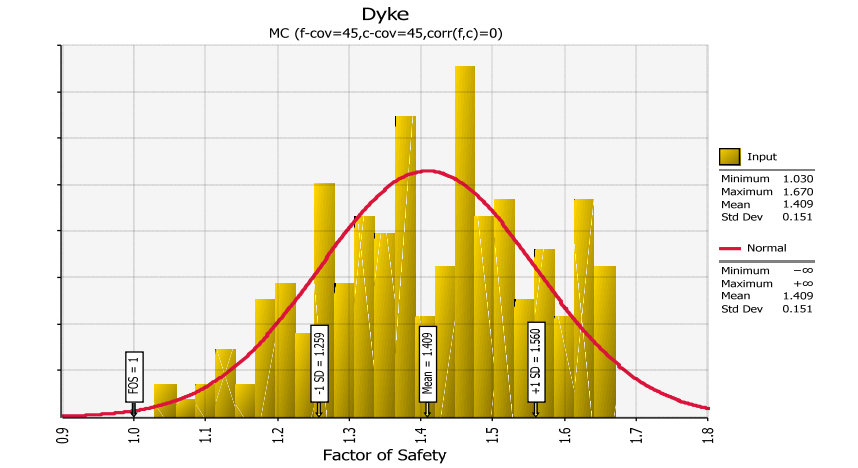

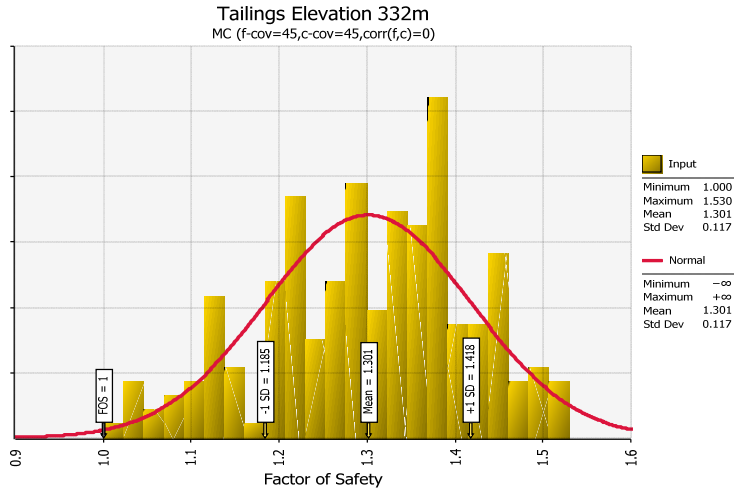

MC (f-cov=45, c-cov=45, corr(f,c)=0)	MEAN	STDEV	Reliability	Probability of Unsatisfactory Performance
Dam	1.43735	0.12769	3.425	0.0003
Tailings Elev 320m	1.531	0.13772	3.856	0.00006
Tailings Elev 324m	1.52625	0.14118	3.728	0.0001
Tailings Elev 328m	1.47455	0.1554	3.054	0.00114
Tailings Elev 330m	1.40915	0.15098	2.710	0.00336
Dyke	1.4093	0.15072	2.716	0.00336
Tailings Elev 332m	1.3013	0.11679	2.580	0.00494

MC (f-cov=45,c-cov=45,corr(f,c)=-0.5)

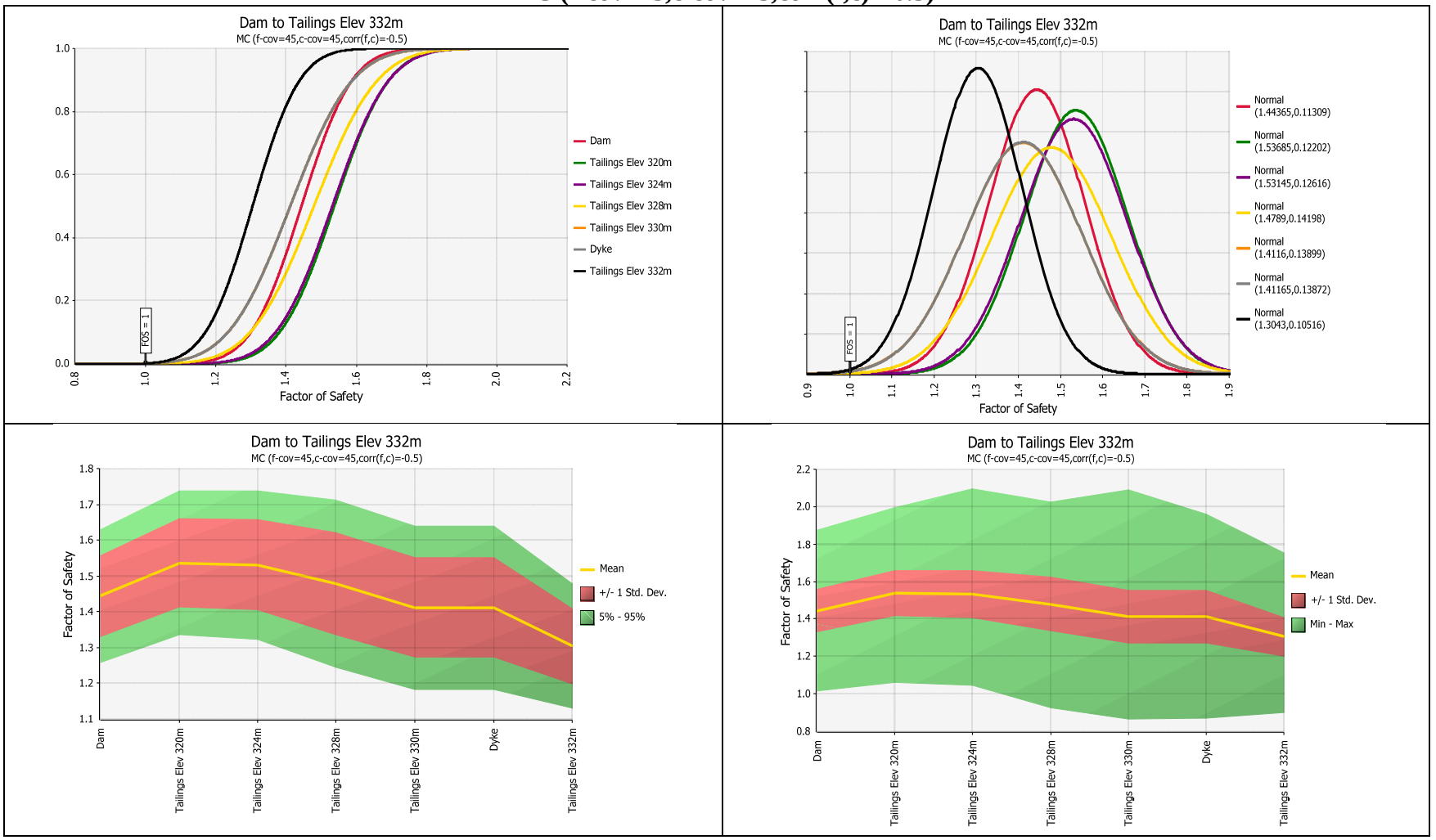

MC (f-cov=45,c-cov=45,corr(f,c)=-0.5)

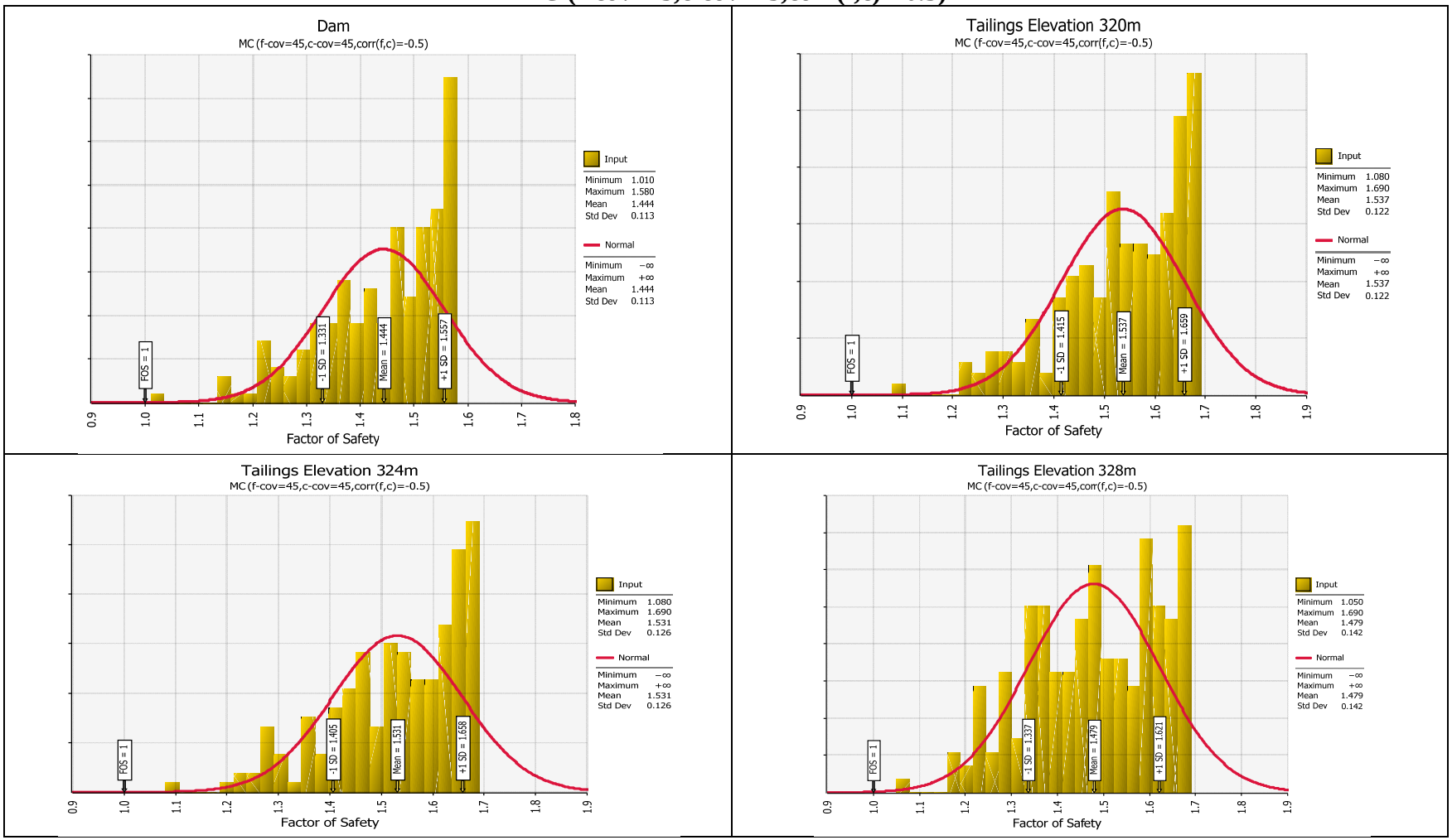

MC (f-cov=45,c-cov=45,corr(f,c)=-0.5)

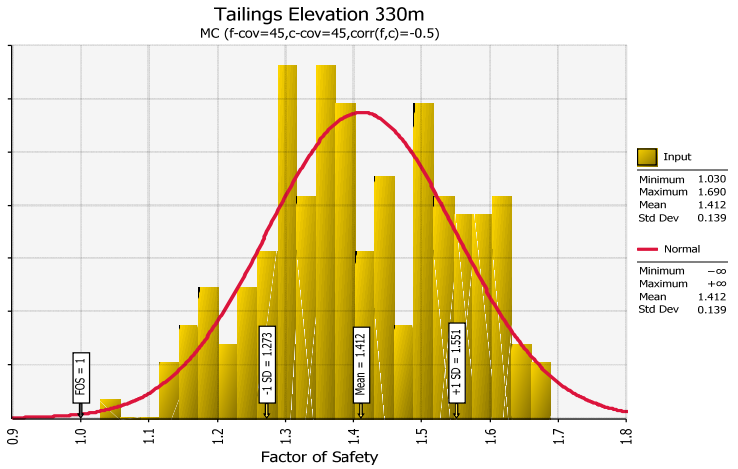

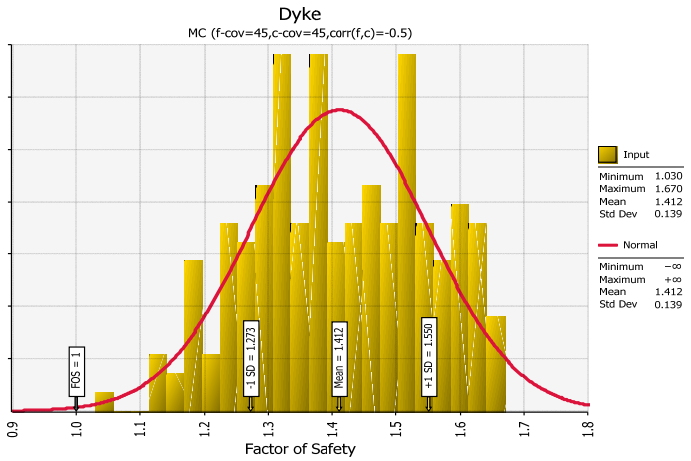

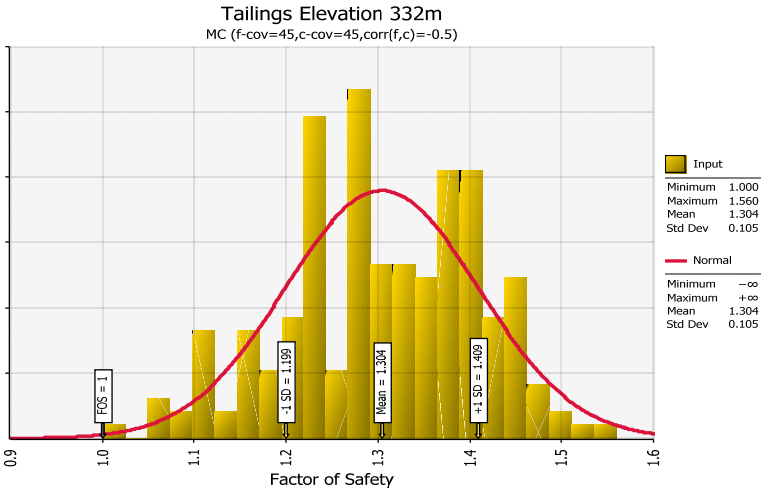

MC (f-cov=45, c-cov=45, corr(f,c)=-0.5)	MEAN	STDEV	Reliability	Probability of Unsatisfactory Performance
Dam	1.44365	0.11309	3.923	0.00004
Tailings Elev 320m	1.53685	0.12202	4.400	0.000001
Tailings Elev 324m	1.53145	0.12616	4.213	0.000001
Tailings Elev 328m	1.4789	0.14198	3.373	0.00038
Tailings Elev 330m	1.4116	0.13899	2.961	0.00154
Dyke	1.41165	0.13872	2.967	0.00154
Tailings Elev 332m	1.3043	0.10516	2.894	0.00193

MC (f-cov=15,c-cov=15,corr(f,c)=0.5,k-cov=150)

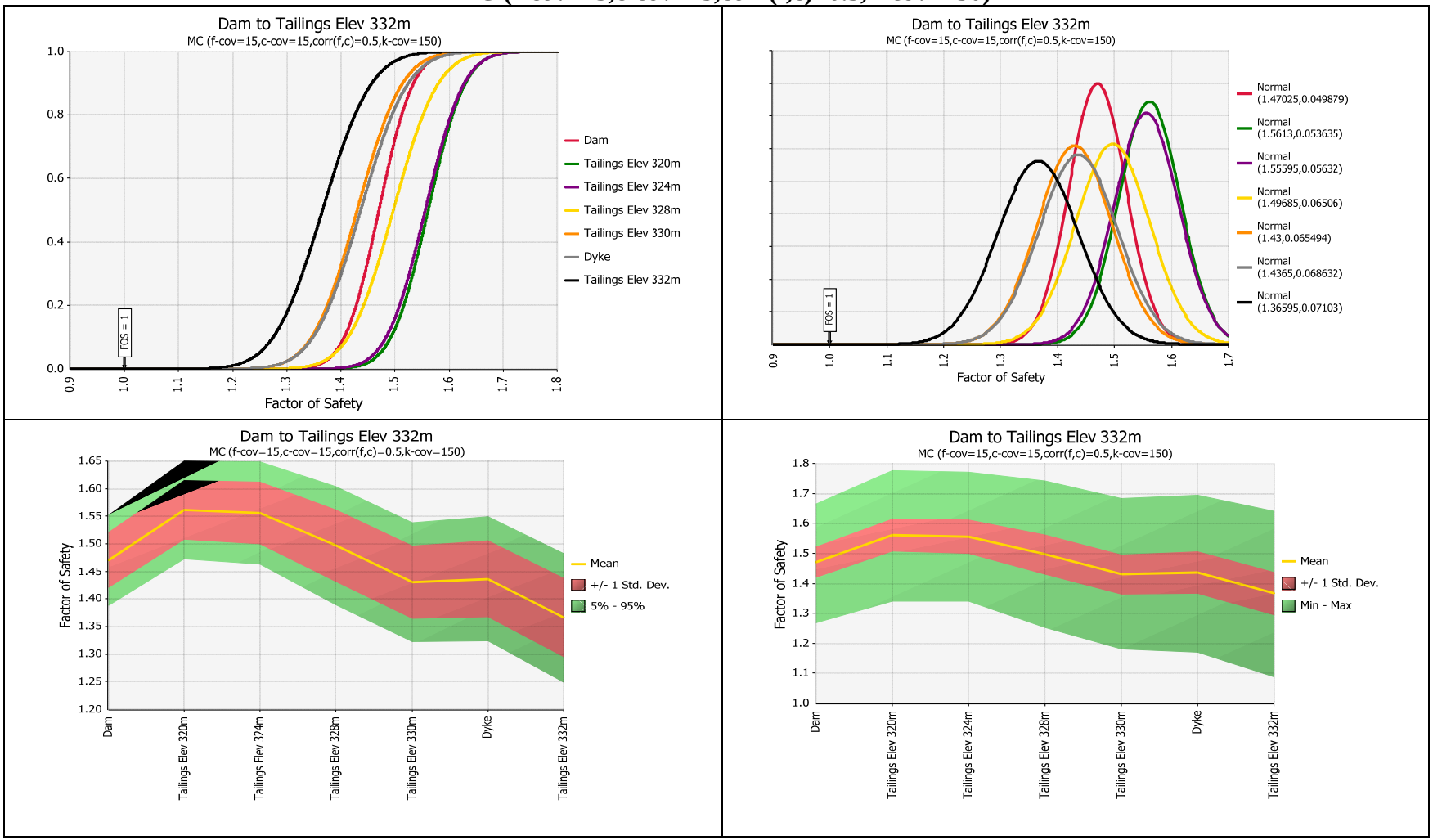

MC (f-cov=15,c-cov=15,corr(f,c)=0.5,k-cov=150)

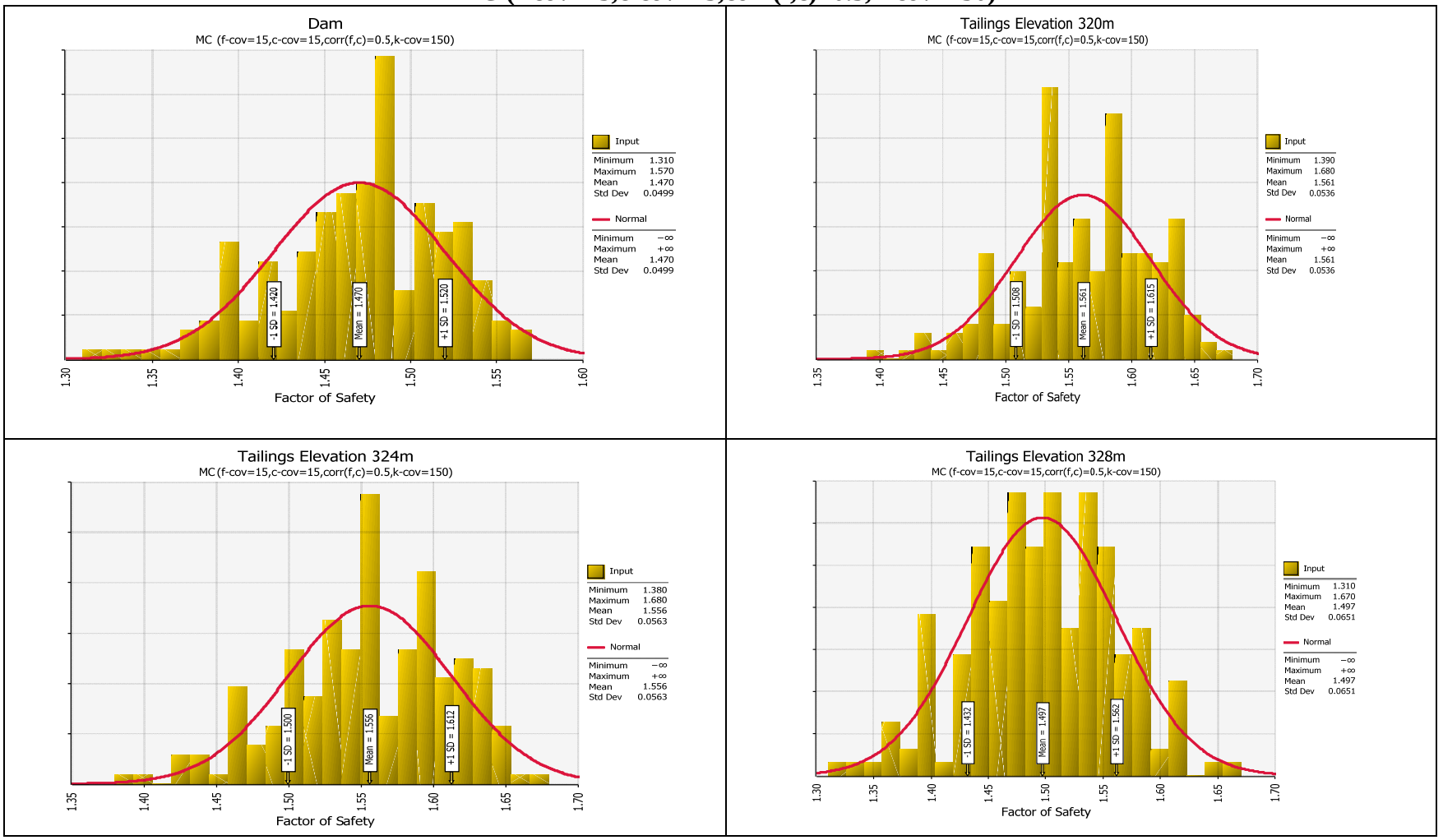

MC (f-cov=15,c-cov=15,corr(f,c)=0.5,k-cov=150)

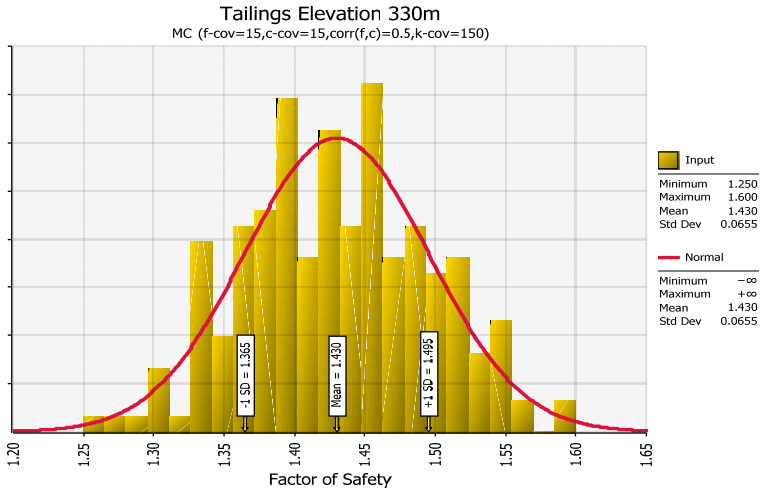

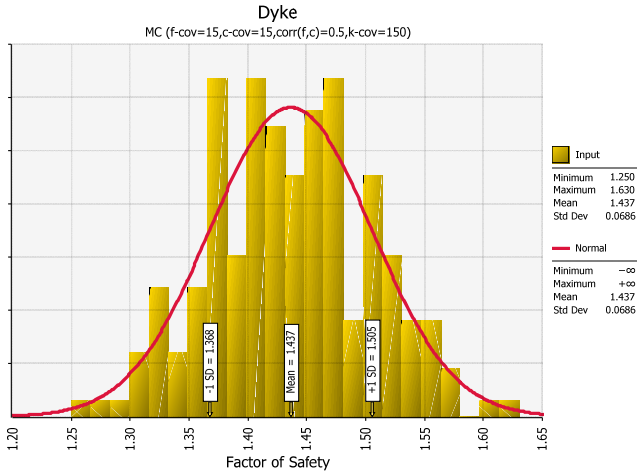

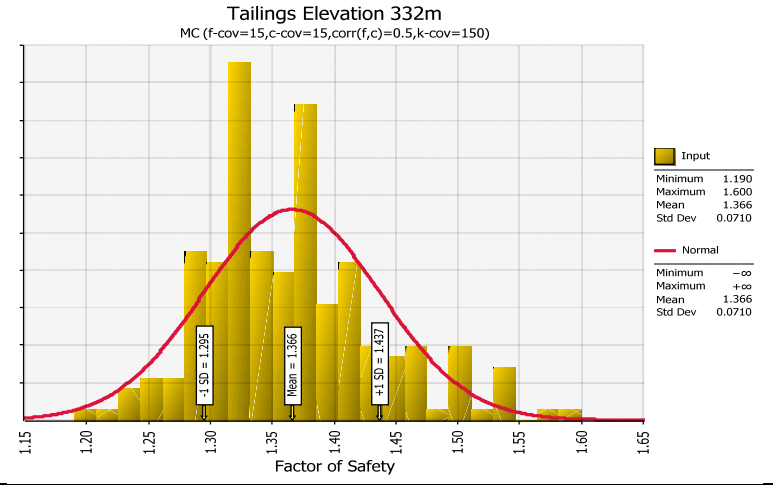

MC (f-cov=15, c-cov=15, corr(f,c)=0.5, k-cov=150)	MEAN	STDEV	Reliability	Probability of Unsatisfactory Performance
Dam	1.47025	0.049879	9.428	0.000001
Tailings Elev 320m	1.5613	0.053635	10.465	0.000001
Tailings Elev 324m	1.55595	0.05632	9.871	0.000001
Tailings Elev 328m	1.49685	0.06506	7.637	0.000001
Tailings Elev 330m	1.43	0.065494	6.565	0.000001
Dyke	1.4365	0.068632	6.360	0.000001
Tailings Elev 332m	1.36595	0.07103	5.152	0.000001

MC (f-cov=15,c-cov=15,corr(f,c)=0,k-cov=150)

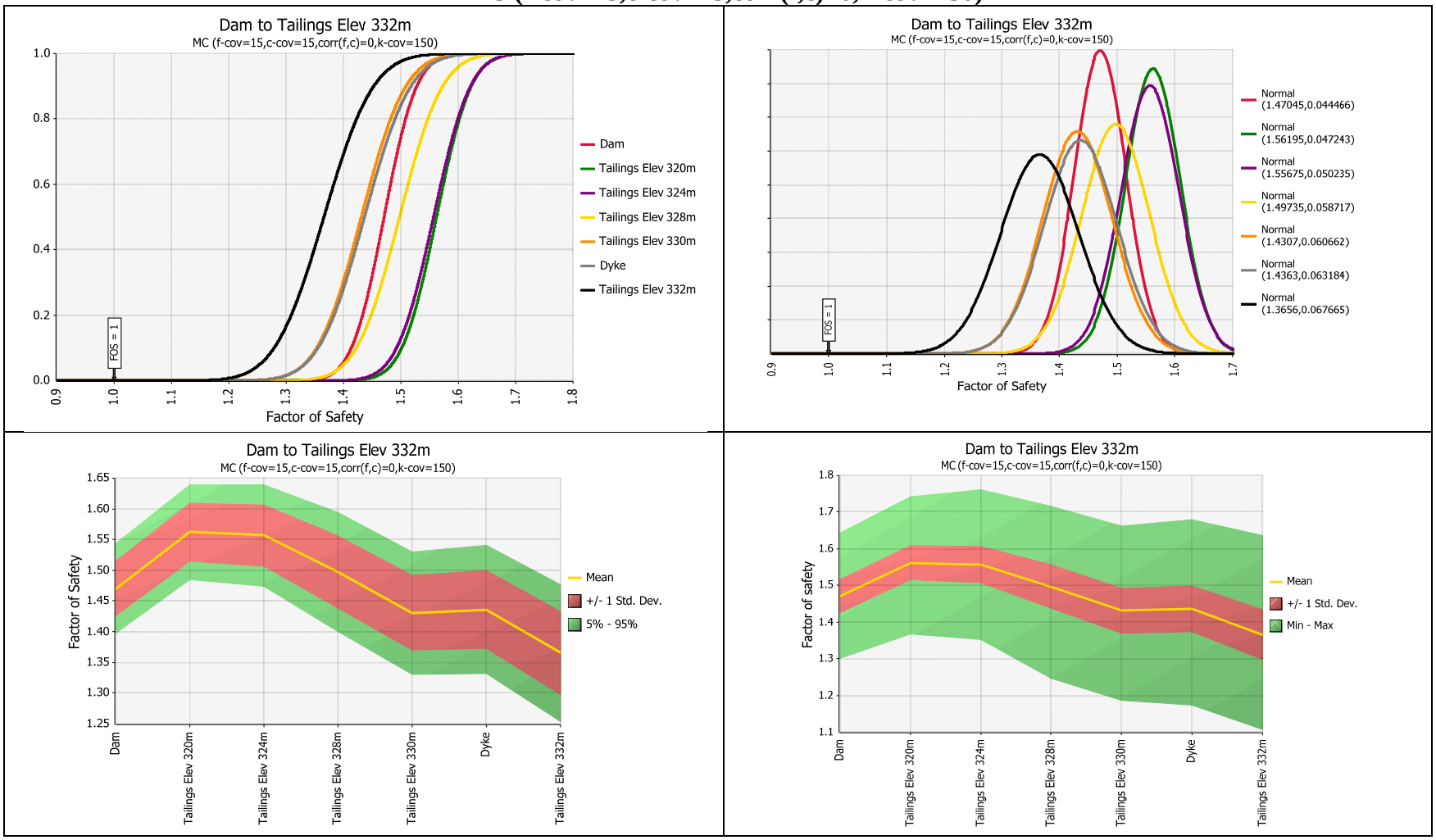

MC (f-cov=15,c-cov=15,corr(f,c)=0,k-cov=150)

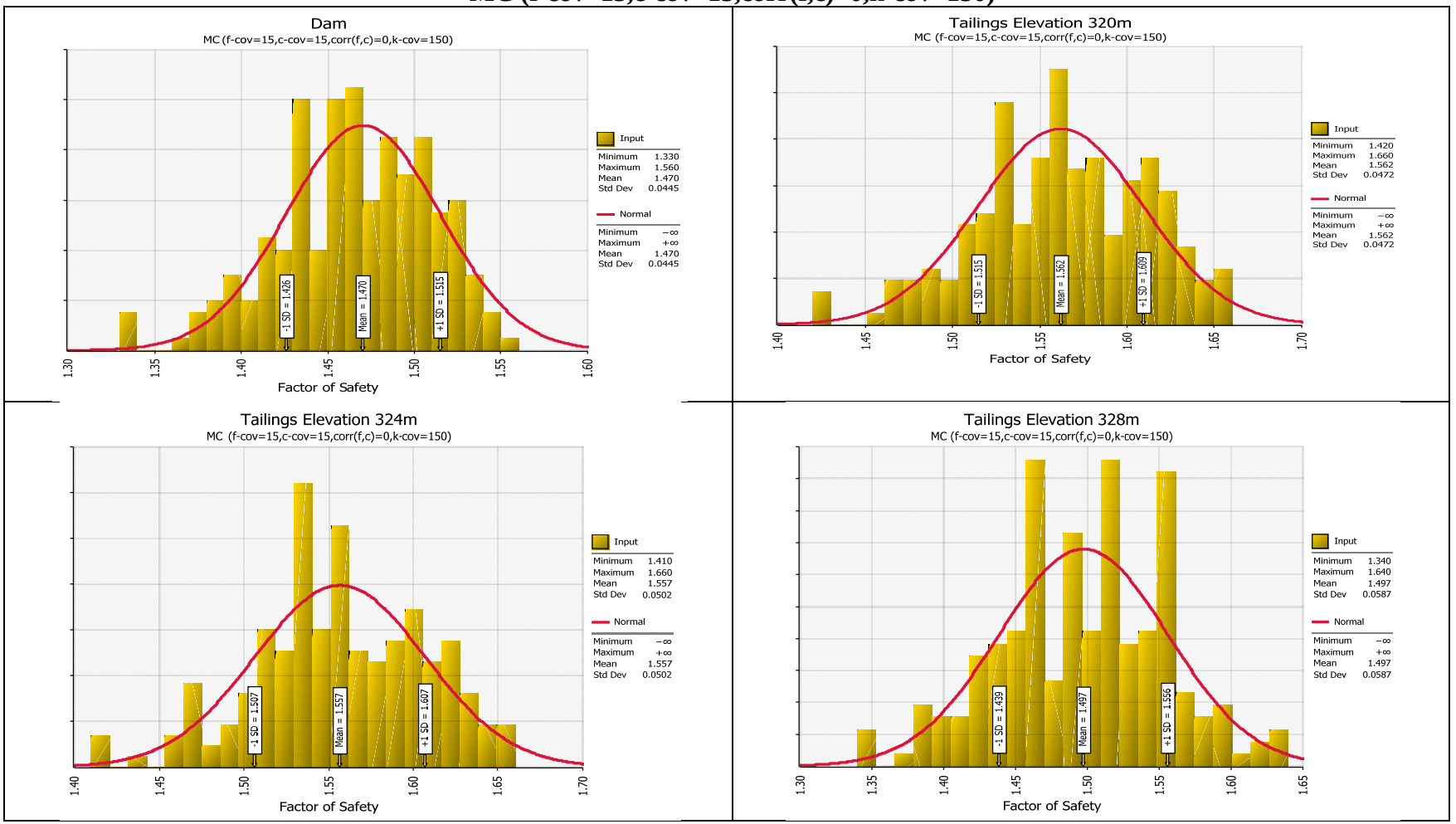

MC (f-cov=15,c-cov=15,corr(f,c)=0,k-cov=150)

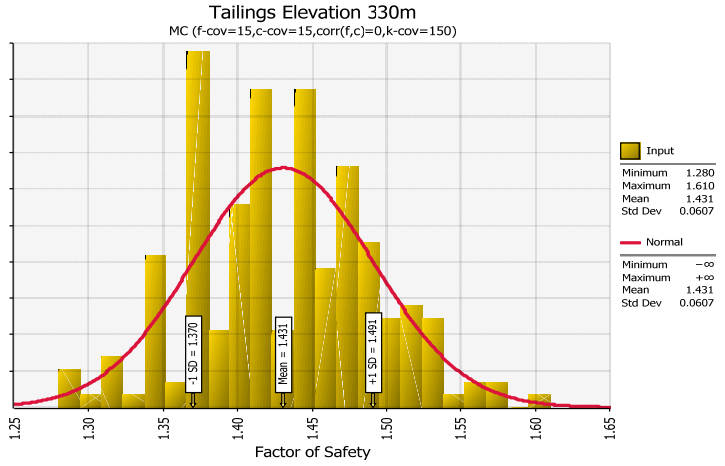

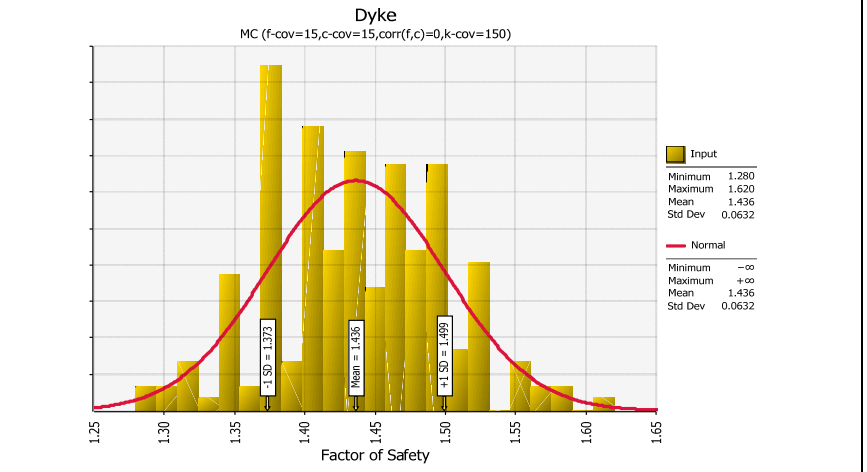

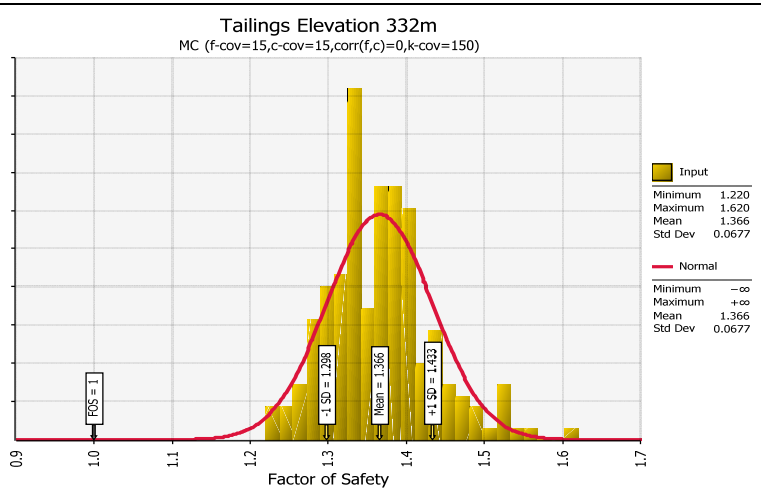

MC (f-cov=15, c-cov=15, corr(f,c)=0, k-cov=150)	MEAN	STDEV	Reliability	Probability of Unsatisfactory Performance
Dam	1.47045	0.044466	10.580	0.000001
Tailings Elev 320m	1.56195	0.047243	11.895	0.000001
Tailings Elev 324m	1.55675	0.050235	11.083	0.000001
Tailings Elev 328m	1.49735	0.058717	8.470	0.000001
Tailings Elev 330m	1.4307	0.060662	7.100	0.000001
Dyke	1.4363	0.063184	6.905	0.000001
Tailings Elev 332m	1.3656	0.067665	5.403	0.000001

MC (f-cov=15,c-cov=15,corr(f,c)=-0.5,k-cov=150)

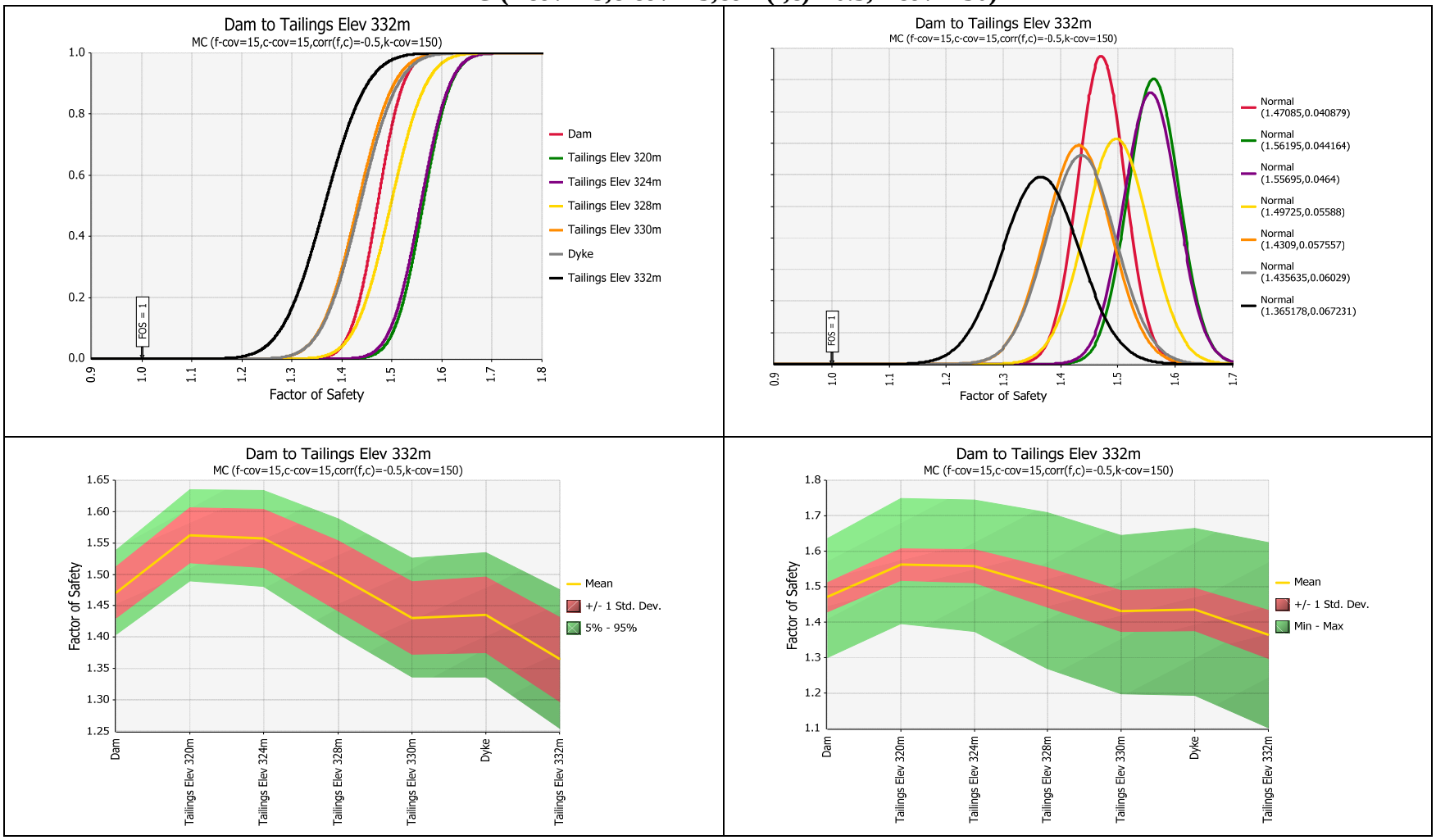

MC (f-cov=15,c-cov=15,corr(f,c)=-0.5,k-cov=150)

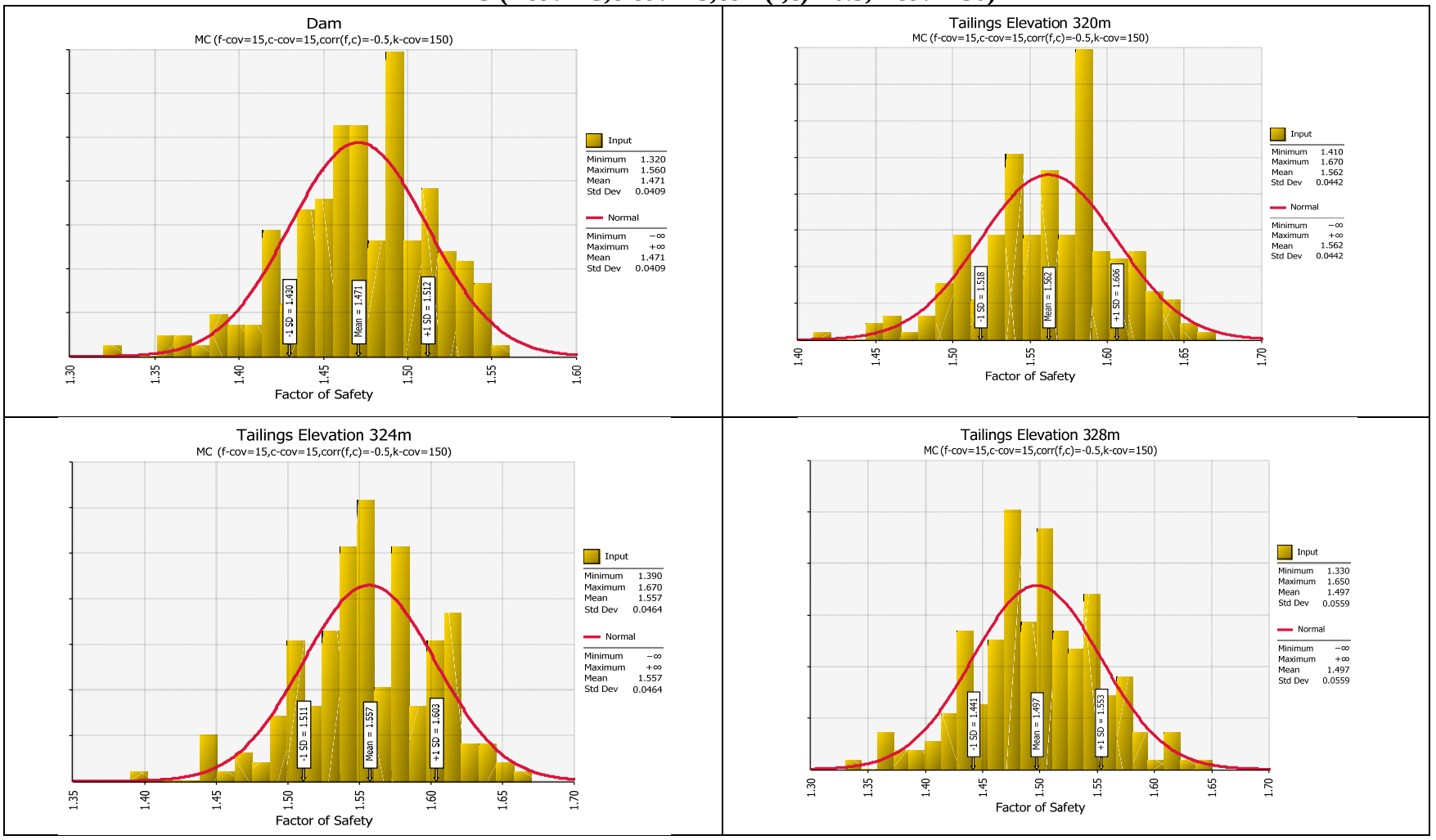

MC (f-cov=15,c-cov=15,corr(f,c)=-0.5,k-cov=150)

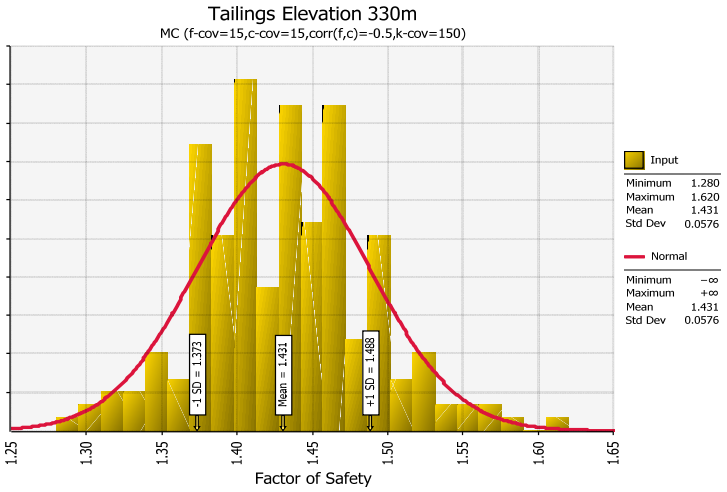

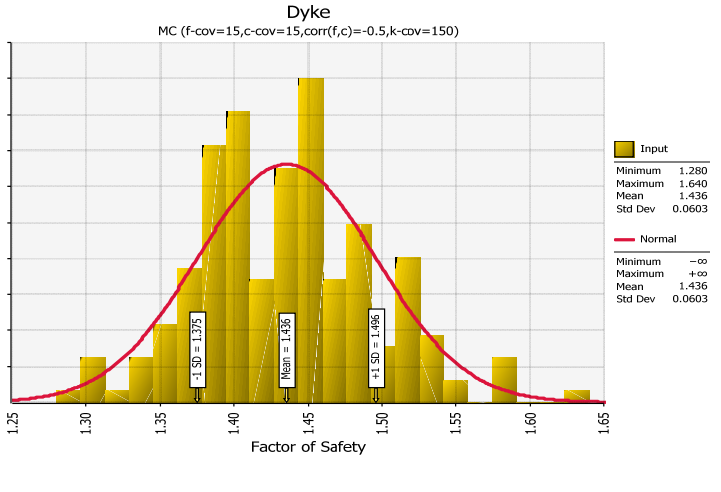

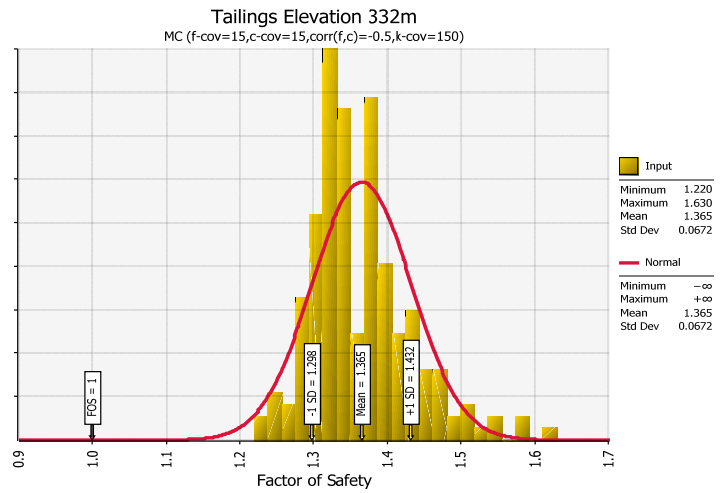

MC (f-cov=15, c-cov=15, corr(f,c)=-0.5, k-cov=150)	MEAN	STDEV	Reliability	Probability of Unsatisfactory Performance
Dam	1.47085	0.040879	11.518	0.000001
Tailings Elev 320m	1.56195	0.044164	12.724	0.000001
Tailings Elev 324m	1.55695	0.0464	12.003	0.000001
Tailings Elev 328m	1.49725	0.05588	8.899	0.000001
Tailings Elev 330m	1.4309	0.057557	7.486	0.000001
Dyke	1.435635	0.06029	7.226	0.000001
Tailings Elev 332m	1.365178	0.067231	5.432	0.000001

MC (f-cov=30,c-cov=30,corr(f,c)=0.5,k-cov=150)

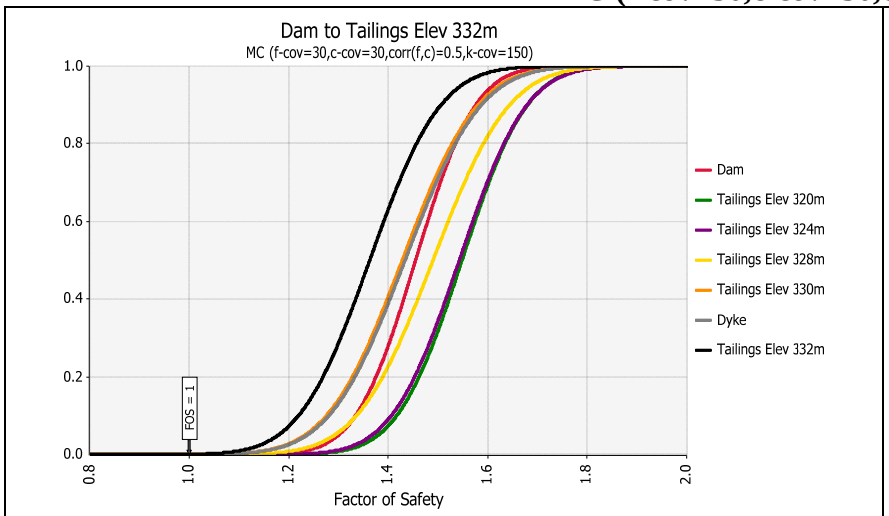

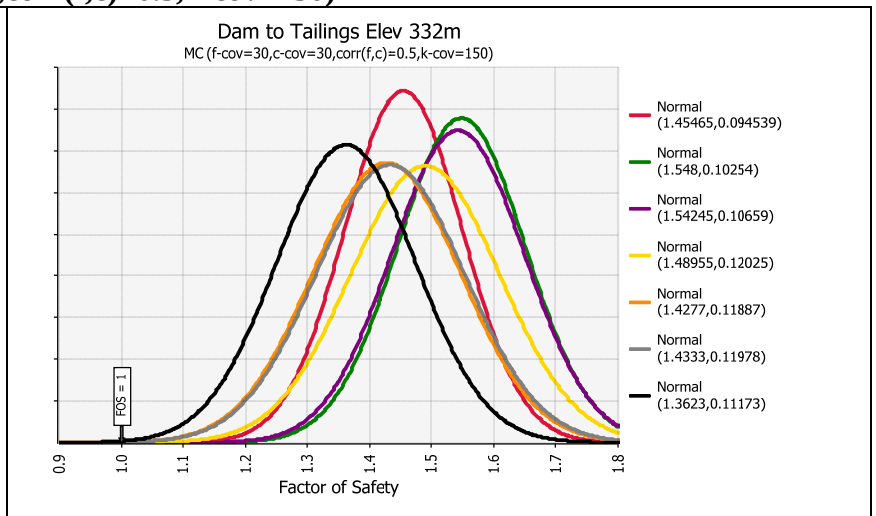

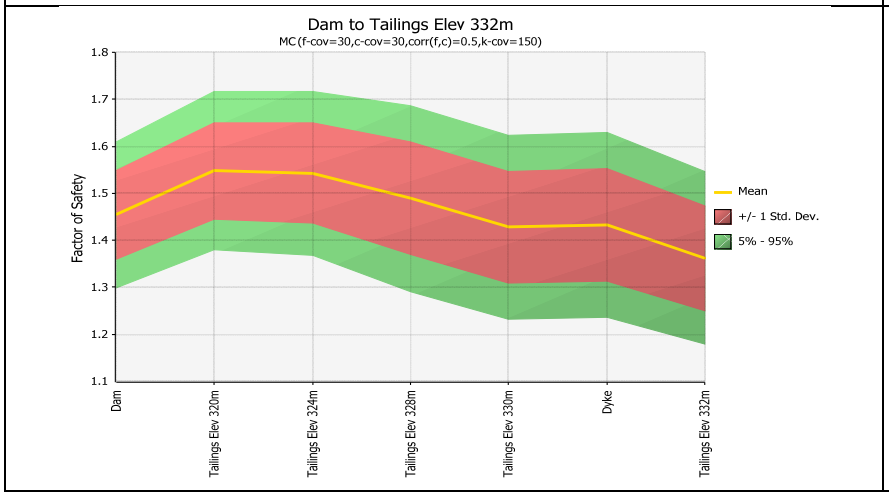

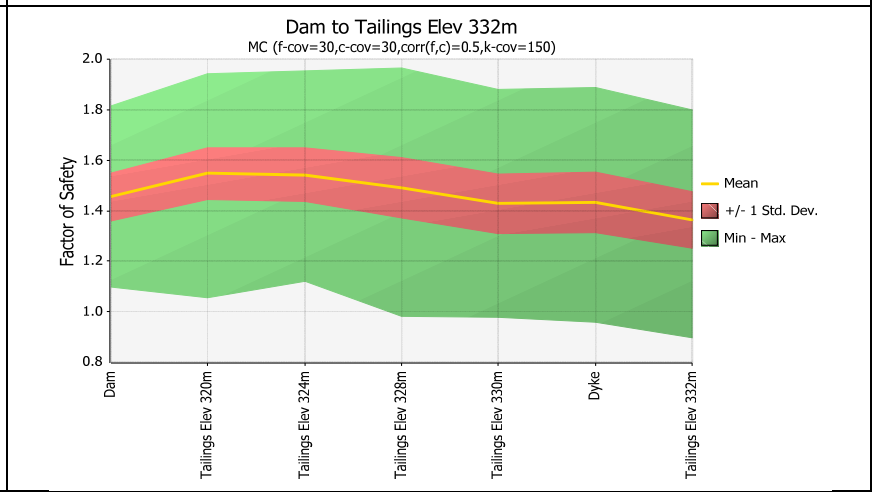

MC (f-cov=30,c-cov=30,corr(f,c)=0.5,k-cov=150)

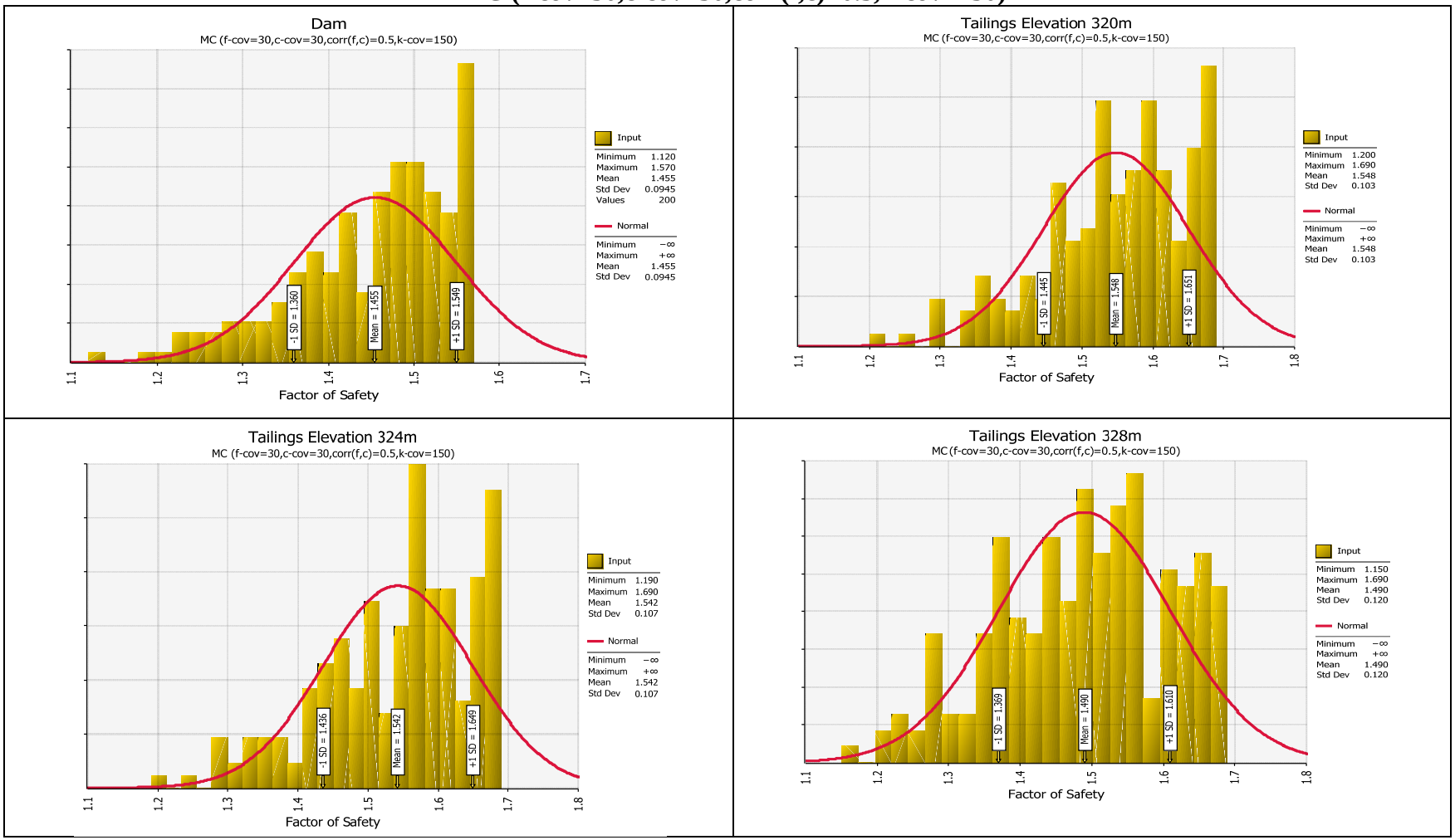

MC (f-cov=30,c-cov=30,corr(f,c)=0.5,k-cov=150)

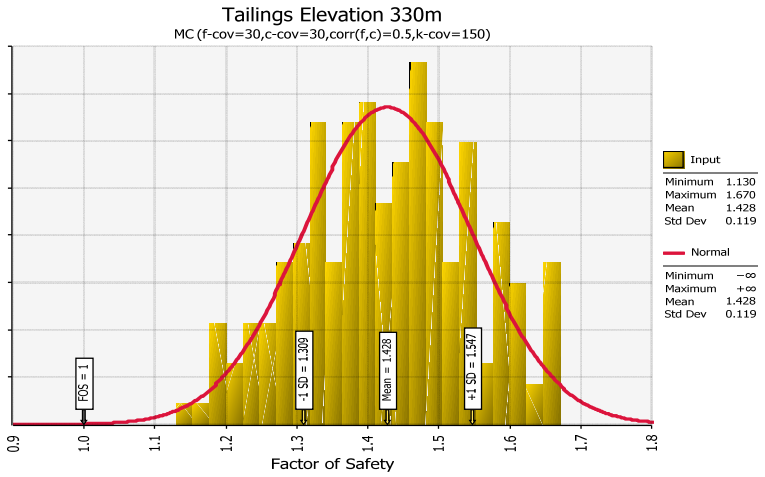

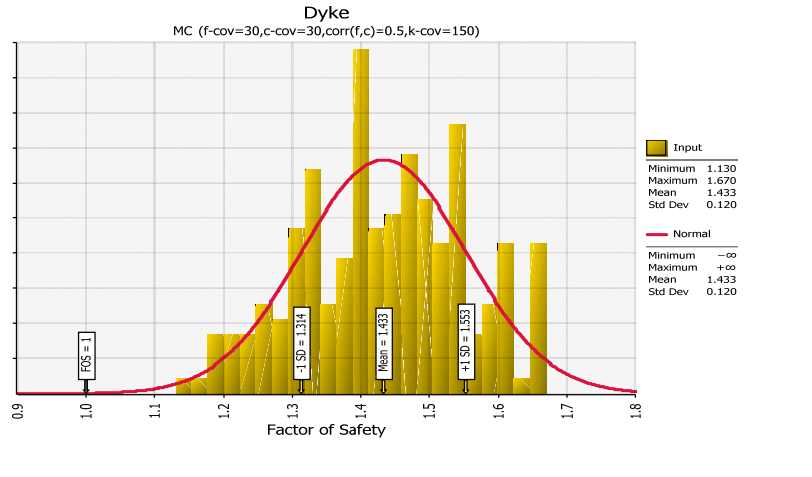

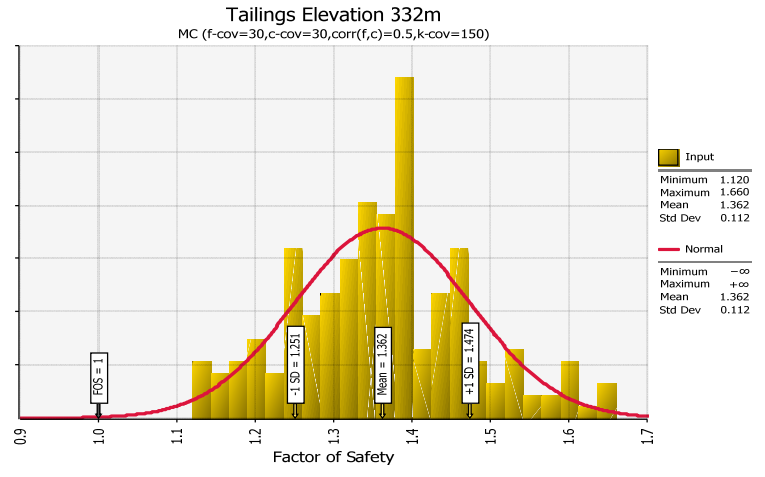

MC (f-cov=30,c-cov=30,corr(f,c)=0.5,k-cov=150)	MEAN	STDEV	Reliability	Probability of Unsatisfactory Performance
Dam	1.45465	0.094539	4.809	0.000001
Tailings Elev 320m	1.548	0.10254	5.344	0.000001
Tailings Elev 324m	1.54245	0.10659	5.089	0.000001
Tailings Elev 328m	1.48955	0.12025	4.071	0.00002
Tailings Elev 330m	1.4277	0.11887	3.598	0.00016
Dyke	1.4333	0.11978	3.617	0.00015
Tailings Elev 332m	1.3623	0.11173	3.243	0.0006

MC (f-cov=30,c-cov=30,corr(f,c)=0,k-cov=150)

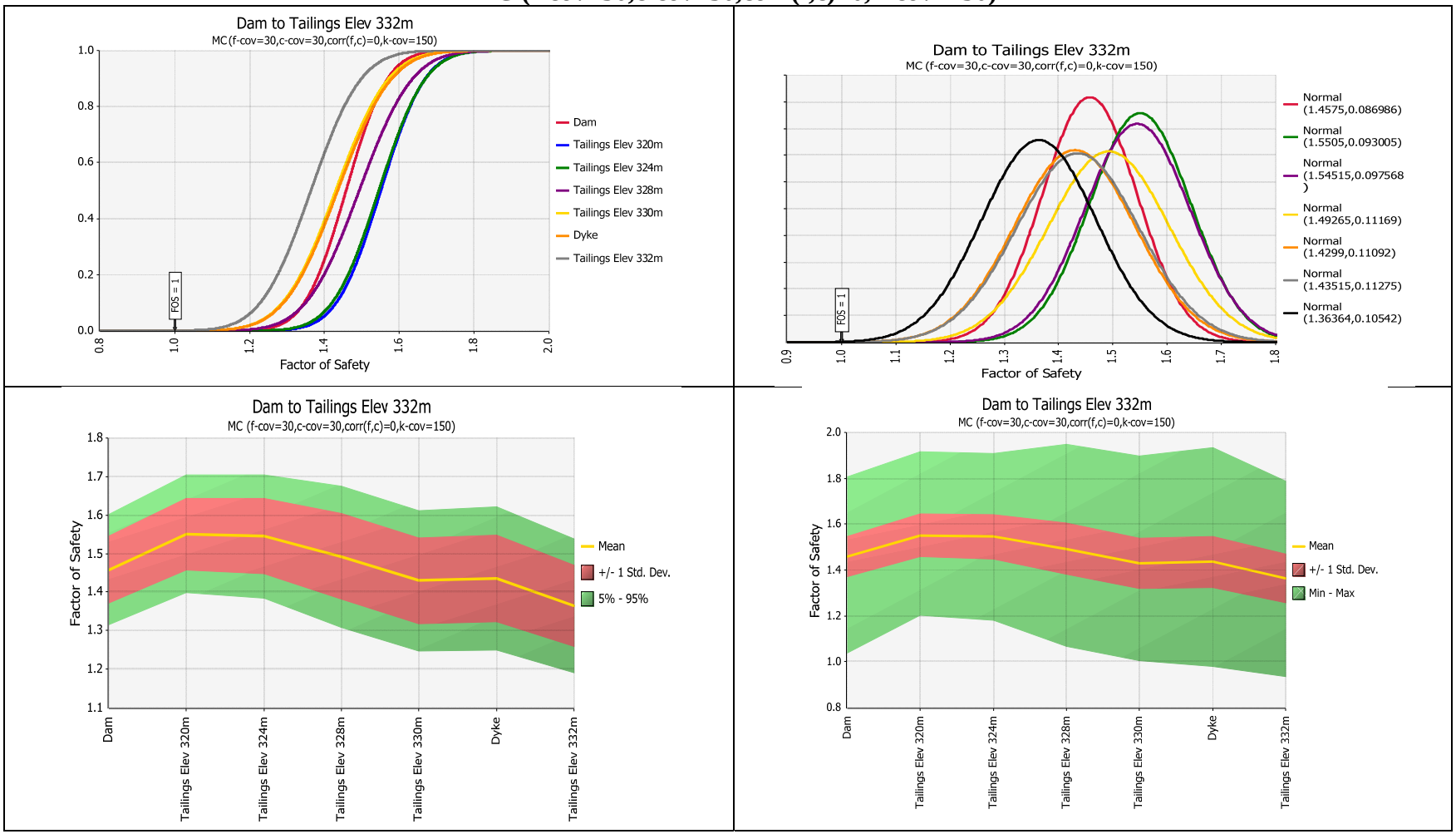

MC (f-cov=30,c-cov=30,corr(f,c)=0,k-cov=150)

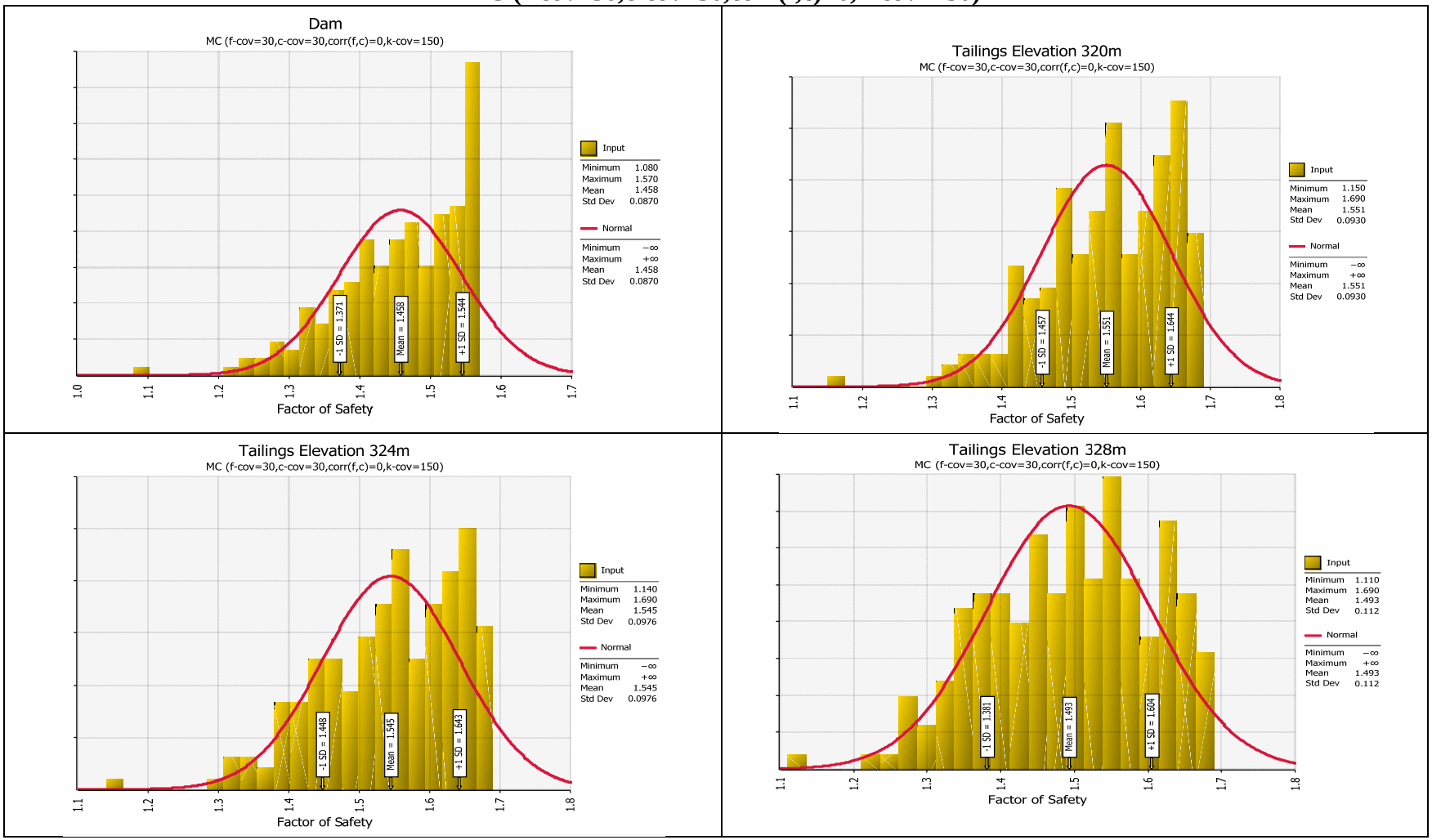

MC (f-cov=30,c-cov=30,corr(f,c)=0,k-cov=150)

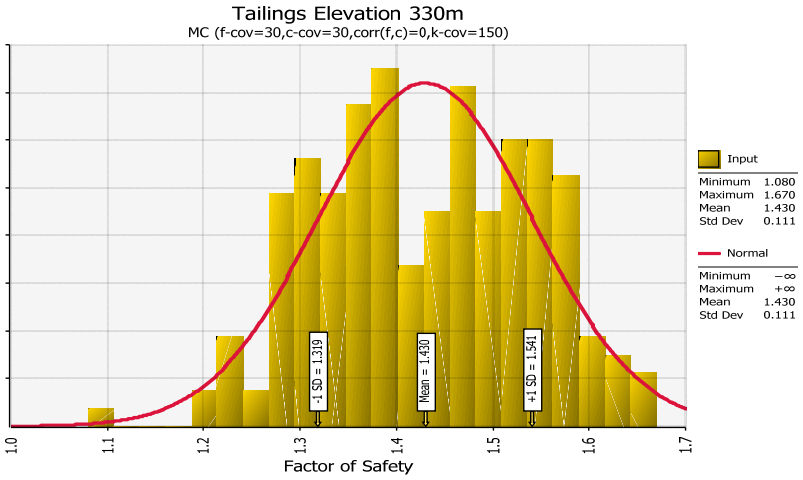

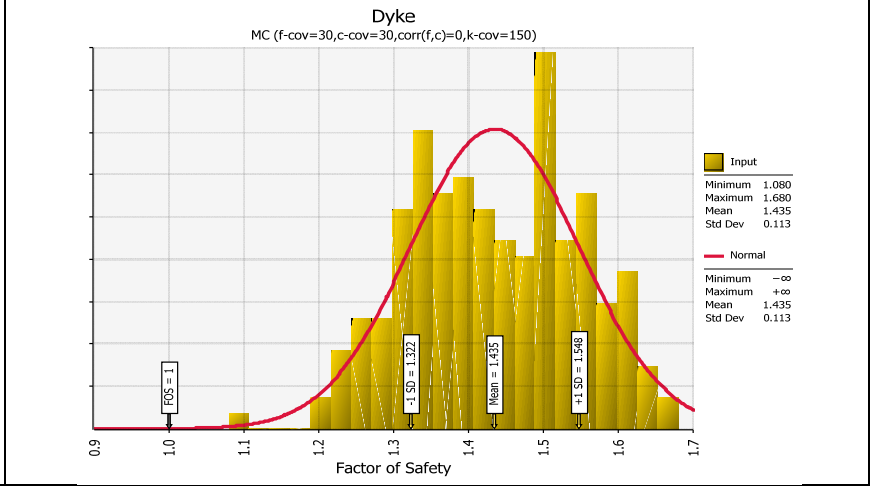

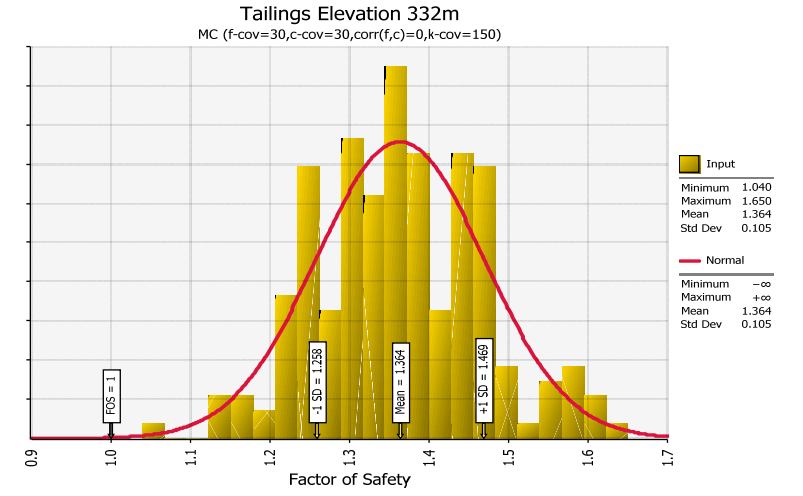

MC (f-cov=30,c-cov=30,corr(f,c)=0,k-cov=150)	MEAN	STDEV	Reliability	Probability of Unsatisfactory Performance
Dam	1.4575	0.086986	5.259	0.000001
Tailings Elev 320m	1.5505	0.093005	5.919	0.000001
Tailings Elev 324m	1.54515	0.097568	5.587	0.000001
Tailings Elev 328m	1.49265	0.11169	4.411	0.000001
Tailings Elev 330m	1.4299	0.11092	3.876	0.00005
Dyke	1.43515	0.11275	3.859	0.00006
Tailings Elev 332m	1.36364	0.10542	3.449	0.00028

MC (f-cov=30,c-cov=30,corr(f,c)=-0.5,k-cov=150)

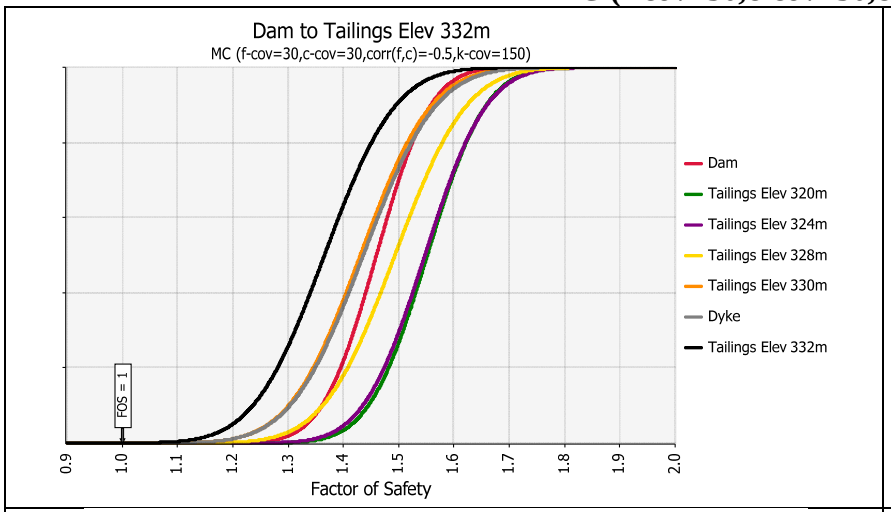

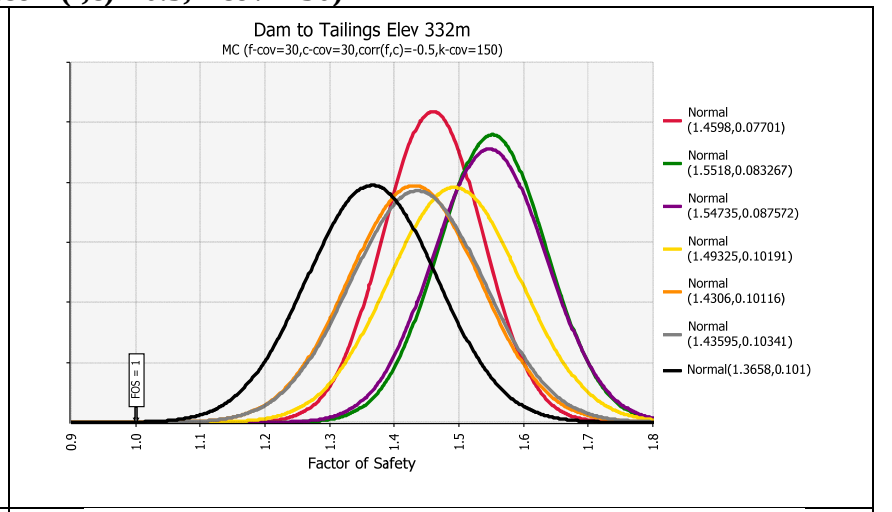

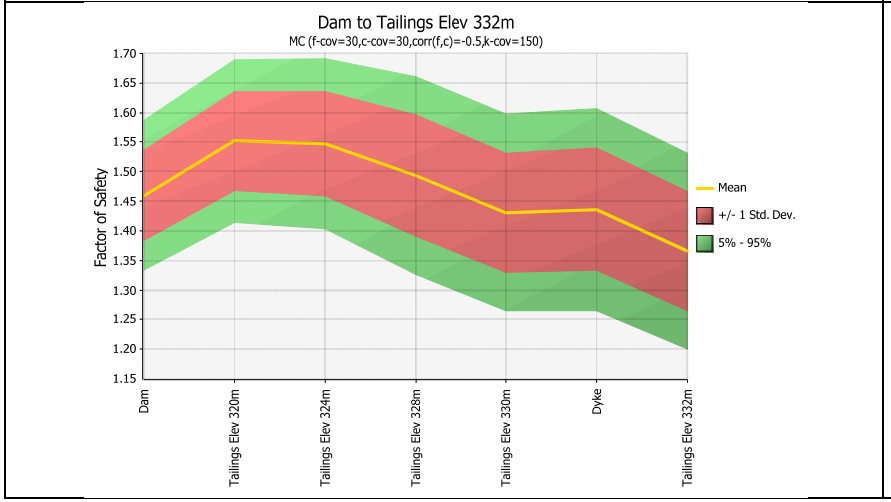

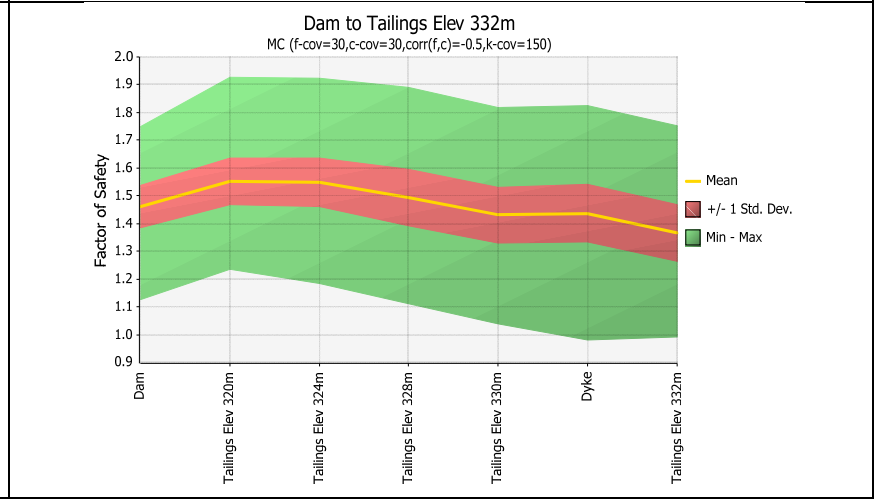

MC (f-cov=30,c-cov=30,corr(f,c)=-0.5,k-cov=150)

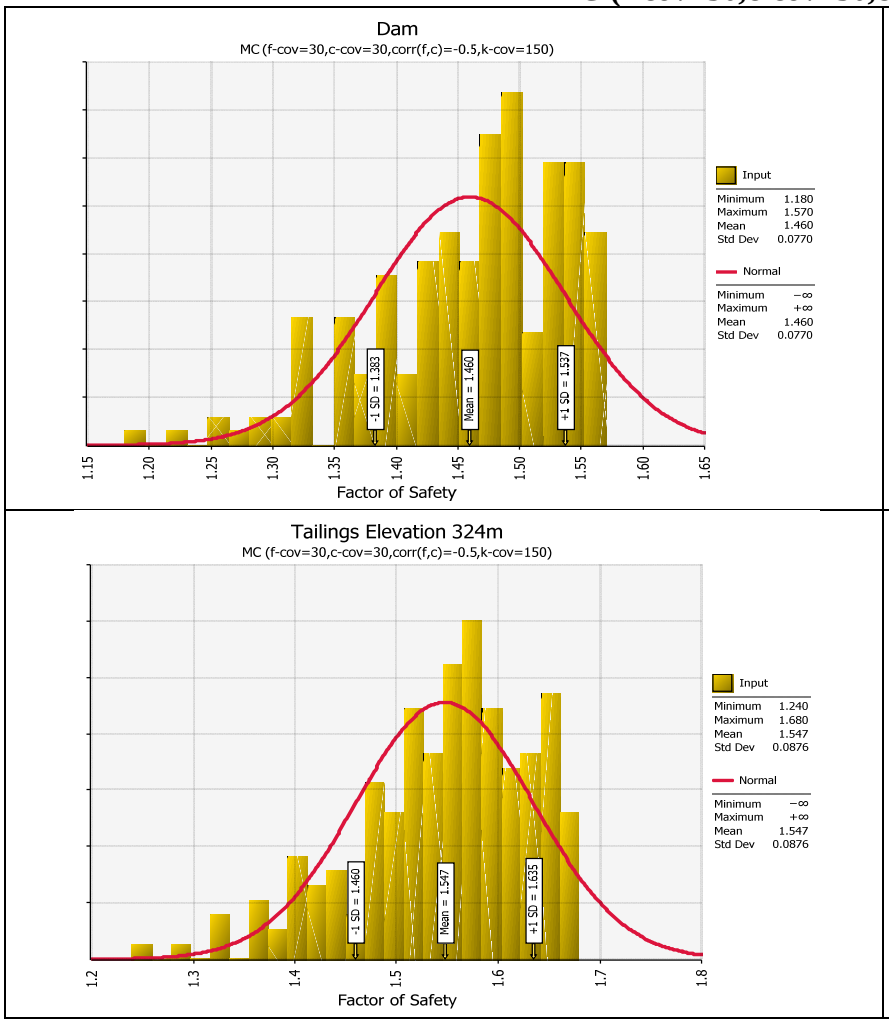

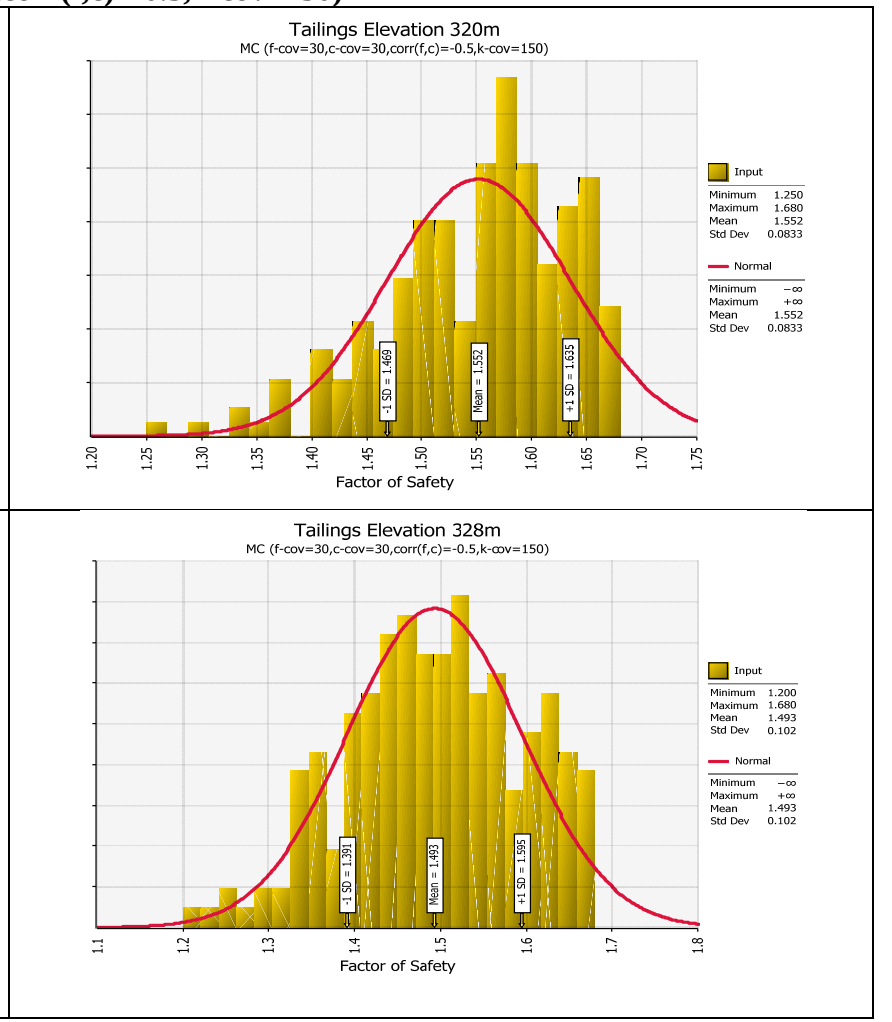

MC (f-cov=30,c-cov=30,corr(f,c)=-0.5,k-cov=150)

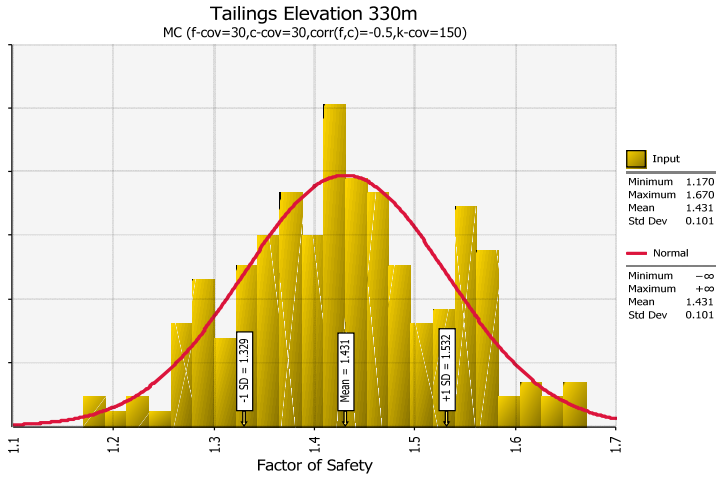

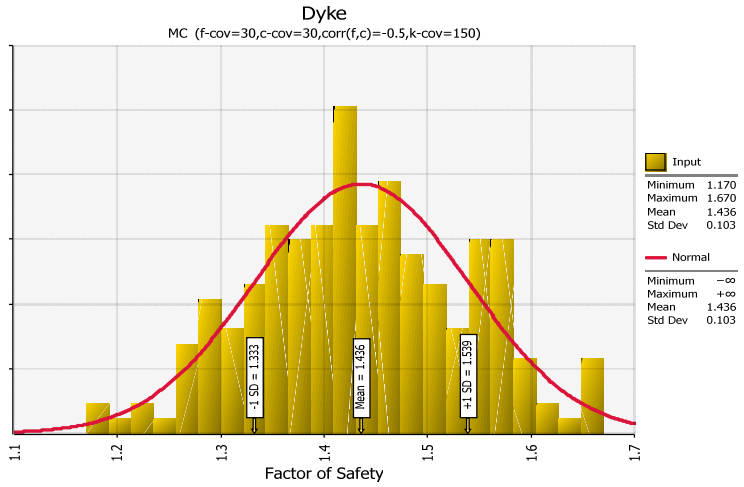

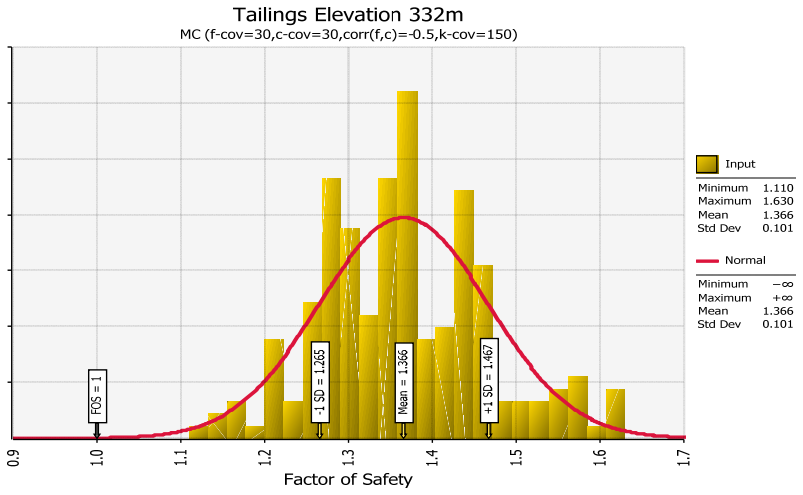

MC (f-cov=30,c-cov=30,corr(f,c)=-0.5,k-cov=150)	MEAN	STDEV	Reliability	Probability of Unsatisfactory Performance
Dam	1.4598	0.07701	5.971	0.000001
Tailings Elev 320m	1.5518	0.083267	6.627	0.000001
Tailings Elev 324m	1.54735	0.087572	6.250	0.000001
Tailings Elev 328m	1.49325	0.10191	4.840	0.000001
Tailings Elev 330m	1.4306	0.10116	4.257	0.000001
Dyke	1.43595	0.10341	4.216	0.000001
Tailings Elev 332m	1.3658	0.101	3.622	0.00015

MC (f-cov=45,c-cov=45,corr(f,c)=0.5,k-cov=150)

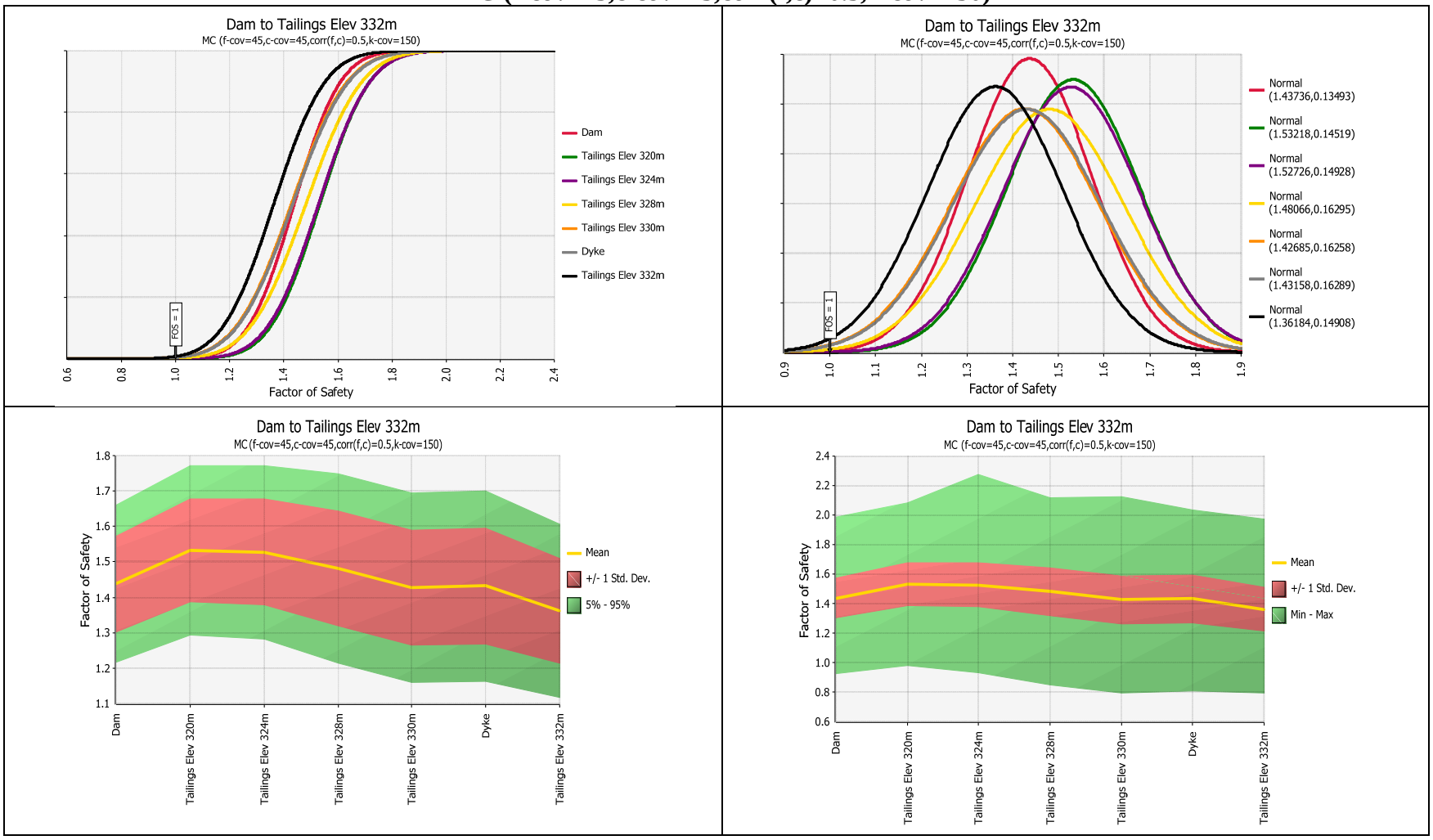

MC (f-cov=45,c-cov=45,corr(f,c)=0.5,k-cov=150)

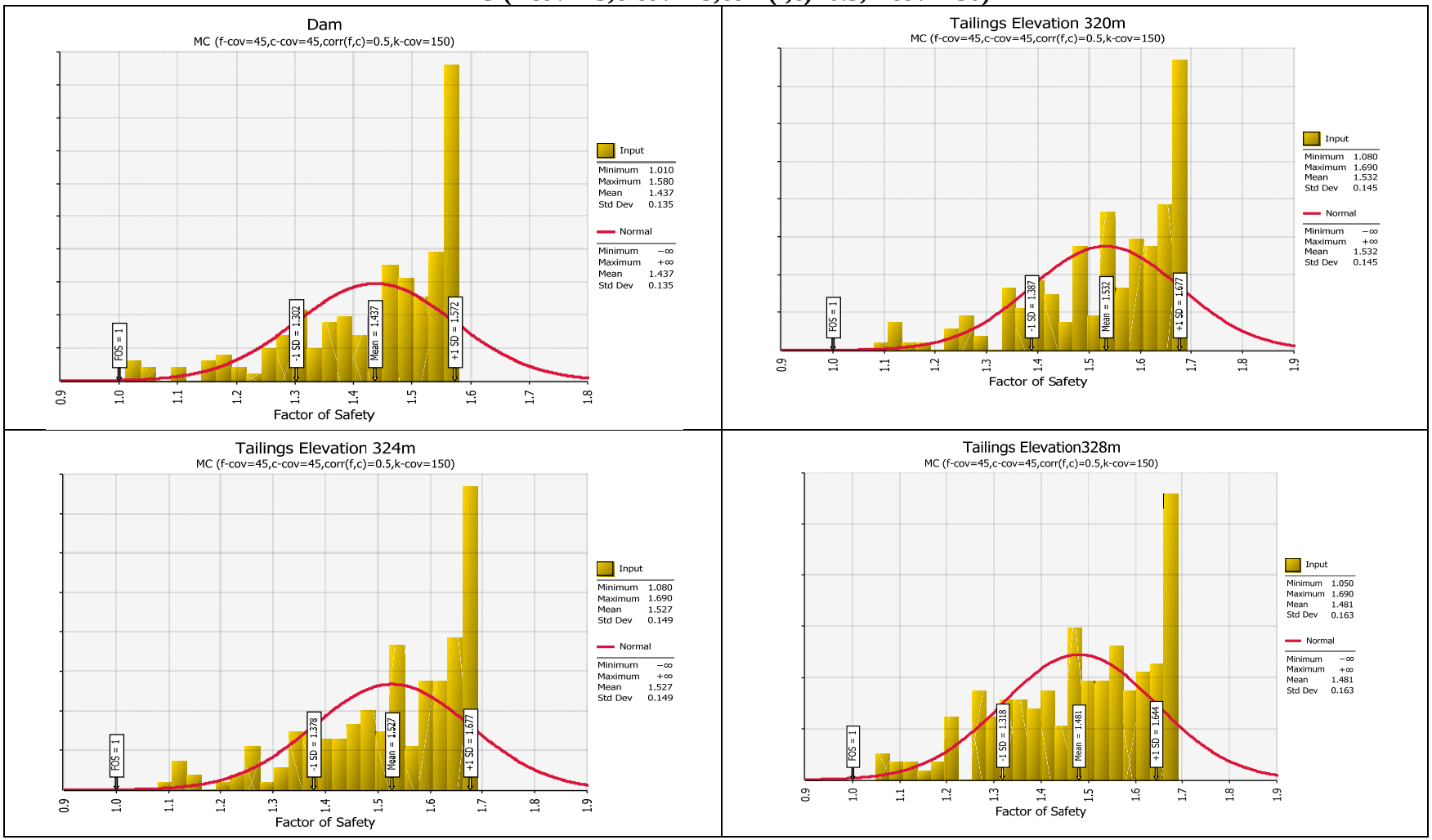

MC (f-cov=45,c-cov=45,corr(f,c)=0.5,k-cov=150)

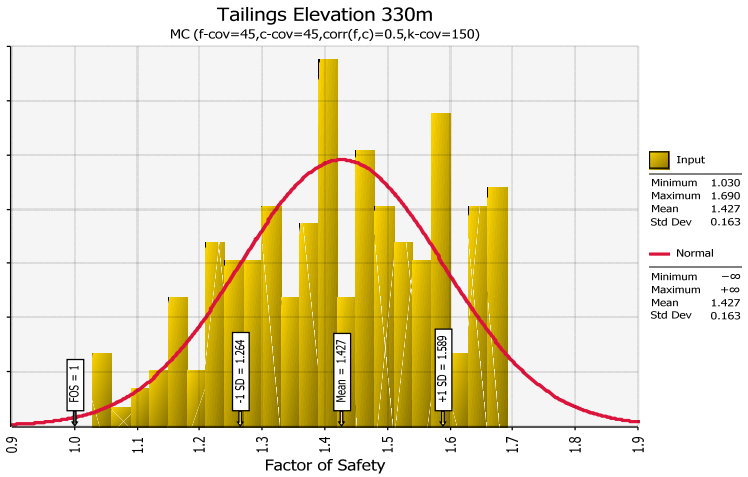

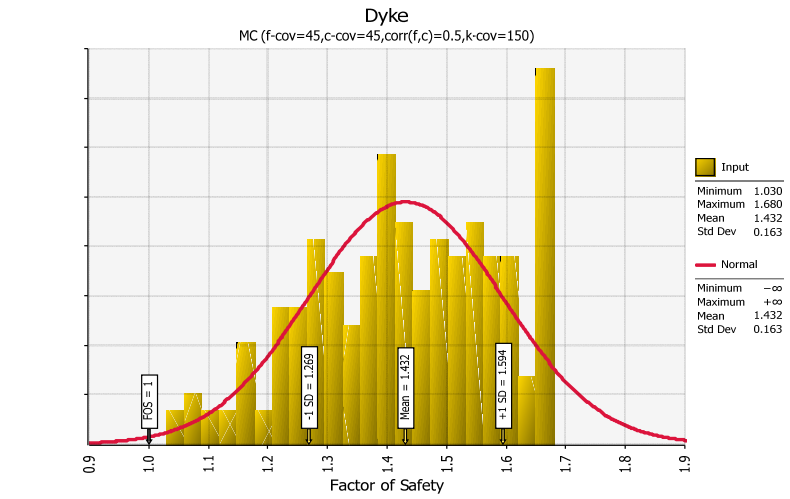

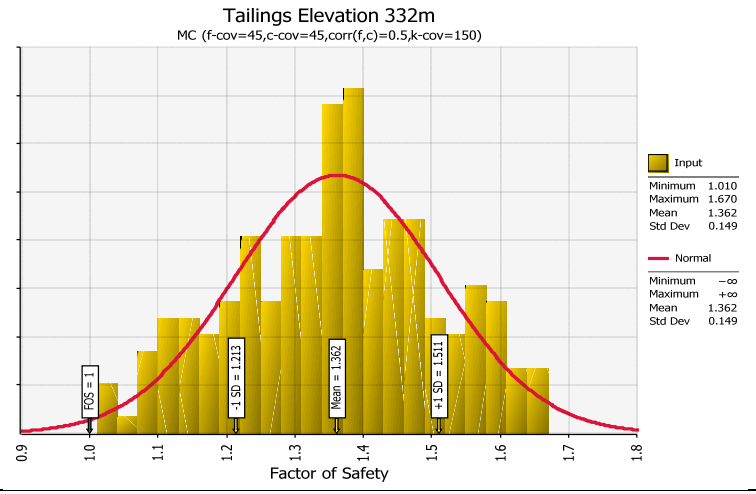

MC (f-cov=45,c-cov=45,corr(f,c)=0.5,k-cov=150)	MEAN	STDEV	Reliability	Probability of Unsatisfactory Performance
Dam	1.43736	0.13493	3.241	0.0006
Tailings Elev 320m	1.53218	0.14519	3.665	0.00012
Tailings Elev 324m	1.52726	0.14928	3.532	0.00021
Tailings Elev 328m	1.48066	0.16295	2.950	0.00159
Tailings Elev 330m	1.42685	0.16258	2.625	0.0044
Dyke	1.43158	0.16289	2.650	0.00402
Tailings Elev 332m	1.36184	0.14908	2.427	0.00755

MC (f-cov=45,c-cov=45,corr(f,c)=0,k-cov=150)

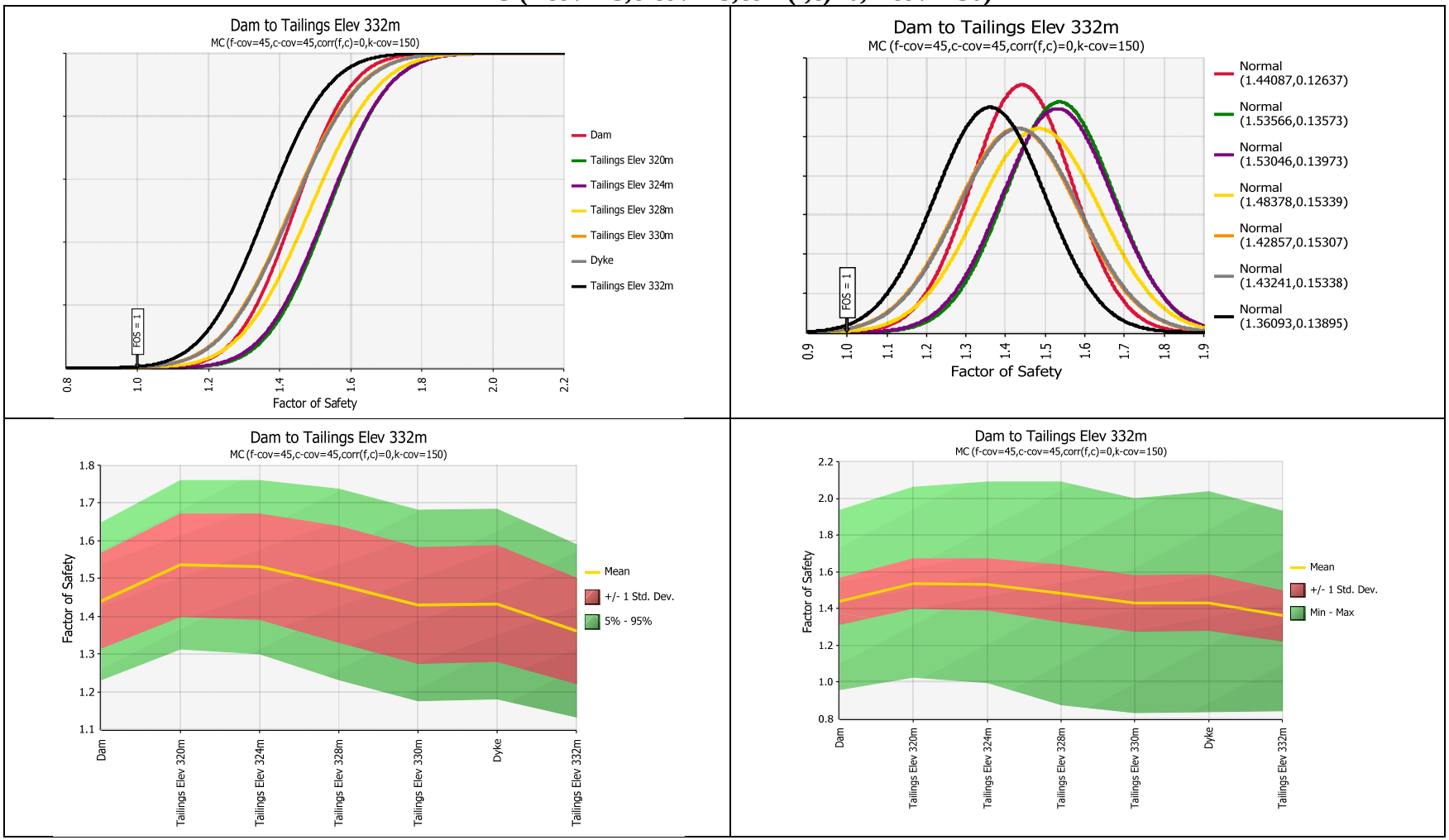

MC (f-cov=45,c-cov=45,corr(f,c)=0,k-cov=150)

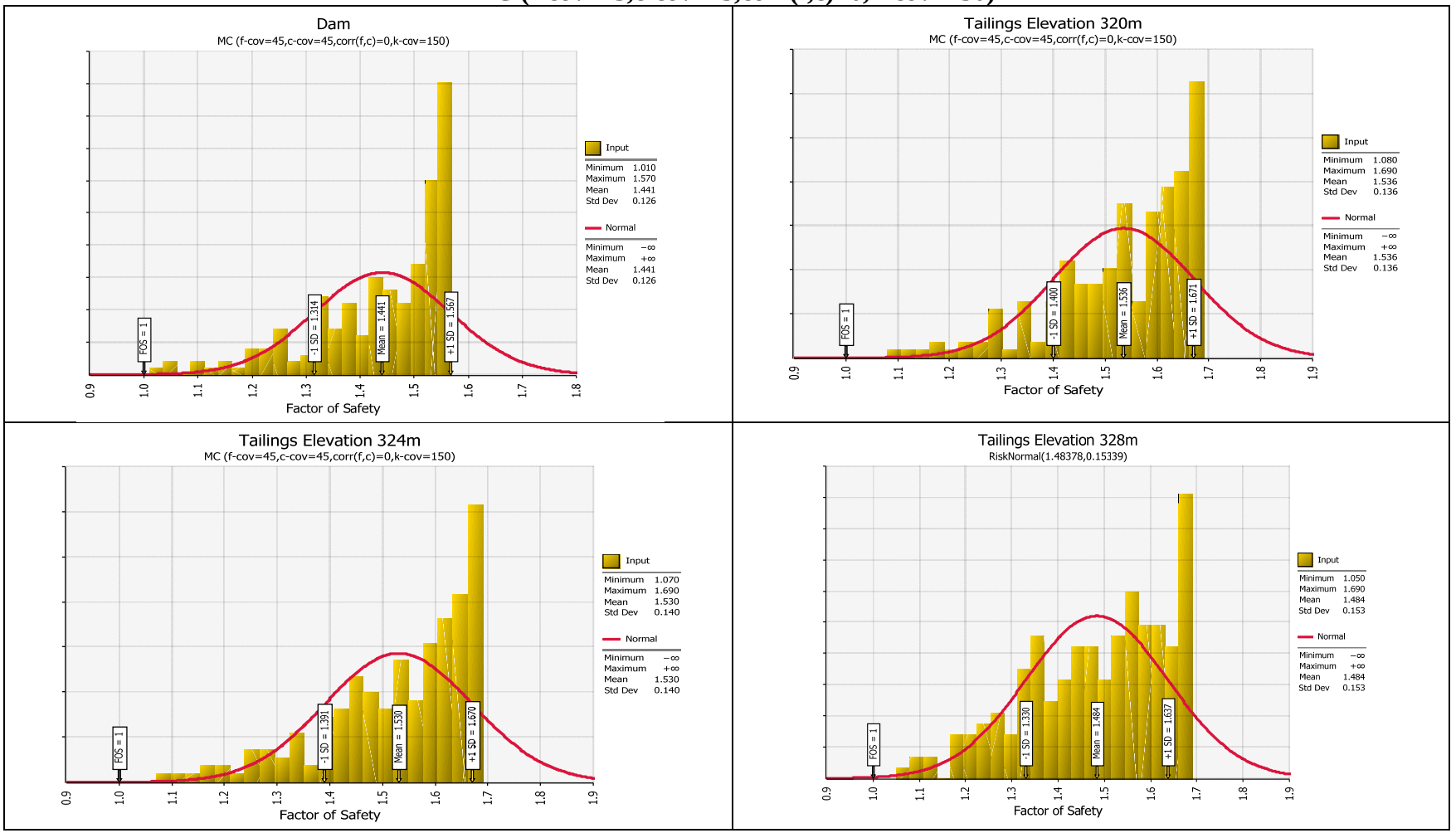

MC (f-cov=45,c-cov=45,corr(f,c)=0,k-cov=150)

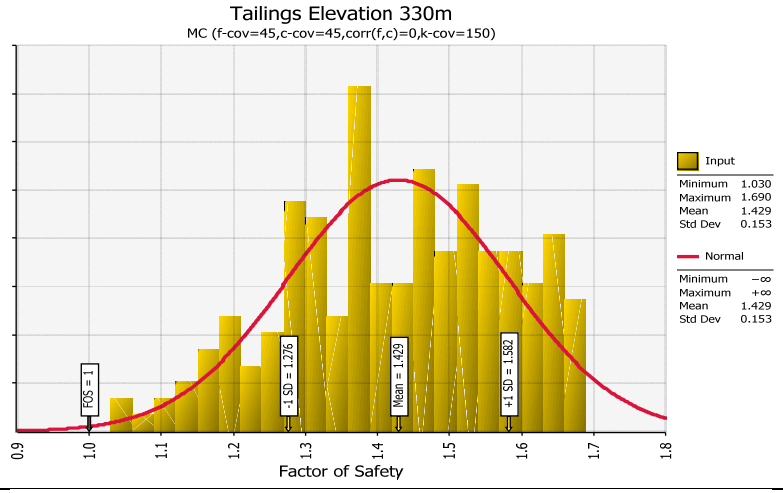

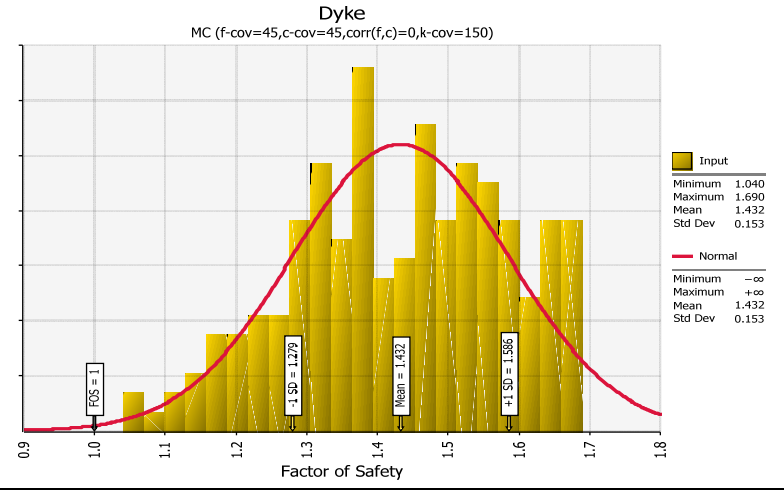

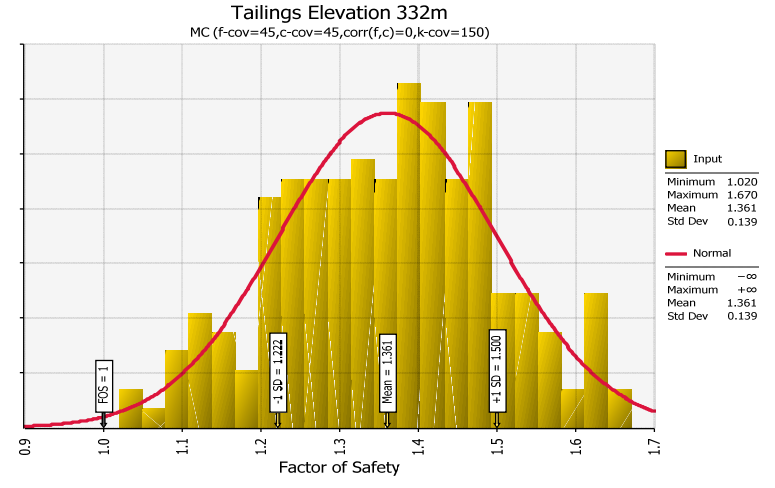

MC (f-cov=45,c-cov=45,corr(f,c)=0,k-cov=150)	MEAN	STDEV	Reliability	Probability of Unsatisfactory Performance
Dam	1.44087	0.12637	3.489	0.00024
Tailings Elev 320m	1.53566	0.13573	3.947	0.00004
Tailings Elev 324m	1.53046	0.13973	3.796	0.00007
Tailings Elev 328m	1.48378	0.15339	3.154	0.00082
Tailings Elev 330m	1.42857	0.15307	2.800	0.00256
Dyke	1.43241	0.15338	2.819	0.0024
Tailings Elev 332m	1.36093	0.13895	2.598	0.00466

MC (f-cov=45,c-cov=45,corr(f,c)=-0.5,k-cov=150)

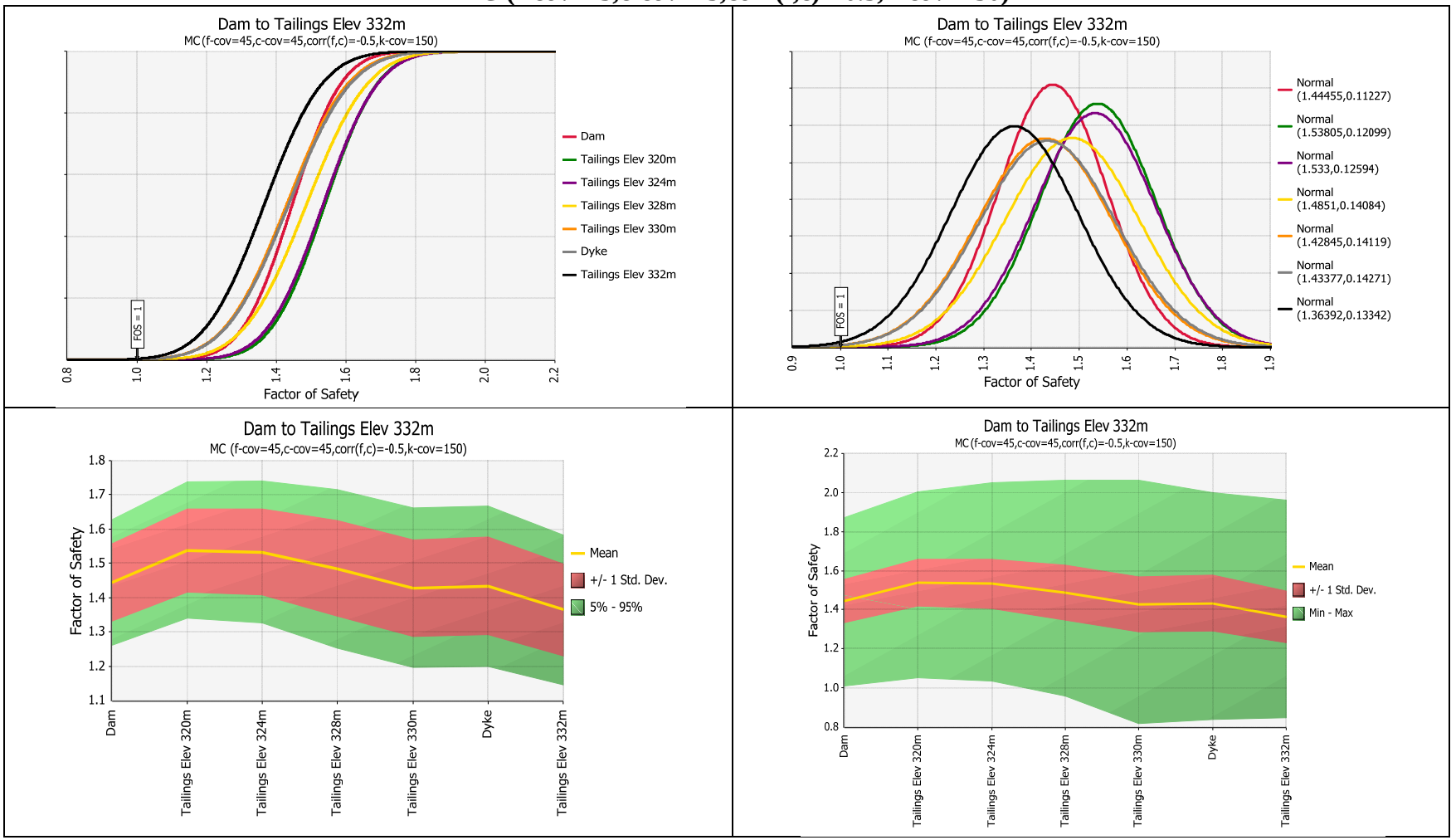

MC (f-cov=45,c-cov=45,corr(f,c)=-0.5,k-cov=150)

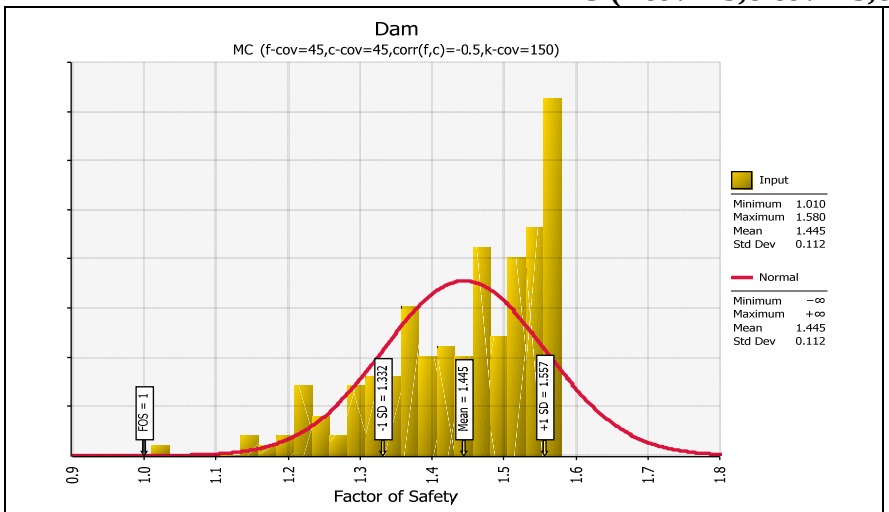

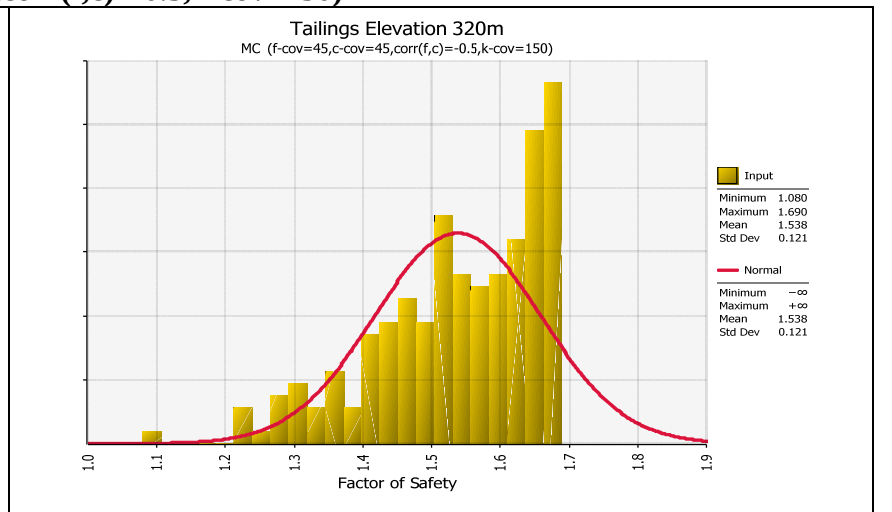

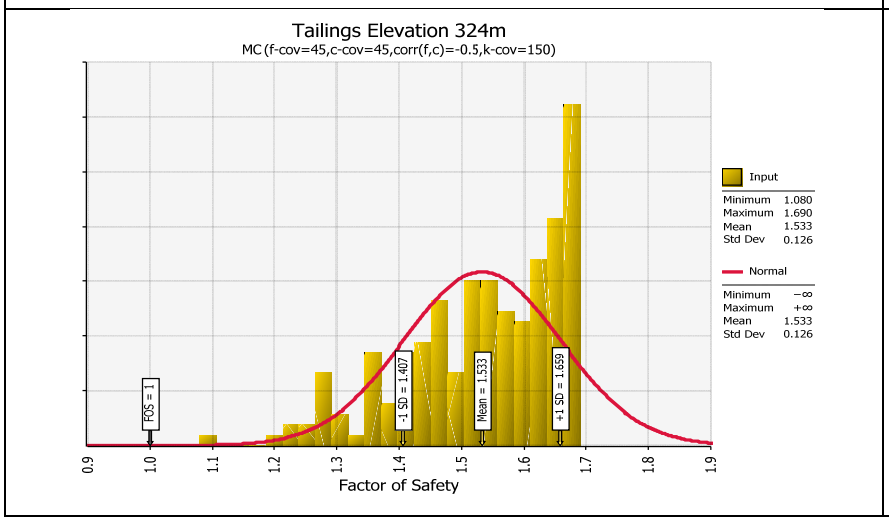

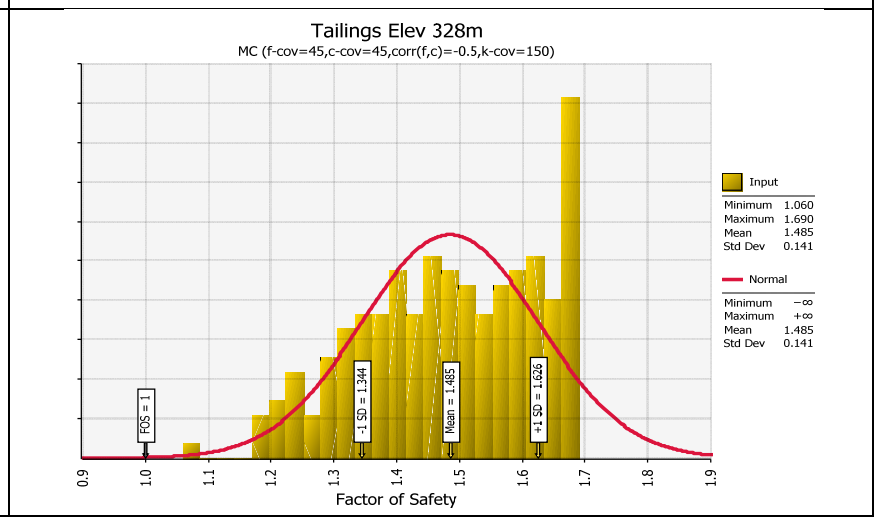

MC (f-cov=45,c-cov=45,corr(f,c)=-0.5,k-cov=150)

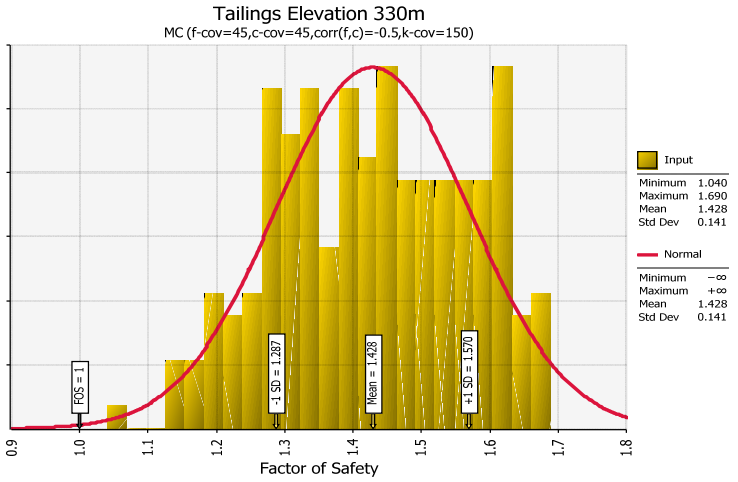

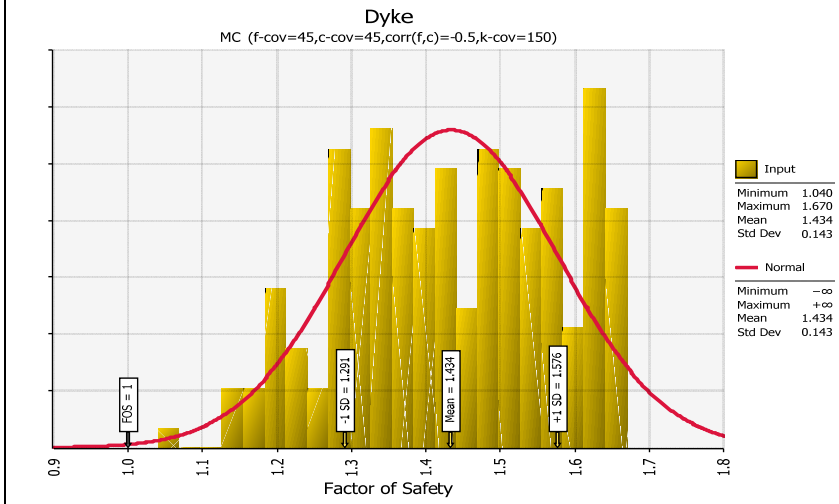

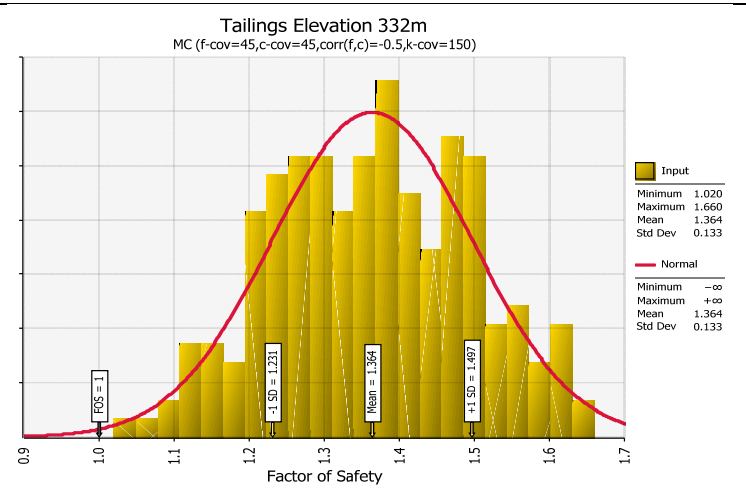

MC (f-cov=45,c-cov=45,corr(f,c)=-0.5,k-cov=150)	MEAN	STDEV	Reliability	Probability of Unsatisfactory Performance
Dam	1.44455	0.11227	3.960	0.00004
Tailings Elev 320m	1.53805	0.12099	4.447	0.000001
Tailings Elev 324m	1.533	0.12594	4.232	0.000001
Tailings Elev 328m	1.4851	0.14084	3.444	0.00029
Tailings Elev 330m	1.42845	0.14119	3.035	0.00118
Dyke	1.43377	0.14271	3.040	0.00118
Tailings Elev 332m	1.36392	0.13342	2.728	0.00317

PEM (f-cov=15, c-cov=15, k-cov=50)

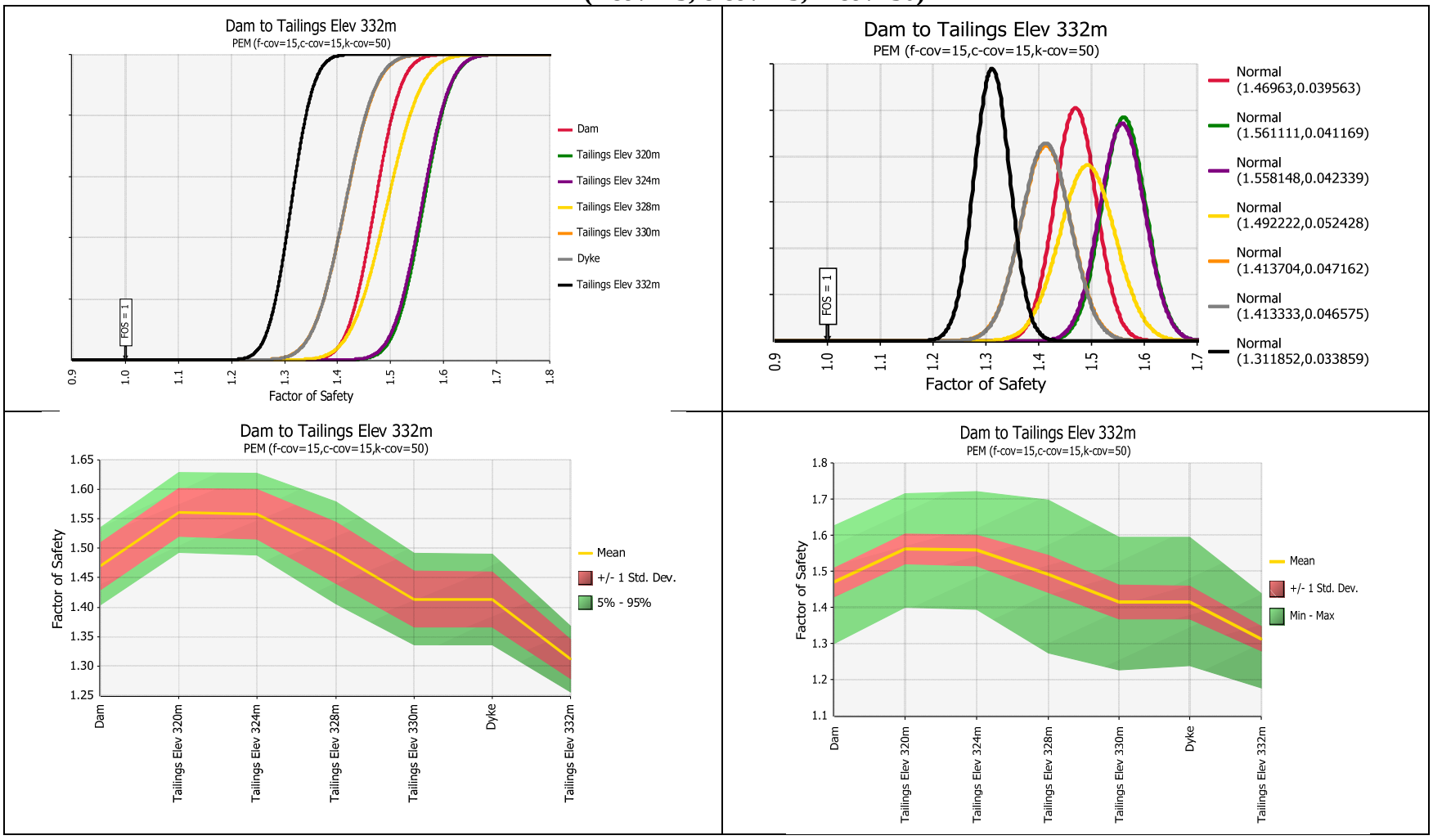

PEM (f-cov=15, c-cov=15, k-cov=50)

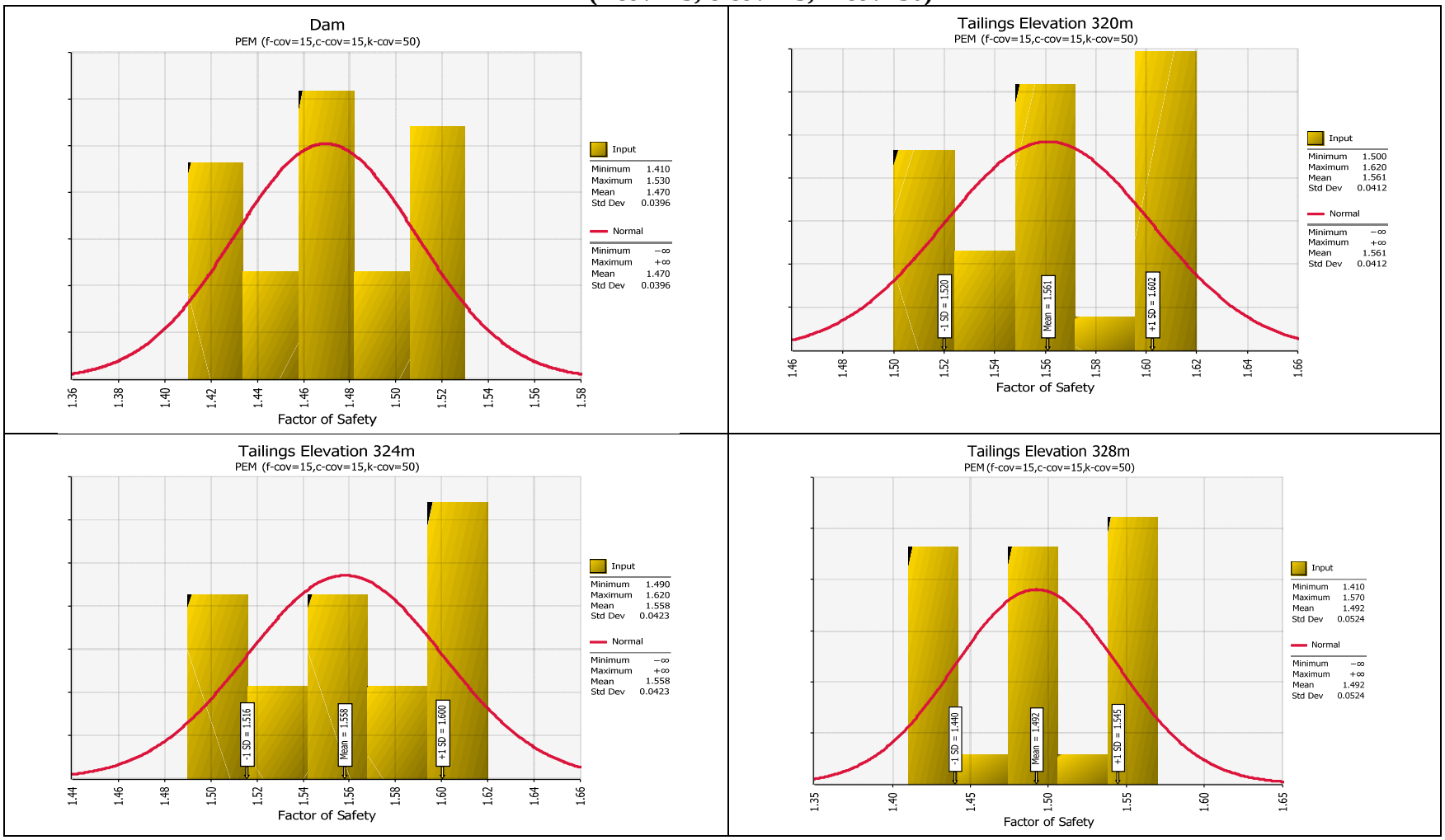

PEM (f-cov=15, c-cov=15, k-cov=50)

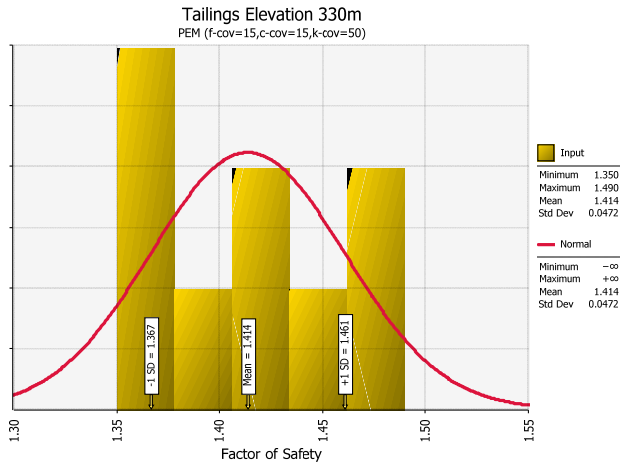

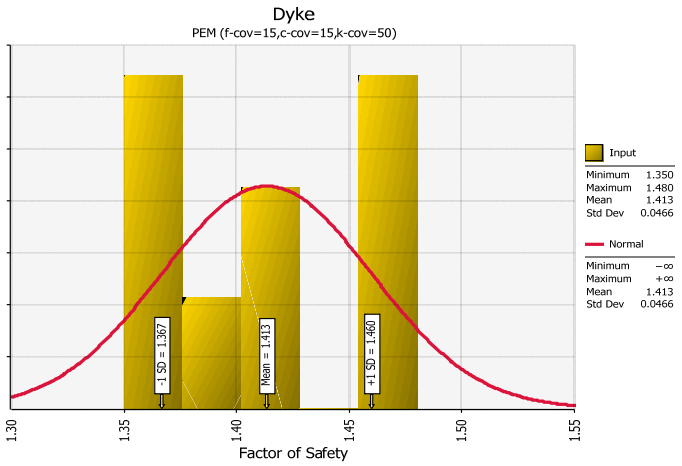

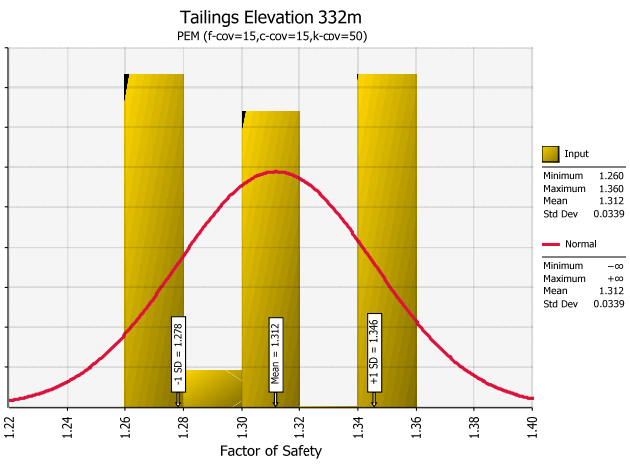

PEM (f-cov=15, c-cov=15, k-cov=50)	MEAN	STDEV	Reliability	Probability of Unsatisfactory Performance
Dam	1.46963	0.039563	11.870	0
Tailings Elev 320m	1.561111	0.041169	13.629	0
Tailings Elev 324m	1.558148	0.042339	13.183	0
Tailings Elev 328m	1.492222	0.052428	9.389	0
Tailings Elev 330m	1.413704	0.047162	8.772	0
Dyke	1.413333	0.046575	8.875	0
Tailings Elev 332m	1.311852	0.033859	9.210	0

PEM (f-cov=30, c-cov=30, k-cov=50)

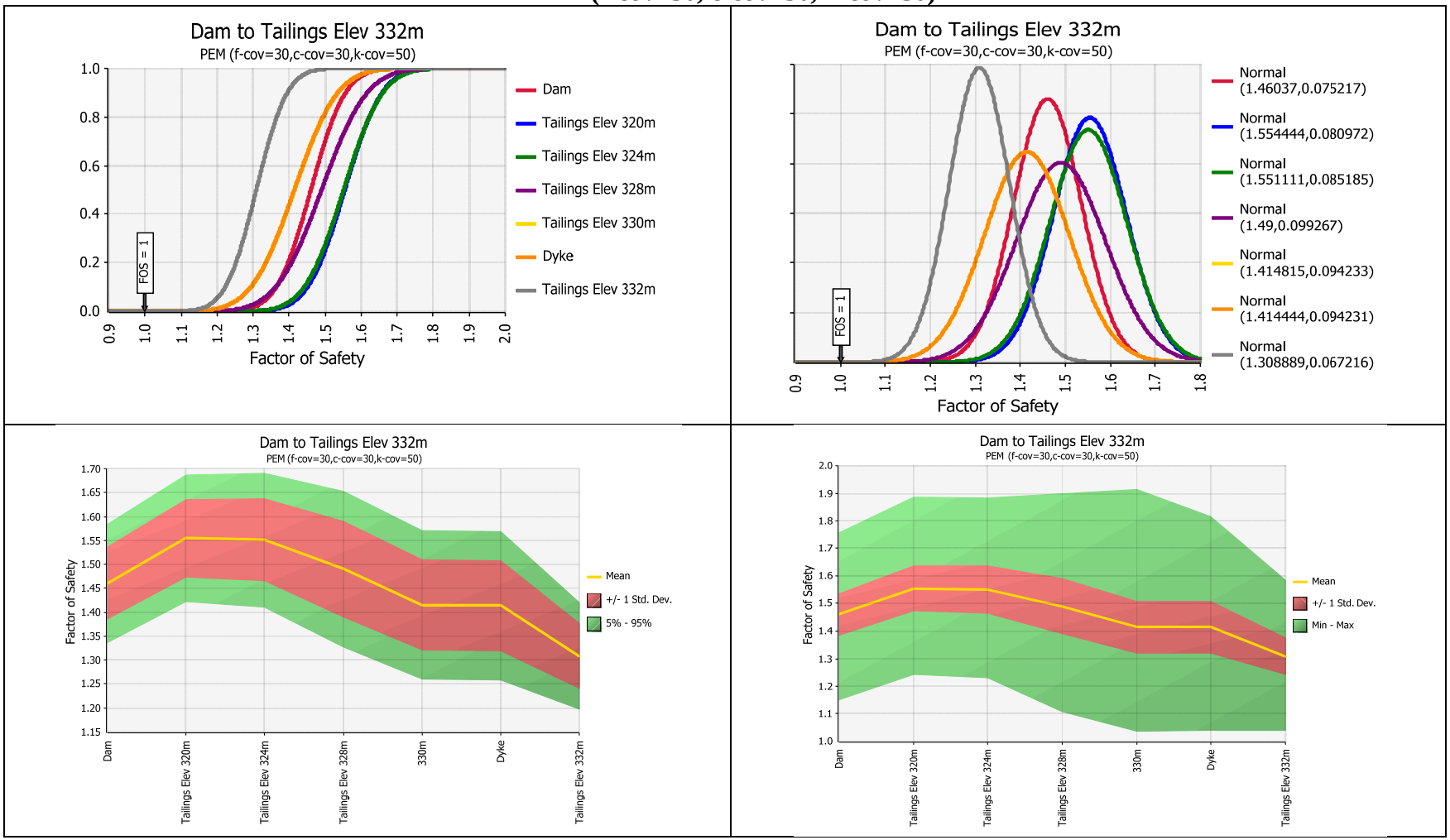

PEM (f-cov=30, c-cov=30, k-cov=50)

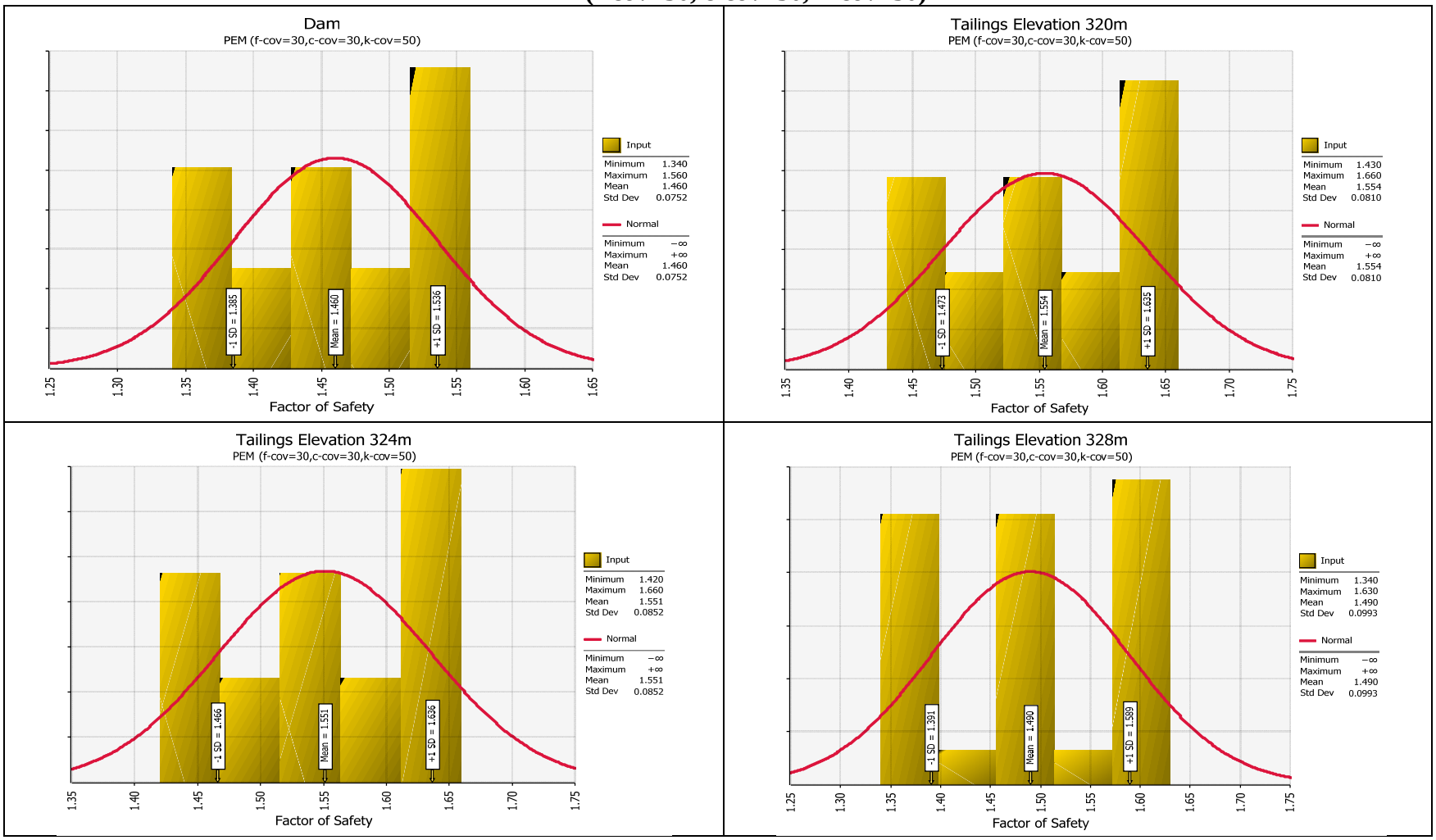

PEM (f-cov=30, c-cov=30, k-cov=50)

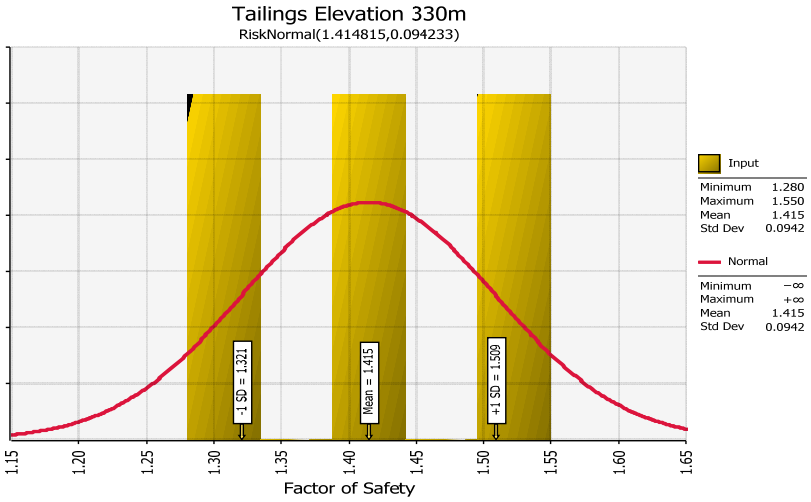

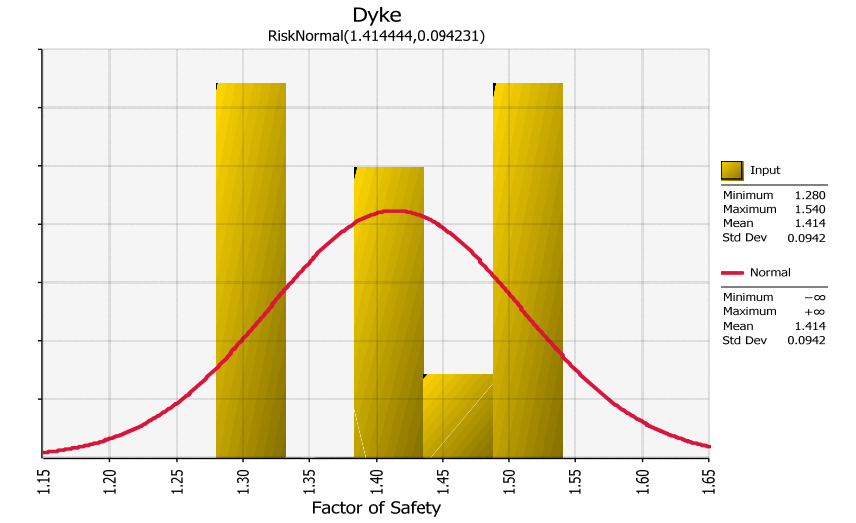

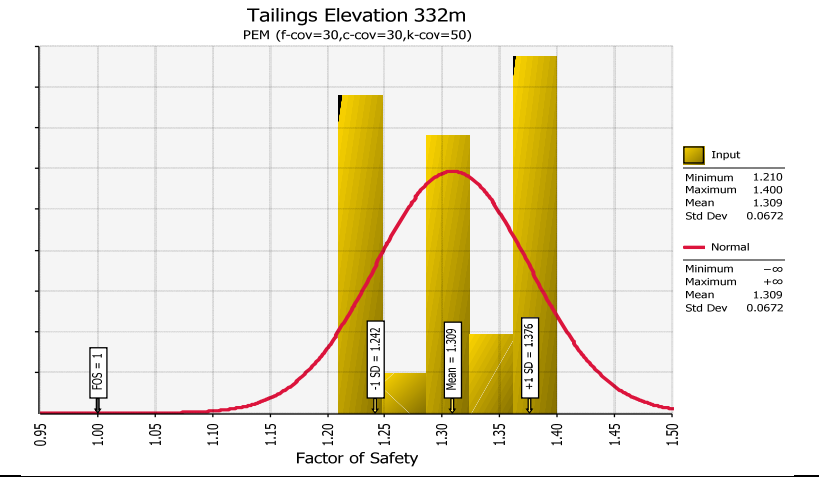

PEM (f-cov=30, c-cov=30, k-cov=50)	MEAN	STDEV	Reliability	Probability of Unsatisfactory Performance
Dam	1.460	0.075	6.121	0
Tailings Elev 320m	1.554	0.081	6.847	0
Tailings Elev 324m	1.551	0.085	6.470	0
Tailings Elev 328m	1.490	0.099	4.936	0
Tailings Elev 330m	1.415	0.094	4.402	0
Dyke	1.414	0.094	4.398	0
Tailings Elev 332m	1.309	0.067	4.595	0

PEM (f-cov=45, c-cov=45, k-cov=50)

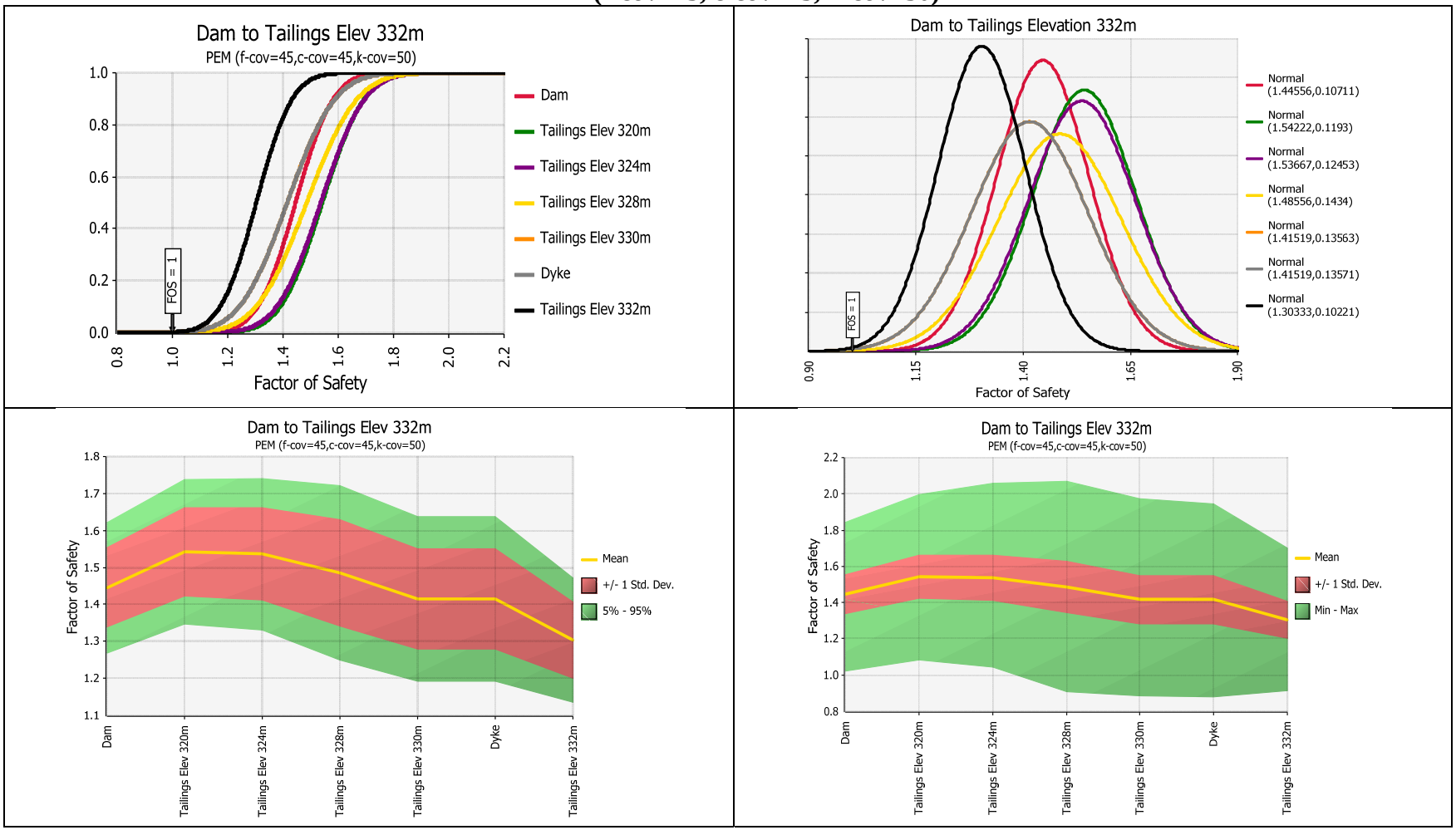

PEM (f-cov=45, c-cov=45, k-cov=50)

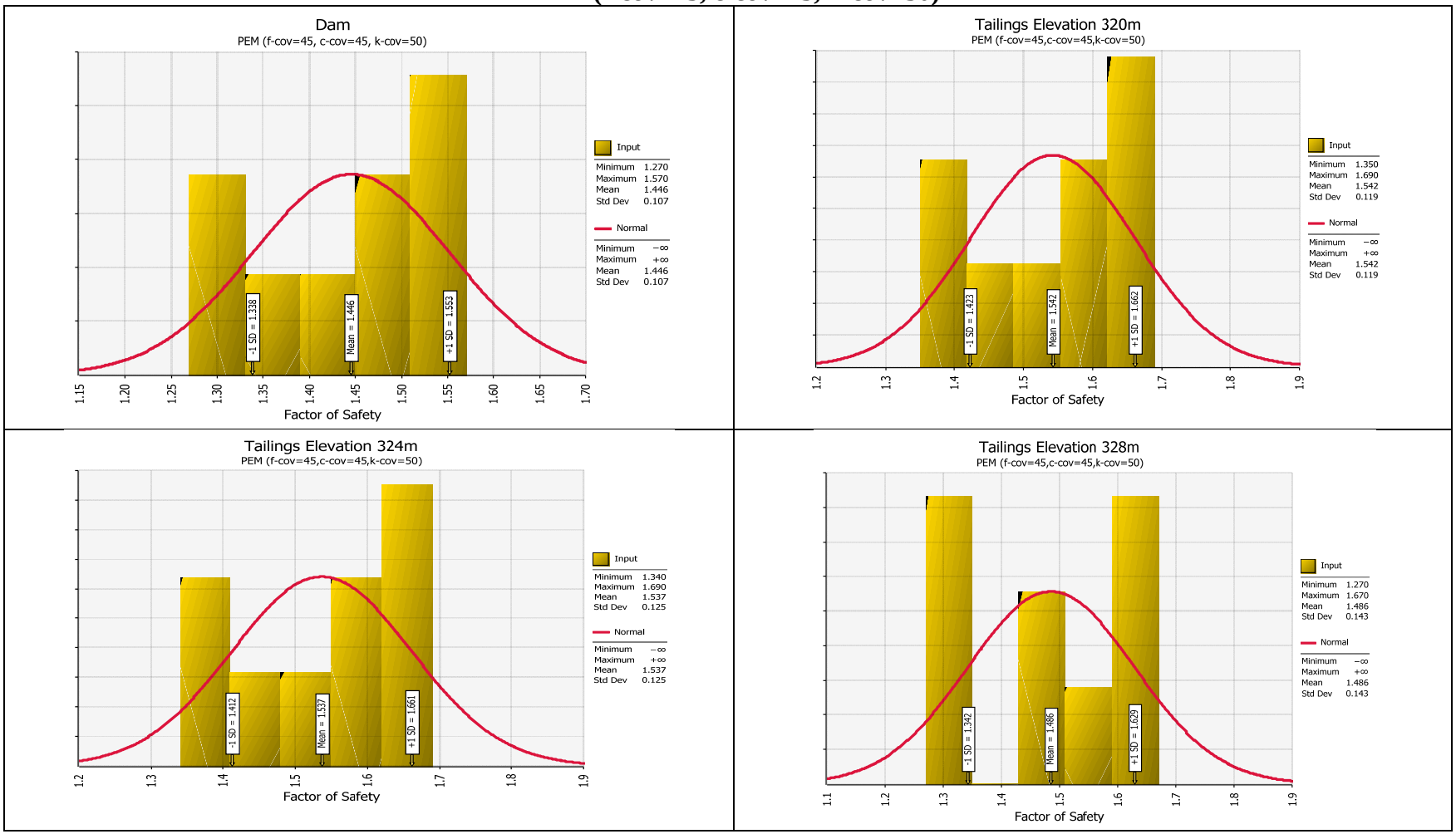

PEM (f-cov=45, c-cov=45, k-cov=50)

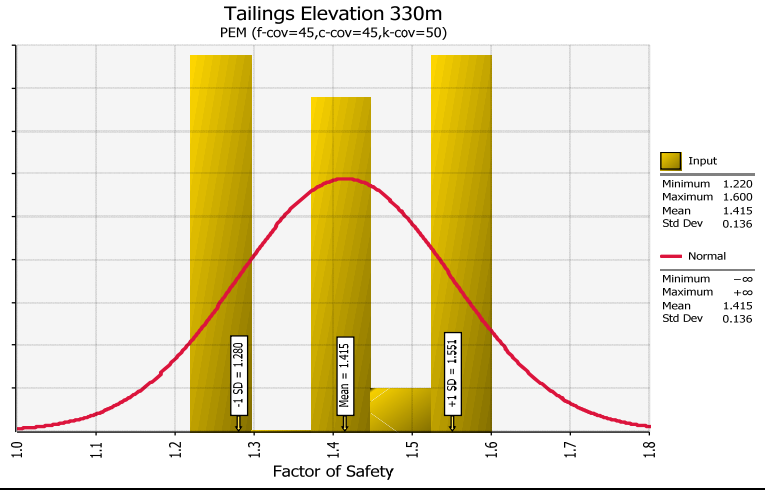

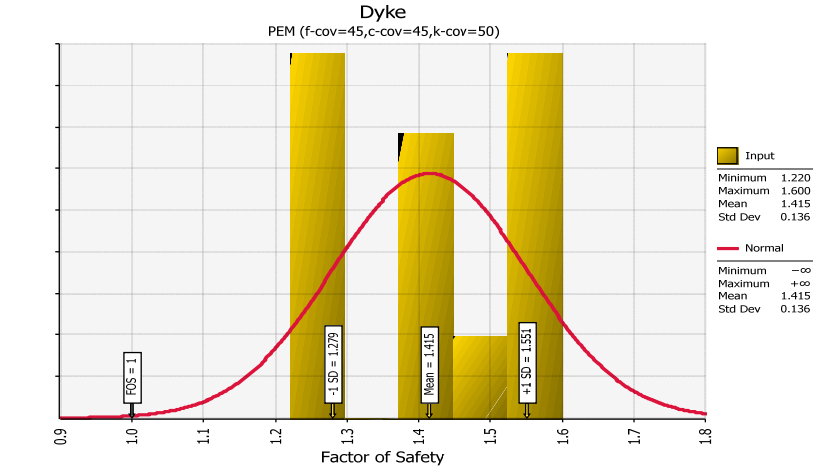

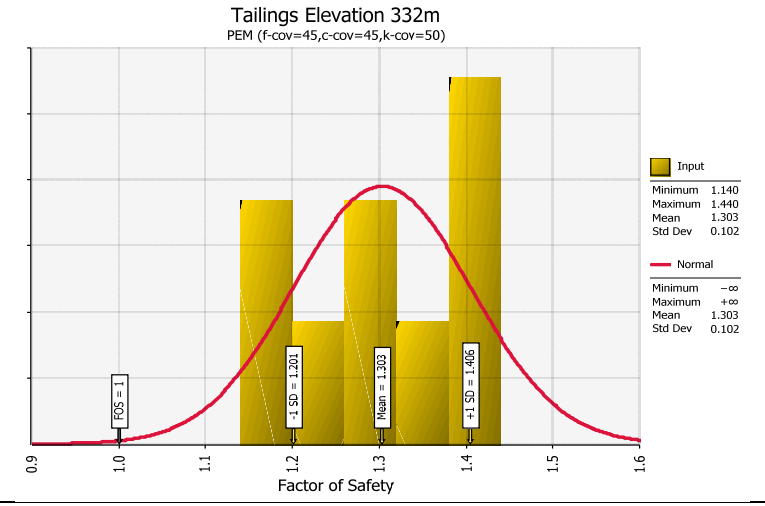

PEM (f-cov=45, c-cov=45, k-cov=50)	MEAN	STDEV	Reliability	Probability of Unsatisfactory Performance
Dam	1.446	0.107	4.160	0
Tailings Elev 320m	1.542	0.119	4.545	0
Tailings Elev 324m	1.537	0.125	4.310	0
Tailings Elev 328m	1.486	0.143	3.386	0.0004
Tailings Elev 330m	1.415	0.136	3.061	0.0011
Dyke	1.415	0.136	3.059	0.0011
Tailings Elev 332m	1.303	0.102	2.968	0.0015

MC (f-cov=30, N)

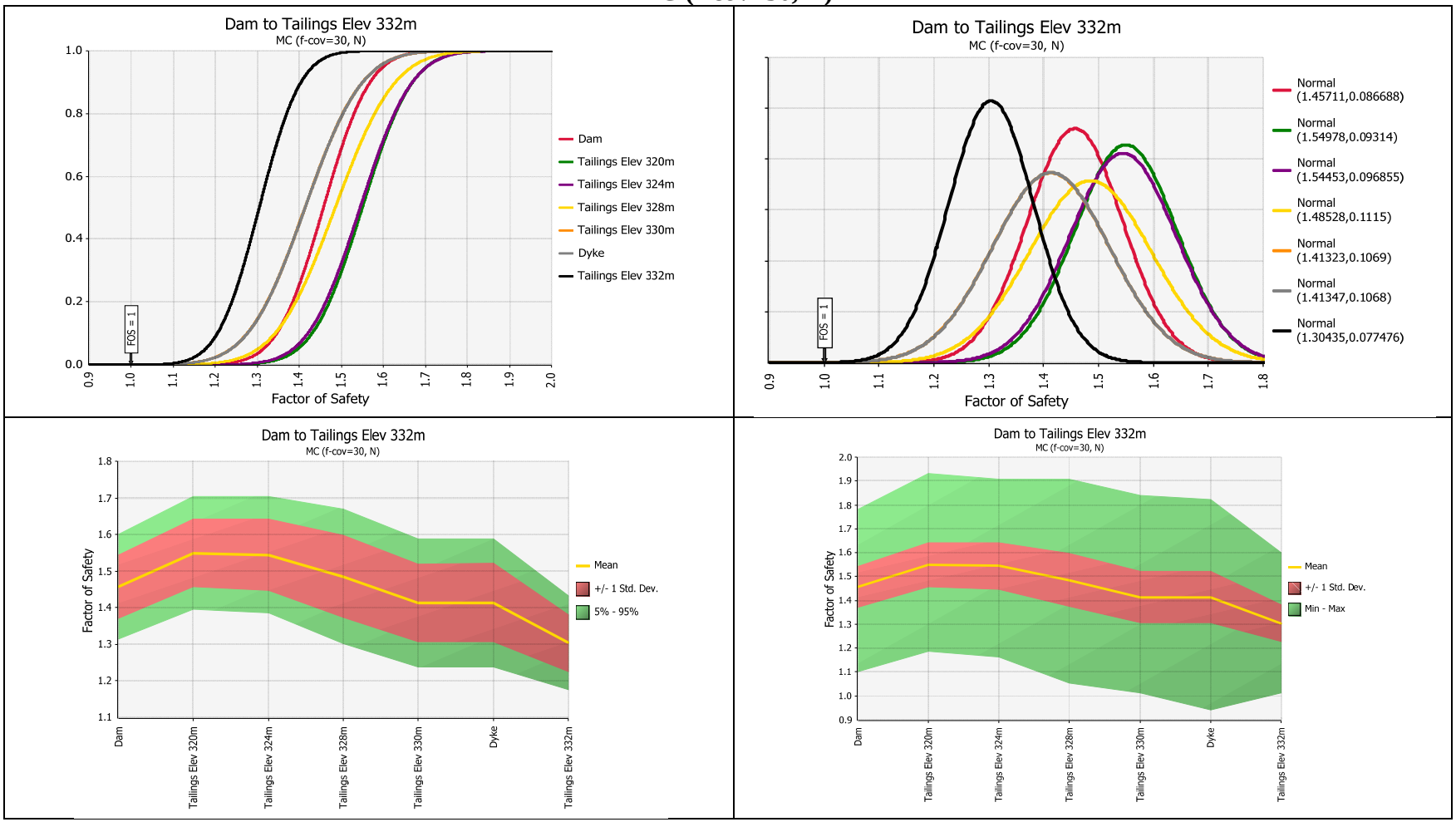
Dam to Tailings Elev 332m
MC (f-cov=30, N)
FOS = 1
Factor of Safety
Dam
Tailings Elev 320m
Tailings Elev 324m
Tailings Elev 328m
Tailings Elev 330m
Dyke
Tailings Elev 332m
Normal (1.45711,0.086688)
Normal (1.54978,0.09314)
Normal (1.54453,0.096855)
Normal (1.48528,0.1115)
Normal (1.41323,0.1069)
Normal (1.41347,0.1068)
Normal (1.30435,0.077476)
Factor of Safety
Mean
+/- 1 Std. Dev.
5% - 95%
Min - Max

MC (f-cov=30, N)

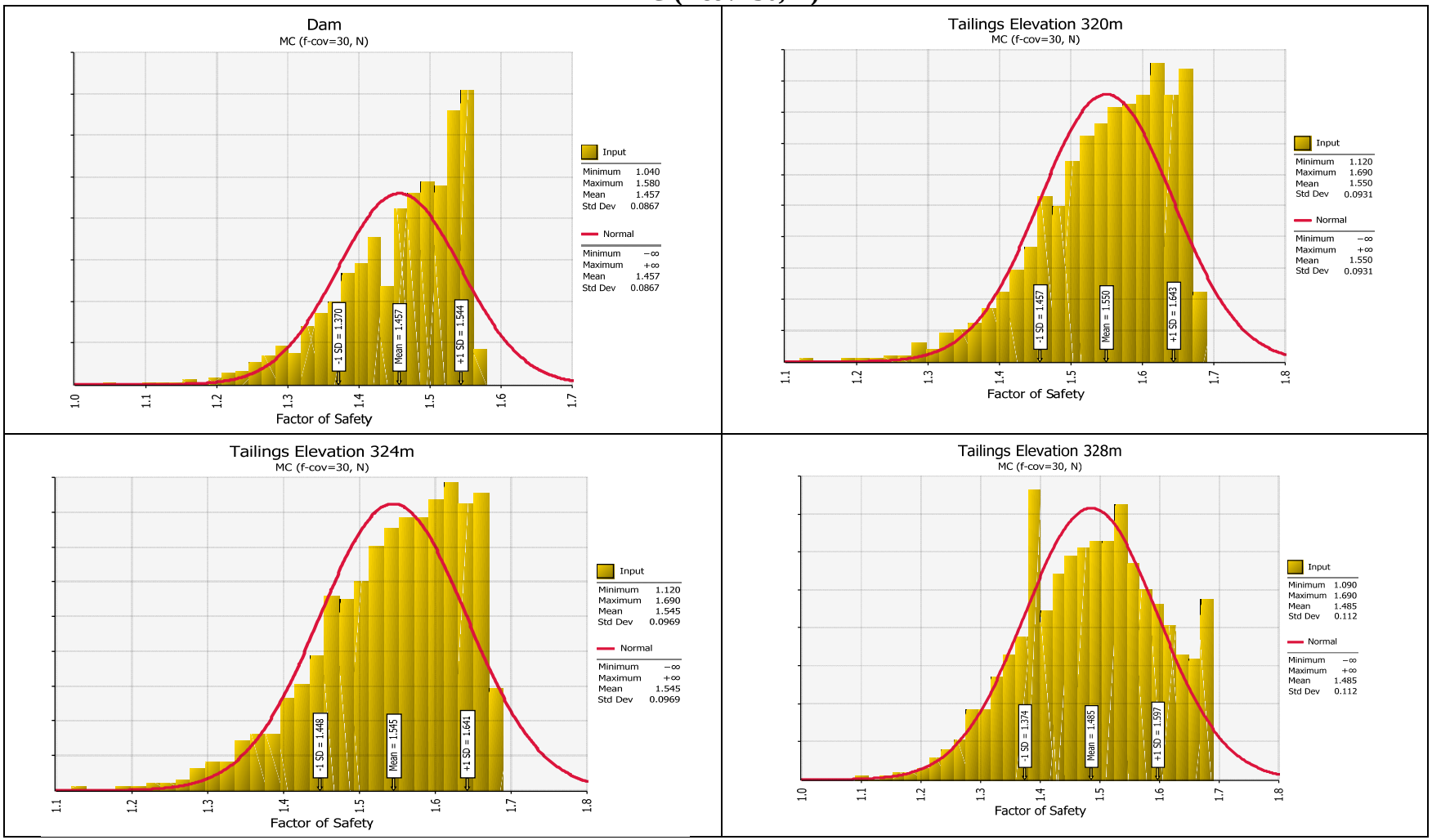
Dam
MC (f-cov=30, N)
Input
Minimum 1.040
Maximum 1.580
Mean 1.457
Std Dev 0.0867
Normal
Minimum −∞
Maximum +∞
Mean 1.457
Std Dev 0.0867
-1 SD = 1.370
Mean = 1.457
+1 SD = 1.544
Factor of Safety
Tailings Elevation 320m
MC (f-cov=30, N)
Input
Minimum 1.120
Maximum 1.690
Mean 1.550
Std Dev 0.0931
Normal
Minimum −∞
Maximum +∞
Mean 1.550
Std Dev 0.0931
-1 SD = 1.457
Mean = 1.550
+1 SD = 1.643
Factor of Safety
Tailings Elevation 324m
MC (f-cov=30, N)
Input
Minimum 1.120
Maximum 1.690
Mean 1.545
Std Dev 0.0969
Normal
Minimum −∞
Maximum +∞
Mean 1.545
Std Dev 0.0969
-1 SD = 1.448
Mean = 1.545
+1 SD = 1.641
Factor of Safety
Tailings Elevation 328m
MC (f-cov=30, N)
Input
Minimum 1.090
Maximum 1.690
Mean 1.485
Std Dev 0.112
Normal
Minimum −∞
Maximum +∞
Mean 1.485
Std Dev 0.112
-1 SD = 1.374
Mean = 1.485
+1 SD = 1.597
Factor of Safety

MC (f-cov=30, N)

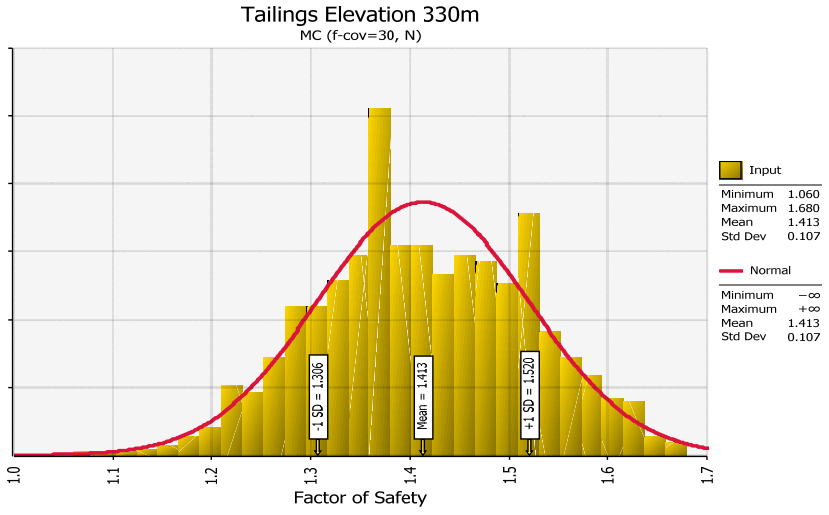

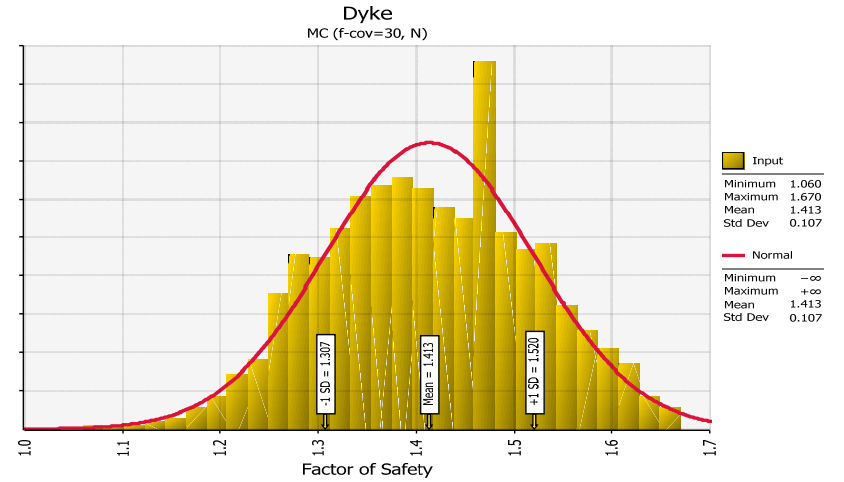

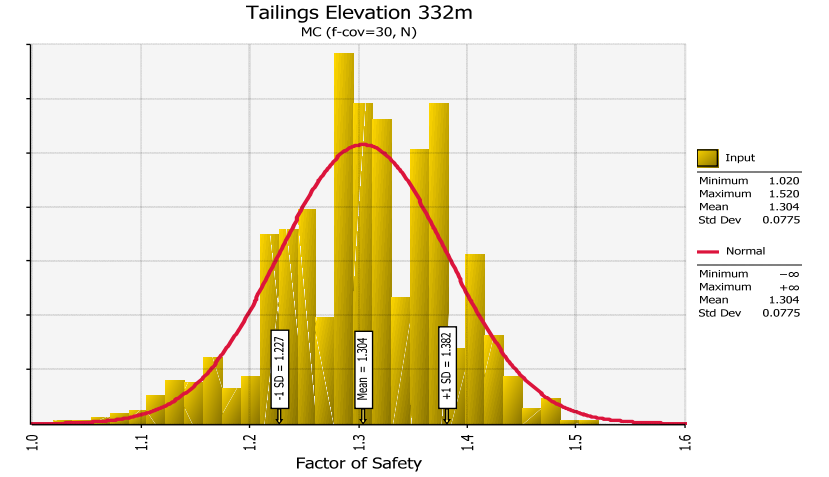

MC Normal PDF ∅ 1,000 runs	MEAN	STDEV	Reliability	Probability of Unsatisfactory Performance
Dam	1.457	0.087	5.273	0
Tailings Elev 320m	1.550	0.093	5.903	0
Tailings Elev 324m	1.545	0.097	5.622	0
Tailings Elev 328m	1.485	0.112	4.352	0
Tailings Elev 330m	1.413	0.107	3.866	0.000055
Dyke	1.413	0.107	3.871	0.00005
Tailings Elev 332m	1.304	0.077	3.928	0.00004

MC (f-cov=30, LN)

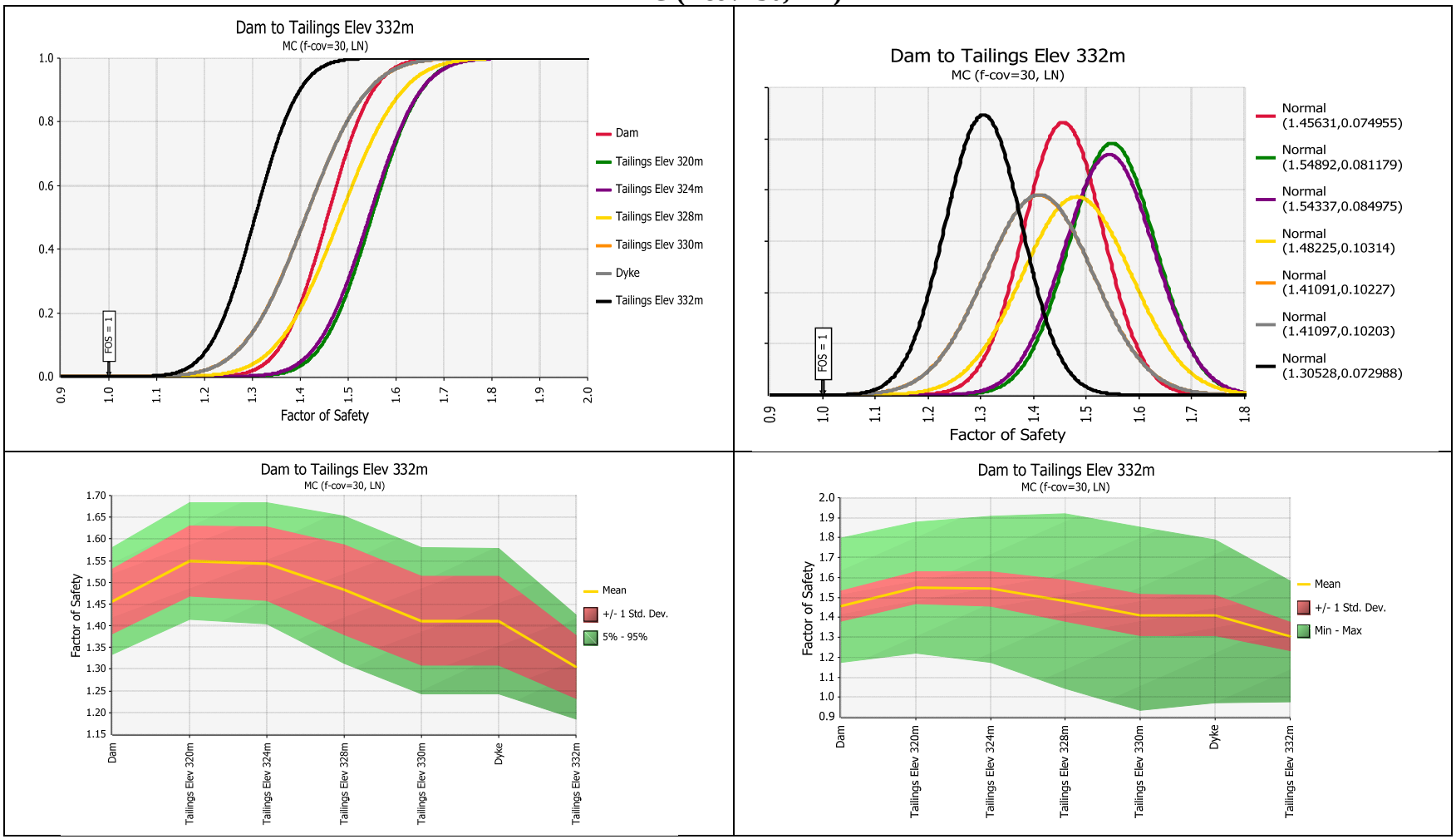
Dam to Tailings Elev 332m
MC (f-cov=30, LN)
Factor of Safety
FOS = 1
Dam
Tailings Elev 320m
Tailings Elev 324m
Tailings Elev 328m
Tailings Elev 330m
Dyke
Tailings Elev 332m
Normal (1.45631,0.074955)
Normal (1.54892,0.081179)
Normal (1.54337,0.084975)
Normal (1.48225,0.10314)
Normal (1.41091,0.10227)
Normal (1.41097,0.10203)
Normal (1.30528,0.072988)
Mean
+/- 1 Std. Dev.
5% - 95%
Min - Max

MC (f-cov=30, LN)

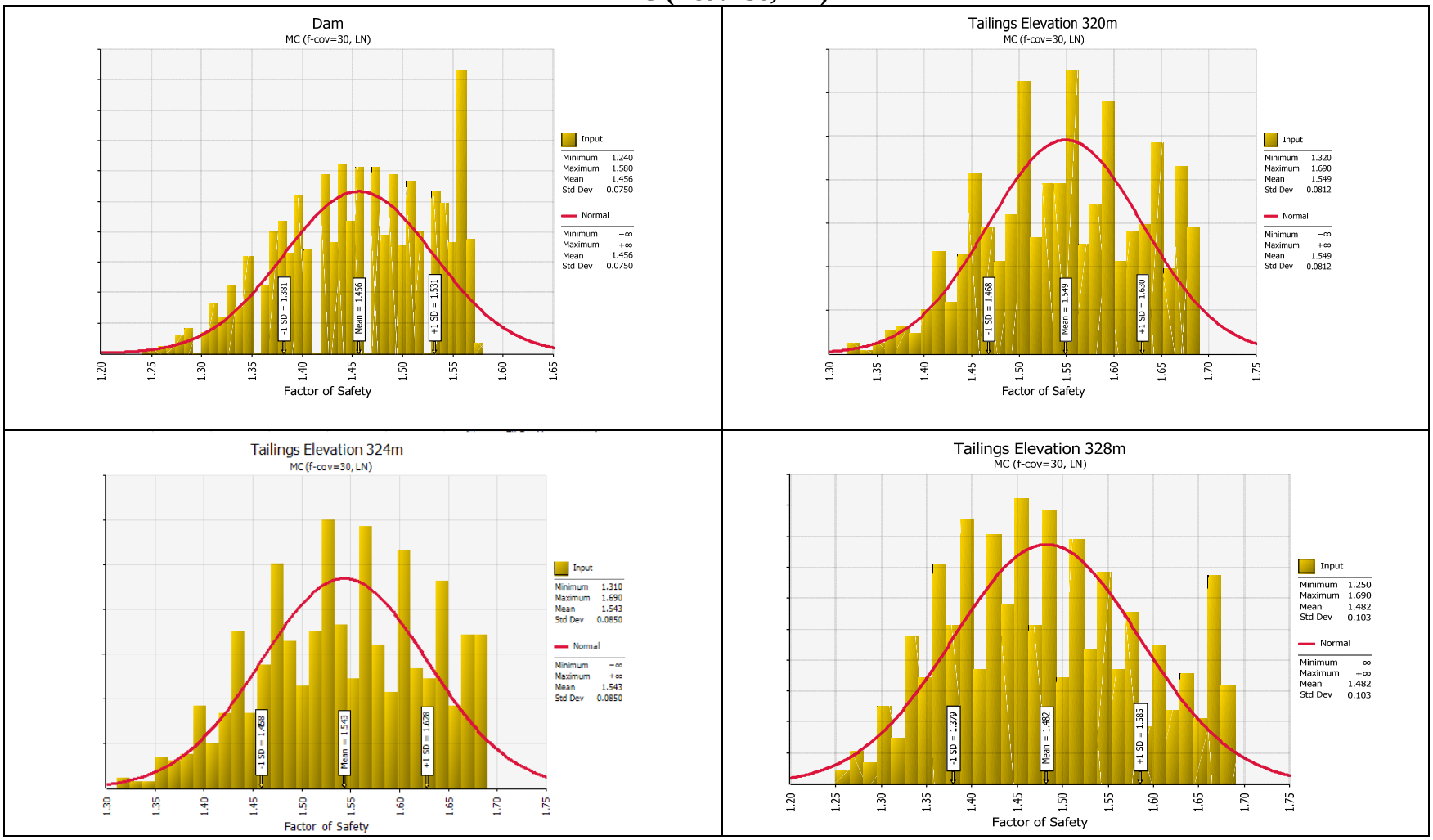
Dam
MC (f-cov=30, LN)
Input
Minimum 1.240
Maximum 1.580
Mean 1.456
Std Dev 0.0750
Normal
Minimum −∞
Maximum +∞
Mean 1.456
Std Dev 0.0750
-1 SD = 1.381
Mean = 1.456
+1 SD = 1.531
Factor of Safety
Tailings Elevation 320m
MC (f-cov=30, LN)
Input
Minimum 1.320
Maximum 1.690
Mean 1.549
Std Dev 0.0812
Normal
Minimum −∞
Maximum +∞
Mean 1.549
Std Dev 0.0812
-1 SD = 1.468
Mean = 1.549
+1 SD = 1.630
Factor of Safety
Tailings Elevation 324m
MC (f-cov=30, LN)
Input
Minimum 1.310
Maximum 1.690
Mean 1.543
Std Dev 0.0850
Normal
Minimum −∞
Maximum +∞
Mean 1.543
Std Dev 0.0850
-1 SD = 1.458
Mean = 1.543
+1 SD = 1.628
Factor of Safety
Tailings Elevation 328m
MC (f-cov=30, LN)
Input
Minimum 1.250
Maximum 1.690
Mean 1.482
Std Dev 0.103
Normal
Minimum −∞
Maximum +∞
Mean 1.482
Std Dev 0.103
-1 SD = 1.379
Mean = 1.482
+1 SD = 1.585
Factor of Safety

MC (f-cov=30, LN)

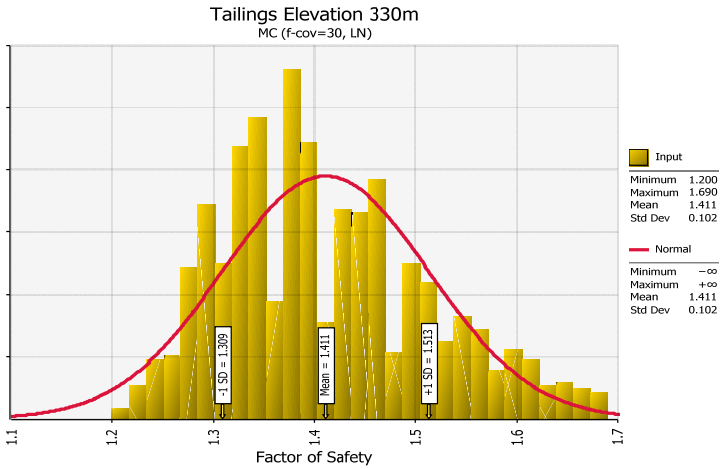

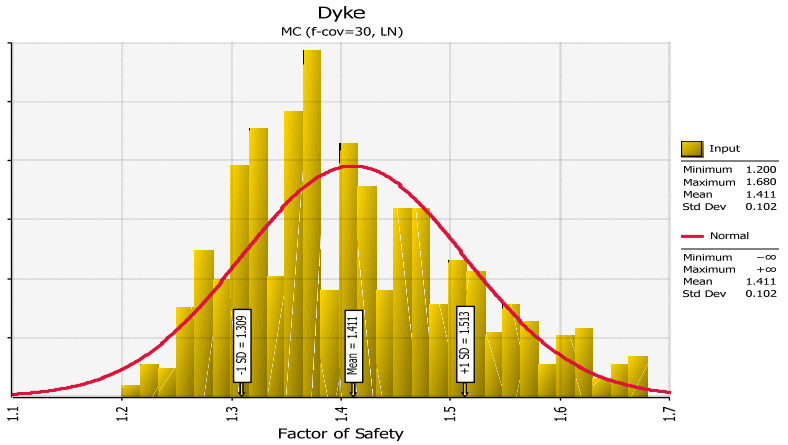

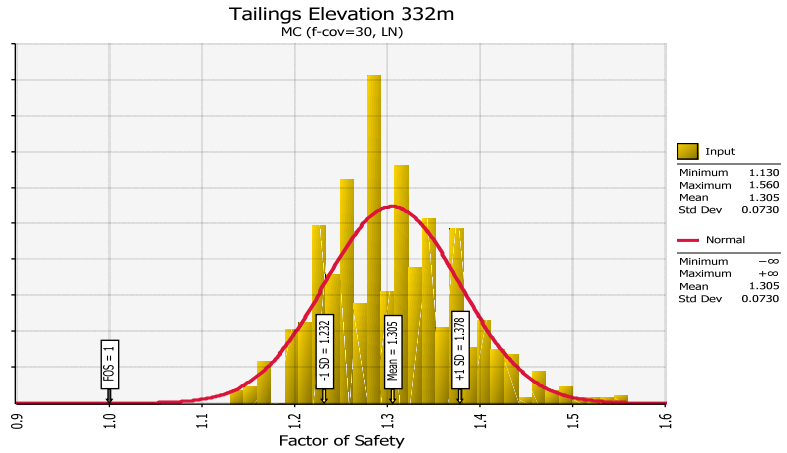

MC LogNormal PDF Ø 1,000 runs	MEAN	STDEV	Reliability	Probability of Unsatisfactory Performance
Dam	1.456	0.075	6.088	0
Tailings Elev 320m	1.549	0.081	6.762	0
Tailings Elev 324m	1.543	0.085	6.394	0
Tailings Elev 328m	1.482	0.103	4.676	0
Tailings Elev 330m	1.411	0.102	4.018	0
Dyke	1.411	0.102	4.028	0
Tailings Elev 332m	1.305	0.073	4.183	0

RMC (f-cov=30, 1000 seeds)

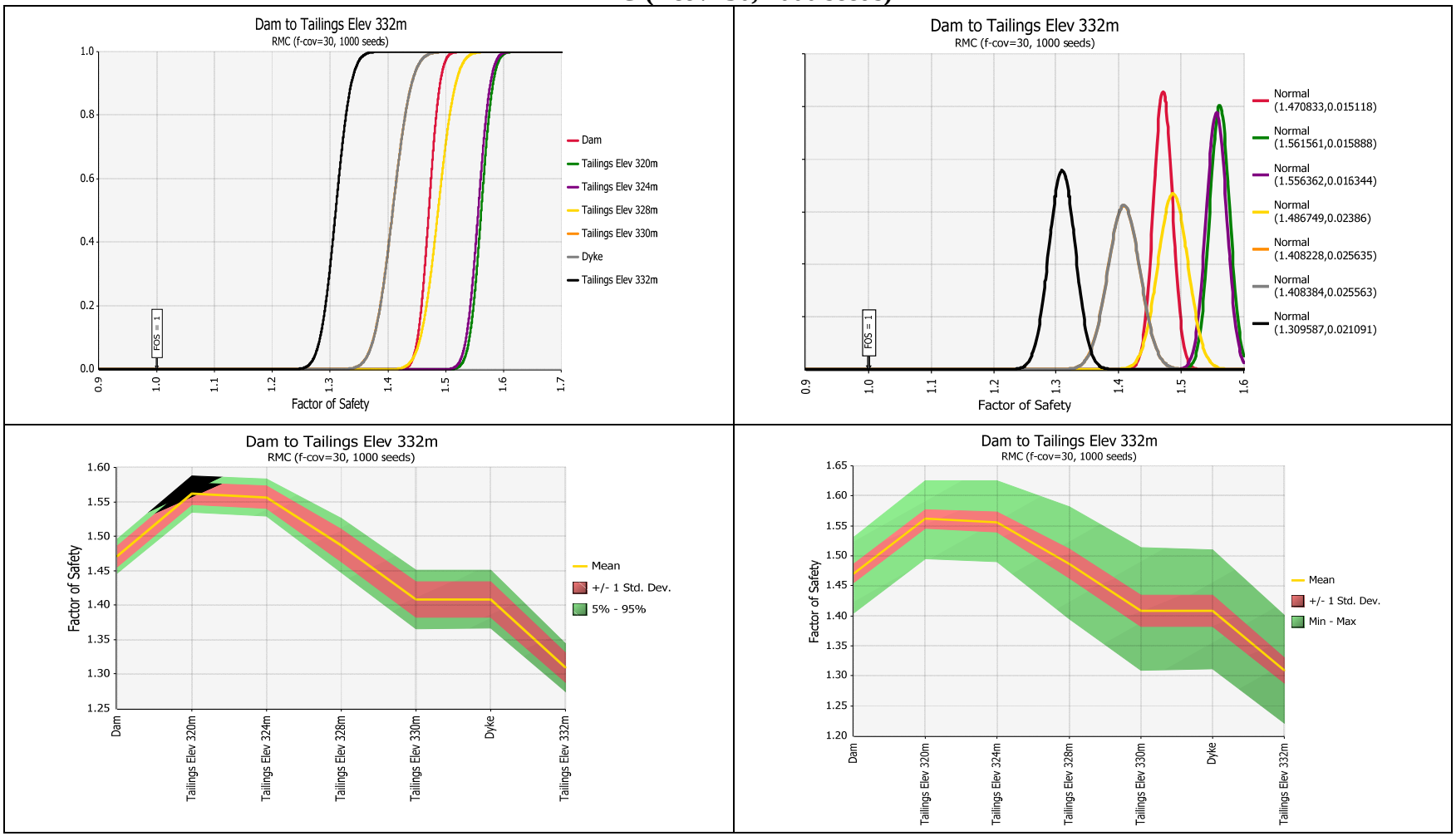

RMC (f-cov=30, 1000 seeds)

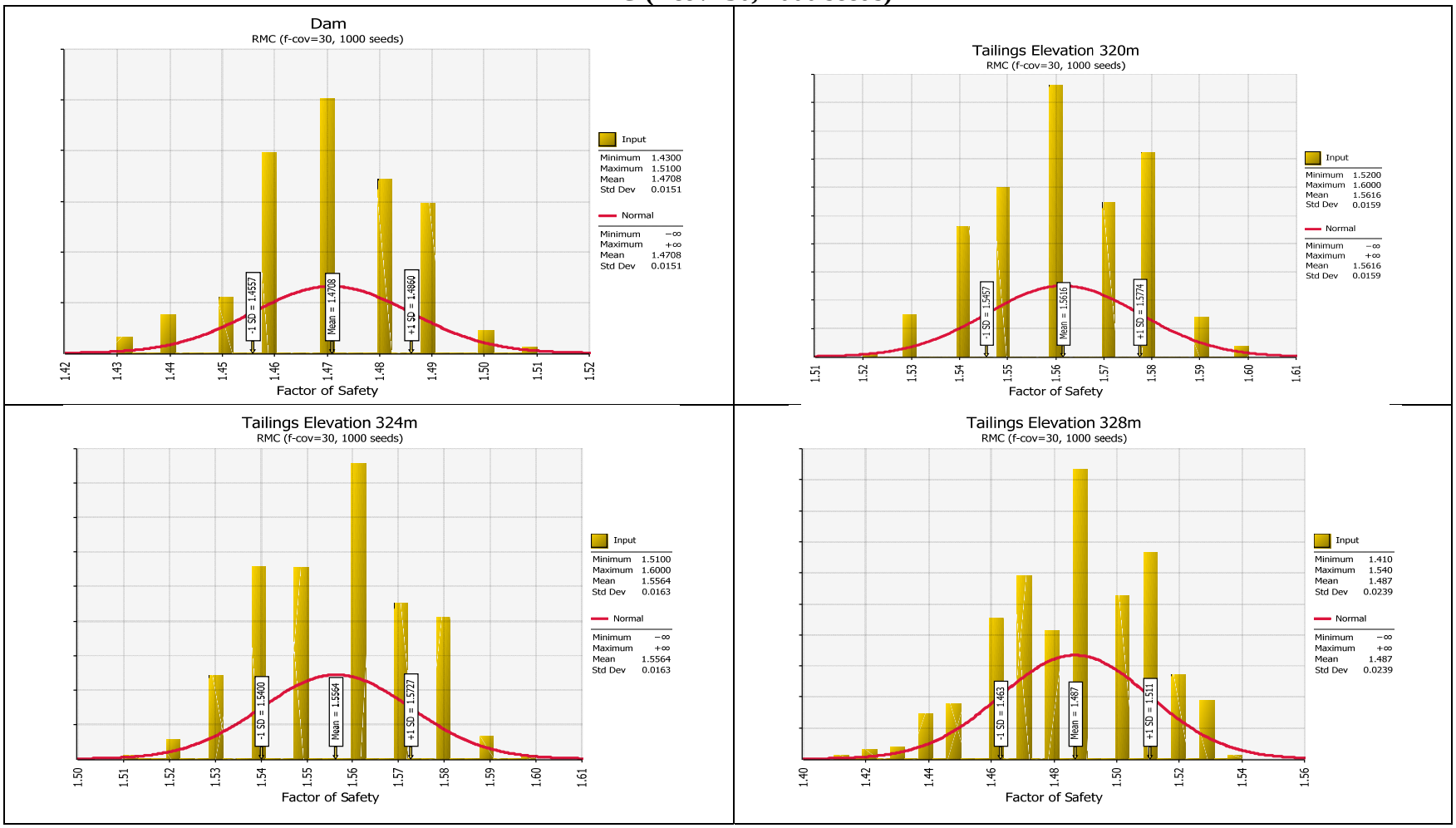

RMC (f-cov=30, 1000 seeds)

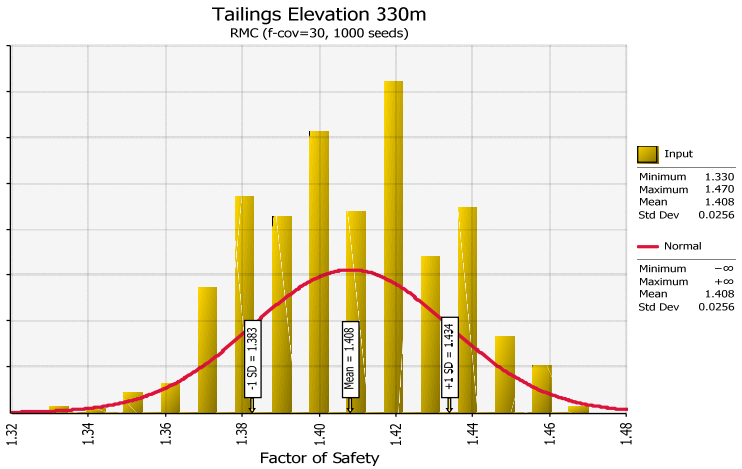

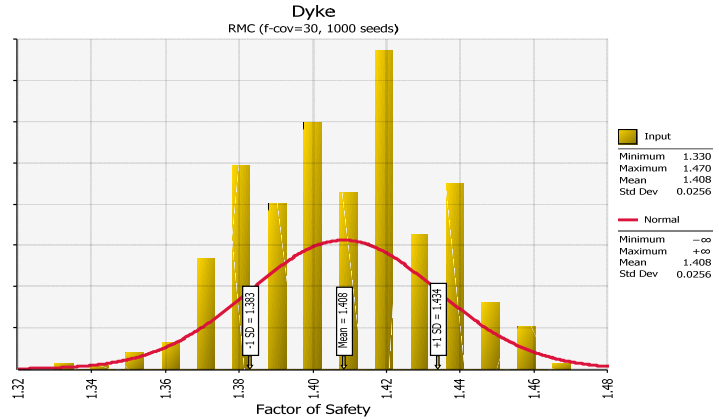

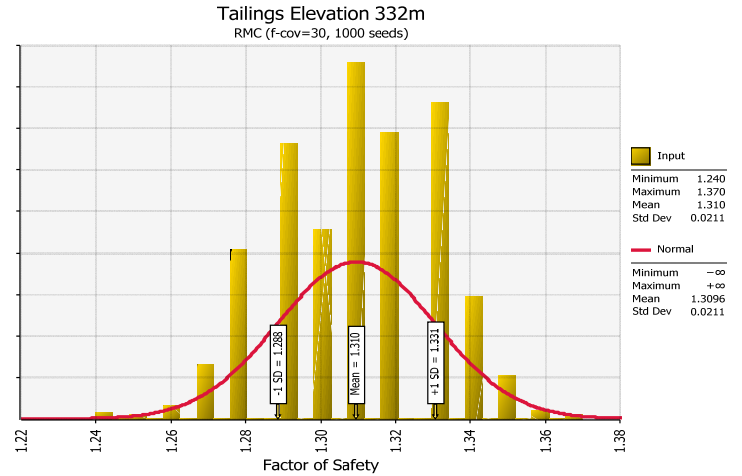

RMC Normal PDF Ø 1,000 seeds	MEAN	STDEV	Reliability	Probability of Unsatisfactory Performance
Dam	1.471	0.015	31.144	0
Tailings Elev 320m	1.562	0.016	35.345	0
Tailings Elev 324m	1.556	0.016	34.041	0
Tailings Elev 328m	1.487	0.024	20.400	0
Tailings Elev 330m	1.408	0.026	15.925	0
Dyke	1.408	0.026	15.976	0
Tailings Elev 332m	1.310	0.021	14.679	0

APPENDIX B – FLAC CODE

```
;1.dat
set echo off
new
; Source: Simple grid
; Grid file: C:\Users\tarek.hamade\Documents\Tarek FLAC\4Four\grid1.grd
config gwflow
;----------Stage1----------
grid 120,28
gen 0.0,0.0 0.0,17.0 100.0,17.0 100.0,0.0 i=1,21 j=1,6
gen 100.0,0.0 100.0,17.0 200.0,17.0 200.0,0.0 i=21,46 j=1,6
gen 200.0,0.0 200.0,17.0 350.0,17.0 350.0,0.0 i=46,121 j=1,6
gen 0.0,17.0 0.0,20.0 100.0,20.0 100.0,17.0 i=1,21 j=6,9
gen 100.0,17.0 100.0,20.0 200.0,20.0 200.0,17.0 i=21,46 j=6,9
gen 200.0,17.0 200.0,20.0 350.0,20.0 350.0,17.0 i=46,121 j=6,9
gen 0.0,20.0 0.0,40.0 100.0,40.0 100.0,20.0 i=1,21 j=9,29
gen 100.0,20.0 100.0,40.0 200.0,40.0 200.0,20.0 i=21,46 j=9,29
gen 200.0,20.0 200.0,40.0 350.0,40.0 350.0,20.0 i=46,121 j=9,29
model elastic i=1,20 j=1,5
model elastic i=21,45 j=1,5
model elastic i=46,120 j=1,5
model elastic i=1,20 j=6,8
model elastic i=21,45 j=6,8
model elastic i=46,120 j=6,8
model elastic i=1,20 j=9,28
model elastic i=21,45 j=9,28
model elastic i=46,120 j=9,28
gen line 0.0,17.0 350.0,17.0
gen line 0.0,20.0 350.0,20.0
gen line 285.0,22.0 295.0,22.0
ini x 295 y 22 i 94 j 11
mark i 94 j 11
```

ini x 285 y 22 i 88 j 11
mark i 88 j 11
ini x 296.67 y 21.33 i 94 j 10
mark i 94 j 10
ini x 298.325 y 20.66 i 95 j 10
mark i 95 j 10
ini x 299.1625 y 20.33 i 96 j 10
mark i 96 j 10
gen line 242.0,36.0 250.0,36.0
ini x 243 y 36 i 68 j 25
ini x 249 y 36 i 70 j 25
gen line 250.0,36.0 285.0,22.0
gen line 242.0,36.0 202.0,20.0
gen line 249.0,36.0 252.0,20.0
gen line 243.0,36.0 240.0,20.0
ini x 243 y 17 i 67 j 6
mark i 67 j 6
ini x 249 y 17 i 71 j 6
mark i 71 j 6
gen line 240.0,20.0 243.0,17.0
gen line 252.0,20.0 249.0,17.0
gen line 0.0,24.0 208.0,24.0
gen line 0.0,28.0 218.0,28.0
gen line 0.0,32.0 228.0,32.0
gen line 0.0,34.0 234.0,34.0
gen line 214.0,37.0 224.0,37.0
ini x 227 y 34 i 59 j 23
gen line 224.0,37.0 227.0,34.0
ini x 211 y 34 i 52 j 23
gen line 214.0,37.0 211.0,34.0
gen line 0.0,36.0 210.0,36.0

```
model null region 102 21
group 'null' region 102 21
group delete 'null'
model elastic i=94,95 j=9
model elastic i=70,71 j=24
model elastic i=66,67 j=24
model elastic i=63,64 j=22
;----------Stage2----------
group 'Foundation:Bedrock' region 52 3
model mohr group 'Foundation:Bedrock'
prop density=2400.0 bulk=1.67E10 shear=7.69E9 cohesion=1.0E7 friction=32.0
dilation=0.0 tension=0.0 group 'Foundation:Bedrock'
group 'Foundation:Clay' region 58 7
model mohr group 'Foundation:Clay'
prop density=1350.0 bulk=2E6 shear=1.2E6 cohesion=50000.0 friction=0.0
dilation=0.0 tension=0.0 group 'Foundation:Clay'
group 'Foundation:Clay' region 89 7
model mohr group 'Foundation:Clay'
prop density=1350.0 bulk=2E6 shear=1.2E6 cohesion=50000.0 friction=0.0
dilation=0.0 tension=0.0 group 'Foundation:Clay'
group 'Foundation:Core' region 68 7
model mohr group 'Foundation:Core'
prop density=1850.0 bulk=1.67E8 shear=7.7E7 cohesion=12000.0 friction=28.0
dilation=0.0 tension=0.0 group 'Foundation:Core'
group 'Dam:Core' region 69 17
model mohr group 'Dam:Core'
prop density=1850.0 bulk=1.67E8 shear=7.7E7 cohesion=12000.0 friction=28.0
dilation=0.0 tension=0.0 group 'Dam:Core'
group 'Foundation:Core' region 71 8
model mohr group 'Foundation:Core'
```

```
prop density=1850.0 bulk=1.67E8 shear=7.7E7 cohesion=12000.0 friction=28.0
dilation=0.0 tension=0.0 group 'Foundation:Core'
group 'Foundation:Core' region 66 8
model mohr group 'Foundation:Core'
prop density=1850.0 bulk=1.67E8 shear=7.7E7 cohesion=12000.0 friction=28.0
dilation=0.0 tension=0.0 group 'Foundation:Core'
group 'Dam:Borrow' region 76 15
model mohr group 'Dam:Borrow'
prop density=1600.0 bulk=2.67E7 shear=1.6E7 cohesion=0.0 friction=35.0
dilation=0.0 tension=0.0 group 'Dam:Borrow'
group 'Dam:Borrow' region 62 15
model mohr group 'Dam:Borrow'
prop density=1600.0 bulk=2.67E7 shear=1.6E7 cohesion=0.0 friction=35.0
dilation=0.0 tension=0.0 group 'Dam:Borrow'
group 'Tailings:Stage1' region 44 11
model mohr group 'Tailings:Stage1'
prop density=1300.0 bulk=6.1E7 shear=8.7E7 cohesion=0.0 friction=28.0
dilation=0.0 tension=0.0 group 'Tailings:Stage1'
group 'Dam:Borrow' region 48 9
model mohr group 'Dam:Borrow'
prop density=1600.0 bulk=2.67E7 shear=1.6E7 cohesion=0.0 friction=35.0
dilation=0.0 tension=0.0 group 'Dam:Borrow'
group 'Tailings:Stage2' region 45 15
model mohr group 'Tailings:Stage2'
prop density=1300.0 bulk=6.1E7 shear=8.7E7 cohesion=0.0 friction=28.0
dilation=0.0 tension=0.0 group 'Tailings:Stage2'
group 'Tailings:Stage1' region 50 12
model mohr group 'Tailings:Stage1'
prop density=1300.0 bulk=6.1E7 shear=8.7E7 cohesion=0.0 friction=28.0
dilation=0.0 tension=0.0 group 'Tailings:Stage1'
group 'Tailings:Stage3' region 49 19
```

```
model mohr group 'Tailings:Stage3'
prop density=1300.0 bulk=6.1E7 shear=8.7E7 cohesion=0.0 friction=28.0
dilation=0.0 tension=0.0 group 'Tailings:Stage3'
group 'Tailings:Stage2' region 55 16
model mohr group 'Tailings:Stage2'
prop density=1300.0 bulk=6.1E7 shear=8.7E7 cohesion=0.0 friction=28.0
dilation=0.0 tension=0.0 group 'Tailings:Stage2'
group 'Tailings:Stage4' region 58 22
model mohr group 'Tailings:Stage4'
prop density=1300.0 bulk=6.1E7 shear=8.7E7 cohesion=0.0 friction=28.0
dilation=0.0 tension=0.0 group 'Tailings:Stage4'
group 'Tailings:Stage3' region 60 20
model mohr group 'Tailings:Stage3'
prop density=1300.0 bulk=6.1E7 shear=8.7E7 cohesion=0.0 friction=28.0
dilation=0.0 tension=0.0 group 'Tailings:Stage3'
group 'Tailings:Stage5' region 48 24
model mohr group 'Tailings:Stage5'
prop density=1300.0 bulk=6.1E7 shear=8.7E7 cohesion=0.0 friction=28.0
dilation=0.0 tension=0.0 group 'Tailings:Stage5'
group 'MiniDam:Borrow' region 54 24
model mohr group 'MiniDam:Borrow'
prop density=1600.0 bulk=2.67E7 shear=1.6E7 cohesion=0.0 friction=35.0
dilation=0.0 tension=0.0 group 'MiniDam:Borrow'
prop tension 1e5
;---------Stage3----------
prop por=0.1 perm=1.0E-11 region 71 4
prop por=0.2 perm=1.0E-10 region 60 7
prop por=0.2 perm=1.0E-10 region 74 6
prop por=0.25 perm=1.0E-10 region 68 7
prop por=0.3 perm=1.0E-6 region 76 15
prop por=0.3 perm=1.0E-6 region 94 9
```

```
prop por=0.3 perm=1.0E-6 region 62 15
prop por=0.25 perm=1.0E-10 region 68 14
prop por=0.3 perm=1.0E-6 region 55 24
prop por=0.4 k11=4.0E-9 k22=4.0E-10 region 39 11
prop por=0.4 k11=4.0E-9 k22=4.0E-10 region 44 15
prop por=0.4 k11=4.0E-9 k22=4.0E-10 region 45 19
prop por=0.4 k11=4.0E-9 k22=4.0E-10 region 45 22
prop por=0.4 k11=4.0E-9 k22=4.0E-10 region 43 24
m null i=1,20
fix x i=21
;----------Stage4----------
fix  x i 1 j 1 25
fix  x i 121 j 1 9
fix  x y j 1
set gravity=9.81
water density=1000.0
;----------Stage5----------
model null  group 'Tailings:Stage5'
model null  group 'MiniDam:Borrow'
model null  group 'Tailings:Stage4'
model null  group 'Tailings:Stage3'
model null  group 'Tailings:Stage2'
model null  group 'Tailings:Stage1'
model null  group 'Dam:Borrow'
model null  group 'Dam:Core'
set flow off
water bulk 0
prop cohesion 1e9 tension 1e5
solve
prop cohesion 1e5 group 'Foundation:Bedrock'
prop cohesion 0.5e5 group 'Foundation:Clay'
```

```
prop cohesion 0.12e5 group 'Foundation:Core'
solve
initial pp 200000.0 var 0.0,-200000.0 j 1 9
fix pp j 9
solve
;----------Stage6----------
def MC1
oo=out('MC_1')
end
set log on
MC1
set log off
ini xdis 0 ydis 0
model mohr group 'Dam:Core'
prop density=1850.0 bulk=1.67E8 shear=7.7E7 cohesion=12000.0 friction=28.0
dilation=0.0 tension=0.0 group 'Dam:Core'
model mohr group 'Dam:Borrow'
prop density=1600.0 bulk=2.67E7 shear=1.6E7 cohesion=0.0 friction=35.0
dilation=0.0 tension=0.0 group 'Dam:Borrow'
free  pp i 48 95 j 9
fix x y j 1,9
ini sat 0 group 'Dam:Core'
ini sat 0 group 'Dam:Borrow'
ini sat 1 j 9
set flow off mech on
water bulk 0
prop cohesion 1e9 tension 1e5 group 'Dam:Core'
prop cohesion 1e9 tension 1e5 group 'Dam:Borrow'
prop por 0.25 perm 1E-10 group 'Dam:Core'
prop por 0.3 perm 1E-6 group 'Dam:Borrow'
solve
```

```
;----------Stage7----------
ini xdis 0 ydis 0
free x y j 2,9
fix x i=21
fix x i=121
fix sat i=1,47   j=9
fix sat i=96,121 j=9
set mech on flow off
water bulk=2e8
solve elastic
prop cohesion 12000 group 'Dam:Core'
solve
prop cohesion 1e4 group 'Dam:Borrow'
solve
set flow=on mech on
set ngw 1 nmech 20
set step 100000000
prop cohesion 1.2e4 i=47 j=9
prop cohesion 1.2e4 i=95 j=9
set fastwb on
set large
solve  auto on age 1e6
;solve for fos
set flow off mech on
water bulk 0
solve fos
def MC1_fos7
oo=out('fos_7')
end
set log on
MC1_fos7
```

```
print fos
set log off
;----------Stage8----------
ini xdis 0 ydis 0
set gwtime 0
model mohr group 'Tailings:Stage1'
prop density=1300.0 bulk=6.1E5 shear=8.7E5 cohesion=0.0 friction=28.0
dilation=0.0 tension=0.0 group 'Tailings:Stage1'
prop tension 1e5 group 'Tailings:Stage1'
m null i=1,20
free pp sat i=1,47 j=9
fix  pp sat i=1,50 j=13
prop perm 1e-10 group 'Dam:Core'
prop perm 1e-6  group 'Dam:Borrow'
prop por=0.4 k11=4.0E-9 k22=4.0E-10 group 'Tailings:Stage1'
; --- undrained response ---
set flow off mech on
water bulk 2e8
solve
;solve for fos
set flow off mech on
water bulk 0
solve fos
def MC1_fos8u
oo=out('fos_8u')
end
set log on
MC1_fos8u
print fos
set log off
; --- drained response ---
```

```
set flow on mech on
water bulk 2e8
set fastwb on
set ngw 1 nmech 20
solve  auto on age 2e6
;solve for fos
set flow off mech on
water bulk 0
solve fos
def MC1_fos8d
oo=out('fos_8d')
end
set log on
MC1_fos8d
print fos
set log off
;----------Stage9----------
ini xdis 0 ydis 0
set gwtime 0
model mohr group 'Tailings:Stage2'
prop density=1300.0 bulk=6.1E5 shear=8.7E5 cohesion=0.0 friction=28.0
dilation=0.0 tension=0.0 group 'Tailings:Stage2'
prop tension 1e5 group 'Tailings:Stage2'
free  pp sat i=1,51 j=13
fix   pp sat i 1 56 j 17
prop por=0.4 k11=4.0E-9 k22=4.0E-10 group 'Tailings:Stage2'
m null i=1,20
; --- undrained response ---
set flow off mech on
water bulk 2e8
solve
```

```
;solve for fos
set flow off mech on
water bulk 0
solve fos
def MC1_fos9u
oo=out('fos_9u')
end
set log on
MC1_fos9u
print fos
set log off
; --- drained response ---
set flow on mech on
water bulk 2e8
set fastwb on
set ngw 1 nmech 20
solve  auto on age 2e6
;solve for fos
set flow off mech on
water bulk 0
solve fos
def MC1_fos9d
oo=out('fos_9d')
end
set log on
MC1_fos9d
print fos
set log off
;----------Stage10---------
ini xdis 0 ydis 0
set gwtime 0
```

```
model mohr group 'Tailings:Stage3'
prop density=1300.0 bulk=6.1E5 shear=8.7E5 cohesion=0.0 friction=28.0
dilation=0.0 tension=0.0 group 'Tailings:Stage3'
prop tension 1e5 group 'Tailings:Stage3'
m null i=1,20
free   pp sat i 1 56 j 17
fix    pp sat i 1 61 j 21
prop por=0.4 k11=4.0E-9 k22=4.0E-10 group 'Tailings:Stage3'
; --- undrained response ---
set flow off mech on
water bulk 2e8
solve
;solve for fos
set flow off mech on
water bulk 0
solve fos
def MC1_fos10u
oo=out('fos_10u')
end
set log on
MC1_fos10u
print fos
set log off
; --- drained response ---
set flow on mech on
water bulk 2e8
set fastwb on
set ngw 1 nmech 20
solve  auto on age 2e6
;solve for fos
set flow off mech on
```

```
water bulk 0
solve fos
def MC1_fos10d
oo=out('fos_10d')
end
set log on
MC1_fos10d
print fos
set log off
;----------Stage11----------
ini xdis 0 ydis 0
set gwtime 0
model mohr group 'Tailings:Stage4'
prop density=1300.0 bulk=6.1E5 shear=8.7E5 cohesion=0.0 friction=28.0
dilation=0.0 tension=0.0 group 'Tailings:Stage4'
prop tension 1e5 group 'Tailings:Stage4'
m null i=1,20
free    pp sat i 1 61 j 21
fix     pp sat i 1 64 j 23
prop por=0.4 k11=4.0E-9 k22=4.0E-10 group 'Tailings:Stage4'
; --- undrained response ---
set flow off mech on
water bulk 2e8
solve
;solve for fos
set flow off mech on
water bulk 0
solve fos
def MC1_fos11u
oo=out('fos_11u')
end
```

```
set log on
MC1_fos11u
print fos
set log off
; --- drained response ---
set flow on mech on
water bulk 2e8
set fastwb on
set ngw 1 nmech 20
solve  auto on age 2e6
;solve for fos
set flow off mech on
water bulk 0
solve fos
def MC1_fos11d
oo=out('fos_11d')
end
set log on
MC1_fos11d
print fos
set log off
;----------Stage12----------
ini xdis 0 ydis 0
set gwtime 0
model mohr group 'MiniDam:Borrow'
prop density=1600.0 bulk=2.67E6 shear=1.6E6 cohesion=0.0 friction=35.0
dilation=0.0 tension=0.0 group 'MiniDam:Borrow'
prop tension 1e5 density 1500 group 'MiniDam:Borrow'
prop por 0.3 perm 1E-6 group 'MiniDam:Borrow'
ini sat 0 group 'MiniDam:Borrow'
m null i=1,20
```

```
; --- (static equilibrium of small dam) ---
fix y i 53 58 j 23
prop cohesion 1e9 group 'MiniDam:Borrow'
set flow off mech on
water bulk 0
solve
free y   i 53 58 j 23
free  pp i 53 58 j 23
ini xdis 0 ydis 0
; --- undrained response ---
set flow off mech on
water bulk 2e8
solve
prop cohesion 1e4 group 'MiniDam:Borrow'
solve
;solve for fos
set flow off mech on
water bulk 0
solve fos
def MC1_fos12u
oo=out('fos_12u')
end
set log on
MC1_fos12u
print fos
set log off
; --- drained response ---
set flow on mech on
water bulk 2e8
set fastwb on
set ngw 1 nmech 20
```

```
solve  auto on age 2e6
;solve for fos
set flow off mech on
water bulk 0
solve fos
def MC1_fos12d
oo=out('fos_12d')
end
set log on
MC1_fos12d
print fos
set log off
;----------Stage13----------
ini xdis 0 ydis 0
set gwtime 0
model mohr group 'Tailings:Stage5'
prop density=1300.0 bulk=6.1E5 shear=8.7E5 cohesion=0.0 friction=28.0
dilation=0.0 tension=0.0 group 'Tailings:Stage5'
prop tension 1e5 group 'Tailings:Stage5'
m null i=1,20
prop por=0.3 perm=1.0E-6 group 'MiniDam:Borrow'
free pp sat i 1 64 j 23
fix  pp sat i 1 51 j 25
prop por=0.4 k11=4.0E-9 k22=4.0E-10 group 'Tailings:Stage5'
; --- undrained response ---
set flow off mech on
water bulk 2e8
solve
;solve for fos
set flow off mech on
water bulk 0
```

```
solve fos
def MC1_fos13u
oo=out('fos_13u')
end
set log on
MC1_fos13u
print fos
set log off
; --- drained response ---
set flow on mech on
water bulk 2e8
set fastwb on
set ngw 1 nmech 20
prop cohesion=1E6 tension=1E6 group 'Tailings:Stage4'
solve  auto on age 2e6
;solve for fos
set flow off mech on
water bulk 0
solve fos
def MC1_fos13d
oo=out('fos_13d')
end
set log on
MC1_fos13d
print fos
set log off
```

APPENDIX C – MATLAB CODE

```
function tarektest=tarektest(filename,template)
% This file is to read a template file and generate a sequence of files
% which have a specific value x replaced by values read from a matrix
[data,TXT,RAW]=xlsread(filename);

rnum=data(:,1);


numvariables=length(data(1,:))-1;


   for i=1:length(rnum)

      inputText = fileread(template);
      newFile = regexprep(inputText,'filenum',num2str(rnum(i)));


      for j=1:numvariables
         num2str(data(i,j+1)),
         newFile = regexprep(newFile,['var' num2str(j)],num2str(data(i,j+1)));
      end


      fid = fopen([num2str(i),'.dat'], 'w');
      fprintf(fid, '%s', newFile);
      fclose(fid);

   end
```

Appendix D – RUBY Code

```
#!/usr/bin/ruby

if ARGV[0].nil?
  puts "Usage #{$0} input.txt"
  exit
else
  if File.exist?(ARGV[0])
    if !File.readable?(ARGV[0])
      puts "file #{ARGV[0]} is not readable!"
      exit
    end
  else
    puts "file #{ARGV[0]} does not exist!"
    exit
  end
end

h = Hash.new{|hash,key| hash[key] = {}}
current_MC = nil
current_fos_k = nil

IO.foreach(ARGV[0]) { |line|

  next if line =~ /^\S$/ # skip blank lines
  next if line =~ /^ \*/ # skip lines starting with *
  next if line =~ /^ From File\*/ # skip these too

  line.sub!( /\r\n/, "\n" ) # convert newlines dos2unix

  if line =~ /^ (MC_\d+)/
    current_MC = $1
```

```
  end

  if line =~ /^ (fos_.*?)\s/
    current_fos_k = $1
  end

  if line =~ /^ Factor of Safety:\s*(\S+)/
    #puts "--- #{current_MC} #{current_fos_k} #{$1} ===" # debug
    h[current_MC][current_fos_k] = $1
  end
}

#require 'yaml' # debug
#puts h.to_yaml # debug

# output csv...

print ","
h[h.keys.sort.first].keys.sort.each { |key|
  print key + ","
}
puts

h.keys.sort.each { |key|
  print key + ","
  h[key].keys.sort.each { |key2|
    print h[key][key2] + ","
  }
  puts
}
```